Path-integral methods for non-adiabatic reaction rates

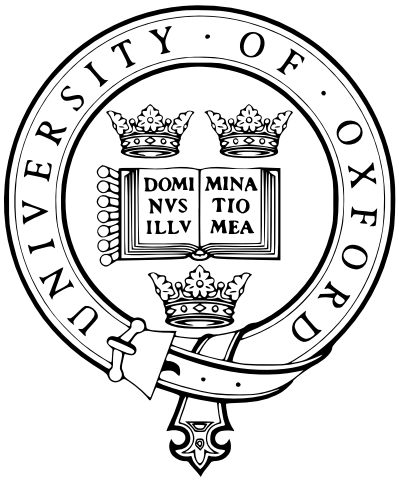

Joseph E. Lawrence

The Queen's College

University of Oxford

A thesis submitted for the degree of

Doctor of Philosophy

Trinity 2020

Path-integral methods for non-adiabatic reaction rates

Joseph E. Lawrence

The Queen's College
University of Oxford

A thesis submitted for the degree of
Doctor of Philosophy

Trinity 2020

Abstract

This thesis discusses recent progress in the development of path-integral methods for non-adiabatic reaction rates in large-scale atomistic simulations. Electronically non-adiabatic reactions are important in a wide range of phenomena, including electron transfer in DNA, enzymatic oxygenation reactions, and the function of light-emitting diodes. Imaginary-time path integrals provide an ideal way to simulate these complex condensed phase reactions, as they are both linearly scaling and capable of accurately describing zero-point energy and tunnelling.

The thesis begins by considering methods for calculating reaction rates in systems that are not fully in either the adiabatic or non-adiabatic limits. Recent work in this area is reviewed, before two new approaches are introduced. The first of these, the non-adiabatic quantum instanton (NAQI), generalises Wolynes theory (valid in the non-adiabatic limit) and the projected quantum instanton (valid in the adiabatic limit) to arbitrary values of electronic coupling. The second approach is a simple formula for interpolating between the results of golden-rule and Born-Oppenheimer rate calculations. This formula can immediately be applied to calculate reaction rates in condensed phase reactions, by combining it with pre-existing path-integral methods in each limit.

Following this, the thesis focusses on the calculation of reaction rates in the golden-rule limit. Again, two new approaches are introduced. The first is an implementation of Wolynes theory which can be used to numerically analytically continue Wolynes theory into the Marcus inverted regime. The second is an alternative path-integral method called the linear golden-rule (LGR) approximation, a size consistent modification of the recently proposed GR-QTST. LGR overcomes the known deficiencies of Wolynes theory, and can be directly applied to calculate reaction rates in the inverted regime. The thesis concludes with a fully atomistic simulation of aqueous ferrous-ferric electron transfer, which addresses recent questions about the nature of the tunnelling in this system.

Acknowledgements

Firstly I would like to thank my supervisor David Manolopoulos, for all of his guidance, encouragement and enthusiasm over the past 4 years. As well as for the many hours of enjoyable discussions about science and politics, both at the board and the pub.

I would also like to thank all of the members of the Manolopoulos group who have helped me reach this point. Special thanks go to Lachlan Lindoy whose advice and knowledge in all areas was invaluable in the completion of this DPhil, to Thomas Fay for many fun and stimulating conversations, and to Theo Fletcher for his collaboration on non-adiabatic rates.

Many thanks also to all the members of the tea group for much needed distraction, entertainment, and cake. To Darren and Jonathan, for many enjoyable lunches as well as great Champions League nights. And to all of the members of the TMCS cohort for an enjoyable first year and catch-ups at conferences.

Most importantly I would like to thank my partner Kathryn Acheson, who has made every aspect of my life over the last 4 years a joy. To her parents Anne and Michael, her sister Isabel, and her grandfather Morrin, for all of their generosity and many great trips to Switzerland. Also many thanks to my grandparents Barbara and Colin for their loving encouragement and many excellent lunches. Finally a huge thanks to my parents for their endless love and support, as well as for great food, walks, and wine.

I would also like to acknowledge the financial support of the Cyril and Phillis Long Scholarship and the University's Clarendon fund.

List of publications

Publications directly related to this thesis

1. *Analytic continuation of Wolynes theory into the Marcus inverted regime*, J. E. Lawrence and D. E. Manolopoulos, J. Chem. Phys. **148**, 102313 (2018).

2. *On the calculation of quantum mechanical electron transfer rates*, J. E. Lawrence, T. Fletcher, L. P. Lindoy and D. E. Manolopoulos, J. Chem. Phys. **151**, 114119 (2019).

3. *Path integral methods for reaction rates in complex systems*, J. E. Lawrence and D. E. Manolopoulos, Farraday Discuss. **221**, 9 (2019).

4. *An analysis of isomorphic RPMD in the golden rule limit*, J. E. Lawrence and D. E. Manolopoulos, J. Chem. Phys. **151**, 244109 (2019).

5. *A general non-adiabatic quantum instanton approximation*, J. E. Lawrence and D. E. Manolopoulos, J. Chem. Phys. **152**, 204117 (2020).

6. *An improved path-integral method for golden-rule rates*, J. E. Lawrence and D. E. Manolopoulos, J. Chem. Phys. **153**, 154113 (2020).

7. *Confirming the role of nuclear tunnelling in aqueous ferrous-ferric electron transfer*, J. E. Lawrence and D. E. Manolopoulos, J. Chem. Phys. **153**, 154114 (2020).

Publications not directly related to this thesis

8. *Magnetoelectroluminescence in organic light-emitting diodes*, J. E. Lawrence, A. M. Lewis, D. E. Manolopoulos and P. J. Hore, J. Chem. Phys. **144**, 214109 (2016).

Declaration of Authorship

This thesis is the result of my own work and includes nothing which is the outcome of work done in collaboration except where specifically indicated in the text. Some of the work described in this thesis has been published in the papers listed above.

This thesis is not substantially the same as any that I have submitted, or, is being concurrently submitted for a degree or diploma or other qualification at the University of Oxford or any other university or similar institution.

Contents

1 Introduction

Rate processes which involve both nuclear quantum effects and the breakdown of the Born-Oppenheimer approximation are important in a wide variety of contexts, ranging from device physics to biology.[1–9] For systems with more than a few degrees of freedom, exact wave-function based approaches are impractical due to the exponential scaling of quantum mechanics with dimensionality. Imaginary-time path-integral techniques,[10–12] which can accurately capture zero-point energy and tunnelling effects and yet scale only linearly with system size, have therefore become popular for studying more complex reactions. Whilst there now exist several such methods which are routinely used to study electronically adiabatic reactions,[13–22] the development of path-integral methods for non-adiabatic reactions is still an area of active research.[23–34]

Under the Born-Oppenheimer approximation, nuclear and electronic motion is separated by assuming that, due to their relatively low mass, the electrons are able to adjust instantaneously to changes in the nuclear positions, always remaining in the ground electronic state.[35] The electronic energy at each nuclear configuration thus gives rise to a potential energy surface on which the nuclei evolve, commonly referred to as the Born-Oppenheimer or adiabatic potential.[36–38] Motion of nuclei on a single potential energy surface underlies the traditional transition state theory perspective of chemical reactions developed by Eyring and others in the 1930s.[39–42] The success of this approach reflects the fact that for many chemical reactions the electronic density changes gradually during

the course of the reaction, and the Born-Oppenheimer approximation is valid. However, if the reaction involves a sudden change in electronic configuration, the electrons may not have time to respond to the nuclear motion and the Born-Oppenheimer approximation may breakdown.[43,44] This can result in transfer of population between electronic states, resulting in a non-adiabatic reaction.*

The prototypical example of a reaction where there is a sudden electronic rearrangement, and which illustrates the key concepts in non-adiabatic rate theory, is electron transfer in solution. The picture of electron transfer, famously developed by Marcus and others,[46–49] consists of two electronic states, which represent the reactant and product electronic configurations and are coupled by the matrix element Δ. These states are not therefore adiabatic states, but rather *diabatic* states. The energies of these diabatic states at each nuclear configuration give rise to diabatic potential energy surfaces, which unlike their adiabatic counterparts may cross in energy.[36–38] A schematic illustration of this for a one dimensional problem with reactant and product diabatic potentials, labelled $V_0(q)$ and $V_1(q)$, and ground and first excited Born-Oppenheimer potentials, labelled $U_0(q)$ and $U_1(q)$, is shown in Fig. 1.1. The coordinate, q, can be thought of in the Marcus picture as corresponding to a collective solvent polarisation coordinate.† Values of q close to the reactant minimum correspond to solvent configurations which stabilise the reactant electronic configuration and values of q near the product minimum to those which stabilise the product electronic configuration. In order for electron transfer to take place thermal fluctuations of the solvent polarisation must take the system to the region near $q^{\ddagger}$, corresponding to the inset of Fig 1.1. If the timescale associated with the tunnelling of the electron from the reactant to product configuration, τ_{e}, was much faster than the timescale associated with the nuclear motion through the region, τ_{n}, then the system would evolve adiabatically and the electron density would change continuously from the reactant to the product configuration. However, due to the large energy barrier typically associated with

*The term adiabatic here refers to the fact the system remains in the same electronic state during the nuclear motion and should not be confused with the concept of adiabatic heat transfer in thermodynamics.[45] As such a non-adiabatic process is just one in which transfer between two or more adiabatic electronic states is important.

†Note that this one dimensional model is just an illustrative example, and in the full multidimensional Marcus theory $V_0(q)$ and $V_1(q)$ are actually free energy surfaces, which are assumed to be harmonic with equal curvature. A formal discussion of Marcus theory is given in Sec. 2.2.3.

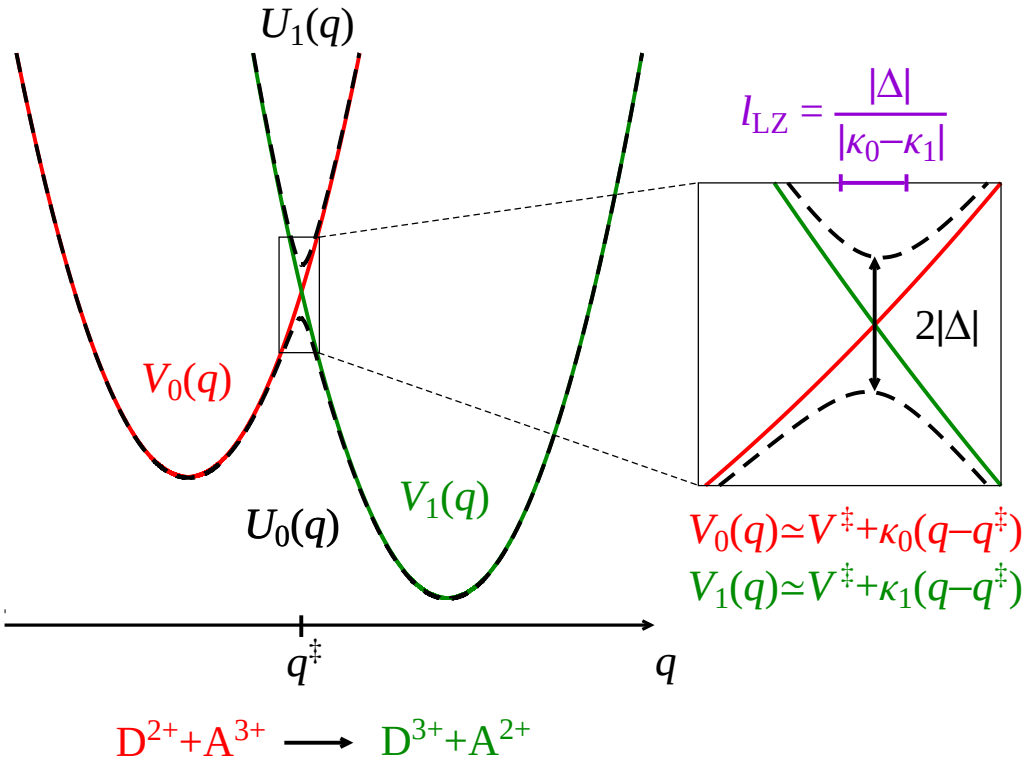

Figure 1.1: Schematic illustration of diabatic (solid lines) and adiabatic (dashed lines) potential energy surfaces for an electron transfer reaction in solution. Inset highlights transition state region, where the character of the adiabatic states change, and shows both the Landau-Zener length, l_{LZ} and the tunnel splitting, $2|\Delta|$. Note that $l_{LZ} = |q_a - q_b|$ where under the linear approximation $V_0(q_a) - V_1(q_a) = |\Delta|$ and $V_1(q_b) - V_0(q_b) = |\Delta|$.

the electron tunnelling from one molecular fragment to the other, the timescale associated with the tunnelling is often very slow and the electrons cannot respond to the change in the nuclear configuration. This means that there is only a small probability of the electron transferring each time a thermal fluctuation takes the system to this region.

Estimates for both of these timescales can be obtained for this simple one dimensional model from the Landau-Zener picture in which the the system moves with constant velocity $v = |\dot{q}|$ through the transition region.[43,44] At the crossing point of the two diabatic states, $q^\ddagger$, the timescale associated with population transfer between the two states is $\tau_e = \hbar/\Delta$. Since the length scale associated with this region is given by $l_{LZ} = |\Delta|/|\kappa_0 - \kappa_1|$, where κ_0 and κ_1 are the derivatives of the diabatic potentials at the crossing point, it follows that the timescale associated with the nuclear motion through the region is

$\tau_n = |\Delta|/v\,|\kappa_0 - \kappa_1|$.* A formal analysis leads to the famous Landau-Zener formula,[43,44]

$$P_{LZ} = \exp\left(-2\pi\frac{\tau_n}{\tau_e}\right) = \exp\left(-\frac{2\pi\Delta^2}{\hbar v\,|\kappa_0 - \kappa_1|}\right), \tag{1.1}$$

which gives the probability for the system to stay on the same diabatic surface as it moves a constant velocity through the region.† Hence if the nuclear timescale is much slower than the electronic timescale, $\tau_n/\tau_e \gg 1$, then the system does not stay on the same diabatic state, but instead evolves adiabatically on the ground Born-Oppenheimer potential and the reaction is said to be in the *adiabatic* limit. However, for many electron transfer reactions the tunnelling matrix element Δ is very small, and can be treated perturbatively, such that the reaction occurs in the opposite *non-adiabatic* limit, where $\tau_n/\tau_e \ll 1$ and $P_{LZ} \sim 1 - 2\pi\tau_n/\tau_e$. In this limit the rate obeys Fermi's golden rule,[50] where the probability of the electron transferring (corresponding to the system staying on the same *adiabat*) and hence the rate of reaction is proportional to Δ^2.

Beyond simple electron transfer reactions in solution, non-adiabatic processes can be important in any reactions which involve a sudden change in electronic configuration. There are many important examples of non-adiabatic reactions in the gas phase,[37] such as the famous $F + H_2 \rightarrow HF + H$ reaction,[51] where coherence effects can be observed due to interference between parts of the wave function which have evolved on different electronic states.[52] These kinds of reactions are interesting in their own right but will not be the focus of the present thesis, in which we will be principally concerned with reactions in the condensed phase where coupling to the thermal environment typically causes rapid decoherence between parts of the wave function on different electronic states. These kinds of reactions are by no means less important, and as well as traditional electron transfer reactions in solution non-adiabatic reactions occur in a wide range of biological processes such as proton coupled electron transfer in enzymes, electron transfer

*Here, as is done throughout the thesis, multiplication is taken to be performed before division such that $a/bc = a/(bc)$.

†Formally it is the probability for a system, prepared initially in state $\psi_0 = (1,0)^T$ at $t = -\infty$, and which evolves under the time dependent Hamiltonian

$$\hat{H}(t) = \begin{pmatrix} \kappa_0 vt & \Delta \\ \Delta & \kappa_1 vt \end{pmatrix}.$$

to be in state $\psi_1 = (0,1)^T$ as $t \rightarrow \infty$.

in photosynthesis, and in electron transfer in DNA,[1–4] as well as in device physics where energy and electron transfer processes in both organic and inorganic semiconductors are important for the function of light emitting diodes and photovoltaics.[6–9]

The use of Marcus theory, which gives a simple analytical expression for the electron transfer rate in the golden-rule limit, to describe this wide range of problems is ubiquitous.[1–9] However, Marcus theory is limited by its assumption that the nuclear motion can be treated classically, by assuming that the resulting diabatic free energies are purely harmonic, and by its perturbative treatment of the electronic coupling, Δ. Due to the cusped nature of the crossing between diabatic surfaces, nuclear tunnelling is often particularly important in non-adiabatic reactions, and there exist many simple analytical theories which extend Marcus theory to allow for the inclusion of nuclear quantum effects.[53–62] However these theories are not generally able to treat complex anharmonic systems, or to capture the non-adiabatic to adiabatic transition; analytical theories which can do the later exist, but again they are generally unable to treat anharmonic problems.[63–72] General simulation techniques, such as Tully's fewest switches surface hopping (FSSH) approach, provide a way to study complex multidimensional and anharmonic atomistic models, however FSSH and other mixed quantum classical treatments typically treat the nuclei classically and hence are not able to describe nuclear tunnelling and zero-point energy effects.[73–77]

In the adiabatic limit path-integral methods have become a popular way to include the effects of both zero-point energy and tunnelling in the calculation of reaction rates in complex multidimensional and anharmonic systems.[13–22] Originally proposed by Feynman, imaginary-time path integrals provide an exact way to calculate thermal expectation values of quantum systems using the classical statistical mechanics of n copies of the system connected by harmonic springs. Importantly, n is independent of the number of physical degrees of freedom in the system and is typically on the order of 10-1000 in chemical applications.[78,79] The resulting simulation is thus no more than n times more expensive than the classical simulation, and hence using modern computer simulation techniques can be applied to complex condensed phase problems. More recently the development of methods such as ring-polymer molecular dynamics

(RPMD),[17–19,80,81] have extended path integrals to calculate approximate dynamical properties whilst accurately describing the effects of zero-point energy and tunnelling. The success of RPMD in the adiabatic limit, particularly for the calculation of reaction rates, and the now routine application of path-integral approaches to large complex systems such as reactions in proteins,[21,22] has led to renewed interest in the use of path integrals to treat non-adiabatic systems.

The earliest application of path-integral techniques to treat non-adiabatic reactions was suggested by Wolynes in 1987.[82] This approach, known as Wolynes theory, is based on making a steepest descent approximation to the time integral of a reactive flux autocorrelation function in the non-adiabatic limit, and leads to a simple imaginary-time path-integral expression for the rate constant that can readily be applied to electron transfer reactions in complex systems.[83–85] More recently, there have been a series of attempts to generalise RPMD to treat non-adiabatic systems.[23–34] Although these methods are in principle applicable to more general problems than Wolynes theory, such as reactions which are intermediate between the adiabatic and non-adiabatic limit, they are typically much more complicated and have shown variable accuracy. In this thesis we will explore the successes and failures of this old and new work, and attempt to develop simple path-integral methods for non-adiabatic reaction rates that are applicable to realistic condensed phase simulations with anharmonic force fields.

The thesis is organised as follows. In Chap. 2 we introduce the background theory which underpins all subsequent chapters. In Chap. 3 we discuss recent attempts to generalise RPMD rate theory to treat non-adiabatic systems, highlighting the challenges associated with the development of a general non-adiabatic rate theory. In Chap. 4 we show that it is possible to develop a non-adiabatic quantum instanton approximation, which can treat reaction rates with arbitrary coupling strength and which reduces to Wolynes theory and the newly proposed projected quantum instanton approximation[86] in the non-adiabatic and adiabatic limits respectively. In Chap. 5 we discuss an alternative approach in which we use a simple interpolation formula to approximate the rate at arbitrary coupling strength from the reaction rates in the Born-Oppenheimer and golden-rule limits. In Chap. 6 we return to focus on the non-adiabatic limit and discuss the

difficulties associated with using Wolynes theory to calculate reaction rates in the inverted regime, suggesting a numerical analytic continuation procedure which overcomes this issue. We continue to explore some of the flaws of Wolynes theory in Chap. 7, where we discuss recent work showing that Wolynes theory breaks down for systems with multiple transition states. We suggest an alternative approach, which we call the linear golden-rule approximation (LGR), that is a size consistent modification of the newly proposed GR-QTST method. Unlike Wolynes theory, LGR, is exact in the high temperature limit and is also capable of calculating reaction rates in the inverted regime without the need for analytic continuation. Chap. 8 applies the methods from the previous two chapters to a fully atomistic model of ferrous-ferric electron transfer, and addresses recent suggestions that multiple tunnelling pathways lead to a breakdown of Wolynes theory and the assumption that the diabatic energy gap can be treated using linear response in this system. Chap. 9 concludes the thesis, and discusses possible future work.

2
Background theory

Contents

Summary

In this chapter we review the basic theory necessary to understand the remainder of the thesis. The first section will introduce basic electronic structure theory, covering the adiabatic basis and the Born-Oppenheimer approximation. We will then go on to briefly discuss the breakdown of the Born-Oppenheimer approximation and some of the difficulties associated with using the adiabatic basis to study non-adiabatic processes. The first section concludes by introducing the idea of a diabatic basis, which will be the starting point for the development of the non-adiabatic methods discussed in the remainder of the thesis. In the second section we will then go on to discuss reaction rate theory, focussing in particular on unimolecular reactions in the condensed phase which is the main focus of this thesis. In addition to giving an overview of reaction rate theory, we will detail the simplifications which can be made in both the adiabatic and non-adiabatic limits, as well as briefly discussing the connection to scattering rate theory which will be used to provide simple exactly soluble test problems later in the thesis. The final section of the chapter will introduce the theory behind imaginary-time path-integral techniques, before going on to discuss two well established methods, RPMD rate theory and Wolynes theory, which can be used to calculate reaction rates in the adiabatic and non-adiabatic limits respectively.

2.1 Adiabatic vs. diabatic representations

2.1.1 Adiabatic basis

The starting point for understanding the coupled motion of electrons and nuclei is the molecular time dependent Schrödinger equation

$$\frac{\partial}{\partial t}\Psi(\mathbf{r},\mathbf{x},t) = -\frac{i}{\hbar}\hat{\mathcal{H}}_{\text{mol}}\Psi(\mathbf{r},\mathbf{x},t) \tag{2.1}$$

where $\hat{\mathcal{H}}_{\text{mol}}$ is the molecular Hamiltonian. The non-relativistic molecular Hamiltonian (ignoring spin-orbit coupling) can be written in the form,[87]

$$\hat{\mathcal{H}}_{\text{mol}} = \hat{T}_{\text{n}} + \hat{T}_{\text{e}} + \hat{V}_{\text{nn}} + \hat{V}_{\text{ee}} + \hat{V}_{\text{ne}} \tag{2.2}$$

where $\hat{T}_\mathrm{n}$ and $\hat{T}_\mathrm{e}$ are the nuclear and electronic kinetic energy operators respectively, and $\hat{V}_\mathrm{nn}$, $\hat{V}_\mathrm{ee}$ and $\hat{V}_\mathrm{ne}$ describe the nuclear-nuclear, electron-electron and nuclear-electron interactions. These Coulombic potential energy operators can be written explicitly as

$$\hat{V}_\mathrm{nn} = \sum_{\nu=1}^{N_\mathrm{n}} \sum_{\mu>\nu}^{N_\mathrm{n}} \frac{Z_\nu Z_\mu \mathrm{e}^2}{4\pi\varepsilon_0 |\boldsymbol{x}_\nu - \boldsymbol{x}_\mu|} \tag{2.3a}$$

$$\hat{V}_\mathrm{ee} = \sum_{\nu=1}^{N_\mathrm{e}} \sum_{\mu>\nu}^{N_\mathrm{e}} \frac{\mathrm{e}^2}{4\pi\varepsilon_0 |\boldsymbol{r}_\nu - \boldsymbol{r}_\mu|} \tag{2.3b}$$

$$\hat{V}_\mathrm{ne} = -\sum_{\nu=1}^{N_\mathrm{e}} \sum_{\mu=1}^{N_\mathrm{n}} \frac{Z_\mu \mathrm{e}^2}{4\pi\varepsilon_0 |\boldsymbol{r}_\nu - \boldsymbol{x}_\mu|} \tag{2.3c}$$

where N_e is the number of electrons in the system, N_n is the number of nuclei in the system, $\boldsymbol{x}_\nu = (x_{\nu x}, x_{\nu y}, x_{\nu z})$ is the 3 dimensional position vector of the ν^th nucleus, $\boldsymbol{r}_\nu = (r_{\nu x}, r_{\nu y}, r_{\nu z})$ is the 3 dimensional position vector of the ν^th electron, e is the elementary charge, Z_ν is the number of protons in nucleus ν and ε_0 is the vacuum permittivity. The kinetic energy terms are

$$\hat{T}_\mathrm{n} = \sum_{\nu=1}^{N_\mathrm{n}} \frac{\hat{\boldsymbol{p}}_{\mathrm{n},\nu}^2}{2m_{\mathrm{n},\nu}} \tag{2.4a}$$

$$\hat{T}_\mathrm{e} = \sum_{\nu=1}^{N_\mathrm{e}} \frac{\hat{\boldsymbol{p}}_{\mathrm{e},\nu}^2}{2m_\mathrm{e}} \tag{2.4b}$$

in which m_e is the mass of an electron, $m_{\mathrm{n},\nu}$ is the nuclear mass of the ν^th atom, $\boldsymbol{p}_{\mathrm{e},\nu}$ is the momentum of the ν^th electron, and $\boldsymbol{p}_{\mathrm{n},\nu}$ is the momentum of the ν^th nucleus. As we are working here in the position representation, the momentum operators are given by

$$\hat{\boldsymbol{p}}_{\mathrm{n},\nu} = -i\hbar\nabla_{\mathrm{n},\nu} \tag{2.5}$$

and

$$\hat{\boldsymbol{p}}_{\mathrm{e},\nu} = -i\hbar\nabla_{\mathrm{e},\nu}, \tag{2.6}$$

where $\nabla_{\mathrm{n},\nu} = (\partial/\partial x_{\nu x}, \partial/\partial x_{\nu y}, \partial/\partial x_{\nu z})$ and $\nabla_{\mathrm{e},\nu} = (\partial/\partial r_{\nu x}, \partial/\partial r_{\nu y}, \partial/\partial r_{\nu z})$.

The usual adiabatic picture of quantum chemistry begins by separating the molecular Hamiltonian into the electronic Hamiltonian,

$$\hat{\mathcal{H}}_\mathrm{e} = \hat{T}_\mathrm{e} + \hat{V}_\mathrm{nn} + \hat{V}_\mathrm{ee} + \hat{V}_\mathrm{ne} \tag{2.7}$$

and the nuclear kinetic energy

$$\hat{\mathcal{H}}_{\text{mol}} = \hat{T}_{\text{n}} + \hat{\mathcal{H}}_{\text{e}}. \tag{2.8}$$

For a fixed set of nuclear coordinates, $\mathbf{x}$, one can then solve the time independent Schrödinger equation for the electronic degrees of freedom

$$\hat{\mathcal{H}}_{\text{e}}\psi_j(\mathbf{r};\mathbf{x}) = U_j(\mathbf{x})\psi_j(\mathbf{r};\mathbf{x}), \tag{2.9}$$

to obtain a complete set of orthonormal (appropriately symmetrised) adiabatic electronic wave functions, $\{\psi_j(\mathbf{r};\mathbf{x})\}$, and their corresponding electronic energies, $\{U_j(\mathbf{x})\}$. As the electronic Hamiltonian $\hat{\mathcal{H}}_{\text{e}}$ is dependent on the nuclear coordinates, the wave functions and also the eigenvalues $U_j(\mathbf{x})$ are also parametrically dependent on $\mathbf{x}$. Importantly, as $\hat{\mathcal{H}}_{\text{e}}$ is Hermitian, for each $\mathbf{x}$ these electronic wave functions form a complete set over the electronic space, and this allows us to expand the total wave function for the nuclei and electrons as a sum over the adiabatic states (the Born-Huang expansion) as[88]

$$\Psi(\mathbf{r},\mathbf{x},t) = \sum_j \chi_j(\mathbf{x},t)\psi_j(\mathbf{r};\mathbf{x}). \tag{2.10}$$

Inserting this into Eq. 2.1, followed by left multiplying by $\psi_j^*(\mathbf{r};\mathbf{x})$ and integrating over the electronic coordinates we can write

$$i\hbar\frac{\partial}{\partial t}\chi_j(\mathbf{x},t) = \sum_k \left(\hat{T}_{\text{n},jk} + U_j(\mathbf{x})\delta_{jk}\right)\chi_k(\mathbf{x},t). \tag{2.11}$$

where

$$\hat{T}_{\text{n},jk} = \int \psi_j^*(\mathbf{r};\mathbf{x})\left(\sum_{\nu=1}^{N_{\text{n}}} -\frac{\hbar^2}{2m_{\text{n},\nu}}\nabla_{\text{n},\nu}^2\right)\psi_k(\mathbf{r};\mathbf{x})\,\mathrm{d}^{3N_{\text{e}}}\mathbf{r} \tag{2.12}$$

is the nuclear kinetic energy operator in the adiabatic basis. This gives a matrix equation for the time evolution of the nuclear expansion coefficients $\chi_j(\mathbf{x},t)$ in the adiabatic basis. Importantly, although the term coming from the electronic Hamiltonian, $U_j(\mathbf{x})$, is diagonal, the nuclear kinetic energy operator, $\hat{T}_{\text{n},jk}$, is not.

In discussing the properties of the nuclear kinetic energy operator it will be helpful to recast Eq. 2.12 in Dirac's bra-ket notation as

$$\hat{T}_{\text{n},jk} = \langle\psi_j| \sum_{\nu=1}^{N_{\text{n}}} -\frac{\hbar^2}{2m_{\text{n},\nu}}\nabla_{\text{n},\nu}^2 |\psi_k\rangle\,, \tag{2.13}$$

where we have suppressed the dependence of the states on the nuclear coordinates, but we stress that throughout they should be read implicitly as $|\psi_k\rangle \equiv |\psi_k(\mathbf{x})\rangle$. By acting the Laplacian operator on the electronic wave function this is often written in the form[37]

$$\hat{T}_{\mathrm{n},jk} = \sum_{\nu=1}^{N_\mathrm{n}} -\frac{\hbar^2}{2m_{\mathrm{n},\nu}} \left(\langle \psi_j | \nabla^2_{\mathrm{n},\nu} \psi_k \rangle + 2 \langle \psi_j | \nabla_{\mathrm{n},\nu} \psi_k \rangle \nabla_{\mathrm{n},\nu} + \delta_{jk} \nabla^2_{\mathrm{n},\nu} \right), \tag{2.14}$$

which can then be simplified by defining the derivative coupling vector $\boldsymbol{d}^\nu_{jk} = \langle \psi_j | \nabla_{\mathrm{n},\nu} \psi_k \rangle$ and the second derivative coupling $D^\nu_{jk} = \langle \psi_j | \nabla^2_{\mathrm{n},\nu} \psi_k \rangle$ to give

$$\hat{T}_{\mathrm{n},jk} = \sum_{\nu=1}^{N_\mathrm{n}} -\frac{\hbar^2}{2m_{\mathrm{n},\nu}} \left(D^\nu_{jk} + 2\boldsymbol{d}^\nu_{jk} \cdot \nabla_{\mathrm{n},\nu} + \delta_{jk} \nabla^2_{\mathrm{n},\nu} \right) \tag{2.15}$$

where the dot product is over the 3 dimensional vector of cartesian components. Note again that $D^\nu_{jk} \equiv D^\nu_{jk}(\mathbf{x})$ and $\boldsymbol{d}^\nu_{jk} \equiv \boldsymbol{d}^\nu_{jk}(\mathbf{x})$.

This can be rewritten in a more symmetric form using the identity,

$$\left[\nabla_{\mathrm{n},\nu}, \boldsymbol{d}^\nu_{jk} \right] = \langle \nabla_{\mathrm{n},\nu} \psi_j | \nabla_{\mathrm{n},\nu} \psi_k \rangle + \langle \psi_j | \nabla^2_{\mathrm{n},\nu} \psi_k \rangle = \sum_l \boldsymbol{d}^{\nu *}_{lj} \cdot \boldsymbol{d}^\nu_{lk} + D^\nu_{jk}, \tag{2.16}$$

where $[A, B] = AB - BA$ denotes a commutator, to give

$$\hat{T}_{\mathrm{n},jk} = \sum_{\nu=1}^{N_\mathrm{n}} -\frac{\hbar^2}{2m_{\mathrm{n},\nu}} \left(\nabla_{\mathrm{n},\nu} \cdot \boldsymbol{d}^\nu_{jk} + \boldsymbol{d}^\nu_{jk} \cdot \nabla_{\mathrm{n},\nu} - \sum_l \boldsymbol{d}^{\nu *}_{lj} \cdot \boldsymbol{d}^\nu_{lk} + \delta_{jk} \nabla^2_{\mathrm{n},\nu} \right), \tag{2.17}$$

or by reintroducing the momentum operators as

$$\hat{T}_{\mathrm{n},jk} = \sum_{\nu=1}^{N_\mathrm{n}} \left(-i\hbar \left(\frac{\hat{\boldsymbol{p}}_{\mathrm{n},\nu}}{2m_{\mathrm{n},\nu}} \cdot \boldsymbol{d}^\nu_{jk} + \boldsymbol{d}^\nu_{jk} \cdot \frac{\hat{\boldsymbol{p}}_{\mathrm{n},\nu}}{2m_{\mathrm{n},\nu}} \right) - \frac{\hbar^2}{2m_{\mathrm{n},\nu}} \sum_l \boldsymbol{d}^\nu_{jl} \cdot \boldsymbol{d}^\nu_{lk} + \delta_{jk} \frac{\hat{\boldsymbol{p}}^2_{\mathrm{n},\nu}}{2m_{\mathrm{n},\nu}} \right). \tag{2.18}$$

Note that we have here also used the fact that $\nabla_{\mathrm{n},\nu} \langle \psi_j | \psi_k \rangle = 0 = \boldsymbol{d}^\nu_{jk} + \boldsymbol{d}^{\nu *}_{kj}$. (This is just an expansion of

$$\hat{T}_{\mathrm{n},jk} = \sum_{\nu=1}^{N_\mathrm{n}} \sum_l \frac{1}{2m_\nu} \left(\hat{\boldsymbol{p}}_{\mathrm{n},\nu} \delta_{jl} - i\hbar \boldsymbol{d}^\nu_{jl} \right) \cdot \left(\hat{\boldsymbol{p}}_{\mathrm{n},\nu} \delta_{lk} - i\hbar \boldsymbol{d}^\nu_{lk} \right), \tag{2.19}$$

which can be obtained simply by inserting $\hat{1} = \sum_l = |\psi_l\rangle\langle\psi_l|$ into the middle of the Laplacian in Eq. 2.13.)

The derivative coupling, $\boldsymbol{d}^\nu_{jk}$, thus couples the nuclear wave function associated with state j, $\chi_j(\mathbf{x}, t)$, to the nuclear wave function associated with state k, $\chi_k(\mathbf{x}, t)$. The strength of this coupling is dependent on both the nuclear velocity and on the magnitude of the

derivative coupling vector $\boldsymbol{d}^{\nu}_{jk}$. Considering the overlap between two adiabatic states for different nuclear coordinates $\mathbf{x}$ and $\mathbf{x} + \delta\mathbf{x}$,

$$\langle \psi_j(\mathbf{x}) | \psi_k(\mathbf{x} + \delta\mathbf{x}) \rangle = \delta_{jk} + \sum_{\nu=1}^{N_\mathrm{n}} \boldsymbol{d}^{\nu}_{jk}(\mathbf{x}) \cdot \delta\boldsymbol{x}_\nu + \ldots, \tag{2.20}$$

it is clear that a large derivative coupling, $\boldsymbol{d}^{\nu}_{jk}$, corresponds to a rapid change in the electronic configuration of the electronic state k, resulting in the physical character of the state changing quickly to look like state j as the ν^{th} nuclear degree of freedom is displaced. Qualitatively therefore, we see that the magnitude of the coupling, $\boldsymbol{d}^{\nu}_{jk} \cdot \hat{\boldsymbol{p}}_{\mathrm{n},\nu}/2m_{\mathrm{n},\nu}$, corresponds to how rapidly in time the character of the electronic states is changing.

2.1.2 Born-Oppenheimer approximation

In much of chemistry, Eq. 2.11 is simplified by making the Born-Oppenheimer approximation, in which it is assumed that the derivative coupling terms can be ignored[35,87]

$$-i\hbar \left(\frac{\hat{\boldsymbol{p}}_{\mathrm{n},\nu}}{2m_{\mathrm{n},\nu}} \cdot \boldsymbol{d}^{\nu}_{jk} + \boldsymbol{d}^{\nu}_{jk} \cdot \frac{\hat{\boldsymbol{p}}_{\mathrm{n},\nu}}{2m_{\mathrm{n},\nu}} \right) - \frac{\hbar^2}{2m_{\mathrm{n},\nu}} \sum_l \boldsymbol{d}^{\nu}_{jl} \cdot \boldsymbol{d}^{\nu}_{lk} \simeq 0. \tag{2.21}$$

This then results in a totally decoupled set of equations for the nuclear wave functions, $\chi_j(\mathbf{x}, t)$, given by

$$i\hbar \frac{\partial}{\partial t} \chi_j(\mathbf{x}, t) = \left(\sum_{\nu=1}^{N_\mathrm{n}} \frac{\hat{\boldsymbol{p}}^2_{\mathrm{n},\nu}}{2m_{\mathrm{n},\nu}} + U_j(\mathbf{x}) \right) \chi_j(\mathbf{x}, t). \tag{2.22}$$

The nuclear wave function $\chi_j(\mathbf{x}, t)$ therefore evolves under an effective Born-Oppenheimer Hamiltonian,

$$\hat{H}_{\mathrm{BO},j} = \sum_{\nu=1}^{N_\mathrm{n}} \frac{\hat{\boldsymbol{p}}^2_{\mathrm{n},\nu}}{2m_{\mathrm{n},\nu}} + U_j(\mathbf{x}), \tag{2.23}$$

where $U_j(\mathbf{x})$ acts as a potential energy surface on which the nuclei evolve, and is therefore often referred to as the Born-Oppenheimer potential energy surface of state j. The standard justification for this approximation is that the nuclei, being much heavier than the electrons, $m_\mathrm{p}/m_\mathrm{e} \simeq 1836$, move much more slowly, and hence the electrons are able to adjust essentially instantaneously to changes in the nuclear coordinates.[35] This is equivalent to saying that the electronic motion is adiabatically separated from the nuclear motion, and hence the regime in which the Born-Oppenheimer approximation is valid is known as the adiabatic limit, and the $U_j(\mathbf{x})$'s are also referred to as the adiabatic potentials.

This is normally a reasonable approximation for nuclear motion near equilibrium, where the nuclear frequencies are usually on the order of $1000\,\mathrm{cm}^{-1}$ and the electronic excitation energy is typically greater than $10,000\,\mathrm{cm}^{-1}$.[89] However, when the nuclear momentum is particularly high, or if two electronic states come close in energy then the Born-Oppenheimer approximation is expected to break down, and the nuclear dynamics becomes "non-adiabatic". Both of these effects are reflected in the form of the left hand side of Eq. 2.21, which is referred to as the non-adiabatic coupling. However, whilst the dependence of the non-adiabatic coupling on the nuclear momentum is explicit in Eq. 2.21, the influence of electronic energy not immediately apparent. To bring it out we consider the adiabatic representation of the operator

$$\begin{aligned}\langle\psi_j|\,\nabla_{\mathrm{n},\nu}\hat{\mathcal{H}}_\mathrm{e}\,|\psi_k\rangle &= \langle\psi_j|\,[\nabla_{\mathrm{n},\nu},\hat{\mathcal{H}}_\mathrm{e}]\,|\psi_k\rangle + \langle\psi_j|\,\hat{\mathcal{H}}_\mathrm{e}\nabla_{\mathrm{n},\nu}\,|\psi_k\rangle \\ &= \langle\psi_j|\,[\nabla_{\mathrm{n},\nu},\hat{\mathcal{H}}_\mathrm{e}]\,|\psi_k\rangle + \langle\psi_j|\,\hat{\mathcal{H}}_\mathrm{e}\,|\nabla_{\mathrm{n},\nu}\psi_k\rangle + \langle\psi_j|\,\hat{\mathcal{H}}_\mathrm{e}\,|\psi_k\rangle\,\nabla_{\mathrm{n},\nu} \\ &= \langle\psi_j|\,[\nabla_{\mathrm{n},\nu},\hat{\mathcal{H}}_\mathrm{e}]\,|\psi_k\rangle + U_j(\mathbf{x})\boldsymbol{d}^\nu_{jk} + U_k(\mathbf{x})\delta_{jk}\nabla_{\mathrm{n},\nu}\end{aligned} \tag{2.24}$$

which is of course equivalent to

$$\langle\psi_j|\,\nabla_{\mathrm{n},\nu}U_k(\mathbf{x})\,|\psi_k\rangle = [\nabla_{\mathrm{n},\nu},U_k(\mathbf{x})]\delta_{jk} + U_k(\mathbf{x})\boldsymbol{d}^\nu_{jk} + U_k(\mathbf{x})\delta_{jk}\nabla_{\mathrm{n},\nu}. \tag{2.25}$$

Thus combining these two equations, the derivative coupling can be written explicitly in terms of the adiabatic energy gap $U_k(\mathbf{x}) - U_j(\mathbf{x})$ as

$$\boldsymbol{d}^\nu_{jk} = \frac{\langle\psi_j|\,[\nabla_{\mathrm{n},\nu},\hat{\mathcal{H}}_\mathrm{e}]\,|\psi_k\rangle}{U_k(\mathbf{x}) - U_j(\mathbf{x})}. \tag{2.26}$$

This highlights the fact that when the adiabatic states come close in energy, the non-adiabatic couplings can become large and the Born-Oppenheimer approximation can break down.

2.1.3 Diabatic basis

Modelling non-adiabatic dynamics in the adiabatic basis, is unfortunately not straightforward. Part of the reason for this is that the derivative coupling can be numerically very poorly behaved, in particular by considering Eq. 2.26, it is clear that the coupling will diverge at conical intersections, where the energy gap between two states goes to zero.[37] For the path-integral methods that we consider in this thesis, a more fundamental

challenge to directly using the adiabatic basis is that we require the kinetic energy operator to be diagonal.

For these reasons it is common when considering non-adiabatic dynamics to work in what is known as a diabatic basis, in which the kinetic energy operator is diagonal.[37,38,90] The transformation from the adiabatic basis considered above, to a diabatic basis is therefore formally defined by a transformation

$$\sum_{jk} \Omega^*_{ja}(\mathbf{x}) \hat{T}_{\mathrm{n},jk} \Omega_{kb}(\mathbf{x}) = \sum_{\nu=1}^{N_\mathrm{n}} \frac{\hat{\boldsymbol{p}}^2_{\mathrm{n},\nu}}{2m_{\mathrm{n},\nu}} \delta_{ab} \tag{2.27}$$

where $\boldsymbol{\Omega}(\mathbf{x})$ is a unitary matrix with elements $(\boldsymbol{\Omega}(\mathbf{x}))_{ja} = \Omega_{ja}(\mathbf{x})$. Expanding the left hand side of this expression in terms of bra-ket notation we have that

$$\begin{aligned} \sum_{jk} \Omega^*_{ja}(\mathbf{x}) \hat{T}_{\mathrm{n},jk} \Omega_{kb}(\mathbf{x}) &= \sum_{jk} \langle \psi_j | \, \Omega^*_{ja}(\mathbf{x}) \left(\sum_{\nu=1}^{N_\mathrm{n}} -\frac{\hbar^2}{2m_{\mathrm{n},\nu}} \nabla^2_{\mathrm{n},\nu} \right) \Omega_{kb}(\mathbf{x}) \, | \psi_k \rangle \\ &= \langle \psi^\mathrm{d}_a | \left(\sum_{\nu=1}^{N_\mathrm{n}} -\frac{\hbar^2}{2m_{\mathrm{n},\nu}} \nabla^2_{\mathrm{n},\nu} \right) | \psi^\mathrm{d}_b \rangle \, , \end{aligned} \tag{2.28}$$

where we have defined the new diabatic basis as $|\psi^\mathrm{d}_a\rangle = \sum_j \Omega_{ja}(\mathbf{x}) \, |\psi_j\rangle$. Evaluating this expression in the same manner as Eqs. 2.13-2.19, it is clear that the right hand side of Eq. 2.27 will be satisfied if the diabatic basis obeys,

$$\langle \psi^\mathrm{d}_a | \nabla_{\mathrm{n},\nu} \psi^\mathrm{d}_b \rangle = 0, \tag{2.29}$$

known as a strict diabatic basis.[90,91] Therefore a diabatic basis is one in which the physical character of the electronic states remains unchanged with nuclear displacement.

Of course, diagonalising the kinetic energy operator comes at the price of the potential energy becoming non-diagonal,

$$\sum_{jk} \Omega^*_{ja}(\mathbf{x}) E_j(\mathbf{x}) \delta_{jk} \Omega_{kb}(\mathbf{x}) = V_{ab}(\mathbf{x}), \tag{2.30}$$

where $V_{ab}(\mathbf{x}) = (\boldsymbol{V}(\mathbf{x}))_{ab}$ is an element of the diabatic potential matrix. Importantly, although the diabatic potential is not diagonal, it is independent of the nuclear momentum, and does not exhibit the divergent behaviour seen in the derivative couplings.[37] Hence, it is much easier to handle than the adiabatic kinetic energy matrix. Confusingly the

off diagonal elements of the diabatic potential matrix are also often referred to as non-adiabatic couplings, it is important to stress that they are fundamentally different to the non-adiabatic couplings in the adiabatic basis discussed above. For the avoidance of doubt we will use non-adiabatic coupling to refer only to the couplings in the *adiabatic* basis, and we will use the term diabatic coupling or electronic coupling for those in the diabatic basis. Defining the nuclear diabatic wave function on diabat a, according to the relation

$$\chi_a^{\mathrm{d}}(\mathbf{x}, t) = \sum_j \Omega_{ja}^*(\mathbf{x})\chi_j(\mathbf{x}, t), \tag{2.31}$$

we can thus transform Eq. 2.11 into the diabatic basis to give

$$i\hbar\frac{\partial}{\partial t}\chi_a^{\mathrm{d}}(\mathbf{x}, t) = \sum_b \left(\frac{\hat{\boldsymbol{p}}_{\mathrm{n},\nu}^2}{2m_{\mathrm{n},\nu}}\delta_{ab} + V_{ab}(\mathbf{x})\right)\chi_b^{\mathrm{d}}(\mathbf{x}). \tag{2.32}$$

This has the same form as the time dependent Schrödinger equation given by the Born-Oppenheimer approximation (Eq. 2.22), except that the nuclear wave functions on each of the *diabatic* states are now coupled by the potential energy and hence can be thought of as moving on a matrix potential energy surface. In the case of zero diabatic coupling these equations again decouple, however, now the nuclei evolve on the diabatic potentials $V_a(\mathbf{x}) = V_{aa}(\mathbf{x})$ and not the adiabatic potentials.

So far, other than saying that they are related to the adiabatic basis via a transformation matrix, $\boldsymbol{\Omega}(\mathrm{x})$, we have not addressed how one might obtain the diabatic states. In general there is no unique way of calculating diabatic states,[90] and as such there are many different approaches that can be taken. Broadly these approaches can be grouped into those which attempt to directly transform from the adiabatic basis to a diabatic basis,[92–96] and those in which the diabatic states are arrived at directly.[97–105] As the calculation of diabatic states is not the focus of this thesis we will just give a brief discussion of some of the difficulties involved, and the methods that can be used.

The simplest choice of diabatic basis is the so-called crude adiabatic basis,[106] in which one simply fixes the parametric dependence of the adiabatic basis on $\mathbf{x}$ to some reference value $\tilde{\mathbf{x}}$, such that

$$\psi_a^{\mathrm{d}}(\mathbf{r}) = \psi_a(\mathbf{r}; \tilde{\mathbf{x}}). \tag{2.33}$$

It is immediately clear that there are a potentially infinite number of choices for a diabatic basis. It is also clear that, unlike in the adiabatic basis where the lowest few adiabatic states are expected to give a good description of most of chemistry, this simple diabatic basis cannot be truncated on the basis of the energy $U_j(\tilde{\mathbf{x}})$ as this will have little to do with the energy of the system away from $\tilde{\mathbf{x}}$. Ideally then, one would first select the adiabatic states that are relevant in the system of interest, and then transform to a diabatic basis within this subspace. (Note that it is not possible to construct a crude adiabatic basis in this reduced space as they will no longer form a complete set). One method that has been suggested to achieve this, is to use Eq. 2.29 to derive a differential equation for the transformation matrix, $\boldsymbol{\Omega}(\mathbf{x})$, which can then be integrated from a reference geometry to give the transformation matrix at a new set of coordinates.[92] This is achieved by using the unitarity of the transformation matrix

$$\sum_a \Omega_{ja}(\mathbf{x}) \langle \psi_a^{\mathrm{d}} | \nabla_{\mathrm{n},\nu} \psi_b^{\mathrm{d}} \rangle = 0, \tag{2.34}$$

to give the following differential equation

$$\sum_k \left(d_{jk}^{\nu\alpha}(\mathbf{x}) \Omega_{kb}(\mathbf{x}) + \delta_{jk} \frac{\partial \Omega_{kb}(\mathbf{x})}{\partial x_{\nu\alpha}} \right) = 0, \tag{2.35}$$

where $\boldsymbol{d}_{jk}^{\nu}(\mathbf{x}) = (d_{jk}^{\nu x}(\mathbf{x}), d_{jk}^{\nu y}(\mathbf{x}), d_{jk}^{\nu z}(\mathbf{x}))$. However, integration of this differential equation is expensive,[37,90] requiring knowledge of the derivative couplings along the path. Furthermore, the resulting transformation matrix is not guaranteed to be uniquely defined, or even to produce a set of strict diabatic states.[90] Hence, in general one can only obtain approximately diabatic states. There exist similar, but more efficient, methods which attempt to minimise the coupling, $\langle \psi_a^{\mathrm{d}} | \nabla_{\mathrm{n},\nu} \psi_b^{\mathrm{d}} \rangle$, in other ways but we will not consider them here.[93–96]

Whilst the transformation from the adiabatic to diabatic representations is in general ill defined, the reverse transformation is not, and is simply given by diagonalisation of the diabatic potential energy matrix $\boldsymbol{V}(\mathbf{x})$. As such, we shall side-step the issue of transforming from the adiabatic basis to the diabatic basis, by working from the outset in a diabatic basis. For non-adiabatic reactions such as electron transfer, it is relatively straightforward to construct diabatic potentials using simple empirical valence bond

approaches.[105] These approaches make use the fact that the electronic character of the diabatic states should remain (at least approximately) independent of the nuclear motion, and hence the diabatic states can be identified with standard force fields corresponding to different electronic configurations.[107–112] These potential energy surfaces can be combined with and modified using additional empirical or ab initio data, to ensure that key features of the potentials are captured correctly, such as reproducing barrier heights on the ground adiabatic potential. A natural extension to this approach is provided by ab initio methods which construct diabatic states based on applying constraints to the electron density, or by identifying diabatic states as eigenstates of operators which are expected physically to remain relatively insensitive to nuclear rearrangements, such as the dipole moment operator.[97–104] As the focus of this thesis is on the development of path-integral methods for the calculation of non-adiabatic reaction rates in condensed phase systems, we will only consider model diabatic systems and atomistic models constructed using empirical force fields. However, in principle the methods that we will discuss can also be applied to diabatic potentials calculated using ab initio techniques.

In developing methods to simulate non-adiabatic reaction rates we will restrict ourselves to consider systems which can be described using two diabatic states. This is sufficient for the description of many processes, such as electron transfer reactions in solution, for which two well defined charge transfer states can be identified.[46–49] We will, however, therefore not explicitly consider reactions which involve many electronic states, such as reactions on the surface of metals[113,114] (where there exist a continuum of electronic states), or reactions where superexchange with higher lying states are important.[67,106,115–118] Despite this, the methods that we will discuss can of course be applied to study reactions which involve population transfer between a sequence of different diabatic states, provided each step can be considered separately, and also to study superexchange reactions which can be treated using a two state model with an effective diabatic coupling.

The Hamiltonian for the two state systems we will consider in this thesis can thus be written in the diabatic representation as

$$\hat{H} = \hat{H}_0|0\rangle\langle 0| + (\hat{H}_1 - \epsilon)|1\rangle\langle 1| + \Delta(\hat{\boldsymbol{q}})(|0\rangle\langle 1| + |1\rangle\langle 0|), \tag{2.36}$$

where (in a simplification of notation) $|0\rangle$ and $|1\rangle$ represent the two diabatic states, $\hat{H}_i$ is the nuclear Hamiltonian on state i,

$$\hat{H}_i = \sum_{\nu=1}^{f} \frac{\hat{p}_\nu^2}{2m_\nu} + V_i(\hat{\boldsymbol{q}}), \tag{2.37}$$

with diabatic potential $V_i(\boldsymbol{q})$, and $\Delta(\boldsymbol{q})$ is the diabatic coupling between the two states. Here we have also introduced a single compressed coordinate vector, $\boldsymbol{q} = (q_1, \ldots, q_f)$, whose elements correspond to the coordinates of each the f degrees of freedom in the system, along with their conjugate momenta $\boldsymbol{p} = (p_1, \ldots, p_f)$. Note that to simplify notation we have dropped the subscript, n, from the label of the masses and momenta of the nuclear degrees of freedom as we will not be explicitly considering electronic coordinates in the remainder of the thesis. Finally we have also included the possibility of an additional external thermodynamic bias, ϵ, towards diabatic state $|1\rangle$. This could of course be included in the definition of the diabatic potential, $V_1(\boldsymbol{q})$, however it will be useful at various points to consider explicitly the effect of a changing driving force on the reaction rate, and hence we include it here to aid discussion in later sections.

Having defined the diabatic potentials it is straightforward to diagonalise the potential energy matrix and obtain the adiabatic potential energy surfaces,

$$U_j(\boldsymbol{q}) = \frac{V_0(\boldsymbol{q}) + V_1(\boldsymbol{q}) - \epsilon}{2} - \frac{(-1)^j}{2}\sqrt{(V_0(\boldsymbol{q}) - V_1(\boldsymbol{q}) + \epsilon)^2 + 4\Delta(\boldsymbol{q})^2}, \tag{2.38}$$

where (as we shall do throughout) we have assumed that the diabatic coupling $\Delta(\boldsymbol{q})$ is purely real. Finally to simplify later discussion of the non-adiabatic limit we define the supremum of the diabatic coupling as

$$\Delta = \sup_{\boldsymbol{q}\in\mathbb{R}^f} \Delta(\boldsymbol{q}), \tag{2.39}$$

and adopt the convention that $\Delta \to 0$ implies that the supremum is being taken to zero whilst $\Delta(\boldsymbol{q})/\Delta$ remains constant for all $\boldsymbol{q}$.

2.2 Exact rate theory

2.2.1 Condensed phase unimolecular rate theory

The central problem that we will be concerned with in this thesis, is calculating the thermal quantum mechanical rate constant, at a temperature T, for transfer from the

reactant state, $|0\rangle$, to the product state, $|1\rangle$. For an arbitrary normalised initial density operator, $\hat{\rho}(0)$, we define the populations of reactants and products as

$$P_r(t) = \mathrm{Tr}[\hat{\rho}(0)\hat{P}_r(t)] \tag{2.40a}$$

$$P_p(t) = \mathrm{Tr}[\hat{\rho}(0)\hat{P}_p(t)], \tag{2.40b}$$

where $\mathrm{Tr}[\dots]$ denotes a trace over the full Hilbert space, $\hat{P}_r$ and $\hat{P}_p$ are operators which project onto the reactants and products respectively, and

$$\hat{A}(t) = e^{+i\hat{H}t/\hbar}\hat{A}e^{-i\hat{H}t/\hbar} \tag{2.41}$$

denotes the Heisenberg time evolved operator. We will mostly be considering the case where the reactants are defined by $\hat{P}_r = |0\rangle\langle 0|$ and the products by $\hat{P}_p = |1\rangle\langle 1|$, however it will be useful at various points to consider more general definitions, and hence for now we will simply assume that $\hat{P}_r$ and $\hat{P}_p$ are projection operators which satisfy $\hat{P}_r + \hat{P}_p = \hat{1}$. As such the rate theory developed in the following section is applicable to any system which can be separated into two regions of phase space corresponding to reactants, r, and products, p. Provided the system obeys rate like behaviour at long time, the dynamics will eventually settle down to satisfy the kinetic equations

$$\dot{P}_r(t) = -kP_r(t) + k'P_p(t), \tag{2.42a}$$

$$\dot{P}_p(t) = -k'P_p(t) + kP_r(t), \tag{2.42b}$$

where k and k' are the forward and reverse rate constants respectively. Using the fact that $P_r(t) + P_p(t) = 1$ in these equations gives

$$\dot{P}_p(t) = k - (k + k')P_p(t) = (k + k')(\langle P_p\rangle - P_p(t)) \tag{2.43}$$

and therefore[119]

$$k = \lim_{t\to\infty} \frac{\dot{P}_p(t)}{1 - P_p(t)/\langle P_p\rangle}, \tag{2.44}$$

where (by detailed balance)

$$\langle P_p\rangle = \frac{k}{k + k'} = \lim_{t\to\infty} P_p(t) = \frac{\mathrm{Tr}\left[e^{-\beta\hat{H}}\hat{P}_p\right]}{\mathrm{Tr}\left[e^{-\beta\hat{H}}\right]} \tag{2.45}$$

is the thermal equilibrium population of the product state, with $\beta = 1/k_B T$. We have introduced the limit as $t \to \infty$ in Eq. 2.44 to stress that the kinetic description only becomes appropriate after an initial transient period. (As $t \to \infty$, both the numerator and denominator of Eq. 2.44 tend to zero, but their ratio remains finite and tends to k.) During this transient period the time dependent rate constant,

$$k(t) = \frac{\dot{P}_p(t)}{1 - P_p(t)/\langle P_p \rangle}, \tag{2.46}$$

may exhibit complex behaviour, characteristic of the molecular processes involved in the relaxation of the initial state, and as such the timescale of this transient period is often referred to as the molecular timescale, τ_{mol}.[120,121]

Note that, as is implied by this definition of the rate constants (Eq. 2.42), we will not be considering systems for which the dynamics remains oscillatory in the long time limit. Furthermore, we shall assume that there exists a separation of timescales, such that the timescale associated with the long time decay of the populations towards equilibrium $\tau_{\text{rxn}} = 1/(k + k')$ is much longer than all other timescales present in the system.[120–124] For a particular initial density, this means that the reaction timescale will be much longer than the molecular timescale which characterises the transient behaviour in $k(t)$, i.e. $\tau_{\text{rxn}} \gg \tau_{\text{mol}}$. Provided this is true, a rate like description is valid and relaxation towards equilibrium, at a temperature T, will always be described by the same rate constants, k and k', independent of the precise details of the initial density $\hat{\rho}(0)$. It is these kinds of systems which we shall restrict ourselves to consider in this thesis. Therefore, in addition to systems where the dynamics is oscillatory, we shall not be considering systems for which the dynamics is rate-like but multi-exponential, or systems in which there are additional degrees of freedom which relax more slowly than the rate process - giving rise to non-equilibrium rate constants.[125–129]

Although the rate fundamentally describes a non-equlibrium process, since it is associated with the specific temperature, T, to which the initial density is relaxing, it can also be thought of as a property of the equilibrium ensemble at that temperature. We can therefore remove explicit reference to the actual non-equilibrium initial density of the system, using linear response theory.[121,130–135] This will allow us to relate the rate to

equilibrium correlation functions, by considering the relaxation of the system due to an infinitesimal perturbation from equilibrium. The resulting expression for the rate will therefore depend only on equilibrium properties of the system at temperature T, and will form the basis of the rate theory in the following sections.

To derive the linear response expression for the rate we begin by considering an initial density of the form,

$$\hat{\rho}(0) = \frac{e^{-\beta(\hat{H}-\eta\hat{P}_r)}}{\mathrm{Tr}[e^{-\beta(\hat{H}-\eta\hat{P}_r)}]}, \tag{2.47}$$

in the limit as the perturbation parameter goes to zero, $\eta \to 0$. (Note that, provided the assumptions stated above are satisfied we need not necessarily use $\hat{P}_r$ as the perturbation, but we do so here as this gives the canonical form of the rate theory). In order to obtain a series expansion for $P_p(t)$ in powers of η, we first make use of the expansion

$$\mathrm{Tr}[e^{-\beta(\hat{H}-\eta\hat{P}_r)}\hat{A}] = \mathrm{Tr}[e^{-\beta\hat{H}}\hat{A}] + \eta\int_0^\beta \mathrm{d}\lambda\ \mathrm{Tr}[e^{-(\beta-\lambda)\hat{H}}\hat{P}_r\, e^{-\lambda\hat{H}}\hat{A}] + O(\eta^2), \tag{2.48}$$

to express both

$$\mathrm{Tr}[e^{-\beta(\hat{H}-\eta\hat{P}_r)}\hat{P}_p(t)] = \mathrm{Tr}[e^{-\beta\hat{H}}\hat{P}_p] + \eta\int_0^\beta \mathrm{d}\lambda\ \mathrm{Tr}[e^{-(\beta-\lambda)\hat{H}}\hat{P}_r\, e^{-\lambda\hat{H}}\hat{P}_p(t)] + O(\eta^2) \tag{2.49}$$

and

$$\frac{1}{\mathrm{Tr}[e^{-\beta(\hat{H}-\eta\hat{P}_r)}]} = \frac{1}{\mathrm{Tr}[e^{-\beta\hat{H}}]}\left(1 - \eta\beta\frac{\mathrm{Tr}[e^{-\beta\hat{H}}\hat{P}_r]}{\mathrm{Tr}[e^{-\beta\hat{H}}]} + O(\eta^2)\right). \tag{2.50}$$

Combining these then gives the time dependent population of the product as

$$P_p(t) = \langle P_p\rangle + \eta\beta\langle P_r\rangle\frac{\tilde{c}_{\mathrm{ss}}(t)}{Q_r} - \eta\beta\langle P_p\rangle\langle P_r\rangle + O(\eta^2), \tag{2.51}$$

where we have defined the Kubo-transformed[132] side-side correlation function

$$\tilde{c}_{\mathrm{ss}}(t) = \frac{1}{\beta}\int_0^\beta \mathrm{d}\lambda\ \mathrm{Tr}[e^{-(\beta-\lambda)\hat{H}}\hat{P}_r\, e^{-\lambda\hat{H}}\hat{P}_p(t)], \tag{2.52}$$

and the reactant partition function as

$$Q_r = \mathrm{Tr}\left[e^{-\beta\hat{H}}\hat{P}_r\right]. \tag{2.53}$$

Taking the time derivative we find that the rate of change of the product population can also be expressed in terms of an equilibrium correlation function as

$$\dot{P}_p(t) = \eta\beta\langle P_r\rangle\frac{\tilde{c}_{\mathrm{fs}}(t)}{Q_r} + O(\eta^2), \tag{2.54}$$

where

$$\tilde{c}_{\mathrm{fs}}(t) = \frac{1}{\beta}\int_0^\beta \mathrm{d}\lambda\, \mathrm{Tr}\left[e^{-(\beta-\lambda)\hat{H}}\hat{F}_p\, e^{-\lambda\hat{H}}\hat{P}_p(t)\right] \tag{2.55}$$

is now the Kubo-transformed flux-side correlation function (just the time derivative of $\tilde{c}_{\mathrm{ss}}(t)$), with $\hat{F}_p$ corresponding to the flux onto products

$$\hat{F}_p = -\frac{i}{\hbar}\left[\hat{H}, \hat{P}_r\right] = +\frac{i}{\hbar}\left[\hat{H}, \hat{P}_p\right]. \tag{2.56}$$

From this we can see that the pre-limit expression for the rate constant can be written as

$$k(t) = \frac{\dot{P}_p(t)}{1 - P_p(t)/\langle P_p\rangle} = \frac{\tilde{c}_{\mathrm{fs}}(t)}{Q_r - \tilde{c}_{\mathrm{ss}}(t)/\langle P_p\rangle} + O(\eta). \tag{2.57}$$

Hence, truncating at lowest order in η gives the linear response expression for the rate constant, solely in terms of equilibrium correlation functions,[119]

$$k = \lim_{t\to\infty} \frac{\tilde{c}_{\mathrm{fs}}(t)}{Q_r - \tilde{c}_{\mathrm{ss}}(t)/\langle P_p\rangle}. \tag{2.58}$$

This expression will be taken as the formal definition of the rate constant, that will be used in the remainder of the thesis. Note that the pre-limit expression for the linear response rate

$$k(t) = \frac{\tilde{c}_{\mathrm{fs}}(t)}{Q_r - \tilde{c}_{\mathrm{ss}}(t)/\langle P_p\rangle} \tag{2.59}$$

is equivalent to the the non-equilibrium expression given by Eq. 2.46, when the initial density is defined as

$$\hat{\rho}(0) = \frac{1}{\beta Q_r}\int_0^\beta \mathrm{d}\lambda\, e^{-(\beta-\lambda)\hat{H}}\hat{P}_r\, e^{-\lambda\hat{H}}. \tag{2.60}$$

Therefore this initial density, which corresponds to a finite perturbation of P_r and P_p from equilibrium, relaxes in the same way as the infinitesimal perturbation considered above.

In order to arrive at the standard expression for the rate we need to make one additional approximation, by introducing the idea of a "plateau time", t_{p} for which[120–122,134]

$$k \simeq \frac{\tilde{c}_{\mathrm{fs}}(t_{\mathrm{p}})}{Q_r}. \tag{2.61}$$

This plateau time is supposed to be sufficiently short that very little population has been transferred to the product state ($P_p(t) \ll 1$), and yet sufficiently long that the population dynamics has settled down to conform to the kinetic behaviour in Eqs. 2.42.

Clearly, therefore, Eq. 2.61 rests on the separation of time scales discussed earlier, and is defined as a time much longer than the molecular time scale associated with the transient behaviour $\tau_{\text{mol}} \ll t_{\text{p}}$, but much shorter than the timescale of the reaction $t_{\text{p}} \ll \tau_{\text{rxn}}$ such that the relaxation to equilibrium appears approximately linear in time. Hence it will be most accurate for slow reactions.

2.2.2 Scattering rates

Although the focus of this thesis is on the development of approximate methods for the study of condensed phase reactions of the kind described by Eq. 2.42, it will be useful at various points to consider simple low dimensional models for which exact results can be calculated for comparison. As such we now briefly make the connection between Eq. 2.58 and the calculation of scattering rate constants. Rather than considering the original formal statistical mechanical arguments of Yamamoto,[134] we will just give a simple qualitative argument to connect the two types of rate constants.

We consider a simple gas phase scattering reaction of the form

$$\text{AB} + \text{C} \rightleftharpoons \text{A} + \text{BC}. \tag{2.62}$$

The phenomenological kinetic scheme for such a bimolecular gas phase reaction can be written as

$$\frac{\text{d[AB]}}{\text{d}t} = -k_{+}[\text{AB}][\text{C}] + k_{-}[\text{A}][\text{BC}] \tag{2.63a}$$

$$\frac{\text{d[A]}}{\text{d}t} = k_{+}[\text{AB}][\text{C}] - k_{-}[\text{A}][\text{BC}], \tag{2.63b}$$

where k_{+} and k_{-} are the usual bimolecular gas phase rate constants and [X] denotes the concentration of species X. The relation between the unimolecular rate constants, k and k', defined by Eq. 2.42 and these bimolecular scattering rate constants can be found by considering a cubic box of volume V, containing just one of each of the molecular fragments A, B and C, in the limit of the box size becoming very large.*

*There is, of course, the implicit assumption here that there is some other process which maintains thermal equilibrium, such as collision with walls of the container, and that this process occurs on a timescale faster than τ_{rxn} but slower than τ_{mol}.

In this case we can rewrite Eq. 2.42 as

$$\frac{\mathrm{d}P_{\mathrm{AB}}}{\mathrm{d}t} = -kP_{\mathrm{AB}} + k'P_{\mathrm{A}} \tag{2.64a}$$

$$\frac{\mathrm{d}P_{\mathrm{A}}}{\mathrm{d}t} = kP_{\mathrm{AB}} - k'P_{\mathrm{A}}, \tag{2.64b}$$

where P_{AB} and P_{A} are now the probabilities that A will be found forming part of a molecule of AB or isolated as a molecule of A respectively. Generalising this to the case where there is only one A molecule, but n_{BC} BC molecules and n_{C} C molecules it is clear that, assuming V is large enough that the interactions of molecules of BC and C as well as 3 body collisions can be ignored, the kinetic scheme in Eq. 2.64 simply becomes

$$\frac{\mathrm{d}P_{\mathrm{AB}}}{\mathrm{d}t} = -kP_{\mathrm{AB}}n_{\mathrm{C}} + k'P_{\mathrm{A}}n_{\mathrm{BC}} \tag{2.65a}$$

$$\frac{\mathrm{d}P_{\mathrm{A}}}{\mathrm{d}t} = kP_{\mathrm{AB}}n_{\mathrm{C}} - k'P_{\mathrm{A}}n_{\mathrm{BC}}. \tag{2.65b}$$

Finally to connect this to Eq. 2.63 we need to consider the case of multiple A molecules, N_{A} in total. Labelling each with an index i, the number of AB molecules in the box is given by

$$n_{\mathrm{AB}} = \sum_{i=1}^{N_{\mathrm{A}}} P_{\mathrm{AB},i} \tag{2.66}$$

and the number of isolated A molecules by

$$n_{\mathrm{A}} = \sum_{i=1}^{N_{\mathrm{A}}} P_{\mathrm{A},i}. \tag{2.67}$$

Assuming that the density of A and AB is also sufficiently low that they can be treated as independent and non interacting, it follows that Eq. 2.65 can be taken to hold for each i individually. Hence, summing over i and dividing by the volume we find that

$$\frac{\mathrm{d}n_{\mathrm{AB}}/V}{\mathrm{d}t} = -kV\frac{n_{\mathrm{AB}}}{V}\frac{n_{\mathrm{C}}}{V} + k'V\frac{n_{\mathrm{A}}}{V}\frac{n_{\mathrm{BC}}}{V} \tag{2.68a}$$

$$\frac{\mathrm{d}n_{\mathrm{A}}/V}{\mathrm{d}t} = kV\frac{n_{\mathrm{AB}}}{V}\frac{n_{\mathrm{C}}}{V} - k'V\frac{n_{\mathrm{A}}}{V}\frac{n_{\mathrm{BC}}}{V}. \tag{2.68b}$$

Therefore, using the definition of the concentration $n_{\mathrm{X}}/V = [\mathrm{X}]$, and comparing Eqs. 2.63 and 2.68 we can see that the rate constants are simply related by $kV = k_+$ and $k'V = k_-$.

Using this (perhaps rather obvious) result, we can now make connection with Yamamoto's original linear response expression for the scattering rate constant k_+ in terms of the flux-side correlation function.[134] We begin by considering the pre-limit linear response expression for k multiplied by V,

$$k(t)V = \frac{\tilde{c}_{\mathrm{fs}}(t)V}{Q_r - \tilde{c}_{\mathrm{ss}}(t)/\langle P_p \rangle}, \tag{2.69}$$

and note that in the limit of a large volume $Q_r \to Q_{\mathrm{AB}}Q_{\mathrm{C}}$, where Q_{AB} and Q_{C} are the molecular partition functions of AB and C respectively. This means that Q_r is proportional to V^2, whereas the correlation functions $\tilde{c}_{\mathrm{ss}}(t)$ and $\tilde{c}_{\mathrm{fs}}(t)$, are only proportional V (due to their dependence on the centre of mass motion). Hence it follows that

$$\lim_{V\to\infty} k(t)V = \lim_{V\to\infty} \frac{\tilde{c}_{\mathrm{fs}}(t)}{Q_r/V}. \tag{2.70}$$

By taking the limit as $V \to \infty$ before taking the limit as $t \to \infty$ we arrive at the standard expression for the scattering rate constant in terms of the Kubo-transformed flux-side correlation function as

$$k_+ = \lim_{t\to\infty}\lim_{V\to\infty} \frac{\tilde{c}_{\mathrm{fs}}(t)}{Q_r/V}. \tag{2.71}$$

Note that taking the limits in this order is physically justified as the molecular timescale τ_{mol} approaches a constant as $V \to \infty$. Hence, comparing with Eq. 2.61 we see that, for scattering rates the plateau time approximation becomes exact, even as $t_{\mathrm{p}} \to \infty$. This reflects the fact that the probability of encounter for a single pair of molecules goes to zero as $V \to \infty$, hence from the point of view of the unimolecular rate constant the reaction is infinitely slow, i.e. $\tau_{\mathrm{mol}}/\tau_{\mathrm{rxn}} \to 0$.

The close connection between the calculation of scattering rates and unimolecular rates in the condensed phase will prove particularly useful throughout the thesis for testing approximate methods. This is because rate constants are typically ill defined for bound systems consisting of a small number of degrees of freedom due to the presence of recurrences. In contrast, a one dimensional scattering model will not recur, as there exists a continuum of product and reactant states, and hence the rate is always well defined.

For the sake of simplicity, in the remainder of the thesis we will use the same notation to refer to scattering quantities and their unimolecular counter part, leaving which is

meant to be determined from context. Hence from now on, for scattering problems we will use k to refer to the scattering rate constant instead of k_+, and we will use Q_r instead of $\lim_{V\to\infty} Q_r/V$ for the reactant partition function per unit volume (or strictly per unit length since all scattering problems we will consider will be one dimensional). Furthermore, we note that since the centre of mass motion can be separated out of both of the reactant partition function and the flux-side correlation function it does not enter the expression for the rate, hence from here on all quantities are defined with the centre of mass motion removed.

Properties of flux correlation functions

Before we conclude this section, we briefly review some important properties of the flux-side correlation function and its time derivative, the flux-flux correlation function. Firstly we note that, since the Kubo-transformed flux-side correlation function is a continuous, real and odd function of time, we can write

$$\lim_{t\to\infty} \tilde{c}_{\mathrm{fs}}(t) = \int_0^\infty \tilde{c}_{\mathrm{ff}}(t)\mathrm{d}t = \frac{1}{2}\int_{-\infty}^\infty \tilde{c}_{\mathrm{ff}}(t)\mathrm{d}t, \tag{2.72}$$

where

$$\tilde{c}_{\mathrm{ff}}(t) = \frac{1}{\beta}\int_0^\beta \mathrm{d}\lambda\, \mathrm{Tr}\left[e^{-(\beta-\lambda)\hat{H}}\hat{F}_p\, e^{-\lambda\hat{H}}\hat{F}_p(t)\right] \tag{2.73}$$

is the Kubo-transformed flux-flux correlation function (the time derivative of $\tilde{c}_{\mathrm{fs}}(t)$). However, one need not use the Kubo-transformed version.[136] In particular by expanding the correlation function in the energy eigenbasis,

$$\hat{H}\,|j\rangle = E_j\,|j\rangle\,, \tag{2.74}$$

we find

$$\int_{-\infty}^\infty \tilde{c}_{\mathrm{ff}}(t)\mathrm{d}t = \frac{1}{\beta}\int_0^\beta \mathrm{d}\lambda \int_{-\infty}^\infty \mathrm{d}t \sum\!\!\!\!\!\!\int_{j,k} e^{-(\beta-\lambda)E_j-\lambda E_k}\,|\langle j|\,\hat{F}_p\,|k\rangle\,|^2 e^{-i(E_j-E_k)t/\hbar}, \tag{2.75}$$

where $\sum\!\!\!\!\!\!\int_{j,k}$ should be understood as being a double sum over the bound states of $\hat{H}$ and a double integral over all continuum states. Recognising the integral over time as giving

the Fourier representation of the delta function, this can be rewritten as

$$\begin{aligned}\int_{-\infty}^{\infty}\tilde{c}_{\mathrm{ff}}(t)\mathrm{d}t &= \frac{2\pi\hbar}{\beta}\int_0^{\beta}\mathrm{d}\lambda\sum\!\!\!\!\!\!\int_{j,k} e^{-(\beta-\lambda)E_j-\lambda E_k}\,|\langle j|\,\hat{F}_p\,|k\rangle|^2\delta(E_j-E_k)\\ &= 2\pi\hbar\sum\!\!\!\!\!\!\int_{j,k} e^{-(\beta-\lambda)E_j-\lambda E_k}\,|\langle j|\,\hat{F}_p\,|k\rangle|^2\delta(E_j-E_k),\end{aligned} \tag{2.76}$$

where the second line now holds for arbitrary λ.* Reinserting the Fourier representation of the delta function, we then see that the time integral of the Kubo-transformed flux-flux correlation function is equivalent to that of alternative equilibrium correlation functions[136]

$$\int_{-\infty}^{\infty}\tilde{c}_{\mathrm{ff}}(t)\mathrm{d}t = \int_{-\infty}^{\infty}\mathrm{Tr}\left[e^{-(\beta-\lambda)\hat{H}}\hat{F}_p\,e^{-\lambda\hat{H}}\hat{F}_p(t)\right]\mathrm{d}t. \tag{2.77}$$

A particularly important example, which we will make use of later, is the "thermally symmetrised" form, which we define as

$$\bar{c}_{\mathrm{ff}}(t) = \mathrm{Tr}\left[e^{-\beta\hat{H}/2}\hat{F}_p\,e^{-\beta\hat{H}/2}\hat{F}_p(t)\right]. \tag{2.78}$$

Just as with the Kubo-transformed correlation function this is a real and even function of time, and this is the form that was preferred by Miller in his alternative, scattering theory based derivation of the flux correlation function formulation of the rate.[136,137] Starting from Eq. 2.76 we can also make the connection to the expression for the scattering rate in terms of the cumulative reaction probability by introducing the identity

$$1 = \int_{-\infty}^{\infty}\mathrm{d}E\delta(E_k-E) \tag{2.79}$$

to give[136]

$$\begin{aligned}\frac{1}{2}\int_{-\infty}^{\infty}\tilde{c}_{\mathrm{ff}}(t)\mathrm{d}t &= \pi\hbar\int_{-\infty}^{\infty}\mathrm{d}E\sum\!\!\!\!\!\!\int_{j,k} e^{-\beta E}\,|\langle j|\,\hat{F}_p\,|k\rangle|^2\delta(E_j-E)\delta(E_k-E)\\ &= \pi\hbar\int_{-\infty}^{\infty}\mathrm{d}E e^{-\beta E}\,\mathrm{Tr}\left[\delta(\hat{H}-E)\hat{F}_p\delta(\hat{H}-E)\hat{F}_p\right]\\ &= \frac{1}{2\pi\hbar}\int_{-\infty}^{\infty}\mathrm{d}E e^{-\beta E}N(E),\end{aligned} \tag{2.80}$$

where $N(E)$ is the cumulative reaction probability, which for a simple one dimensional scattering model is equivalent to the barrier transmission probability.

*Provided that the sums are convergent, which will certainly be true for $\lambda \in [0,\beta]$

2.2.3 Golden-rule limit

As discussed earlier many electronically non-adiabatic reactions can be very accurately described using Fermi's golden rule, where the rate is proportional to Δ^2.[46–49] The golden-rule rate can therefore be formally defined according to the relation*

$$k_{\mathrm{GR}} = \beta^2 \Delta^2 k_2 \tag{2.81}$$

where

$$k_2 = \lim_{t\to\infty} \lim_{\Delta\to 0} \frac{k(t)}{\beta^2\Delta^2}. \tag{2.82}$$

As with the scattering rates we define these limits to be taken in such a way that $\Delta \to 0$ before $t \to \infty$, which can be justified by noting that $\lim_{\Delta\to 0} \tau_{\mathrm{mol}}/\tau_{\mathrm{rxn}} = 0$. This means that the plateau time approximation (Eq. 2.61) becomes exact and the plateau time can be taken to infinity,

$$k_2 = \lim_{t\to\infty} \lim_{\Delta\to 0} \frac{\tilde{c}_{\mathrm{fs}}(t)}{\beta^2\Delta^2 Q_r}. \tag{2.83}$$

Following the same reasoning as Eq. 2.72-2.77 this can be equivalently rewritten in terms of the thermally symmetrised flux-flux correlation function as

$$k_2 = \frac{1}{2Q_r} \int_{-\infty}^{\infty} \lim_{\Delta\to 0} \frac{\bar{c}_{\mathrm{ff}}(t)}{\beta^2\Delta^2}\, \mathrm{d}t. \tag{2.84}$$

In this limit it is natural to define $\hat{P}_r = |0\rangle\langle 0|$ and $\hat{P}_p = |1\rangle\langle 1|$ such that the flux operator becomes

$$\hat{F}_p = \frac{i\Delta(\hat{\boldsymbol{q}})}{\hbar}(|0\rangle\langle 1| - |1\rangle\langle 0|). \tag{2.85}$$

Inserting this into Eq. 2.84, and using the fact that $\langle i|\, e^{-i\hat{H}t/\hbar}\, |j\rangle = O(\Delta)$ for $i \neq j$, it is then straightforward to see that the correlation function can be expanded as

$$\bar{c}_{\mathrm{ff}}(t) = 2\,\mathrm{Re}\left(\mathrm{tr_n}\left[e^{-(\beta/2+it/\hbar)\hat{H}_0}\frac{\Delta(\hat{\boldsymbol{q}})}{\hbar}e^{-(\beta/2-it/\hbar)(\hat{H}_1-\epsilon)}\frac{\Delta(\hat{\boldsymbol{q}})}{\hbar}\right]\right) + O(\Delta^4), \tag{2.86}$$

where $\mathrm{tr_n}[\dots]$ denotes a trace over nuclear coordinates only. Inserting this into Eq. 2.84 it follows that the golden-rule rate is given by,

$$k_{\mathrm{GR}} = \frac{1}{\hbar^2 Q_r} \int_{-\infty}^{\infty} \mathrm{tr_n}\left[e^{-(\beta/2+it/\hbar)\hat{H}_0}\Delta(\hat{\boldsymbol{q}})e^{-(\beta/2-it/\hbar)(\hat{H}_1-\epsilon)}\Delta(\hat{\boldsymbol{q}})\right]\mathrm{d}t, \tag{2.87}$$

*We include the factor of β^2 here such that k_2 also has the units of a rate constant.

note that we are able to drop the Re(...) as the imaginary part of the integrand is odd. Again, following a similar argument to the scattering case above (Eqs. 2.74-2.77) we can expand using the eigenvectors of $\hat{H}_0$ and $\hat{H}_1$ to show that the golden-rule rate can also equivalently be written as,[138,139]

$$k_{\mathrm{GR}} = \frac{1}{\hbar^2 Q_r} \int_{-\infty}^{\infty} \mathrm{tr_n}\left[e^{-(\beta-\lambda+it/\hbar)\hat{H}_0} \Delta(\hat{\boldsymbol{q}}) e^{-(\lambda-it/\hbar)(\hat{H}_1-\epsilon)} \Delta(\hat{\boldsymbol{q}}) \right] \mathrm{d}t, \tag{2.88}$$

independent of the choice of λ.

Much of the thesis will be focussed on systems for which the diabatic coupling is defined or assumed to be a constant, such that $\Delta(\boldsymbol{q}) = \Delta$, allowing us to simplify the notation. For example the golden-rule rate can then be written as[138,139]

$$k_{\mathrm{GR}} = \frac{\Delta^2}{\hbar^2 Q_r} \int_{-\infty}^{\infty} c_{\mathrm{GR}}(t + i\lambda\hbar)\mathrm{d}t, \tag{2.89}$$

where we have introduced the golden-rule "correlation function"

$$c_{\mathrm{GR}}(t + i\lambda\hbar) = \mathrm{tr_n}\left[e^{-(\beta-\lambda+it/\hbar)\hat{H}_0} e^{-(\lambda-it/\hbar)(\hat{H}_1-\epsilon)} \right]. \tag{2.90}$$

Note in passing that $c_{\mathrm{GR}}(t)$ as defined in Eq. 2.90 is a convergent representation of an analytic function of complex time t, for $0 \leq \mathrm{Im}(t) \leq \beta\hbar$, and that, although in general it is not convergent outside of this strip, it does always have a unique analytic continuation. This is an important point that we will come back to later.

Instead of writing the rate in terms of $c_{\mathrm{GR}}(t)$ we can highlight the effect of the bias, ϵ, on the golden-rule rate by writing it as

$$k_{\mathrm{GR}}(\epsilon) = \frac{\Delta^2}{Q_r\hbar^2} e^{\lambda\epsilon} \int_{-\infty}^{\infty} c_\lambda(t) e^{-i\epsilon t/\hbar}\mathrm{d}t \tag{2.91}$$

where

$$c_\lambda(t) = \mathrm{tr_n}\left[e^{-(\beta-\lambda+it/\hbar)\hat{H}_0} e^{-(\lambda-it/\hbar)\hat{H}_1} \right]. \tag{2.92}$$

This illustrates the fact that changing the bias simply alters the correlation function $c_{\mathrm{GR}}(t + i\lambda\hbar)$ by introducing a sinusoidal oscillation, $e^{-i\epsilon t/\hbar}$, and a multiplicative factor of $e^{+\lambda\epsilon}$. Of course $e^{-i\epsilon t/\hbar}$ can also be recognised as the kernel of a Fourier transform, and this allows us to write the rate in the form

$$k(\epsilon) = \frac{2\pi\Delta^2}{Q_r\hbar} \rho_\lambda(\epsilon) e^{-\beta F(\lambda)+\lambda\epsilon}, \tag{2.93}$$

where $\rho_\lambda(E)$ is a probability distribution given by the Fourier transform

$$\rho_\lambda(E) = \frac{1}{2\pi\hbar}\int_{-\infty}^{\infty}\left\langle e^{-i\hat{H}_0 t/\hbar}e^{+i\hat{H}_1 t/\hbar}\right\rangle_\lambda e^{-iEt/\hbar}\mathrm{d}t, \tag{2.94}$$

in which

$$\left\langle e^{-i\hat{H}_0 t/\hbar}e^{+i\hat{H}_1 t/\hbar}\right\rangle_\lambda = \frac{c_\lambda(t)}{c_\lambda(0)} \tag{2.95}$$

is just the correlation function (for $\epsilon = 0$) normalised to one at $t = 0$, and the Boltzmann factor,

$$e^{-\beta F_{\mathrm{GR}}(\lambda)} = \mathrm{tr}_\mathrm{n}\left[e^{-(\beta-\lambda)\hat{H}_0}e^{-\lambda\hat{H}_1}\right] = c_\lambda(0), \tag{2.96}$$

is just the correlation function evaluated on the imaginary axis. Note that to prove $\rho_\lambda(E)$ is a probability density one can first show that it is positive everywhere by expanding the correlation function in eigenstates of $\hat{H}_0$ and $\hat{H}_1$,[140] or by recognising that it is proportional to the rate constant, and then simply using the inverse Fourier transform to identify that it is normalised. Importantly, as the distribution is just the Fourier transform of the normalised correlation function, moments of the distribution are related to time derivatives of the correlation function at $t = 0$, and hence by analyticity to derivatives of the free energy, $F_{\mathrm{GR}}(\lambda)$.

For completeness we will now give a brief derivation of the relation between the first two moments of the exact distribution $\rho_\lambda(E)$ and the first two derivatives of the free energy $F_{\mathrm{GR}}(\lambda)$, as these derivatives will play an important role in approximate theories discussed later. We begin by considering the 1st central moment of the distribution which is defined as,

$$\mu_{1,\lambda} = \int_{-\infty}^{\infty} E\rho_\lambda(E)\mathrm{d}E. \tag{2.97}$$

Inserting the definition of the distribution into this expression this gives

$$\mu_{1,\lambda} = \frac{1}{2\pi\hbar}\int_{-\infty}^{\infty}\int_{-\infty}^{\infty}\left\langle e^{-i\hat{H}_0 t/\hbar}e^{+i\hat{H}_1 t/\hbar}\right\rangle_\lambda E e^{-iEt/\hbar}\mathrm{d}E\mathrm{d}t. \tag{2.98}$$

Then replacing the multiplication by E with a derivative with respect to time and integrating by parts leads to

$$\mu_{1,\lambda} = \frac{-i}{2\pi}\int_{-\infty}^{\infty}\int_{-\infty}^{\infty}\left\langle \frac{\partial}{\partial t}e^{-i\hat{H}_0 t/\hbar}e^{+i\hat{H}_1 t/\hbar}\right\rangle_\lambda e^{-iEt/\hbar}\mathrm{d}E\mathrm{d}t, \tag{2.99}$$

which can then be integrated over E to give

$$\mu_{1,\lambda} = -i\hbar \int_{-\infty}^{\infty} \left\langle \frac{\partial}{\partial t} e^{-i\hat{H}_0 t/\hbar} e^{+i\hat{H}_1 t/\hbar} \right\rangle_{\lambda} \delta(t) \mathrm{d}t. \tag{2.100}$$

This then immediately simplifies to

$$\mu_{1,\lambda} = -\frac{\mathrm{tr_n}\left[(\hat{V}_0 - \hat{V}_1) e^{-(\beta-\lambda)\hat{H}_0} e^{-\lambda \hat{H}_1}\right]}{\mathrm{tr_n}\left[e^{-(\beta-\lambda)\hat{H}_0} e^{-\lambda \hat{H}_1}\right]} = \beta F'_{\mathrm{GR}}(\lambda), \tag{2.101}$$

and hence we see that the first moment is directly proportional to the first derivative of the free energy at λ. We can apply the same process to evaluate the second central moment,

$$\mu_{2,\lambda} = \int_{-\infty}^{\infty} (E^2 - \mu_{1,\lambda}^2) \rho_{\lambda}(E) \mathrm{d}E \tag{2.102}$$

from which it follows that

$$\mu_{2,\lambda} = -\hbar^2 \int_{-\infty}^{\infty} \left\langle \frac{\partial^2}{\partial t^2} e^{-i\hat{H}_0 t/\hbar} e^{+i\hat{H}_1 t/\hbar} \right\rangle_{\lambda} \delta(t) \mathrm{d}t - \mu_{1,\lambda}^2. \tag{2.103}$$

This then simplifies to give the second central moment in terms of the second derivative of the free energy,

$$\mu_{2,\lambda} = \frac{\mathrm{tr_n}\left[(\hat{V}_0 - \hat{V}_1) e^{-(\beta-\lambda)\hat{H}_0} (\hat{V}_0 - \hat{V}_1) e^{-\lambda \hat{H}_1}\right]}{\mathrm{tr_n}\left[e^{-(\beta-\lambda)\hat{H}_0} e^{-\lambda \hat{H}_1}\right]} - \mu_{1,\lambda}^2 = -\beta F''_{\mathrm{GR}}(\lambda). \tag{2.104}$$

Classical golden-rule

In the high temperature ($\beta \to 0$) limit the golden-rule expression for the rate simplifies significantly and reduces to the classical golden-rule expression[141,142]

$$k_{\text{cl-GR}}(\epsilon) = \frac{2\pi}{Q_r \hbar} \langle \Delta^2(\boldsymbol{q}) \delta(V_-(\boldsymbol{q}) + \epsilon) \rangle_{\mathrm{cl},\lambda} e^{-\beta F_{\text{cl-GR}}(\lambda) + \lambda \epsilon} \tag{2.105}$$

where $V_-(\boldsymbol{q}) = V_0(\boldsymbol{q}) - V_1(\boldsymbol{q})$ is the diabatic energy gap,

$$e^{-\beta F_{\text{cl-GR}}(\lambda)} = \frac{1}{(2\pi\hbar)^f} \int \mathrm{d}^f \boldsymbol{p} \int \mathrm{d}^f \boldsymbol{q} e^{-(\beta-\lambda) H_0(\boldsymbol{p},\boldsymbol{q}) - \lambda H_1(\boldsymbol{p},\boldsymbol{q})} \tag{2.106}$$

is the high temperature limit of the correlation function on the imaginary axis,* and the expectation value is taken in the classical ensemble with

$$\langle A(\boldsymbol{q}) \rangle_{\mathrm{cl},\lambda} = \frac{\int \mathrm{d}^f \boldsymbol{p} \int \mathrm{d}^f \boldsymbol{q}\, A(\boldsymbol{q}) e^{-(\beta-\lambda) H_0(\boldsymbol{p},\boldsymbol{q}) - \lambda H_1(\boldsymbol{p},\boldsymbol{q})}}{\int \mathrm{d}^f \boldsymbol{p} \int \mathrm{d}^f \boldsymbol{q}\, e^{-(\beta-\lambda) H_0(\boldsymbol{p},\boldsymbol{q}) - \lambda H_1(\boldsymbol{p},\boldsymbol{q})}}. \tag{2.107}$$

*Note that throughout the thesis we will adopt the convention that,

$$\int \mathrm{d}^N \boldsymbol{x} \equiv \int_{-\infty}^{\infty} \mathrm{d}x_1 \cdots \int_{-\infty}^{\infty} \mathrm{d}x_N.$$

In the case of constant diabatic coupling this simply becomes

$$k_{\text{cl-GR}}(\epsilon) = \frac{2\pi\Delta^2}{Q_r\hbar}\left\langle\delta(V_-(\boldsymbol{q})+\epsilon)\right\rangle_{\text{cl},\lambda} e^{-\beta F_{\text{cl-GR}}(\lambda)+\lambda\epsilon} \tag{2.108}$$

and hence we see that in the classical limit the probability distribution, $\rho_\lambda(\epsilon)$, is just the probability density at the diabatic crossing point $V_-(\boldsymbol{q}) = -\epsilon$,

$$\rho_{\text{cl},\lambda}(E) = \left\langle\delta(V_-(\boldsymbol{q})+E)\right\rangle_{\text{cl},\lambda}. \tag{2.109}$$

Marcus theory

Starting from the exact classical golden-rule expression we can derive the famous Marcus theory expression for the rate[46–49] by simply assuming that the free-energy in the reactant or product ensembles is a parabolic function of the diabatic energy gap, consistent with the central limit theorem. The free energy in the reactant ensemble as a function of the diabatic energy gap is defined as

$$\Phi_0(E) = -\frac{1}{\beta}\ln\left(\left\langle\delta(V_-(\boldsymbol{q})-E)\right\rangle_{\text{cl},0}\right) = -\frac{1}{\beta}\ln\left(\rho_{\text{cl},0}(-E)\right) \tag{2.110}$$

and in the product ensemble as

$$\Phi_1(E) = -\frac{1}{\beta}\ln\left(\left\langle\delta(V_-(\boldsymbol{q})-E)\right\rangle_{\text{cl},\beta}\right) - (\Delta F+\epsilon) = -\frac{1}{\beta}\ln\left(\rho_{\text{cl},\beta}(-E)\right) - (\Delta F+\epsilon), \tag{2.111}$$

where ΔF is the classical free energy difference between reactants and products,

$$\Delta F = -\frac{1}{\beta}\ln\left(\frac{\text{tr}_{\text{cl,n}}\left[e^{-\beta H_0}\right]}{\text{tr}_{\text{cl,n}}\left[e^{-\beta H_1}\right]}\right). \tag{2.112}$$

Hence we see that the Marcus assumption of parabolic free energy surfaces is equivalent to assuming that $\rho_{\text{cl},\lambda}(E)$ is Gaussian,

$$\rho_{\text{MT},\lambda}(E) = \sqrt{\frac{\beta}{4\pi\Lambda}}e^{-\frac{\beta}{4\Lambda}\left(E+\Delta F-\Lambda\left(1-\frac{2\lambda}{\beta}\right)\right)^2}, \tag{2.113}$$

where Λ is the Marcus theory reorganisation energy, and is equivalent to assuming that the central limit theorem can be invoked. By comparison with Eq. 2.108 we then arrive at the famous Marcus theory expression for the golden-rule rate[46–49]

$$k_{\text{MT}} = \frac{\Delta^2}{\hbar}\sqrt{\frac{\pi\beta}{\Lambda}}e^{-\beta(\Lambda-\Delta F-\epsilon)^2/4\Lambda}. \tag{2.114}$$

In order to relate the Marcus reorganisation energy, which appears in this expression, to classical expectation values of the system, we note that the relationship between $\rho_{\mathrm{cl},\lambda}(E)$ and $F_{\text{cl-GR}}(\lambda)$ means that the Marcus approximation is equivalent to assuming that the classical free energy obeys

$$-\beta(F_{\text{cl-GR}}(\lambda) - F_{\text{cl-GR}}(0)) \simeq -\beta(F_{\mathrm{MT}}(\lambda) - F_{\mathrm{MT}}(0)) = \lambda \Delta F + \beta\Lambda\left(\frac{\lambda^2}{\beta^2} - \frac{\lambda}{\beta}\right). \quad (2.115)$$

Hence, by differentiating with respect to λ and comparing to $F'_{\text{cl-GR}}(\lambda = 0)$ we see that the Marcus reorganisation energy can be defined as

$$\Lambda = \Delta F - \langle V_- \rangle_{\mathrm{cl},0}. \quad (2.116)$$

This definition is obviously not unique, in particular we could alternatively compare to the derivative at $\lambda = \beta$ giving

$$\Lambda = -\Delta F + \langle V_- \rangle_{\mathrm{cl},\beta}. \quad (2.117)$$

For systems in which Marcus theory is exact these two definitions will give the same result, but in general they will be different. We will give a more detailed discussion of the different possible definitions of the Marcus reorganisation energy in Chap. 8, however, for now we take Eq. 2.116 as the definition of the reorganisation energy unless stated otherwise. The definition of the Marcus inverted regime, $\epsilon + \Delta F > \Lambda$, for which the rate decreases with increasing driving force, can thus be equivalently defined as $\epsilon > -\langle V_- \rangle_{\mathrm{cl},0}$. The implications of this inequality will be discussed later in the thesis.

2.2.4 Born-Oppenheimer rate constant

Although the focus of this thesis is on the calculation of electronically non-adiabatic reaction rates, having discussed the limit of weak electronic coupling, $\Delta \to 0$, we now consider the opposite regime in which one can assume the Born-Oppenheimer approximation is valid.[35] The Born-Oppenheimer approximation to the rate can be calculated whenever the reactants and products can be separated by a position space dividing surface. This is certainly the case for an activated reaction in the normal Marcus

regime, where the projection operators $\hat{P}_r$ and $\hat{P}_p$ onto the reactant and product states can equally well be replaced by

$$\hat{P}_r = \theta(-s(\hat{\boldsymbol{q}})) \quad \text{and} \quad \hat{P}_p = \theta(s(\hat{\boldsymbol{q}})), \tag{2.118}$$

where $\theta(x)$ is the Heaviside step function, and $s(\boldsymbol{q}) = 0$ defines a position space dividing surface, which separates the reactants, $s(\boldsymbol{q}) < 0$, from the products, $s(\boldsymbol{q}) > 0$. The operator describing flux onto products then becomes

$$\hat{F}_p = \sum_{\nu=1}^{f} \left\{ \delta(s(\hat{\boldsymbol{q}})) \frac{\partial s(\hat{\boldsymbol{q}})}{\partial q_\nu} \frac{\hat{p}_\nu}{2m_\nu} + \frac{\hat{p}_\nu}{2m_\nu} \delta(s(\hat{\boldsymbol{q}})) \frac{\partial s(\hat{\boldsymbol{q}})}{\partial q_\nu} \right\}. \tag{2.119}$$

Assuming the population on the upper adiabatic state is negligible and making the Born-Oppenheimer approximation one then arrives at the thermally symmetrised Born-Oppenheimer flux-side correlation function,

$$\bar{c}_{\text{BO-fs}}(t) = \text{tr}_\text{n} \left[e^{-\beta \hat{H}_\text{BO}/2} \hat{F}_p e^{-\beta \hat{H}_\text{BO}/2} e^{+i\hat{H}_\text{BO}t/\hbar} \hat{P}_p e^{-i\hat{H}_\text{BO}t/\hbar} \right], \tag{2.120}$$

or the Kubo-transformed version

$$\tilde{c}_{\text{BO-fs}}(t) = \frac{1}{\beta} \int_0^\beta \text{d}\lambda \, \text{tr}_\text{n} \left[e^{-(\beta-\lambda)\hat{H}_\text{BO}} \hat{F}_p e^{-\lambda \hat{H}_\text{BO}} e^{+i\hat{H}_\text{BO}t/\hbar} \hat{P}_p e^{-i\hat{H}_\text{BO}t/\hbar} \right], \tag{2.121}$$

where

$$\hat{H}_\text{BO} = \hat{T} + U_0(\hat{\boldsymbol{q}}) \tag{2.122}$$

is just the Born-Oppenheimer Hamiltonian for the lower adiabatic surface. We note that for the two state systems considered here $s(\boldsymbol{q}) = V_0(\boldsymbol{q}) - V_1(\boldsymbol{q})$ provides a natural choice of dividing surface, although as will be discussed later it may not always be the best choice.

Classical limit

The classical ($\beta \to 0$) limit of the Born-Oppenheimer flux-side correlation function is simply[121]

$$c_\text{fs}(t) = \frac{1}{(2\pi\hbar)^f} \int \text{d}^f \boldsymbol{p} \int \text{d}^f \boldsymbol{q} \, e^{-\beta H_\text{BO}(\boldsymbol{p},\boldsymbol{q})} \dot{\theta}(s(\boldsymbol{q}(0))) \theta(s(\boldsymbol{q}(t))), \tag{2.123}$$

where the classical flux through the dividing surface, $s(\boldsymbol{q}) = 0$, at $t = 0$ is given by

$$\dot{\theta}(s(\boldsymbol{q}(0))) = \delta(s(\boldsymbol{q})) \dot{s}(\boldsymbol{q}(0)) = \sum_{\nu=1}^{f} \delta(s(\boldsymbol{q})) \frac{\partial s(\boldsymbol{q})}{\partial q_\nu} \frac{p_\nu}{m_\nu}, \tag{2.124}$$

and the coordinates are evolved according to the classical equations of motion

$$\dot{q}_\nu = \frac{\partial H_{\mathrm{BO}}}{\partial p_\nu} \tag{2.125a}$$

$$\dot{p}_\nu = -\frac{\partial H_{\mathrm{BO}}}{\partial q_\nu}. \tag{2.125b}$$

The classical Born-Oppenheimer rate is then given by

$$k_{\mathrm{cl-BO}} = \lim_{t\to\infty} \frac{c_{\mathrm{fs}}(t)}{Q_r - \int_0^t c_{\mathrm{fs}}(t)\,\mathrm{d}t / \langle P_p \rangle_{\mathrm{cl}}}, \tag{2.126}$$

where the classical equilibrium population of products is

$$\langle P_p \rangle_{\mathrm{cl}} = \frac{\int \mathrm{d}^f \boldsymbol{p} \int \mathrm{d}^f \boldsymbol{q} e^{-\beta H_{\mathrm{BO}}(\boldsymbol{p},\boldsymbol{q})} \theta(s(\boldsymbol{q}))}{\int \mathrm{d}^f \boldsymbol{p} \int \mathrm{d}^f \boldsymbol{q} e^{-\beta H_{\mathrm{BO}}(\boldsymbol{p},\boldsymbol{q})}}, \tag{2.127}$$

and the classical reactant partition function is

$$Q_r = \frac{1}{(2\pi\hbar)^f} \int \mathrm{d}^f \boldsymbol{p} \int \mathrm{d}^f \boldsymbol{q} e^{-\beta H_{\mathrm{BO}}(\boldsymbol{p},\boldsymbol{q})} \theta(-s(\boldsymbol{q})). \tag{2.128}$$

Classical transition state theory

Starting from the exact expression for the classical Born-Oppenheimer rate given by Eq. 2.126 we can derive the classical transition state theory expression for the rate by considering the $t \to 0^+$ limit rather than the $t \to \infty$ limit of $k_{\text{cl-BO}}(t)$. To do this we note that

$$\begin{aligned} \lim_{t\to 0^+} \delta(s(\boldsymbol{q}(0)))\theta(s(\boldsymbol{q}(t))) &= \lim_{t\to 0^+} \delta(s(\boldsymbol{q}(0)))\theta(s(\boldsymbol{q}(0)) + \dot{s}(\boldsymbol{q}(0))t + \dots) \\ &= \delta(s(\boldsymbol{q}(0)))\theta(\dot{s}(\boldsymbol{q}(0))) \end{aligned} \tag{2.129}$$

and therefore the classical transition state theory rate is given by[121]

$$k_{\text{cl-TST}} = \lim_{t\to 0^+} \frac{c_{\mathrm{fs}}(t)}{Q_r} \tag{2.130}$$

with

$$\lim_{t\to 0^+} c_{\mathrm{fs}}(t) = \frac{1}{(2\pi\hbar)^f} \int \mathrm{d}^f \boldsymbol{p} \int \mathrm{d}^f \boldsymbol{q} e^{-\beta H_{\mathrm{BO}}(\boldsymbol{p},\boldsymbol{q})} \delta(s(\boldsymbol{q}))\dot{s}(\boldsymbol{q})\theta(\dot{s}(\boldsymbol{q})). \tag{2.131}$$

By considering the behaviour of a trajectory as it moves away from the dividing surface, one can see that the transition state theory approximation is equivalent to assuming that trajectories do not recross the dividing surface. Unlike the exact classical rate,

the transition state theory rate is therefore strongly dependent on the precise choice of dividing surface used to define the reactants and products. Despite this, transition state theory is a very useful and popular method because it does not require the propagation of classical trajectories and hence just depends on static equilibrium properties of the system. Furthermore, provided the dividing surface is chosen so that it minimises recrossing, the transition state theory rate can be very accurate.

2.3 Imaginary-time path-integral approaches to reaction rates

Unfortunately, for all but simple model problems, direct evaluation of the exact quantum rate is not possible due to the exponential scaling of the Hilbert space with the number of degrees of freedom. However, for static equilibrium properties, it is possible to avoid this exponential scaling by using imaginary-time path integrals,[10–12] which allow one to calculate quantum thermal expectation values using an extended classical phase space.[78,79] This approach is therefore linearly scaling and hence applicable to arbitrarily complex condensed phase systems. Whilst reaction rates are fundamentally a time dependent property, the success of classical transition state theory illustrates that they are often dominated by short time behaviour in a small region of phase space, which can be thought of as the bottleneck of the reaction. By generalising the ideas of classical transition state theory, one might therefore hope that imaginary-time path integrals would provide an accurate approach to calculating quantum mechanical reaction rates. This idea has been at the heart of the development of many approximate quantum rate theories,[13–16,82,143–148] and will form the basis for the development of non-adiabatic rate theories discussed in this thesis. This section begins by introducing the basic theory of imaginary-time path integrals, before discussing two important reaction rate theories which are applicable in the Born-Oppenheimer and golden-rule limits respectively, and will provide a foundation for the methods discussed in later chapters.

2.3.1 Background theory

For notational simplicity we begin by just considering a single surface Hamiltonian of the form

$$\hat{H} = \hat{T} + V(\hat{\boldsymbol{q}}) \tag{2.132}$$

where $\hat{T}$ is the kinetic energy operator

$$\hat{T} = \sum_{\nu=1}^{f} \frac{\hat{p}_\nu^2}{2m_\nu}, \tag{2.133}$$

and we will leave the generalisation to multiple electronic states to the following chapter. In order to derive the path-integral expression for a matrix element of the Boltzmann operator one begins by splitting the operator into n parts according to

$$\langle \boldsymbol{q}| \, e^{-\beta\hat{H}} \, |\boldsymbol{q}'\rangle = \langle \boldsymbol{q}| \, (e^{-\beta\hat{H}/n})^n \, |\boldsymbol{q}'\rangle \, . \tag{2.134}$$

Then by introducing $n-1$ identity operators, in the form

$$\hat{1} = \int \mathrm{d}^f \boldsymbol{q}_j |\boldsymbol{q}_j\rangle\langle\boldsymbol{q}_j|, \tag{2.135}$$

between each of the n terms, and defining $\beta_n = \beta/n$ we can write

$$\langle \boldsymbol{q}| \, e^{-\beta\hat{H}} \, |\boldsymbol{q}'\rangle = \int \mathrm{d}^f \boldsymbol{q}_1 \cdots \int \mathrm{d}^f \boldsymbol{q}_{n-1} \, \langle \boldsymbol{q}_0| \, e^{-\beta_n\hat{H}} \, |\boldsymbol{q}_1\rangle \ldots \langle \boldsymbol{q}_{n-1}| \, e^{-\beta_n\hat{H}} \, |\boldsymbol{q}_n\rangle \tag{2.136}$$

where we have defined $\boldsymbol{q} = \boldsymbol{q}_0$ and $\boldsymbol{q}' = \boldsymbol{q}_n$. The benefit of having separated the Boltzmann operator into n parts is that we can then use the symmetric Suzuki-Trotter expansion[149,150]

$$e^{-\beta_n\hat{H}} = e^{-\beta_n\hat{V}/2} e^{-\beta_n\hat{T}} e^{-\beta_n\hat{V}/2} + O(\beta_n^3) \tag{2.137}$$

in order to approximate the matrix elements as

$$\langle \boldsymbol{q}_j| \, e^{-\beta_n\hat{H}} \, |\boldsymbol{q}_{j+1}\rangle \simeq e^{-\beta_n V(\boldsymbol{q}_j)/2} e^{-\beta_n V(\boldsymbol{q}_{j+1})/2} \, \langle \boldsymbol{q}_j| \, e^{-\beta_n\hat{T}} \, |\boldsymbol{q}_{j+1}\rangle \, , \tag{2.138}$$

which can be made as accurate as necessary by simply increasing the value of n. In order to evaluate the matrix element of the kinetic energy term we introduce a resolution of the identity in terms of the momentum eigenstates,

$$\hat{1} = \int \mathrm{d}^f \boldsymbol{p}_j |\boldsymbol{p}_j\rangle\langle\boldsymbol{p}_j|, \tag{2.139}$$

to give

$$\begin{aligned}\langle \boldsymbol{q}_j | \, e^{-\beta_n \hat{T}} \, | \boldsymbol{q}_{j+1} \rangle &= \int \mathrm{d}^f \boldsymbol{p}_j \, \langle \boldsymbol{q}_j | \boldsymbol{p}_j \rangle \, \langle \boldsymbol{p}_j | \boldsymbol{q}_{j+1} \rangle \, e^{-\beta_n \sum_{\nu=1}^{f} p_{\nu,j}^2 / 2m_\nu} \\ &= \frac{1}{(2\pi\hbar)^f} \int \mathrm{d}^f \boldsymbol{p}_j \, e^{i \boldsymbol{p}_j \cdot (\boldsymbol{q}_j - \boldsymbol{q}_{j+1})/\hbar} e^{-\beta_n \sum_{\nu=1}^{f} p_{\nu,j}^2 / 2m_\nu}.\end{aligned} \tag{2.140}$$

This is a simple Gaussian integral which can be done by completing the square and shifting the contour of integration to give

$$\langle \boldsymbol{q}_j | \, e^{-\beta_n \hat{T}} \, | \boldsymbol{q}_{j+1} \rangle = \prod_{\nu=1}^{f} \sqrt{\frac{m_\nu}{2\pi\beta_n\hbar^2}} \exp\left(-\beta_n m_\nu \frac{(q_{\nu,j} - q_{\nu,j+1})^2}{2\beta_n^2\hbar^2} \right). \tag{2.141}$$

Defining $\omega_n = 1/\beta_n\hbar$ and reintroducing the integral over momentum we can then insert this into Eq. 2.138 to give

$$\langle \boldsymbol{q}_j | \, e^{-\beta_n \hat{H}} \, | \boldsymbol{q}_{j+1} \rangle \simeq \frac{1}{(2\pi\hbar)^f} \int \mathrm{d}^f \boldsymbol{p}_j e^{-\beta_n \left[\sum_{\nu=1}^{f} \left\{ p_{\nu,j}^2 / 2m_\nu + m_\nu \omega_n^2 (q_{\nu,j} - q_{\nu,j+1})^2 / 2 \right\} + \left(V(\boldsymbol{q}_j) + V(\boldsymbol{q}_{j+1}) \right)/2 \right]}, \tag{2.142}$$

which when combined with Eq. 2.136 gives a discrete path-integral approximation to $\langle \boldsymbol{q} | \, e^{-\beta \hat{H}} \, | \boldsymbol{q}' \rangle$, with an error of $O(\beta_n^2)$ (since we have made n approximations of $O(\beta_n^3)$).

The utility of this expression can be seen by considering the quantum partition function in terms of position eigenstates,

$$Q = \mathrm{tr}_\mathrm{n} \left[e^{-\beta \hat{H}} \right] = \int \mathrm{d}^f \boldsymbol{q} \, \langle \boldsymbol{q} | \, e^{-\beta \hat{H}} \, | \boldsymbol{q} \rangle \,, \tag{2.143}$$

which when combined with Eqs. 2.136 & 2.142 allows us to write

$$\mathrm{tr}_\mathrm{n} \left[e^{-\beta \hat{H}} \right] = \lim_{n \to \infty} \frac{1}{(2\pi\hbar)^{nf}} \int \mathrm{d}^{nf} \mathbf{q} \int \mathrm{d}^{nf} \mathbf{p} \, e^{-\beta_n H_n(\mathbf{p}, \mathbf{q})}, \tag{2.144}$$

where we have introduced the notation $\mathbf{q} = \{\boldsymbol{q}_0, \ldots, \boldsymbol{q}_{n-1}\}$ and similarly for the momentum $\mathbf{p} = \{\boldsymbol{p}_0, \ldots, \boldsymbol{p}_{n-1}\}$ and due to the cyclic permutation of the trace we have $\boldsymbol{q}_0 = \boldsymbol{q}_n$ and $\boldsymbol{p}_0 = \boldsymbol{p}_n$. The corresponding classical Hamiltonian is then given by

$$H_n(\mathbf{p}, \mathbf{q}) = h_n(\mathbf{p}, \mathbf{q}) + \sum_{j=1}^{n} V(\boldsymbol{q}_j) \tag{2.145}$$

where $h_n(\mathbf{p}, \mathbf{q})$ (the free ring-polymer Hamiltonian) is given by

$$h_n(\mathbf{p}, \mathbf{q}) = \sum_{j=1}^{n} \sum_{\nu=1}^{f} \left[\frac{p_{j,\nu}^2}{2m_\nu} + \frac{1}{2} m_\nu \omega_n^2 (q_{j+1,\nu} - q_{j,\nu})^2 \right]. \tag{2.146}$$

Considering the terms in this Hamiltonian we see that each set of position coordinates, $\boldsymbol{q}_j$, is connected to its neighbours via harmonic springs, and that, due to the cyclic symmetry of the trace, the n different sets of coordinates thus form a ring. This ring can be thought of as a classical ring-polymer, and each of the $\boldsymbol{q}_j$'s are often referred to as "beads" of the ring. We therefore see that the exact quantum partition function is "isomorphic" to the classical partition function of an n bead ring polymer in the limit that n goes to infinity.[78,79] The utility of this expression, however, is that for practical purposes in chemistry, the number of beads, n, needed to converge the calculation of properties of interest is typically on the order of 10-1000 and importantly is independent of the size of the system.[22] To understand why this is the case note that for a system to be in the high temperature limit it should be approximately true that $\beta\hbar\omega_{\max} \ll 1$, and correspondingly for the path-integral system one requires $\beta\hbar\omega_{\max} \ll n$, hence for $\hbar\omega_{\max} \simeq 2000\,\mathrm{cm}^{-1}$ and $k_\mathrm{B}T \simeq 200\,\mathrm{cm}^{-1}$ (i.e. near 300 K) we have $\beta\hbar\omega_{\max} \simeq 10$. With a naive implementation path-integral methods are thus typically 10-1000 times more expensive than the equivalent classical simulation, and, whilst they will not be a focus of this thesis, there now exist a large number of methods which can be used to significantly reduce this cost, allowing path integrals to be applied to large scale atomistic simulations.[151–157]

In general the calculation of even classical absolute partition functions is a very hard problem, fortunately however, one is usually only interested in calculating thermal expectation values,

$$\langle A \rangle = \frac{\mathrm{tr_n}\left[\hat{A}e^{-\beta\hat{H}}\right]}{\mathrm{tr_n}\left[e^{-\beta\hat{H}}\right]}. \tag{2.147}$$

Provided the operator of interest is simply a function of position, the path-integral expression for the thermal quantum expectation value is straightforward to obtain using,

$$\mathrm{tr_n}\left[A(\hat{\boldsymbol{q}})e^{-\beta\hat{H}}\right] = \int \mathrm{d}^f\boldsymbol{q} A(\boldsymbol{q}) \left\langle \boldsymbol{q}\right| e^{-\beta\hat{H}} \left|\boldsymbol{q}\right\rangle, \tag{2.148}$$

in conjunction with the path-integral expression for $\left\langle \boldsymbol{q}\right| e^{-\beta\hat{H}} \left|\boldsymbol{q}\right\rangle$ to give

$$\begin{aligned}\mathrm{tr_n}\left[A(\hat{\boldsymbol{q}})e^{-\beta\hat{H}}\right] &= \lim_{n\to\infty} \frac{1}{(2\pi\hbar)^{nf}} \int \mathrm{d}^{nf}\mathbf{q} \int \mathrm{d}^{nf}\mathbf{p}\, A(\boldsymbol{q}_0) e^{-\beta_n H_n(\mathbf{p},\mathbf{q})} \\ &= \lim_{n\to\infty} \frac{1}{(2\pi\hbar)^{nf}} \int \mathrm{d}^{nf}\mathbf{q} \int \mathrm{d}^{nf}\mathbf{p}\, \frac{1}{n}\sum_{j=1}^{n} A(\boldsymbol{q}_j) e^{-\beta_n H_n(\mathbf{p},\mathbf{q})},\end{aligned} \tag{2.149}$$

where in the second line we have made use of the cyclic symmetry of the ring polymer. We can therefore approximate the quantum expectation value as an expectation value in the ring-polymer ensemble as

$$\langle A(\hat{\boldsymbol{q}})\rangle \simeq \left\langle \frac{1}{n}\sum_{j=1}^{n} A(\boldsymbol{q}_j)\right\rangle = \frac{\int \mathrm{d}^{nf}\mathbf{q}\int \mathrm{d}^{nf}\mathbf{p}\,\frac{1}{n}\sum_{j=1}^{n} A(\boldsymbol{q}_j)e^{-\beta_n H_n(\mathbf{p},\mathbf{q})}}{\int \mathrm{d}^{nf}\mathbf{q}\int \mathrm{d}^{nf}\mathbf{p}\,e^{-\beta_n H_n(\mathbf{p},\mathbf{q})}}. \tag{2.150}$$

Hence the calculation of quantum thermal expectation values is equivalent to the calculation of a classical expectation value in the extended phase space of the ring polymer.

It will also be helpful at various points to work with continuous (rather than discrete) path-integral notation. To understand the connection between the continuous path-integral notation and the discrete form we recognise that, in the limit as $n \to \infty$ the ring-polymer beads can be considered as forming a continuous set of points on a cyclic path. We can thus define the corresponding path as a function of imaginary time, τ,* according to the relation[10–12]

$$\boldsymbol{q}(\tau_j) = \boldsymbol{q}(j\Delta\tau_n) = \boldsymbol{q}(j\beta_n\hbar) = \boldsymbol{q}_j, \tag{2.151}$$

such that $\boldsymbol{q}(0) = \boldsymbol{q}(\beta\hbar)$. With this definition we can also use the Riemann definition of an integral to relate a sum over beads to an integral around the ring according to

$$\int_0^{\beta\hbar} A(\boldsymbol{q}(\tau))\mathrm{d}\tau = \lim_{n\to\infty}\sum_{j=1}^{n} A(\boldsymbol{q}(\tau_j))\,\Delta\tau_n = \lim_{n\to\infty}\sum_{j=1}^{n} A(\boldsymbol{q}_j)\beta_n\hbar, \tag{2.152}$$

and the definition of a derivative to identify the imaginary-time velocity

$$\dot{\boldsymbol{q}}(\tau_j) = \lim_{n\to\infty}\frac{\boldsymbol{q}(\tau_j+\Delta\tau_n)-\boldsymbol{q}(\tau_j)}{\Delta\tau_n} = \lim_{n\to\infty}\frac{\boldsymbol{q}_{j+1}-\boldsymbol{q}_j}{\beta_n\hbar}. \tag{2.153}$$

Hence functions which depend on a finite fraction of the ring-polymer beads become functionals of the imaginary-time path in the infinite n limit. We can therefore view the discrete path-integral expressions given in Eq. 2.149 above as corresponding to

*Note the use of the term imaginary time is simply a reflection of the fact that the real time propagator is equivalent to the Boltzmann operator,

$$\langle \boldsymbol{q}|\, e^{-\beta\hat{H}}\,|\boldsymbol{q}'\rangle = \langle \boldsymbol{q}|\, e^{-it\hat{H}/\hbar}\,|\boldsymbol{q}'\rangle\,,$$

when $t = -i\beta\hbar$.

a functional integral over all possible cyclic paths in the limit as $n \to \infty$, which we write as[10–12]

$$\begin{aligned} \mathrm{tr_n}\left[A(\hat{\boldsymbol{q}})e^{-\beta\hat{H}}\right] &= \oint \mathcal{D}\boldsymbol{q}(\tau)\, A(\boldsymbol{q}(0))e^{-S[\boldsymbol{q}(\tau)]/\hbar} \\ &= \oint \mathcal{D}\boldsymbol{q}(\tau)\, A[\boldsymbol{q}(\tau)]e^{-S[\boldsymbol{q}(\tau)]/\hbar}. \end{aligned} \tag{2.154}$$

Here the position dependent part of the ring-polymer Hamiltonian has been replaced by the Euclidean action around the path

$$S[\boldsymbol{q}(\tau)] = \int_0^{\beta\hbar} \sum_{\nu=1}^{f} \frac{1}{2} m_\nu \dot{q}_\nu^2(\tau) + V(\boldsymbol{q}(\tau))\, \mathrm{d}\tau, \tag{2.155}$$

the average around the ring of A has been replaced by the functional

$$A[\boldsymbol{q}(\tau)] = \frac{1}{\beta\hbar}\int_0^{\beta\hbar} A(\boldsymbol{q}(\tau))\mathrm{d}\tau = \lim_{n\to\infty}\frac{1}{n}\sum_{j=1}^{n} A(\boldsymbol{q}_j), \tag{2.156}$$

and the kinetic energy of the beads has been integrated over to give the functional integration measure

$$\lim_{n\to\infty}\left(\prod_{\nu=1}^{f}\sqrt{\frac{m_\nu}{2\pi\beta_n\hbar^2}}\right)^n \mathrm{d}\boldsymbol{q}_1 \ldots \mathrm{d}\boldsymbol{q}_n \equiv \mathcal{D}\boldsymbol{q}(\tau), \tag{2.157}$$

with the integral sign, $\oint$, indicating that all paths form closed loops. We will not attempt to give a more rigorous mathematical foundation to the meaning of these continuous path-integral expressions, and for the purpose of this thesis the continuous path-integral expression can just be thought of as a convenient short hand for the $n \to \infty$ limit of the discrete path-integral expression. Note that as has been done here, throughout the thesis we will adopt the convention of using square brackets to denote a functional of the imaginary-time path, and brackets to denote a function.

Before we conclude this subsection we note that at various points it will be helpful to work, not in terms of the bead coordinates but instead, in the normal mode representation of the free ring polymer. The transformation to the normal mode representation can be written as,

$$\tilde{\boldsymbol{q}}_k = \sum_{j=1}^{n} C_{jk}\boldsymbol{q}_j \tag{2.158}$$

$$\tilde{\boldsymbol{p}}_k = \sum_{j=1}^{n} C_{jk} \boldsymbol{p}_j \tag{2.159}$$

where the $\tilde{\boldsymbol{q}}_k$ and $\tilde{\boldsymbol{p}}_k$ are the positions and momenta of the k^{th} normal mode. For an even number of beads, n, the transformation matrix is given by

$$C_{jk} = \begin{cases} \sqrt{1/n} & \text{if } k = 0 \\ \sqrt{2/n}\cos(2\pi jk/n) & \text{if } 1 \leq k \leq n/2 - 1 \\ \sqrt{1/n}(-1)^j & \text{if } k = n/2 \\ \sqrt{2/n}\sin(2\pi jk/n) & \text{if } n/2 + 1 \leq k \leq n - 1. \end{cases} \tag{2.160}$$

This transformation is useful as it diagonalises the spring term in the free ring-polymer Hamiltonian, such that

$$h_n(\mathbf{p}, \mathbf{q}) = \sum_{k=0}^{n-1} \sum_{\nu=1}^{f} \left[\frac{\tilde{p}_{k,\nu}^2}{2m_\nu} + \frac{1}{2} m_\nu \omega_k^2 \tilde{q}_{k,\nu}^2 \right], \tag{2.161}$$

where the normal mode frequencies ω_k are given by

$$\omega_k = 2\omega_n \sin(k\pi/n). \tag{2.162}$$

Note that $k = 0$ normal mode is proportional to the centroid of the ring polymer

$$\bar{\boldsymbol{q}} = \frac{1}{n} \sum_{j=1}^{n} \boldsymbol{q}_j = \frac{1}{\sqrt{n}} \tilde{\boldsymbol{q}}_0. \tag{2.163}$$

2.3.2 RPMD rate theory

Before we discuss ring-polymer molecular dynamics (RPMD) rate theory,[17–19] we first give a short discussion of Born-Oppenheimer (adiabatic) quantum transition state theories. The development of a quantum generalisation of classical transition state theory turns out to be a rather challenging task, and as such there are many different approaches that have been taken over the years. We will not have time to discuss all of these approaches here, but instead will focus on highlighting approaches most closely related to RPMD, which has become a "go to" way for including nuclear quantum effects in the calculation of chemical reaction rates, particularly in the condensed phase.[20,21,158,159]

The difficulty in generalising classical transition state theory can be understood by considering the behaviour of the flux-flux and flux-side correlation functions for the simple one dimensional Hamiltonian

$$\hat{H}_{\text{BO}} = \frac{\hat{p}^2}{2m} + V^{\ddagger}. \tag{2.164}$$

This is obviously a rather artificial problem, but it is helpful to illustrate the behaviour of the flux correlation function in the limit of a wide barrier where there is no tunnelling. In this case the thermally symmetrised flux-side correlation function can simply be evaluated to give

$$\bar{c}_{\mathrm{fs}}(t) = \frac{e^{-\beta V^{\ddagger}}}{2\pi\beta\hbar} \frac{2t/\beta\hbar}{\sqrt{1 + (2t/\beta\hbar)^2}} \tag{2.165}$$

and hence the thermally symmetrised flux-flux correlation function is given by

$$\bar{c}_{\mathrm{ff}}(t) = \frac{e^{-\beta V^{\ddagger}}}{4\pi[1 + (2t/\beta\hbar)^2]^{3/2}(\beta\hbar/2)^2}. \tag{2.166}$$

Importantly, we see that it is only in the limit as $\beta\hbar \to 0$ that the flux-side correlation function becomes discontinuous and hence, unlike in the classical limit, $\bar{c}_{\mathrm{fs}}(t)$ tends to zero as $t \to 0^+$. This means that finding a quantum generalisation of transition state theory is not straightforward, and as such there are a variety of different methods which attempt to generalise the ideas of classical transition state theory to include nuclear quantum effects. The difficulties associated with developing a quantum generalisation of transition state theory were recognised as far back as Wigner, who identified the lack of a configurational analogue of the classical Boltzmann factor, and the fact that the uncertainty principle precludes defining the velocity of the system when it is confined to the transition state as fundamental challenges to the development of a quantum transition state theory.[41,160,161] Of course Wigner did not know about path integrals, which, as we have just seen, certainly overcome the first of his barriers to the development of a quantum transition state theory.

Over the past 50 years there has been a steady development of imaginary-time path-integral methods for including the effects of nuclear tunnelling and zero-point energy on adiabatic reaction rates. The earliest of these was the thermal instanton approximation introduced by Miller in 1975, which uses a single imaginary-time trajectory to capture the effect of nuclear tunnelling.[143] Although this approximation can be very accurate, it is only applicable to problems in which the rate is dominated by a single tunnelling path.[144–146] It cannot be used for reactions in solution, in which the configuration space of the solvent leads to multiple contributing tunnelling paths. In order to overcome this problem, methods which use statistical sampling of imaginary-time paths (as described

above) are required. One of the earliest methods to do this was centroid density quantum transition state theory (QTST),[13] which uses the potential of mean force on the centroid of the imaginary-time path in place of the classical potential energy surface in classical TST. Whilst successful, QTST has two main drawbacks, firstly although it is very accurate for systems with symmetric barriers, QTST is much less accurate for asymmetric barriers in the deep tunnelling regime, and secondly for liquid systems the exponential sensitivity on the choice of dividing surface can lead to significant over estimation of the rate. RPMD rate theory, improves on QTST in both of these areas.[18,19] Firstly and perhaps most importantly, it is a fully dynamical method and like classical rate theory it gives a rate which is rigorously independent of dividing surface. Secondly, it is also more accurate than QTST in the deep tunnelling regime. Its accuracy in the deep tunnelling regime has been explained in terms of the short time accuracy of RPMD by showing that the optimum ring-polymer transition state theory is connected to the semi-classical instanton approximation, and more recently has been shown to correspond to the $t \to 0^+$ limit of a generalised quantum flux-side correlation function.[147,148] This short discussion has of course not been able to cover all of the path-integral methods for calculating reaction rates, in particular we have not discussed the quantum instanton approximation,[15,16] which uses a short time approximation to the flux-flux correlation function to approximate the rate, and to which we shall return in Chap. 4.

In the remainder of this section we give an overview of the theory behind the Born-Oppenheimer version of RPMD rate theory, leaving non-adiabatic generalisations to Chap. 3. RPMD is not only applicable to reaction rates, but gives a general prescription for approximating Kubo-transformed correlation functions[132] for operators which depend solely on position,

$$\tilde{c}_{AB}(t) = \frac{1}{\beta}\int_0^\beta \mathrm{d}\lambda \ \mathrm{tr_n}\left[e^{-(\beta-\lambda)\hat{H}}A(\hat{\boldsymbol{q}})\, e^{-\lambda\hat{H}}B(\hat{\boldsymbol{q}}(t))\right]. \tag{2.167}$$

The RPMD approximation to this Kubo-transformed correlation function is given by[17]

$$\tilde{c}_{AB}(t) \simeq \frac{1}{(2\pi\hbar)^{nf}}\int \mathrm{d}^{nf}\mathbf{p}\int \mathrm{d}^{nf}\mathbf{q} e^{-\beta_n H_n(\mathbf{p},\mathbf{q})}A_n(\mathbf{q}(0))B_n(\mathbf{q}(t)), \tag{2.168}$$

where $A_n(\mathbf{q})$ and $B_n(\mathbf{q})$ are just the average of the respective operator around the ring

$$A_n(\mathbf{q}) = \frac{1}{n}\sum_{j=1}^{n} A(\boldsymbol{q}_j) \tag{2.169}$$

and

$$B_n(\mathbf{q}) = \frac{1}{n}\sum_{j=1}^{n} B(\boldsymbol{q}_j). \tag{2.170}$$

For a system evolving solely on the ground adiabatic state, the ring-polymer Hamiltonian is given by,

$$H_n(\mathbf{p},\mathbf{q}) = h_n(\mathbf{p},\mathbf{q}) + \sum_{j=1}^{n} U_0(\boldsymbol{q}_j). \tag{2.171}$$

RPMD approximates the true quantum dynamics by simply evolving the ring-polymer according to the classical dynamics generated by $H_n(\mathbf{p},\mathbf{q})$, such that

$$\dot{q}_{j,\nu} = \frac{\partial H_n}{\partial p_{j,\nu}} \tag{2.172a}$$

$$\dot{p}_{j,\nu} = -\frac{\partial H_n}{\partial q_{j,\nu}}. \tag{2.172b}$$

Hence, RPMD is simply classical dynamics in the extended classical phase space of the ring polymer. It is straightforward to show, using the results from Sec. 2.3.1, that at $t = 0$ the correlation function gives the exact quantum result. For non-zero time it can be shown that for non-linear operators of position RPMD gives correlation functions with a leading error term of $O(t^3)$.[162,163]

One can use this prescription to directly approximate the Kubo-transformed side-side (and hence by differentiation also the flux-side) correlation functions.[18] However, as RPMD is just classical dynamics in the extended phase space of the ring polymer, the RPMD approximation to the rate is independent of the precise choice of dividing surface, provided that it separates reactants from products. One is therefore free to use a dividing surface, $s(\mathbf{q}) = 0$, which is an arbitrary function of the bead positions.[19] The n-bead RPMD approximation to the Born-Oppenheimer rate constant is therefore[119]

$$k_{\mathrm{BO}} \simeq k_{\mathrm{RPMD}} = \lim_{t\to\infty} \frac{c_{\mathrm{fs}}(t)}{Q_r - \int_0^t c_{\mathrm{fs}}(t)\,\mathrm{d}t/\langle P_p\rangle}, \tag{2.173}$$

where $c_{\mathrm{fs}}(t)$ is an RPMD flux-side correlation function

$$c_{\mathrm{fs}}(t) = \frac{1}{(2\pi\hbar)^{nf}} \int \mathrm{d}^{nf}\mathbf{p} \int \mathrm{d}^{nf}\mathbf{q} e^{-\beta_n H_n(\mathbf{p},\mathbf{q})} \dot{\theta}(s(\mathbf{q}))\theta(s(\mathbf{q}(t))), \tag{2.174}$$

the flux through the dividing surface $s(\mathbf{q}) = 0$ at time $t = 0$ is given by

$$\dot{\theta}(s(\mathbf{q})) = \delta(s(\mathbf{q})) \sum_{j=1}^{n} \sum_{\nu=1}^{f} \frac{\partial s(\mathbf{q})}{\partial q_{j,\nu}} \frac{p_{j,\nu}}{m_\nu}, \tag{2.175}$$

Q_r is the reactant and product partition function

$$Q_r = \frac{1}{(2\pi\hbar)^{nf}} \int \mathrm{d}^{nf}\mathbf{p} \int \mathrm{d}^{nf}\mathbf{q}\, e^{-\beta_n H_n(\mathbf{p},\mathbf{q})} \theta(-s(\mathbf{q})), \tag{2.176}$$

and $\langle P_p \rangle$ is the equilibrium population of the products

$$\langle P_p \rangle = \frac{\int \mathrm{d}^{nf}\mathbf{p} \int \mathrm{d}^{nf}\mathbf{q}\, e^{-\beta_n H_n(\mathbf{p},\mathbf{q})} \theta(s(\mathbf{q}))}{\int \mathrm{d}^{nf}\mathbf{p} \int \mathrm{d}^{nf}\mathbf{q}\, e^{-\beta_n H_n(\mathbf{p},\mathbf{q})}} \tag{2.177}$$

both of which of course RPMD gets exactly correct as they are just time independent properties.

Since the RPMD rate is just a classical rate in the extended phase space of the ring polymer, it can be calculated using any of the techniques that have been developed over the years for overcoming the rare event problem in the calculation of classical reaction rates, such as the Bennett-Chandler method.[120,164] RPMD rate theory also has a number of other desirable features, including the following:

1. It is a full-dimensional theory in which all degrees of freedom are treated on an equal footing.

2. It is parameter-free: a given reaction at a given temperature has a unique RPMD rate, which can be converged simply by increasing the number of ring-polymer beads.

3. The RPMD rate constant is independent of the choice of the dividing surface,[19] and it is rigorously consistent with the quantum mechanical equilibrium constant (i.e., the forward and reverse RPMD rates exactly satisfy the quantum mechanical detailed balance condition).

4. The theory becomes exact in the high-temperature (classical) limit, and it is also exact for the shallow tunnelling through a parabolic barrier.[18]

5. In the low temperature (deep tunnelling) regime, where the classical rate is too small by several orders of magnitude, the RPMD rate is typically within a factor of two of the exact quantum mechanical result. Moreover it provides an approximate bound on the exact result, because RPMD is known to underestimate the rates of symmetric reactions and to overestimate those of asymmetric reactions. This has been found to be the case for a variety of reactions for which the exact quantum mechanical rates could be computed for comparison,[165–168] and also established theoretically from the connection between RPMD rate theory and semiclassical instanton theory.[144]

No other electronically adiabatic reaction rate theory shares all of these desirable features and is also routinely applicable to the calculation of chemical reaction rates in complex (anharmonic and multidimensional) systems such as liquids.

2.3.3 Wolynes theory

Before we discuss non-adiabatic generalisations of RPMD in the next chapter, we first discuss a much older path-integral method applicable to the golden-rule limit, Wolynes theory.[82] The Wolynes theory approximation is different in spirit to RPMD rate theory, as it does not try to directly approximate the correlation function, but instead uses a steepest descent approximation to the integral in Eq. 2.89 resulting in an approximate expression which only depends on the correlation function and its derivatives at $t = 0$. The resulting expression can then be evaluated exactly using imaginary-time path integrals.

Starting from the exact expression for the golden-rule rate given in Eq. 2.89 Wolynes suggested evaluating the rate using the steepest descent (saddle point) approximation.[169] Noting that the correlation function, $c_{\mathrm{GR}}(t)$, is purely real on the imaginary axis, it follows that one expects there to be a saddle point of the function on this axis. Additionally due to the relation between $c_{\mathrm{GR}}(t)$ and the flux-flux correlation function, it is also expected that this will be the dominant saddle point, and hence using the saddle point approximation

to the integral about this point is expected to give a good approximation to the rate. The saddle point approximation can be understood by considering the cumulant expansion of the golden-rule correlation function

$$\ln\left(\frac{c_{\mathrm{GR}}(t+i\lambda\hbar)}{c_{\mathrm{GR}}(i\lambda\hbar)}\right) = \frac{i(\mu_{1,\lambda}-\epsilon)t}{\hbar} - \frac{\mu_{2,\lambda}t^2}{2\hbar^2} + \dots. \tag{2.178}$$

Since the exact rate is independent of the choice of λ we we are free to choose λ such that

$$\ln\left(\frac{c_{\mathrm{GR}}(t+i\lambda_{\mathrm{sp}}\hbar)}{c_{\mathrm{GR}}(i\lambda_{\mathrm{sp}}\hbar)}\right) = -\frac{\mu_{2,\lambda_{\mathrm{sp}}}t^2}{2\hbar^2} + \dots, \tag{2.179}$$

due to the analyticity of the function this point is therefore a minimum on the imaginary axis (i.e. in λ) and a maximum of the function along the real axis. Hence it is a saddle point of the function, with the saddle point condition given by $\mu_{1,\lambda_{\mathrm{sp}}} \equiv \beta F_{\mathrm{GR}}(\lambda_{\mathrm{sp}}) = \epsilon$. Close to this point along the real axis the function therefore looks approximately Gaussian, and hence, provided the function decays sufficiently quickly we may truncate this at second order to give

$$\begin{aligned} k_{\mathrm{GR}} \simeq k_{\mathrm{WT}} &= \frac{\Delta^2}{\hbar^2 Q_r}\int_{-\infty}^{\infty} c_{\mathrm{GR}}(i\lambda_{\mathrm{sp}}\hbar)\exp\left(-\frac{\mu_{2,\lambda_{\mathrm{sp}}}t^2}{2\hbar^2}\right)\mathrm{d}t \\ &= \frac{\Delta^2}{\hbar^2 Q_r}\int_{-\infty}^{\infty}\exp\left(-\frac{\mu_{2,\lambda_{\mathrm{sp}}}t^2}{2\hbar^2}\right)\mathrm{d}t\, e^{-\beta F_{\mathrm{GR}}(\lambda_{\mathrm{sp}})+\lambda_{\mathrm{sp}}\epsilon}. \end{aligned} \tag{2.180}$$

Performing the integral over time and using the fact that $-\beta F''_{\mathrm{GR}}(\lambda_{\mathrm{sp}}) = \mu_{2,\lambda_{\mathrm{sp}}}$ then gives the Wolynes expression for the rate[82]

$$k_{\mathrm{WT}} = \frac{\Delta^2}{Q_r\hbar}\sqrt{\frac{2\pi}{-\beta F''_{\mathrm{GR}}(\lambda_{\mathrm{sp}})}}e^{-\beta F_{\mathrm{GR}}(\lambda_{\mathrm{sp}})+\lambda_{\mathrm{sp}}\epsilon}. \tag{2.181}$$

More formally the steepest descent approximation is an asymptotic expansion of an integral of the form[169]

$$I(\alpha) = \int_C f(z)e^{\alpha g(z)}\mathrm{d}z \tag{2.182}$$

where $f(z)$ and $g(z)$ are complex analytic functions. The steepest descent approximation is (in the case of a single saddle point) defined as

$$I(\alpha) \sim f(z_0)\sqrt{\frac{2\pi}{\alpha|g''(z_0)|}}e^{\alpha g(z_0)} \quad \text{as} \quad \alpha \to \infty \tag{2.183}$$

where z_0 is the saddle point of $g(z_0)$ defined such that $g'(z_0) = 0$. As we will see in Appendix 2.A in the case of the spin-boson model the asymptotic parameter that we are assuming is very large in Wolynes theory is the Marcus reorganisation energy $\beta\Lambda$, hence Wolynes theory is expected to be most accurate in highly activated systems.

The advantage of the steepest descent approximation is that the resulting rate constant can be evaluated in a straightforward way using imaginary-time path-integral techniques. To see this we can begin by expanding the imaginary-time correlation function in the position eigenbasis as

$$e^{-\beta F_{\mathrm{GR}}(\lambda)} = \mathrm{tr_n}\left[e^{-(\beta-\lambda)\hat{H}_0} e^{-\lambda \hat{H}_1}\right] = \int \mathrm{d}^f \boldsymbol{q} \int \mathrm{d}^f \boldsymbol{q}' \, \langle \boldsymbol{q}| \, e^{-(\beta-\lambda)\hat{H}_0} \, |\boldsymbol{q}'\rangle \, \langle \boldsymbol{q}'| \, e^{-\lambda \hat{H}_1} \, |\boldsymbol{q}\rangle \,. \quad (2.184)$$

Then using an $n - l$ bead path-integral approximation to $\langle \boldsymbol{q}| \, e^{-(\beta-\lambda)\hat{H}_0} \, |\boldsymbol{q}'\rangle$ and an l bead path-integral approximation to $\langle \boldsymbol{q}'| \, e^{-\lambda \hat{H}_1} \, |\boldsymbol{q}\rangle$, where $l/n = \lambda_l/\beta$, gives

$$e^{-\beta F_{\mathrm{GR}}(\lambda_l)} \simeq \frac{1}{(2\pi\hbar)^{nf}} \int \mathrm{d}^{nf}\mathbf{p} \int \mathrm{d}^{nf}\mathbf{q} \; e^{-\beta_n H_n^{(l)}(\mathbf{p},\mathbf{q})}, \quad (2.185)$$

where the Hamiltonian is given by

$$H_n^{(l)}(\mathbf{p},\mathbf{q}) = h_n(\mathbf{p},\mathbf{q}) + \sum_{j=0}^{l} w_{jl} V_1(\boldsymbol{q}_j) + \sum_{j=l}^{n} w_{jl} V_0(\boldsymbol{q}_j) \quad (2.186)$$

in which the w_{jl} are just the usual trapezium rule weights

$$w_{jl} = \begin{cases} 0 & \text{if } j = l \text{ and } l \in \{0, n\} \\ \frac{1}{2} & \text{if } j \in \{0, l, n\} \text{ and } l \notin \{0, n\} \\ 1 & \text{otherwise.} \end{cases} \quad (2.187)$$

When $l = 0$, this Hamiltonian is simply the standard ring-polymer Hamiltonian on the reactant diabat, and when $l = n$ it is the ring-polymer Hamiltonian on the product diabat. But for intermediate values of l, beads $l + 1$ to $l - 1$ are on the reactant diabat, beads 1 to $l - 1$ are on the product diabat, and beads 0 and l are on the average of the two diabats, as illustrated for a specific case in Fig. 2.1.

Using the definitions of $F'_{\mathrm{GR}}(\lambda)$ and $F''_{\mathrm{GR}}(\lambda)$ given in Eqs. 2.101 and 2.104, it is straightforward to show that

$$-\beta F'_{\mathrm{GR}}(\lambda_l) = \left\langle V_-(\boldsymbol{q}_0) \right\rangle_{\lambda_l}, \quad (2.188)$$

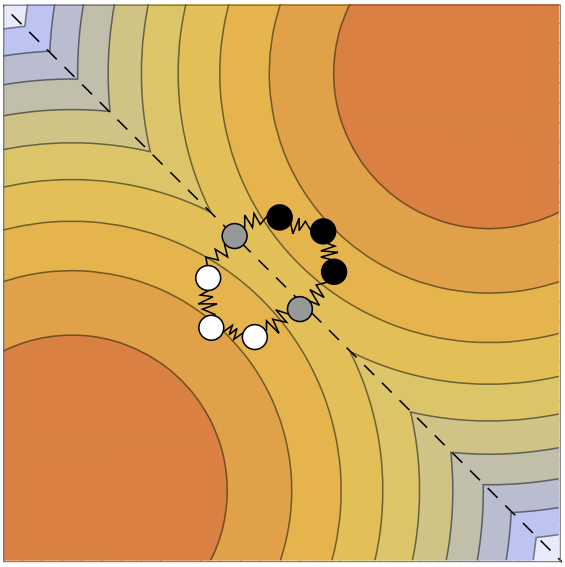

Figure 2.1: Schematic illustration of the ring-polymer Hamiltonian $H_n^{(l)}(\mathbf{p},\mathbf{q})$ in Eq. 2.186 for a problem with $f = 2$, $n = 8$, and $l = 4$. Beads 5 to 7 are on the reactant diabat (white), beads 1 to 3 are on the product diabat (black), and beads 0 and 4 are on the average of the two diabats (grey).

and

$$-\beta F''_{\mathrm{GR}}(\lambda_l) = \left\langle V_-(\boldsymbol{q}_0)V_-(\boldsymbol{q}_l)\right\rangle_{\lambda_l} - \left\langle V_-(\boldsymbol{q}_0)\right\rangle^2_{\lambda_l} \quad , \tag{2.189}$$

where

$$\langle A(\mathbf{q})\rangle_{\lambda_l} = \frac{\int \mathrm{d}^{nf}\mathbf{p} \int \mathrm{d}^{nf}\mathbf{q}\ e^{-\beta_n H_n^{(l)}(\mathbf{p},\mathbf{q})} A(\mathbf{q})}{\int \mathrm{d}^{nf}\mathbf{p} \int \mathrm{d}^{nf}\mathbf{q}\ e^{-\beta_n H_n^{(l)}(\mathbf{p},\mathbf{q})}}. \tag{2.190}$$

Hence, recognising that for unimolecular reactions the reactant partition function is given simply by,

$$Q_r = \mathrm{tr_n}\left[e^{-\beta\hat{H}_0}\right] = e^{-\beta F_{\mathrm{GR}}(0)} \tag{2.191}$$

it follows that the Wolynes expression for the rate can be evaluated in three stages:

1. Evaluate $F'_{\mathrm{GR}}(\lambda)$ at a series of different values of λ to find the saddle point λ_{sp}, which satisfies $\beta F'_{\mathrm{GR}}(\lambda_{\mathrm{sp}}) = \epsilon$.

2. Integrate
$$\int_0^{\lambda_{\mathrm{sp}}} F'_{\mathrm{GR}}(\lambda)\mathrm{d}\lambda = F_{\mathrm{GR}}(\lambda_{\mathrm{sp}}) - F_{\mathrm{GR}}(0), \tag{2.192}$$
to obtain the Boltzmann factor $e^{-\beta F_{\mathrm{GR}}(\lambda_{\mathrm{sp}})}/Q_r$.

3. Evaluate the prefactor using $F''_{\mathrm{GR}}(\lambda_{\mathrm{sp}})$.

The simplicity with which these quantities can be evaluated makes it straightforward to apply Wolynes theory to arbitrarily complex (anharmonic and multi-dimensional) condensed phase problems.[83–85] The theory exactly recovers Marcus theory in the high temperature limit for the spin-boson model, and it is known to be very accurate even at extremely low temperatures, where nuclear quantum effects can increase the rate over the Marcus theory prediction by several orders of magnitude.

As it does not involve any real time dynamics, Wolynes theory can be thought of as a kind of quantum transition state theory. Importantly however, in contrast to the adiabatic limit, the difficulty of choosing an optimum dividing surface is avoided in the non-adiabatic limit, as the bottleneck of the reaction is by definition the non-adiabatic transition from $|0\rangle$ to $|1\rangle$. This is reflected in the classical limit, where the golden-rule rate (Eq. 2.105) is given exactly by a transition state theory like expression (i.e. it just depends on a time independent configurational average). Note however that although Wolynes theory can be thought of as a kind of quantum transition state theory (in the sense that it does not involve real time), it does not in general recover the classical golden-rule rate in the high temperature limit.[170]

One might hope that it was also possible to develop an exact transition state theory expression for the quantum rate, and Appendix 2.B discusses this idea in more detail. Unfortunately in the quantum case the transition state dividing surface involves the kinetic as well as potential energy and hence an exact *purely configurational* imaginary-time transition state theory is not possible. An alternative approach to Wolynes theory would therefore be to try and develop an approximate imaginary-time transition state theory, which *does* reduce to the classical golden-rule expression, by finding a purely configurational approximation to the exact quantum golden-rule expression. We will return to this idea in Chaps. 7 and 8.

Note that just as with the adiabatic case, the discrete path-integral expressions can be written in continuous form as

$$\begin{aligned} e^{-\beta F_{\mathrm{GR}}(\lambda)} &= \mathrm{tr}_{\mathrm{n}}\left[e^{-(\beta-\lambda)\hat{H}_0}e^{-\lambda\hat{H}_1}\right] \\ &= \oint \mathcal{D}\boldsymbol{q}(\tau)\, e^{-S^{(\lambda)}[\boldsymbol{q}(\tau)]/\hbar} \end{aligned} \tag{2.193}$$

where now the Euclidean action is given by

$$S^{(\lambda)}[\boldsymbol{q}(\tau)] = S_0^{(\lambda)}[\boldsymbol{q}(\tau)] + S_1^{(\lambda)}[\boldsymbol{q}(\tau)] \tag{2.194}$$

with

$$S_0^{(\lambda)}[\boldsymbol{q}(\tau)] = \int_{\lambda\hbar}^{\beta\hbar} \sum_{\nu=1}^{f} \frac{1}{2} m_\nu \dot{q}_\nu^2(\tau) + V_0(\boldsymbol{q}(\tau)) \mathrm{d}\tau \tag{2.195}$$

and

$$S_1^{(\lambda)}[\boldsymbol{q}(\tau)] = \int_{0}^{\lambda\hbar} \sum_{\nu=1}^{f} \frac{1}{2} m_\nu \dot{q}_\nu^2(\tau) + V_1(\boldsymbol{q}(\tau)) \mathrm{d}\tau. \tag{2.196}$$

Equally we can also therefore write the derivatives of the free energy $F_{\mathrm{GR}}(\lambda)$ as

$$-\beta F'_{\mathrm{GR}}(\lambda) = \left\langle V_-(\boldsymbol{q}(0)) \right\rangle_\lambda \tag{2.197}$$

and

$$-\beta F''_{\mathrm{GR}}(\lambda) = \left\langle V_-(\boldsymbol{q}(0)) V_-(\boldsymbol{q}(\lambda\hbar)) \right\rangle_\lambda - \left\langle V_-(\boldsymbol{q}(0)) \right\rangle_\lambda \left\langle V_-(\boldsymbol{q}(\lambda\hbar)) \right\rangle_\lambda \tag{2.198}$$

where now the expectation value is defined as

$$\langle A[\boldsymbol{q}(\tau)] \rangle_\lambda = \frac{\oint \mathcal{D}\boldsymbol{q}(\tau) e^{-S^{(\lambda)}[\boldsymbol{q}(\tau)]/\hbar} A[\boldsymbol{q}(\tau)]}{\oint \mathcal{D}\boldsymbol{q}(\tau) e^{-S^{(\lambda)}[\boldsymbol{q}(\tau)]/\hbar}}. \tag{2.199}$$

We introduce these expressions now as we will make use of them at various points in later chapters to help simplify the presentation of other imaginary-time path-integral methods in the golden-rule limit.

Finally before we conclude the chapter, for completeness we note that it is relatively straightforward to generalise the Wolynes approximation to systems with non-constant diabatic coupling. This can be achieved by simply rewriting the exact rate as

$$k_{\mathrm{GR}} = \frac{1}{Q_r \hbar^2} \int_{-\infty}^{\infty} \frac{\mathrm{tr_n}\left[e^{-(\beta-\lambda+it/\hbar)\hat{H}_0} \Delta(\hat{\boldsymbol{q}}) e^{-(\lambda-it/\hbar)\hat{H}_1} \Delta(\hat{\boldsymbol{q}}) \right]}{\mathrm{tr_n}\left[e^{-(\beta-\lambda+it/\hbar)\hat{H}_0} e^{-(\lambda-it/\hbar)\hat{H}_1} \right]} c_{\mathrm{GR}}(t + i\lambda\hbar) \mathrm{d}t \tag{2.200}$$

and applying the steepest descent approximation, as in Eq. 2.183, identifying $c_{\mathrm{GR}}(t + i\lambda\hbar)$ with $e^{\alpha g(z)}$ to give

$$k_{\mathrm{WT}} = \frac{\left\langle \Delta(\boldsymbol{q}(0)) \Delta(\boldsymbol{q}(\lambda_{\mathrm{sp}}\hbar)) \right\rangle_{\lambda_{\mathrm{sp}}}}{Q_r \hbar} \sqrt{\frac{2\pi}{-\beta F''_{\mathrm{GR}}(\lambda_{\mathrm{sp}})}} e^{-\beta F_{\mathrm{GR}}(\lambda_{\mathrm{sp}}) + \lambda_{\mathrm{sp}}\epsilon}. \tag{2.201}$$

Physically this is equivalent to assuming that the time dependence of $\Delta(\boldsymbol{q})$ is slow compared to the transient behaviour of $c_{\mathrm{GR}}(t + i\lambda_{\mathrm{sp}}\hbar)$.[171,172] Alternatively one can of course include the coupling in the cumulant expansion, which then requires the calculation of additional terms involving the time derivatives of the coupling. As we will only study systems in this thesis for which the coupling is taken to be a constant, i.e. satisfying the Condon approximation,[173] we shall not consider this matter in any more detail.

2.A Appendix: Exact rate for the spin-boson model in the golden-rule limit

The spin-boson model assumes that from the perspective of the electron transfer the nuclear potentials in both charge transfer states can be modelled as being purely harmonic with the same frequencies in both states,[53,54,59,60,173]

$$V_0(\boldsymbol{q}) = \sum_{\nu=1}^{f} \frac{1}{2} m\omega_\nu^2 \left(q_\nu + \frac{c_\nu}{m\omega_\nu^2} \right)^2 \tag{2.202a}$$

$$V_1(\boldsymbol{q}) = \sum_{\nu=1}^{f} \frac{1}{2} m\omega_\nu^2 \left(q_\nu - \frac{c_\nu}{m\omega_\nu^2} \right)^2 . \tag{2.202b}$$

To derive the exact expression for the rate in this system we note that

$$\mathrm{tr_n}\left[e^{-(\beta-\lambda)\hat{H}_0} e^{-\lambda\hat{H}_1} \right] = \prod_{\nu=1}^{f} \mathrm{tr}_\nu \left[e^{-(\beta-\lambda)\hat{H}_{0,\nu}} e^{-\lambda\hat{H}_{1,\nu}} \right] \tag{2.203}$$

where $\mathrm{tr}_\nu[\dots]$ denotes a trace over the ν^{th} nuclear degree of freedom and

$$\hat{H}_{i,\nu} = \frac{\hat{p}_\nu^2}{2m_\nu} + V_{i,\nu}(\hat{q}_\nu) \tag{2.204}$$

with

$$V_{0,\nu}(q_\nu) = \frac{1}{2} m\omega_\nu^2 (q_\nu + \xi_\nu)^2 \tag{2.205a}$$

$$V_{1,\nu}(q_\nu) = \frac{1}{2} m\omega_\nu^2 (q_\nu - \xi_\nu)^2, \tag{2.205b}$$

in which $m\omega_\nu^2\xi_\nu = c_\nu$. Hence we need only consider a single degree of freedom, with the multidimensional case a simple generalisation. Hence for notational simplicity in the

following we consider first just a one dimensional model $f = 1$ with the potentials

$$V_0(q) = \frac{1}{2}m\omega^2(q+\xi)^2 \tag{2.206a}$$

$$V_1(q) = \frac{1}{2}m\omega^2(q-\xi)^2. \tag{2.206b}$$

We begin by writing

$$\mathrm{tr_n}\left[e^{-(\beta-\lambda)\hat{H}_0}e^{-\lambda\hat{H}_1}\right] = \int_{-\infty}^{\infty}\mathrm{d}q\int_{-\infty}^{\infty}\mathrm{d}q'\,\langle q|\,e^{-(\beta-\lambda)\hat{H}_0}\,|q'\rangle\,\langle q'|\,e^{-\lambda\hat{H}_1}\,|q\rangle \tag{2.207}$$

and make use of the imaginary-time propagator for a harmonic oscillator[12] which gives

$$\langle q|\,e^{-(\beta-\lambda)\hat{H}_0}\,|q'\rangle = \sqrt{\frac{m\omega}{2\pi\hbar\sinh((\beta-\lambda)\hbar\omega)}}\exp\left(g(q,q')\right) \tag{2.208}$$

where

$$g(q,q') = \frac{-m\omega\left(((q+\xi)^2+(q'+\xi)^2)\cosh((\beta-\lambda)\hbar\omega)-2(q+\xi)(q'+\xi)\right)}{2\hbar\sinh((\beta-\lambda)\hbar\omega)} \tag{2.209}$$

and

$$\langle q'|\,e^{-\lambda\hat{H}_1}\,|q\rangle = \sqrt{\frac{m\omega}{2\pi\hbar\sinh(\lambda\hbar\omega)}}\exp\left(h(q,q')\right) \tag{2.210}$$

where

$$h(q,q') = \frac{-m\omega\left(((q-\xi)^2+(q'-\xi)^2)\cosh(\lambda\hbar\omega)-2(q-\xi)(q'-\xi)\right)}{2\hbar\sinh(\lambda\hbar\omega)}. \tag{2.211}$$

Performing the Gaussian integrals over q and q', followed by some tedious algebra one arrives at the following expression for the correlation function on the imaginary axis

$$\mathrm{tr_n}\left[e^{-(\beta-\lambda)\hat{H}_0}e^{-\lambda\hat{H}_1}\right] = \frac{\exp\left(\frac{-2m\xi^2\omega}{\hbar}\left[\frac{1-\cosh(\lambda\hbar\omega)}{\tanh(\beta\hbar\omega/2)}+\sinh(\lambda\hbar\omega)\right]\right)}{2\sinh(\beta\hbar\omega/2)}. \tag{2.212}$$

This can then be straightforwardly analytically continued ($\lambda = -it/\hbar$) to give

$$\mathrm{tr_n}\left[e^{-\beta\hat{H}_0}e^{-it\hat{H}_0/\hbar}e^{it\hat{H}_1/\hbar}\right] = \frac{\exp\left(\frac{-2m\xi^2\omega}{\hbar}\left[\frac{1-\cos(\omega t)}{\tanh(\beta\hbar\omega/2)}-i\sin(\omega t)\right]\right)}{2\sinh(\beta\hbar\omega/2)}. \tag{2.213}$$

Hence generalising to the full multidimensional case gives

$$\mathrm{tr_n}\left[e^{-\beta\hat{H}_0}e^{-it\hat{H}_0/\hbar}e^{it\hat{H}_1/\hbar}\right] = \frac{\exp\left(\sum_{\nu=1}^{f}\frac{-2c_\nu^2}{m\omega_\nu^3\hbar}\left[\frac{1-\cos(\omega_\nu t)}{\tanh(\beta\hbar\omega_\nu/2)}-i\sin(\omega_\nu t)\right]\right)}{\prod_{\nu=1}^{f}2\sinh(\beta\hbar\omega_\nu/2)}, \tag{2.214}$$

where we have also replaced the displacements, ξ_ν, with the couplings, c_ν using the identity $m\omega_\nu^2\xi_\nu = c_\nu$.

Dividing by the reactant partition function,

$$Q_r = \frac{1}{\prod_{\nu=1}^{f} 2\sinh(\beta\hbar\omega_\nu/2)}, \tag{2.215}$$

and introducing the spectral density

$$J(\omega) = \frac{\pi}{2}\sum_{\nu=1}^{f}\frac{c_\nu^2}{m\omega_\nu}\delta(\omega-\omega_\nu). \tag{2.216}$$

we can rewrite the exact correlation function for the spin-boson model in the form[53,54,59,60]

$$\frac{c_{\mathrm{GR}}(t)}{Q_r} = \exp\left(-i\epsilon t/\hbar - \phi(t)/\hbar\right) \tag{2.217}$$

where

$$\phi(t) = \frac{4}{\pi}\int_0^\infty \frac{J(\omega)}{\omega^2}\left[\frac{1-\cos(\omega t)}{\tanh(\beta\hbar\omega/2)} - i\sin(\omega t)\right]\mathrm{d}\omega. \tag{2.218}$$

It is therefore straightforward to obtain the exact golden-rule rate for the spin-boson model by simply numerically integrating the correlation function. Note that to improve the numerical accuracy it is often helpful to shift the contour of integration to pass through the saddle point $t = i\lambda_{\mathrm{sp}}\hbar$.

In the high temperature limit ($\beta\hbar \to 0$) the exact golden-rule rate for the spin-boson model simply reduces to the Marcus theory expression Eq. 2.114. To see this we begin by defining the Marcus theory reorganisation energy

$$\Lambda = \frac{4}{\pi}\int_0^\infty \frac{J(\omega)}{\omega}\mathrm{d}\omega. \tag{2.219}$$

Then making the substitution $x = \beta\hbar\omega$

$$\frac{c_{\mathrm{GR}}(t)}{Q_r} = \exp\left(-i\epsilon t/\hbar - \frac{4\beta}{\pi}\int_0^\infty \frac{J(x/\beta\hbar)}{x^2}\left[\frac{1-\cos\left(xt/\beta\hbar\right)}{\tanh(x/2)} - i\sin\left(xt/\beta\hbar\right)\right]\mathrm{d}x\right). \tag{2.220}$$

and using the fact that

$$\lim_{\beta\hbar\to 0}\frac{J(x/\beta\hbar)}{x} = \frac{\pi\Lambda}{4}\delta(x) \tag{2.221}$$

along with the Laurent expansion

$$\coth(x/2) = \frac{2}{x} + \frac{x}{6} + O(x^3), \tag{2.222}$$

we can simplify the correlation function in the high temperature limit as

$$\frac{c_{\mathrm{GR}}(t)}{Q_r} = \exp\left(-i\epsilon t/\hbar - \beta\Lambda\left(\frac{t^2}{\beta^2\hbar^2} - i\frac{t}{\beta\hbar}\right)\right). \tag{2.223}$$

Integrating this over time then gives the Marcus expression for the rate[46–49]

$$k_{\mathrm{MT}} = \frac{\Delta^2}{\hbar}\sqrt{\frac{\pi\beta}{\Lambda}}e^{-\beta(\Lambda-\epsilon)^2/4\Lambda}. \tag{2.224}$$

Before we conclude this section we briefly comment on the accuracy of the saddle point approximation made in Wolynes theory. Defining the normalised spectral density as

$$\frac{\tilde{J}(\omega)}{\omega} = \frac{J(\omega)}{\Lambda\omega} \tag{2.225}$$

and the relative driving force as $\tilde{\epsilon} = \epsilon/\Lambda$, we can rewrite the correlation function as

$$\frac{c_{\mathrm{GR}}(t)}{Q_r} = \exp\left(\beta\Lambda\left(-i\tilde{\epsilon}t/\beta\hbar - \tilde{\phi}(t)/\beta\hbar\right)\right) \tag{2.226}$$

where

$$\tilde{\phi}(t) = \frac{4}{\pi}\int_0^\infty \frac{\tilde{J}(\omega)}{\omega^2}\left[\frac{1-\cos(\omega t)}{\tanh(\beta\hbar\omega/2)} - i\sin(\omega t)\right]\mathrm{d}\omega. \tag{2.227}$$

Hence we see that for the spin-boson model Wolynes theory is asymptotic to the exact rate as $\beta\Lambda \to \infty$.

2.B Appendix: Exact path-integral golden-rule transition state theory

In this appendix we explore the formal development of a path-integral generalisation of the classical golden-rule expression for the rate given in Eq. 2.108. The aim is to derive a path-integral expression for the exact golden-rule rate, which, analogous to the classical theory, has the form of a transition state theory. None of the remaining chapters relies on the theory developed in this section. The resulting theory is also not directly applicable to realistic simulations, and hence is therefore at the present time of purely theoretical interest as an illustration of the challenges associated with the development of a practical path-integral rate theory in the golden-rule limit. However, we note that the theory developed here is similar both in spirit and in form to the theories discussed

in Chap. 7, which at present have no first principles derivation. Throughout this section we shall employ the Condon approximation, assuming that Δ is constant.

We begin by considering the generalisation of the exact path-integral expression for the correlation function on the imaginary axis (Eq. 2.185) to a general complex time,

$$\mathrm{tr_n}\left[e^{-\tau_0\hat{H}_0/\hbar}e^{-\tau_1\hat{H}_1/\hbar}\right] = \lim_{n\to\infty}\frac{1}{(2\pi\hbar)^{nf}}\int \mathrm{d}^{nf}\mathbf{p}\int \mathrm{d}^{nf}\mathbf{q}e^{-S^{(l)}_{0,n}(\mathbf{p},\mathbf{q},\tau_0)/\hbar - S^{(l)}_{1,n}(\mathbf{p},\mathbf{q},\tau_1)/\hbar} \tag{2.228}$$

where

$$S^{(l)}_{0,n}(\mathbf{p},\mathbf{q},\tau_0) = \frac{\tau_0}{n-l}\sum_{j=l}^{n-1}\left(\sum_{\nu=1}^{f}\left[\frac{p^2_{j,\nu}}{2m_\nu} + \frac{m_\nu(q_{j+1,\nu}-q_{j,\nu})^2}{2\tau_0^2/(n-l)^2}\right] + \frac{V_0(\boldsymbol{q}_{j+1})+V_0(\boldsymbol{q}_j)}{2}\right) \tag{2.229}$$

and

$$S^{(l)}_{1,n}(\mathbf{p},\mathbf{q},\tau_1) = \frac{\tau_1}{l}\sum_{j=0}^{l-1}\left(\sum_{\nu=1}^{f}\left[\frac{p^2_{j,\nu}}{2m_\nu} + \frac{m_\nu(q_{j+1,\nu}-q_{j,\nu})^2}{2\tau_1^2/l^2}\right] + \frac{V_1(\boldsymbol{q}_{j+1})+V_1(\boldsymbol{q}_j)}{2}\right) \tag{2.230}$$

with $l/n = \mathrm{Re}(\tau_1/(\tau_0+\tau_1))$ and $\tau_0+\tau_1 = \beta\hbar$. Now making use of the relations

$$\frac{1}{\tau_0/(n-l)} = \frac{1}{\beta_n\hbar + it/(n-l)} = \frac{1}{\beta_n\hbar}\left(1 - \frac{it}{(n-l)\beta_n\hbar} - \frac{t^2/(n-l)^2\beta_n^2\hbar^2}{1+it/(n-l)\beta_n\hbar}\right) \tag{2.231}$$

and

$$\frac{1}{\tau_1/l} = \frac{1}{\beta_n\hbar - it/l} = \frac{1}{\beta_n\hbar}\left(1 + \frac{it}{l\beta_n\hbar} - \frac{t^2/l^2\beta_n^2\hbar^2}{1-it/l\beta_n\hbar}\right) \tag{2.232}$$

it follows that we can separate the exponent into those terms which involve real time and those which do not as,

$$S^{(l)}_{0,n}(\mathbf{p},\mathbf{q},\tau_0)/\hbar = \beta_n H^{(l)}_{0,n}(\mathbf{p},\mathbf{q}) + \frac{it}{(n-l)\hbar}E^{(l)}_{0,n}(\mathbf{p},\mathbf{q}) - \frac{t^2/(n-l)^2\hbar^2}{\beta_n + it/(n-l)\hbar}W^{(l)}_{0,n}(\mathbf{p},\mathbf{q}) \tag{2.233}$$

and

$$S^{(l)}_{1,n}(\mathbf{p},\mathbf{q},\tau_1)/\hbar = \beta_n H^{(l)}_{1,n}(\mathbf{p},\mathbf{q}) - \frac{it}{l\hbar}E^{(l)}_{1,n}(\mathbf{p},\mathbf{q}) - \frac{t^2/l^2\hbar^2}{\beta_n - it/l\hbar}W^{(l)}_{1,n}(\mathbf{p},\mathbf{q}). \tag{2.234}$$

Here, $H^{(l)}_n(\mathbf{p},\mathbf{q}) = H^{(l)}_{0,n}(\mathbf{p},\mathbf{q}) + H^{(l)}_{1,n}(\mathbf{p},\mathbf{q})$ is just the Hamiltonian from Wolynes theory (Eq. 2.186) separated into contributions from state $|0\rangle$,

$$H^{(l)}_{0,n}(\mathbf{p},\mathbf{q}) = \sum_{j=l}^{n-1}\left(\sum_{\nu=1}^{f}\left[\frac{p^2_{j,\nu}}{2m_\nu} + \frac{m_\nu\omega_n^2(q_{j+1,\nu}-q_{j,\nu})^2}{2}\right] + \frac{V_0(\boldsymbol{q}_{j+1})+V_0(\boldsymbol{q}_j)}{2}\right), \tag{2.235}$$

and state $|1\rangle$,

$$H^{(l)}_{1,n}(\mathbf{p},\mathbf{q}) = \sum_{j=0}^{l-1}\left(\sum_{\nu=1}^{f}\left[\frac{p^2_{j,\nu}}{2m_\nu} + \frac{m_\nu\omega_n^2(q_{j+1,\nu}-q_{j,\nu})^2}{2}\right] + \frac{V_1(\boldsymbol{q}_{j+1}) + V_1(\boldsymbol{q}_j)}{2}\right), \tag{2.236}$$

with the $W^{(l)}_{j,n}(\mathbf{p},\mathbf{q})$ terms corresponding to the contributions to the spring energy from beads associated with state $|0\rangle$,

$$W^{(l)}_{0,n}(\mathbf{p},\mathbf{q}) = \sum_{j=l}^{n-1}\sum_{\nu=1}^{f}\frac{m_\nu\omega_n^2(q_{j+1,\nu}-q_{j,\nu})^2}{2}, \tag{2.237}$$

and state $|1\rangle$

$$W^{(l)}_{1,n}(\mathbf{p},\mathbf{q}) = \sum_{j=0}^{l-1}\sum_{\nu=1}^{f}\frac{m_\nu\omega_n^2(q_{j+1,\nu}-q_{j,\nu})^2}{2}. \tag{2.238}$$

The remaining terms are analogous to the primitive energy estimator,[12] with the spring terms having the opposite sign to the ring-polymer Hamiltonian

$$E^{(l)}_{0,n}(\mathbf{p},\mathbf{q}) = H^{(l)}_{0,n}(\mathbf{p},\mathbf{q}) - 2W^{(l)}_{0,n}(\mathbf{p},\mathbf{q}) \tag{2.239}$$

$$E^{(l)}_{1,n}(\mathbf{p},\mathbf{q}) = H^{(l)}_{1,n}(\mathbf{p},\mathbf{q}) - 2W^{(l)}_{1,n}(\mathbf{p},\mathbf{q}). \tag{2.240}$$

Now we make use of the integral identity

$$\int_{-\infty}^{\infty} e^{-(a+ic)x^2+bx}\mathrm{d}x = \int_{-\infty}^{\infty} e^{-(a+ic)x^2}e^{\frac{b^2}{4(a+ic)}}\mathrm{d}x \tag{2.241}$$

for $a, b, c \in \mathbb{R}$ and $a > 0$, which will allow us to rewrite the exponent as a solely linear function of time. This is achieved by recognising that

$$\begin{aligned}\int_{-\infty}^{\infty}\mathrm{d}p_{j,\nu}\exp\left(-\left(\beta_n + \frac{it}{(n-l)\hbar}\right)\frac{p^2_{j,\nu}}{2m_\nu} + \frac{t^2/(n-l)^2\hbar^2}{\beta_n + it/(n-l)\hbar}\frac{m_\nu\omega_n^2(q_{j+1,\nu}-q_{j,\nu})^2}{2}\right)\\ = \int_{-\infty}^{\infty}\mathrm{d}p_{j,\nu}\exp\left(-\left(\beta_n + \frac{it}{(n-l)\hbar}\right)\frac{p^2_{j,\nu}}{2m_\nu} + \frac{t}{(n-l)\hbar}p_{j,\nu}\omega_n(q_{j+1,\nu}-q_{j,\nu})\right)\end{aligned} \tag{2.242}$$

and

$$\begin{aligned}\int_{-\infty}^{\infty}\mathrm{d}p_{j,\nu}\exp\left(-\left(\beta_n - \frac{it}{l\hbar}\right)\frac{p^2_{j,\nu}}{2m_\nu} + \frac{t^2/l^2\hbar^2}{\beta_n - it/l\hbar}\frac{m_\nu\omega_n^2(q_{j+1,\nu}-q_{j,\nu})^2}{2}\right)\\ = \int_{-\infty}^{\infty}\mathrm{d}p_{j,\nu}\exp\left(-\left(\beta_n - \frac{it}{l\hbar}\right)\frac{p^2_{j,\nu}}{2m_\nu} - \frac{t}{l\hbar}p_{j,\nu}\omega_n(q_{j+1,\nu}-q_{j,\nu})\right),\end{aligned} \tag{2.243}$$

such that we can replace the time dependent spring terms in Eqs. 2.233 and 2.234 with

$$\frac{t^2/(n-l)^2\hbar^2}{\beta_n + it/(n-l)\hbar} W^{(l)}_{0,n}(\mathbf{p},\mathbf{q}) \to \frac{t}{(n-l)\hbar} \sum_{j=l}^{n-1} \sum_{\nu=1}^{f} p_{j,\nu}\omega_n(q_{j+1,\nu} - q_{j,\nu}) \tag{2.244}$$

and

$$\frac{t^2/l^2\hbar^2}{\beta_n - it/l\hbar} W^{(l)}_{1,n}(\mathbf{p},\mathbf{q}) \to -\frac{t}{l\hbar} \sum_{j=0}^{l-1} \sum_{\nu=1}^{f} p_{j,\nu}\omega_n(q_{j+1,\nu} - q_{j,\nu}). \tag{2.245}$$

It follows that we can write

$$\mathrm{tr_n}\left[e^{-\tau_0\hat{H}_0/\hbar} e^{-\tau_1\hat{H}_1/\hbar}\right] = \lim_{n\to\infty} \frac{1}{(2\pi\hbar)^{nf}} \int \mathrm{d}^{nf}\mathbf{p} \int \mathrm{d}^{nf}\mathbf{q} e^{-\tilde{S}^{(l)}_{0,n}(\mathbf{p},\mathbf{q},\tau_0)/\hbar - \tilde{S}^{(l)}_{1,n}(\mathbf{p},\mathbf{q},\tau_1)/\hbar} \tag{2.246}$$

with

$$\tilde{S}^{(l)}_{0,n}(\mathbf{p},\mathbf{q},\tau_0)/\hbar = \beta_n H^{(l)}_{0,n}(\mathbf{p},\mathbf{q}) + \frac{it}{(n-l)\hbar}\left(E^{(l)}_{0,n}(\mathbf{p},\mathbf{q}) - \sum_{j=l}^{n-1}\sum_{\nu=1}^{f} ip_{j,\nu}\omega_n(q_{j+1,\nu} - q_{j,\nu})\right) \tag{2.247}$$

and

$$\tilde{S}^{(l)}_{1,n}(\mathbf{p},\mathbf{q},\tau_1)/\hbar = \beta_n H^{(l)}_{1,n}(\mathbf{p},\mathbf{q}) - \frac{it}{l\hbar}\left(E^{(l)}_{1,n}(\mathbf{p},\mathbf{q}) - \sum_{j=0}^{l-1}\sum_{\nu=1}^{f} ip_{j,\nu}\omega_n(q_{j+1,\nu} - q_{j,\nu})\right). \tag{2.248}$$

This gives an expression in which the exponent is purely linear in real time. However, due to the terms of the form

$$ip_{j,\nu}\omega_n(q_{j+1,\nu} - q_{j,\nu}), \tag{2.249}$$

we cannot integrate over time to give a delta function as the coefficient of time in the exponent is not pure imaginary, and the resulting expression therefore suffers the usual sign problem, which plagues real time path-integral methods.

We can, at least, integrate over time analytically if we first make use of another integral identity

$$\int_{-\infty}^{\infty} e^{-ax^2 - ib(x+ic)^2}\mathrm{d}x = \int_{-\infty}^{\infty} e^{-a(x-ic)^2 - ibx^2}\mathrm{d}x \tag{2.250}$$

for $a, b, c \in \mathbb{R}$ and $a > 0$. As, having factorised the kinetic energy terms, this allows us to rewrite

$$\begin{aligned} &\int_{-\infty}^{\infty} \mathrm{d}p_{j,\nu} \exp\left(-\beta_n \frac{p^2_{j,\nu}}{2m_\nu} - \frac{it}{(n-l)\hbar}\frac{\left(p_{j,\nu} + i\omega_n m_\nu(q_{j+1,\nu} - q_{j,\nu})\right)^2}{2m_\nu}\right) \\ &= \int_{-\infty}^{\infty} \mathrm{d}p_{j,\nu} \exp\left(-\beta_n \frac{\left(p_{j,\nu} - i\omega_n m_\nu(q_{j+1,\nu} - q_{j,\nu})\right)^2}{2m_\nu} - \frac{it}{(n-l)\hbar}\frac{p^2_{j,\nu}}{2m_\nu}\right) \end{aligned} \tag{2.251}$$

and

$$\begin{aligned}&\int_{-\infty}^{\infty} \mathrm{d}p_{j,\nu} \exp\left(-\beta_n \frac{p_{j,\nu}^2}{2m_\nu} + \frac{it}{l\hbar}\frac{\left(p_{j,\nu} + i\omega_n m_\nu (q_{j+1,\nu} - q_{j,\nu})\right)^2}{2m_\nu}\right)\\ &= \int_{-\infty}^{\infty} \mathrm{d}p_{j,\nu} \exp\left(-\beta_n \frac{\left(p_{j,\nu} - i\omega_n m_\nu (q_{j+1,\nu} - q_{j,\nu})\right)^2}{2m_\nu} + \frac{it}{l\hbar}\frac{p_{j,\nu}^2}{2m_\nu}\right).\end{aligned} \tag{2.252}$$

Hence we can then analytically integrate over time to give

$$\begin{aligned}&\frac{1}{2\pi\hbar}\int_{-\infty}^{\infty} \mathrm{tr}_\mathrm{n}\left[e^{-((\beta-\lambda)+it/\hbar)\hat{H}_0} e^{-(\lambda - it/\hbar)\hat{H}_1}\right]\mathrm{d}t\\ &= \lim_{n\to\infty}\frac{1}{(2\pi\hbar)^{nf}}\int \mathrm{d}^{nf}\mathbf{p}\int \mathrm{d}^{nf}\mathbf{q} e^{-\beta_n \mathcal{H}_n^{(l)}(\mathbf{p},\mathbf{q}) + i\beta_n\theta_n(\mathbf{p},\mathbf{q})}\delta\left(\bar{\mathcal{H}}_{-,n}^{(l)}(\mathbf{p},\mathbf{q})\right)\end{aligned} \tag{2.253}$$

where the Hamiltonian is given by

$$\mathcal{H}_n^{(l)}(\mathbf{p},\mathbf{q}) = \mathcal{H}_{0,n}^{(l)}(\mathbf{p},\mathbf{q}) + \mathcal{H}_{1,n}^{(l)}(\mathbf{p},\mathbf{q}) \tag{2.254}$$

and the argument of the delta function is the difference in the average energy between the beads associated with state $|0\rangle$ and state $|1\rangle$,

$$\bar{\mathcal{H}}_{-,n}^{(l)}(\mathbf{p},\mathbf{q}) = \frac{1}{n-l}\mathcal{H}_{0,n}^{(l)}(\mathbf{p},\mathbf{q}) - \frac{1}{l}\mathcal{H}_{1,n}^{(l)}(\mathbf{p},\mathbf{q}), \tag{2.255}$$

with

$$\mathcal{H}_{0,n}^{(l)}(\mathbf{p},\mathbf{q}) = \sum_{j=l}^{n-1}\left(\sum_{\nu=1}^{f}\frac{p_{j,\nu}^2}{2m_\nu} + \frac{V_0(\boldsymbol{q}_{j+1}) + V_0(\boldsymbol{q}_j)}{2}\right), \tag{2.256}$$

and

$$\mathcal{H}_{1,n}^{(l)}(\mathbf{p},\mathbf{q}) = \sum_{j=0}^{l-1}\left(\sum_{\nu=1}^{f}\frac{p_{j,\nu}^2}{2m_\nu} + \frac{V_1(\boldsymbol{q}_{j+1}) + V_1(\boldsymbol{q}_j)}{2}\right). \tag{2.257}$$

Unfortunately this does not remove the practical difficulties associated with the real time path integral, as we are still left with the phase term

$$\theta_n(\mathbf{p},\mathbf{q}) = \sum_{j=0}^{n-1}\sum_{\nu=1}^{f}\omega_n p_{j,\nu}(q_{j+1,\nu} - q_{j,\nu}). \tag{2.258}$$

The resulting path-integral expression for the golden-rule rate,*

$$k_\mathrm{GR} = \frac{2\pi\Delta^2}{\hbar Q_r}\lim_{n\to\infty}\frac{1}{(2\pi\hbar)^{nf}}\int \mathrm{d}^{nf}\mathbf{p}\int \mathrm{d}^{nf}\mathbf{q} e^{-\beta_n \mathcal{H}_n^{(l)}(\mathbf{p},\mathbf{q}) + i\beta_n\theta_n(\mathbf{p},\mathbf{q})}\delta\left(\bar{\mathcal{H}}_{-,n}^{(l)}(\mathbf{p},\mathbf{q})\right), \tag{2.259}$$

is therefore impractical without further approximation.

*Defined here just in the case of $\epsilon = 0$.

We note that Eq. 2.259 is closely related to the expression for the Born-Oppenheimer Matsubara dynamics time-correlation function.[174] This is of course not a coincidence, and can be explained by noting that we have essentially performed several of the steps used in Ref. 175 in reverse. In fact it is also possible to derive this expression following essentially the same arguments as in the original Matsubara derivation[174] by using a modified version of the generalised Wigner transform from that work. Matsubara dynamics is a purely classical dynamics that conserves the exact quantum Boltzmann distribution, and can be systematically derived from an exact generalised Kubo-transformed correlation function.[174] It has been used to provide a unified framework to understand approximate path-integral methods such as RPMD and CMD, that can be shown to correspond to making different approximations to the Matsubara Liouvillian.[175] The key difference here is that there is no real time dynamics, i.e. no Liouvillian appears, and in this sense Eq. 2.259 corresponds to an exact path-integral transition state theory expression for the golden-rule rate. Just as RPMD and CMD can be related to the Matsubara time-correlation function, one might speculatively hope that it would be possible to develop accurate approximations to this expression which were applicable to the simulation of condensed phase non-adiabatic reactions. Apart from noting the connection between this expression and the approximate methods discussed in Chap. 7, further analysis is unfortunately beyond the scope of this thesis.

3

Non-adiabatic generalisations of RPMD rate theory

Contents

Summary

In this chapter we discuss non-adiabatic generalisations of ring-polymer molecular dynamics, focussing on methods which are designed for the calculation of non-adiabatic reaction rates. We will begin by giving a brief summary of some of the different approaches that have been taken to generalising RPMD to treat non-adiabatic systems, before discussing the simplest non-adiabatic generalisation of RPMD, Mean Field RPMD (MF-RPMD). This will provide the theoretical foundation for a discussion of three methods which have been explicitly designed for the calculation of non-adiabatic reaction rates: Kinetically Constrained RPMD (KC-RPMD), State Space Path Integrals (SS-PI) and isomorphic RPMD (iso-RP). We will discuss each of these methods in turn, focussing on their limitations and highlighting the difficulties associated with developing an accurate path-integral method for calculating non-adiabatic reaction rates.

3.1 Introduction

Because of the success of RPMD in the adiabatic limit, there have been several attempts to generalise it to treat non-adiabatic systems.[23–34] Unfortunately however, at present each of these methods has its limitations. The simplest way to calculate non-adiabatic reaction rates using RPMD is to avoid finding a non-adiabatic generalisation altogether. This can be done for electron transfer reactions by explicitly including an electron as a distinguishable particle, however this is limited to systems where using a one electron pseudo-potential is valid,[23,24] and as such we will not consider it further here. One of the first non-adiabatic generalisations of RPMD was an extension of Tully's fewest switches surface hopping,[73] in which the ring polymer is evolved on the usual adiabatic surfaces and the electronic variables are either evolved using the centroid potential energy and derivative couplings, or using the average around the ring.[25] This approach does not however use the exact Boltzmann distribution, a flaw which the "isomorphic RPMD" method[33,34] (discussed in Sec. 3.5) attempts to fix. A non-adiabatic generalisation of RPMD, known simply as Non-adiabatic RPMD,[26] which is based on the well-known (Meyer-Miller,[74] Stock-Thoss[75]) classical electron mapping approach has also been

proposed. This method does not correctly preserve the quantum mechanical Boltzmann distribution,[26,176] and hence is not well suited to the calculation of rates. Mapping variable RPMD[27] is a modified version of non-adiabatic RPMD which *does* preserve the quantum Boltzmann distribution, but it introduces a pathological sign problem that arises from a cancellation between positively and negatively weighted regions of the ring-polymer phase space in the mapping basis. In the remainder of this chapter we will discuss in more detail three of the most recently proposed non-adiabatic generalisations of RPMD: Kinetically Constrained RPMD, the State Space Path Integral method and isomorphic RPMD. We will see that each of these methods has issues which limit their applicability to the calculation of non-adiabatic reaction rates, highlighting the challenges associated with developing an accurate path-integral method for these rates.

Sec. 3.2, introduces the most primitive non-adiabatic generalisation of RPMD, Mean Field RPMD.[177] This will provide the theoretical basis for brief discussion of both the Kinetically Constrained RPMD approach[29–31] in Sec. 3.3, and the State Space Path Integral rate method[28] in Sec. 3.4. Finally, in Sec. 3.5, we will give a detailed analysis of the golden-rule limit of the newest non-adiabatic generalisation of RPMD, the "isomorphic" RPMD method.[33,34]

3.2 Mean Field RPMD

The most basic generalisation of RPMD is Mean Field RPMD (MF-RPMD), in which the electronic degrees of freedom are integrated out to give a single thermally averaged (or "mean field") ring-polymer potential on which the nuclei evolve. Although this formalism is in principle applicable to systems with many electronic states, in line with the rest of this thesis we will consider just a two level system, for which the Hamiltonian can be written in the diabatic representation as

$$\hat{H} = \sum_{\nu=1}^{f} \frac{\hat{p}_\nu^2}{2m_\nu}\mathbf{1} + \boldsymbol{V}(\hat{\boldsymbol{q}}) \tag{3.1}$$

where $\mathbf{1}$ is the 2×2 identity matrix and $\boldsymbol{V}(\hat{\boldsymbol{q}})$ is the diabatic potential matrix

$$\boldsymbol{V}(\hat{\boldsymbol{q}}) = \begin{pmatrix} V_0(\hat{\boldsymbol{q}}) & \Delta(\hat{\boldsymbol{q}}) \\ \Delta(\hat{\boldsymbol{q}}) & V_1(\hat{\boldsymbol{q}}) - \epsilon \end{pmatrix}. \tag{3.2}$$

To derive MF-RPMD we begin by performing an imaginary-time path-integral discretisation of the Boltzmann operator following the same argument as in Chap. 2. The point at which the derivation differs is in Eq. 2.138 where in the multi-level case,

$$\langle \boldsymbol{q}_j | \, e^{-\beta_n \hat{H}} \, | \boldsymbol{q}_{j+1} \rangle \simeq e^{-\beta_n \boldsymbol{V}(\boldsymbol{q}_j)/2} e^{-\beta_n \boldsymbol{V}(\boldsymbol{q}_{j+1})/2} \, \langle \boldsymbol{q}_j | \, e^{-\beta_n \hat{T}} \, | \boldsymbol{q}_{j+1} \rangle \,, \tag{3.3}$$

and since the diabatic potential matrices at different values of $\boldsymbol{q}$ do not in general commute it follows that

$$e^{-\beta_n \boldsymbol{V}(\boldsymbol{q}_j)/2} e^{-\beta_n \boldsymbol{V}(\boldsymbol{q}_{j+1})/2} \neq e^{-\beta_n \boldsymbol{V}(\boldsymbol{q}_j)/2 - \beta_n \boldsymbol{V}(\boldsymbol{q}_{j+1})/2}. \tag{3.4}$$

Using this the resulting expression for the full quantum partition function can be written as

$$\mathrm{Tr}\left[e^{-\beta \hat{H}}\right] = \lim_{n\to\infty} \frac{1}{(2\pi\hbar)^{nf}} \int \mathrm{d}^{nf}\mathbf{q} \int \mathrm{d}^{nf}\mathbf{p} \, e^{-\beta_n h_n(\mathbf{p},\mathbf{q})} \mu(\mathbf{q}), \tag{3.5}$$

where $h_n(\mathbf{p},\mathbf{q})$ is the free ring-polymer Hamiltonian (given in Eq. 2.146), the potential term is given by

$$\mu(\mathbf{q}) = \mathrm{tr_e}\left[\mathcal{T} \prod_{j=1}^{n} e^{-\beta_n \boldsymbol{V}(\boldsymbol{q}_j)}\right], \tag{3.6}$$

in which $\mathrm{tr_e}[\dots]$ denotes a trace over the electronic degrees of freedom only, and $\mathcal{T}$ denotes the fact that the product is ordered by bead index j. Provided $\mu(\mathbf{q}) > 0$, we can define the mean field ring-polymer Hamiltonian as[177–180]

$$H_n^{\mathrm{MF}}(\mathbf{p},\mathbf{q}) = h_n(\mathbf{p},\mathbf{q}) + V_n^{\mathrm{MF}}(\mathbf{q}), \tag{3.7}$$

where the potential is given by

$$V_n^{\mathrm{MF}}(\mathbf{q}) = -\frac{1}{\beta_n} \ln\left(\mu(\mathbf{q})\right), \tag{3.8}$$

such that[177–180]

$$\mathrm{Tr}\left[e^{-\beta \hat{H}}\right] = \lim_{n\to\infty} \frac{1}{(2\pi\hbar)^{nf}} \int \mathrm{d}^{nf}\mathbf{q} \int \mathrm{d}^{nf}\mathbf{p} \, e^{-\beta_n H_n^{\mathrm{MF}}(\mathbf{p},\mathbf{q})}. \tag{3.9}$$

Assuming that a position space dividing surface, $s(\mathbf{q}) = 0$, can be used to separate the reactants and products then the MF-RPMD approximation to the rate is just given by

$$k \simeq k_{\mathrm{MF}} = \lim_{t\to\infty} \frac{c_{\mathrm{fs}}(t)}{Q_r - \int_0^t c_{\mathrm{fs}}(t)\,\mathrm{d}t / \langle P_p \rangle}, \tag{3.10}$$

where $c_{\mathrm{fs}}(t)$ is a MF-RPMD flux-side correlation function

$$c_{\mathrm{fs}}(t) = \frac{1}{(2\pi\hbar)^{nf}} \int \mathrm{d}^{nf}\mathbf{p} \int \mathrm{d}^{nf}\mathbf{q} e^{-\beta_n H_n^{\mathrm{MF}}(\mathbf{p},\mathbf{q})} \dot{\theta}(s(\mathbf{q}))\theta(s(\mathbf{q}(t))), \tag{3.11}$$

and the dynamics is simply the classical dynamics generated by the mean field Hamiltonian

$$\dot{q}_{j,\nu} = \frac{\partial H_n^{\mathrm{MF}}}{\partial p_{j,\nu}} \tag{3.12a}$$

$$\dot{p}_{j,\nu} = -\frac{\partial H_n^{\mathrm{MF}}}{\partial q_{j,\nu}}. \tag{3.12b}$$

Although the MF-RPMD rates can be reasonably accurate when the reaction is close to the adiabatic limit, they will clearly break down in the golden-rule limit. This can be understood by noting that the exact rate satisfies $k(\Delta = 0) = 0$, however the MF-RPMD rate will clearly always be non-zero, as it is just an adiabatic rate on the thermally averaged potential, and so $k_{\mathrm{MF}}(\Delta = 0) \neq 0$.

Before we discuss other non-adiabatic generalisations of RPMD it is helpful to introduce the idea of ring-polymer "kinks".[61] To do this we consider expanding the matrix product in terms of individual matrix elements as

$$\mu(\mathbf{q}) = \mathrm{tr}_{\mathrm{e}}\left[\mathcal{T}\prod_{j=1}^{n} e^{-\beta_n \boldsymbol{V}(\boldsymbol{q}_j)}\right] = \prod_{j=1}^{n}\left(\sum_{\sigma_j=0}^{1}\left\langle\sigma_j\right| e^{-\beta_n \boldsymbol{V}(\boldsymbol{q}_j)}\left|\sigma_{j+1}\right\rangle\right), \tag{3.13}$$

where as with the positions and momenta the state variable obeys cyclic boundary conditions $\sigma_0 = \sigma_n$. Each set of possible values $\{\sigma_j\}_{j=0}^{n-1}$ can be thought of as a different imaginary-time path in the state space, and every time $\sigma_{j+1} - \sigma_j \neq 0$ can be considered as a hop from one diabatic state to the other, and is referred to as a kink. Due to the cyclic symmetry there must always be an even number of kinks, and hence they are also often grouped together as so-called kink pairs. In the two level case the only paths which have no kinks are those in which the system stays entirely on the reactant diabat or entirely on the product diabat, and we can therefore define the contribution to the distribution from paths which contain kinks as

$$\mu_{\mathrm{kinks}}(\mathbf{q}) = \mu(\mathbf{q}) - e^{-\beta_n \sum_j V_0(\boldsymbol{q}_j)} - e^{-\beta_n \sum_j \left(V_1(\boldsymbol{q}_j) - \epsilon\right)}. \tag{3.14}$$

3.3 Kinetically Constrained RPMD

The Kinetically Constrained RPMD (KC-RPMD) approach is rather complicated, and as such we will not give a full description of the method here, instead we will just give a brief summary of the main idea behind the method and discuss the accuracy it has shown in simple test cases.[29,30] The key idea behind the KC-RPMD method is to introduce an additional continuous variable, y, which reports on the existence of kinks in the ring-polymer distribution by writing the exact distribution as

$$\mu(\mathbf{q}) = \int_{-\infty}^{\infty} \mu_{\text{kinks}}(\mathbf{q}) f(y,0) + e^{-\beta_n \sum_j V_0(\boldsymbol{q}_j)} f(y,-1) + e^{-\beta_n \sum_j \left(V_1(\boldsymbol{q}_j)-\epsilon\right)} f(y,1)\mathrm{d}y, \tag{3.15}$$

where the integral of $f(y,a)$ over y is 1. In the simplest version this function is chosen to be a limit representation of the rectangular function $f(y,a) = \text{rect}(y-a)$ with

$$\text{rect}(x) = \begin{cases} 0, & \text{if } |x| > \frac{1}{2} \\ \frac{1}{2}, & \text{if } |x| = \frac{1}{2} \\ 1, & \text{if } |x| < \frac{1}{2}. \end{cases} \tag{3.16}$$

The idea is to then introduce an associated mass and momentum for y leading to a dynamical variable, and to fit the mass to give the correct golden-rule rate in the classical limit.[30] However, as this would not work in the Marcus inverted regime (where kinked configurations between the minimum of the reactant well and the product surface dominate) an additional modification is required, and this is where the method becomes rather complicated. To avoid the problem in the inverted regime, $\mu(\mathbf{q})$ is replaced with $\mu_{\text{KC}}(\mathbf{q})$ where

$$\mu_{\text{KC}}(\mathbf{q}) = \int_{-\infty}^{\infty} \mu_{\text{kinks}}(\mathbf{q}) f(y,0)\delta\left(\frac{w(\bar{\boldsymbol{q}})}{\eta}\right) + e^{-\beta_n \sum_j V_0(\boldsymbol{q}_j)} f(y,-1) + e^{-\beta_n \sum_j \left(V_1(\boldsymbol{q}_j)-\epsilon\right)} f(y,1)\mathrm{d}y, \tag{3.17}$$

in which the kinked contribution has been modified by the introduction of a delta function which constrains the configurations for which kinks can exist to those where the centroid of the ring polymer obeys $w(\bar{\boldsymbol{q}}) = 0$, with the constraint function given by[29]

$$w(\boldsymbol{q}) = \frac{V_0(\boldsymbol{q}) - V_1(\boldsymbol{q}) + \epsilon}{\Delta(\boldsymbol{q})}. \tag{3.18}$$

The parameter η is then determined numerically such that the probability density for the system to be found at the crossing points of the diabats is unchanged; the resulting

expression is rather complicated and does not add to the present discussion so we will not include it here.

Note that by modifying the distribution, KC-RPMD no longer obeys the exact quantum statistics, and hence loses one of the most important features of the original Born-Oppenheimer RPMD. It is therefore clear that as the reaction approaches the adiabatic limit KC-RPMD will not reduce to the original RPMD rate theory. Due to the number of parameters which must be determined numerically it is not very easy to perform a theoretical analysis of the accuracy of KC-RPMD, however we note that the results given in the original two papers outlining the method showed variable accuracy.[29,30] In particular, in the second paper on KC-RPMD (Ref. 30) KC-RPMD is compared to the exact rates for a simple spin-boson model which is approximately in the golden-rule limit (system A3 of that paper), and it was found that KC-RPMD overestimates the exact rate by as much as a factor of 6 in the case of moderate to strong friction. In contrast for the same system the Marcus theory rate is only 30% too small and the Wolynes theory rate is within 5% of the exact rate. It thus appears that KC-RPMD is not a generally reliable approach for including nuclear quantum effects in non-adiabatic reaction rates.

3.4 State Space Path Integrals

A conceptually much simpler approach, is the State Space Path Integral (SS-PI) method, proposed by Duke and Ananth.[28] In this approach the initial distribution in the mean field correlation function is modified, so that it only contains kinked configurations. The SS-PI approximation to the rate is defined in terms of the plateau time of this modified correlation function as

$$k_{\text{SS-PI}}(\Delta) = \frac{c_{\text{SS-fs}}(t_{\text{p}})}{Q_r}. \tag{3.19}$$

There are two different variants of the approach, the simpler of the two is the "solvent reaction coordinate" version, in which the flux-side correlation function is approximated as

$$c_{\text{SS-fs}}(t) = \frac{1}{(2\pi\hbar)^{nf}} \int \mathrm{d}^{nf}\mathbf{p} \int \mathrm{d}^{nf}\mathbf{q} e^{-\beta_n h_n(\mathbf{p},\mathbf{q})} \mu_{\text{kinks}}(\mathbf{q}) \dot{\theta}(s(\mathbf{q})) \theta(s(\mathbf{q}(t))), \tag{3.20}$$

where the dividing surface is given by

$$s(\mathbf{q}) = V_{-}(\bar{\boldsymbol{q}}) + \epsilon \tag{3.21}$$

with $V_{-}(\boldsymbol{q}) = V_0(\boldsymbol{q}) - V_1(\boldsymbol{q})$, and importantly the dynamics is still generated by the mean field Hamiltonian (Eq. 3.12). To get a better understanding of this approach we note that $\mu_{\text{kinks}}(\mathbf{q})$ is just the difference between $\mu(\mathbf{q})$ evaluated at the true Δ and at $\Delta = 0$, i.e.

$$\mu_{\text{kinks}}(\mathbf{q}) = \mu(\mathbf{q}, \Delta) - \mu(\mathbf{q}, \Delta = 0). \tag{3.22}$$

Hence, by assuming the dynamics generated by $H_n^{\text{MF}}(\mathbf{p}, \mathbf{q})$ is approximately independent of Δ, we can write the SS-PI rate in terms of the MF-RPMD rate as

$$k_{\text{SS-PI}}(\Delta) \simeq k_{\text{MF}}(\Delta) - k_{\text{MF}}(\Delta = 0). \tag{3.23}$$

Note that this approximation becomes exact as one approaches the golden-rule limit. We thus see that the SS-PI approximation can be thought of as a modified version of MF-RPMD where the unphysical zeroth order contribution to the rate is removed.

The SS-PI rate is certainly an improvement on the MF-RPMD rate, as it correctly predicts that the rate is proportional to Δ^2 in the golden-rule limit, however it is not clear in general what approximation one is making and hence how accurate it will be. One notable deficiency of the method is that it breaks down in the high temperature limit. To see this we consider a simple one dimensional scattering model with diabatic potentials

$$\begin{aligned} V_0(q) &= Ae^{+q/L} \\ V_1(q) &= Ae^{-q/L}, \end{aligned} \tag{3.24}$$

with $\epsilon = 0$ and a constant Δ. Noting that the classical (one bead) limit of $\mu(\mathbf{q})$ is given by

$$\mu_{\text{cl}}(q) = 2e^{-\beta(V_0(q)+V_1(q))/2} \cosh\left(\frac{\beta}{2}\sqrt{(V_0(q) - V_1(q))^2 + 4\Delta^2}\right) \tag{3.25}$$

it follows straightforwardly that the mean field rate in the classical limit is given by

$$\beta\hbar Q_r k_{\text{cl-MF}}(\Delta) = \frac{1}{2\pi} 2e^{-\beta A} \cosh(\beta\Delta). \tag{3.26}$$

Using this, in conjunction with Eq. 3.23, we see that in the classical limit the SS-PI approximation to the golden-rule rate is given by

$$\beta\hbar Q_r k_{\text{SS-PI}}(\Delta) = \frac{\beta^2\Delta^2}{2\pi} e^{-\beta A}. \tag{3.27}$$

In contrast the exact classical golden-rule rate for this system is given by,

$$\beta\hbar Q_r k_{\text{cl-GR}}(\Delta) = \frac{\beta^2\Delta^2}{2\pi}\sqrt{\frac{2\pi^3 mL^2}{\beta^3 A^2\hbar^2}}e^{-\beta A}. \tag{3.28}$$

Hence we see that there is an uncontrolled error in going from the exact result to the SS-PI rate. Whilst for some systems the factor of $\sqrt{2\pi^3 mL^2/\beta^3 A^2\hbar^2}$ may be close to 1, this will not be true in general. Without a formal argument explaining the general regime in which SS-PI gives a good approximation to the rate, it thus seems that it does not provide a viable approach to calculating reaction rates in complex systems. Despite this we note that Duke and Ananth did find reasonably close agreement between the exact rate and the SS-PI rate for a spin-boson model showing moderate quantum enhancement, when the reaction was approximately symmetric. The reasons for this agreement will be discussed in more detail in the following chapter.

Duke and Ananth also proposed an alternative approach involving a further modification to the flux-side correlation function, in which the distribution is restricted to just contain imaginary-time paths which spend an equal amount of imaginary time on each of the surfaces. This allowed them to calculate reaction rates in the Marcus inverted regime, however they found that this approach significantly under-predicted the rate,[28] essentially failing to capture nuclear tunnelling.

3.5 An analysis of iso-RPMD in the golden-rule limit

Recently Tao, Shushkov and Miller have proposed a new method, called isomorphic ring-polymer molecular dynamics (iso-RPMD or iso-RP),[33,34] which aims to extend the Born-Oppenheimer ring-polymer molecular dynamics (RPMD) method[17–21] to systems with multiple electronic states. The iso-RPMD ansatz is to construct an "isomorphic" multi-state Hamiltonian for a ring polymer of classical nuclei that is consistent with the quantum mechanical partition function, and then to combine this with a pre-existing mixed quantum-classical (MQC) dynamics approximation such as Tully's fewest switches surface hopping.[73]

One potential application for iso-PRMD is the study of thermal reactions which involve transitions between two different electronic states.[181] In the adiabatic limit, in

which excited electronic states do not make any contribution to the canonical quantum mechanical partition function, it is clear that iso-RPMD will work well, since it reduces in this limit to the standard RPMD approximation (in which the dynamics of the ring polymer takes place on the ground adiabatic Born-Oppenheimer potential energy surface). However, how well it can be expected to work in the opposite non-adiabatic limit is less clear. This is what we shall investigate in the remainder of this chapter.

3.5.1 Isomorphic RPMD

To set the scene for this investigation, let us begin by introducing the iso-RPMD formalism.[33,34] Again although this formalism is in principle applicable to systems with many electronic states, it will be sufficient for our purposes to consider just a two level system. The "isomorphic" RPMD for this two level system is based on writing the exact quantum partition function

$$Q = \mathrm{Tr}\left[e^{-\beta\hat{H}}\right] \tag{3.29}$$

in the form

$$Q = \lim_{n\to\infty}\left(\frac{n}{2\pi\hbar}\right)^{nf}\int \mathrm{d}^{nf}\mathbf{p}\int \mathrm{d}^{nf}\mathbf{q}\ \mathrm{tr_e}\left[e^{-\beta \boldsymbol{H}_n^{\mathrm{iso}}(\mathbf{p},\mathbf{q})}\right], \tag{3.30}$$

where $\mathrm{tr_e}[\dots]$ denotes a trace over the electronic degrees of freedom. The isomorphic ring-polymer Hamiltonian $\boldsymbol{H}_n^{\mathrm{iso}}(\mathbf{p},\mathbf{q})$ is

$$\boldsymbol{H}_n^{\mathrm{iso}}(\mathbf{p},\mathbf{q}) = h_n^{\mathrm{iso}}(\mathbf{p},\mathbf{q})\mathbf{1} + \boldsymbol{V}_n^{\mathrm{iso}}(\mathbf{q}), \tag{3.31}$$

where

$$h_n^{\mathrm{iso}}(\mathbf{p},\mathbf{q}) = \sum_{j=1}^{n}\sum_{\nu=1}^{f}\left\{\frac{p_{j,\nu}^2}{2m_{n,\nu}} + \frac{1}{2}m_{n,\nu}\omega_n^2(q_{j+1,\nu}-q_{j,\nu})^2\right\} \tag{3.32}$$

is the isomorphic free ring-polymer Hamiltonian, with $m_{n,\nu} = m_\nu/n$. The isomorphic diabatic potential energy matrix is

$$\boldsymbol{V}_n^{\mathrm{iso}}(\mathbf{q}) = \begin{pmatrix} V_{0,n}^{\mathrm{iso}}(\mathbf{q}) & \Delta_n^{\mathrm{iso}}(\mathbf{q}) \\ \Delta_n^{\mathrm{iso}}(\mathbf{q}) & V_{1,n}^{\mathrm{iso}}(\mathbf{q}) - \epsilon \end{pmatrix}, \tag{3.33}$$

where the diagonal elements are chosen to be[33]

$$V_{i,n}^{\mathrm{iso}}(\mathbf{q}) = \frac{1}{n}\sum_{j=1}^{n} V_i(\boldsymbol{q}_j). \tag{3.34}$$

We note that, in this formalism the simulation is performed at a temperature T rather than nT, and this is balanced by a change in the definition of the mass of the particles, which are reduced by a factor of n. These two ways of thinking about the path-integral simulation are equivalent in the adiabatic case, but the definition used in iso-RPMD is more appropriate in this context as it means that the total potential energy converges with bead number, which is important due to the influence of the potential energy on the electronic dynamics.

In order to ensure that the iso-RP partition function exactly reproduces the quantum partition function in the infinite n limit, Tao *et al.*[33] require that $\Delta_n^{\mathrm{iso}}(\mathbf{q})$ is chosen so that

$$\mathrm{tr_e}\left[e^{-\beta \boldsymbol{H}_n^{\mathrm{iso}}(\mathbf{p},\mathbf{q})}\right] = e^{-\beta h_n^{\mathrm{iso}}(\mathbf{p},\mathbf{q})}\mu(\mathbf{q}). \tag{3.35}$$

This leads to the following expression for the isomorphic coupling[33]

$$\Delta_n^{\mathrm{iso}}(\mathbf{q})^2 = \frac{1}{\beta^2}\,\mathrm{acosh}^2\left[\frac{\mu(\mathbf{q})}{2}e^{\beta(V_{+,n}^{\mathrm{iso}}(\mathbf{q})-\epsilon)/2}\right] - \frac{\left(V_{-,n}^{\mathrm{iso}}(\mathbf{q})+\epsilon\right)^2}{4}, \tag{3.36}$$

where

$$V_{\pm,n}^{\mathrm{iso}}(\mathbf{q}) = V_{0,n}^{\mathrm{iso}}(\mathbf{q}) \pm V_{1,n}^{\mathrm{iso}}(\mathbf{q}). \tag{3.37}$$

Note that in general $\mu(\mathbf{q})$ can become negative,[182] which leads to a complex $\Delta_n^{\mathrm{iso}}(\mathbf{q})$ and a non-hermitian $\boldsymbol{V}_n^{\mathrm{iso}}(\mathbf{q})$. However, when $\Delta(\boldsymbol{q})$ has a constant sign, one can show that $\mu(\mathbf{q}) > 0$,[182] so $\Delta_n^{\mathrm{iso}}(\mathbf{q})$ is real and $\boldsymbol{V}_n^{\mathrm{iso}}(\mathbf{q})$ is real and symmetric for all values of $\mathbf{q}$. We shall therefore assume that $\Delta(\boldsymbol{q})$ has a constant sign from this point on.

All of the above is simply a rearrangement of a formally exact expression for the quantum mechanical partition function. The isomorphic RPMD ansatz is to take the classical multi-state Hamiltonian $\boldsymbol{H}_n^{\mathrm{iso}}(\mathbf{p},\mathbf{q})$ and use it with a mixed quantum classical (MQC) dynamics method, such as Tully's fewest switches surface hopping.[73] This is an appealingly simple idea, but how well does it work? In the following we will consider the more specific question of whether or not iso-RPMD can give accurate reaction rates in the non-adiabatic (golden-rule) limit, and in particular whether it can capture nuclear quantum effects such as tunnelling and zero-point energy in this limit.

3.5.2 Golden-rule limit

As we saw in Chap. 2 the exact quantum mechanical rate constant for transfer from state $|0\rangle$ to state $|1\rangle$ in the golden-rule limit can be written as

$$k_{\mathrm{GR}} = \frac{1}{Q_r \hbar^2} \int_{-\infty}^{\infty} \mathrm{tr_n} \left[e^{-\beta \hat{H}_0} e^{-i\hat{H}_0 t/\hbar} \Delta(\hat{\boldsymbol{q}}) e^{+i(\hat{H}_1 - \epsilon)t/\hbar} \Delta(\hat{\boldsymbol{q}}) \right] \mathrm{d}t, \tag{3.38}$$

where Q_r is the reactant partition function. The classical limit of Eq. 3.38, which becomes exact at high temperatures where the ring polymer can be replaced by a single bead, is simply[141,142]

$$k_{\text{cl-GR}} = \left\langle \frac{2\pi}{\hbar} \Delta^2(\boldsymbol{q}) \delta(V_-(\boldsymbol{q}) + \epsilon) \right\rangle_{\mathrm{cl},0}, \tag{3.39}$$

where $V_-(\boldsymbol{q}) = V_0(\boldsymbol{q}) - V_1(\boldsymbol{q})$ is the diabatic energy gap. Unfortunately, it is well known that many MQC dynamics methods do not give the correct rate in the high-temperature, non-adiabatic limit (i.e., are not consistent with Eq. 3.39). In particular, the original formulation of Tully's fewest switches surface hopping[73] suffers from "over coherence". There has been a concerted effort to fix this problem with decoherence corrections,[183–191] but that is not the focus of the present study. Here we shall simply sidestep the issue by assuming that the MQC method used with iso-RPMD *does* reduce to Eq. 3.39 in the one bead limit.

Having made this assumption, we need not consider the specific details of the MQC dynamics, and can simply make use of the isomorphism to write down the iso-RP expression for the golden-rule rate

$$k_{\mathrm{iso}} = \lim_{n\to\infty} \left\langle \frac{2\pi}{\hbar} \Delta_n^{\mathrm{iso}}(\mathbf{q})^2 \delta(V_{-,n}^{\mathrm{iso}}(\mathbf{q}) + \epsilon) \right\rangle_{0,n}^{\mathrm{iso}}, \tag{3.40}$$

where the ring-polymer thermal average is defined as

$$\langle A(\mathbf{q}) \rangle_{0,n}^{\mathrm{iso}} = \frac{\int \mathrm{d}^{nf}\mathbf{p} \int \mathrm{d}^{nf}\mathbf{q}\, e^{-\beta H_{0,n}^{\mathrm{iso}}(\mathbf{p},\mathbf{q})} A(\mathbf{q})}{\int \mathrm{d}^{nf}\mathbf{p} \int \mathrm{d}^{nf}\mathbf{q}\, e^{-\beta H_{0,n}^{\mathrm{iso}}(\mathbf{p},\mathbf{q})}}, \tag{3.41}$$

with $H_{0,n}^{\mathrm{iso}}(\mathbf{p},\mathbf{q}) = h_n^{\mathrm{iso}}(\mathbf{p},\mathbf{q}) + V_{0,n}^{\mathrm{iso}}(\mathbf{q})$.

We can further simplify Eq. (3.40) by taking the golden-rule limit of the iso-RP coupling $\Delta_n^{\mathrm{iso}}(\mathbf{q})^2$. To keep the notation as simple as possible, we shall do this only

in the special case where $\Delta(\boldsymbol{q}) = \Delta$ is a constant (the Condon approximation[173]). The more general case of a coordinate-dependent Δ can also be treated but it does not add anything useful to our discussion.

The golden-rule limit of $\Delta_n^{\mathrm{iso}}(\mathbf{q})^2$ is worked out for constant Δ in Appendix 3.A, where it is shown to lead to a golden-rule iso-RP rate in the infinite n limit that can be written in the path-integral notation introduced in Sec. 2.3.3 as

$$k_{\mathrm{iso}} = \frac{2\pi}{\beta\hbar Q_r}\int_0^\beta d\lambda \Big\langle \Delta^2 \delta(V_-^{\mathrm{iso}}[\boldsymbol{q}(\tau)] + \epsilon)\Big\rangle_\lambda e^{-\beta F_{\mathrm{GR}}(\lambda)+\lambda\epsilon}. \tag{3.42}$$

Where the isomorphic diabatic energy gap in Eq. 3.37 has become

$$V_-^{\mathrm{iso}}[\boldsymbol{q}(\tau)] = V_0^{\mathrm{iso}}[\boldsymbol{q}(\tau)] - V_1^{\mathrm{iso}}[\boldsymbol{q}(\tau)], \tag{3.43}$$

with

$$V_i^{\mathrm{iso}}[\boldsymbol{q}(\tau)] = \frac{1}{\beta\hbar}\int_0^{\beta\hbar} V_i(\boldsymbol{q}(\tau))\,\mathrm{d}\tau. \tag{3.44}$$

3.5.3 Example calculation

In order to assess the accuracy of Eq. 3.42, and facilitate our analysis, we shall consider the prototypical model of condensed phase electron transfer, the spin-boson model

$$V_0(\boldsymbol{q}) = \sum_{\nu=1}^{f}\frac{1}{2}\omega_\nu^2\Big(q_\nu + \frac{c_\nu}{\omega_\nu^2}\Big)^2 \tag{3.45}$$

$$V_1(\boldsymbol{q}) = \sum_{\nu=1}^{f}\frac{1}{2}\omega_\nu^2\Big(q_\nu - \frac{c_\nu}{\omega_\nu^2}\Big)^2, \tag{3.46}$$

again with constant Δ. The effect of the nuclear motion on the electronic dynamics of this model (and hence the rate of transfer from state 0 to state 1) is fully characterised by the spectral density

$$J(\omega) = \frac{\pi}{2}\sum_{\nu=1}^{f}\frac{c_\nu^2}{\omega_\nu}\delta(\omega-\omega_\nu), \tag{3.47}$$

in which we have chosen to work in mass-scaled coordinates such that $m_\nu = 1$.

Due to the simplicity of this problem it is possible to obtain closed form expressions for each of the terms appearing in Eq. 3.42. The λ-dependent Boltzmann factor can be written as

$$\frac{e^{-\beta F_{\mathrm{GR}}(\lambda)}}{Q_r} = e^{-\beta(F_{\mathrm{GR}}(\lambda)-F_{\mathrm{GR}}(0))} = e^{-\beta\Delta F_{\mathrm{GR}}(\lambda)} \tag{3.48}$$

where, using the exact expression given in Appendix 2.A, we have

$$\Delta F_{\mathrm{GR}}(\lambda) = \frac{4}{\pi}\int_0^\infty \frac{J(\omega)}{\beta\hbar\omega^2}\Big[\frac{1-\cosh(\omega\lambda\hbar)}{\tanh(\omega\beta\hbar/2)} + \sinh(\omega\lambda\hbar)\Big]\mathrm{d}\omega. \tag{3.49}$$

Furthermore, using the fact that $V_-^{\mathrm{iso}}[\boldsymbol{q}(\tau)]$ only depends on the average (centroid) of the imaginary-time path, $\bar{\boldsymbol{q}} = \frac{1}{\beta\hbar}\int_0^{\beta\hbar}\boldsymbol{q}(\tau)\,\mathrm{d}\tau$, it is straightforward to show that

$$\Big\langle \delta(V_-^{\mathrm{iso}}[\boldsymbol{q}(\tau)] + \epsilon)\Big\rangle_\lambda = \frac{1}{2}\sqrt{\frac{\beta}{\pi\Lambda}}e^{-\beta\frac{(\Lambda-\epsilon)^2}{4\Lambda}+\Lambda\lambda\left(1-\frac{\lambda}{\beta}\right)-\lambda\epsilon}, \tag{3.50}$$

where

$$\Lambda = \frac{4}{\pi}\int_0^\infty \frac{J(\omega)}{\omega}\mathrm{d}\omega \tag{3.51}$$

is the Marcus theory reorganisation energy.

Note that in the high temperature limit $\Delta F_{\mathrm{GR}}(\lambda) \to \Lambda\frac{\lambda}{\beta}(1-\frac{\lambda}{\beta})$, and hence the λ dependence of Eq. 3.48 exactly cancels the λ dependence of Eq. 3.50. In this limit the isomorphic rate correctly reduces to the rate given by Marcus theory: $k_{\mathrm{iso}} \to k_{\mathrm{MT}}$ as $\beta \to 0$ where[46–49]

$$k_{\mathrm{MT}} = \frac{\Delta^2}{\hbar}\sqrt{\frac{\beta\pi}{\Lambda}}e^{-\beta\frac{(\Lambda-\epsilon)^2}{4\Lambda}}. \tag{3.52}$$

Unfortunately, however, it is already clear that there is an issue with the iso-RP rate at lower temperatures. Since $\Delta F_{\mathrm{GR}}(\lambda)$ is independent of ϵ we see that the iso-RP rate retains the Marcus theory dependence on ϵ at all temperatures. Hence the ratio of the iso-RP rate to the Marcus rate is independent of the driving force, $k_{\mathrm{iso}}/k_{\mathrm{MT}} = A$, and so on a plot of the logarithm of the rate as a function of the driving force the iso-RP rate is simply a vertically shifted version of the famous Marcus parabola. This clearly does not capture the behaviour of the correct quantum mechanical rate at low temperatures.

To demonstrate this, we shall consider two models with Brownian Oscillator spectral densities[64,192,193]

$$J(\omega) = \frac{\Lambda}{2}\frac{\gamma\Omega^2\omega}{(\omega^2-\Omega^2)^2+\gamma^2\omega^2}, \tag{3.53}$$

and with parameters chosen to be representative of typical condensed phase electron transfer reactions. Model 1 is weakly quantum mechanical with $\beta\Omega = 2$, $\gamma = \Omega$, and $\beta\Lambda = 60$, corresponding to a reaction coordinate frequency of $\Omega \approx 400\ \mathrm{cm}^{-1}$ and a

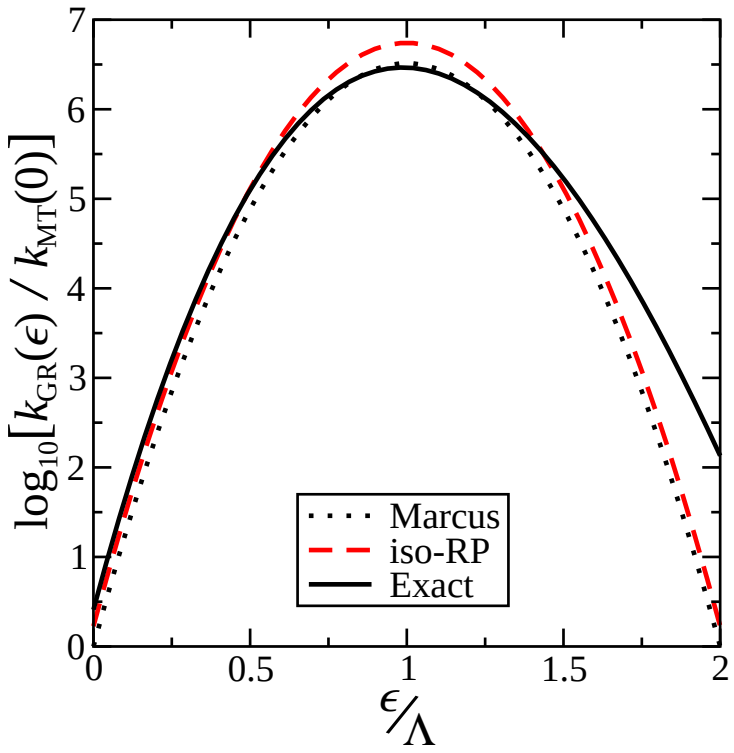

Figure 3.1: Reaction rate constants as a function of the driving force for model 1, a spin-boson model with $\beta\Omega = 2$, $\gamma = \Omega$, and $\beta\Lambda = 60$. Although it may seem as though the curvature of the iso-RP curve is larger (more negative) than that of the Marcus curve, this is an optical illusion: the logarithm of the iso-RP rate is in fact just vertically shifted from the Marcus theory parabola.

Marcus reorganisation energy of $\Lambda \approx 1.5$ eV at 300 K. Model 2 is more strongly quantum mechanical with $\beta\Omega = 6$, $\gamma = \Omega$, and $\beta\Lambda = 60$, corresponding to a reaction coordinate frequency of $\Omega \approx 1200$ cm^{-1}. These parameters are roughly comparable to those obtained in the classic experimental paper on the Marcus inverted regime by Miller *et al.*,[194] who extracted 1500 cm^{-1} as the characteristic inner sphere frequency, along with a total reorganisation energy of 1.2 eV, for a series of organic electron transfers in tetrahydrofuran. The approximately 40% to 60% split of the reorganisation energy into inner-sphere and outer-sphere contributions they obtained experimentally is also broadly compatible with the Brownian Oscillator spectral density for model 2, in which 60% of the reorganisation energy comes from modes with frequencies less than $\omega \approx 1000$ cm^{-1} at 300 K.

Figure 3.1 compares the iso-RP rate for model 1 as a function of the driving force,

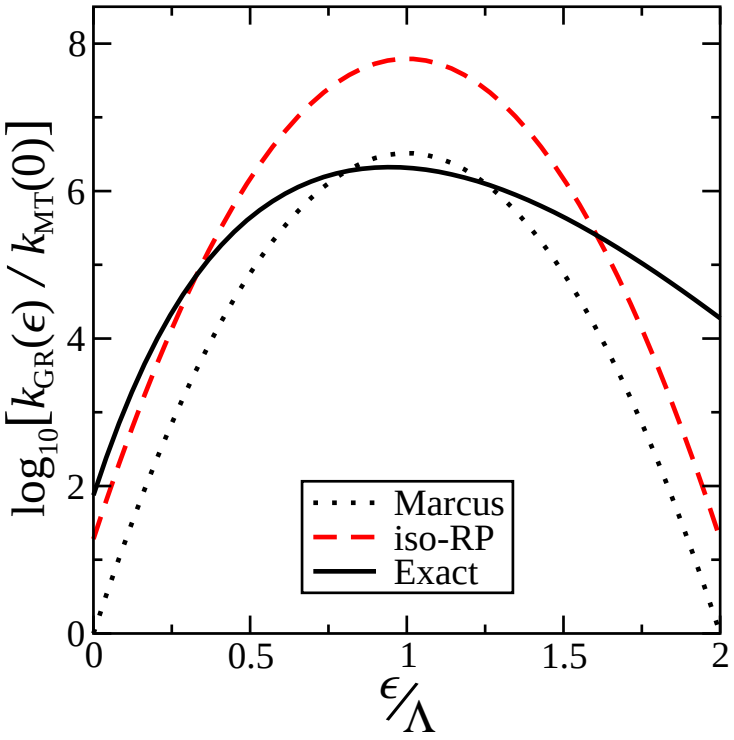

Figure 3.2: As in Fig. 3.1 but for model 2, a more strongly quantum mechanical spin-boson model with $\beta\Omega = 6$, $\gamma = \Omega$, and $\beta\Lambda = 60$.

ϵ, with both the exact quantum mechanical rate and the classical rate (given by Marcus theory). The isomorphic rate is unable to capture the dependence of the exact rate on the driving force, retaining the parabolic form seen in Marcus theory and failing to reproduce the large increase in the rate in the inverted regime due to nuclear quantum effects. The largest error is in the inverted regime: when the bias is twice the reorganisation energy the iso-RP rate is too small by nearly 2 orders of magnitude. In contrast it is reasonably accurate in the case of zero bias ($\epsilon = 0$), where $k_{iso}/k_{MT} = 1.7$ compared to $k_{GR}/k_{MT} = 2.6$ for the exact rate. Perhaps the most worrying aspect of the results in Fig. 3.1, however, is that the iso-RP rate seems to be significantly less accurate than the Marcus rate in the activationless case ($\epsilon = \Lambda$), where it predicts a quantum enhancement whereas the exact rate is actually slightly smaller than the Marcus rate.

The overestimation of the rate in the activationless case is even more striking in

model 2, as shown in Fig. 3.2. Here the iso-RP rate is over 30 times larger than the exact rate at $\epsilon = \Lambda$. Moreover the error is again largest deep in the inverted regime, with the iso-RP rate underestimating the exact rate by nearly 3 orders of magnitude at $\epsilon = 2\Lambda$, and it is again smallest for symmetric electron transfer ($\epsilon = 0$), where the iso-RP rate is a factor of 4 too small.

3.5.4 Analysis

To understand the behaviour of the iso-RP rate it is helpful to consider another approximate method for calculating reaction rates in the golden-rule limit, namely Wolynes theory,[82]

$$k_{\mathrm{WT}} = \frac{\Delta^2}{Q_r\hbar}\sqrt{\frac{2\pi}{-\beta F''_{\mathrm{GR}}(\lambda_{\mathrm{sp}})}}e^{-\beta F_{\mathrm{GR}}(\lambda_{\mathrm{sp}})+\lambda_{\mathrm{sp}}\epsilon}. \tag{3.54}$$

Wolynes theory is well known to be very accurate for the spin-boson model. It correctly recovers the Marcus theory rate in the high-temperature limit ($k_{\mathrm{WT}} \to k_{\mathrm{MT}}$ as $\beta \to 0$), and it is also remarkably accurate at lower temperatures, where the path-integral distribution corresponding to $e^{-\beta F_{\mathrm{GR}}(\lambda_{\mathrm{sp}})}$ is dominated by imaginary-time paths close to the golden-rule instanton.[170,195,196] For example, for our strongly quantum mechanical model 2 at zero bias, $k_{\mathrm{WT}}/k_{\mathrm{GR}} = 0.98$, and in the activationless case $k_{\mathrm{WT}}/k_{\mathrm{GR}} = 1.00$.

It is clear that one of the main differences between k_{WT} and k_{iso} is that in Wolynes theory the Boltzmann factor $e^{-\beta F_{\mathrm{GR}}(\lambda)}$ is evaluated at $\lambda = \lambda_{\mathrm{sp}}$, whereas the iso-RP rate [Eq. 3.42] involves an integral over all values of λ in the interval $[0,\beta]$. This difference can be used to explain the behaviour of the iso-RP rate. We begin by noting that the (ϵ independent) ratio of the iso-RP rate to the Marcus theory rate is given by

$$\frac{k_{\mathrm{iso}}}{k_{\mathrm{MT}}} = \frac{1}{\beta}\int_0^\beta \mathrm{d}\lambda \frac{e^{-\beta\Delta F_{\mathrm{GR}}(\lambda)}}{e^{-\beta\Delta F_{\mathrm{MT}}(\lambda)}}, \tag{3.55}$$

where $\Delta F_{\mathrm{MT}}(\lambda) = \Lambda\frac{\lambda}{\beta}\left(1-\frac{\lambda}{\beta}\right)$ is the high temperature limit of $\Delta F_{\mathrm{GR}}(\lambda)$. Then since $k_{\mathrm{WT}} \to k_{\mathrm{MT}}$ as $\beta \to 0$ we can write

$$\frac{k_{\mathrm{WT}}(\epsilon)}{k_{\mathrm{MT}}(\epsilon)} = \sqrt{\frac{F''_{\mathrm{MT}}(\lambda_{\mathrm{MT}})}{F''_{\mathrm{GR}}(\lambda_{\mathrm{sp}})}}\frac{e^{-\beta\Delta F_{\mathrm{GR}}(\lambda_{\mathrm{sp}})+\lambda_{\mathrm{sp}}\epsilon}}{e^{-\beta\Delta F_{\mathrm{MT}}(\lambda_{\mathrm{MT}})+\lambda_{\mathrm{MT}}\epsilon}} \tag{3.56}$$

where

$$\lambda_{\mathrm{MT}}(\epsilon) = \frac{\beta(\Lambda-\epsilon)}{2\Lambda} \tag{3.57}$$

is the high temperature limit of λ_{sp}. Now assuming that both $\lambda_{\mathrm{sp}}(\epsilon) \approx \lambda_{\mathrm{MT}}(\epsilon)$ and $F''_{\mathrm{GR}}(\lambda_{\mathrm{sp}}) \approx F''_{\mathrm{MT}}(\lambda_{\mathrm{MT}})$ continue to hold at lower temperatures (at least approximately), we see that

$$\frac{e^{-\beta\Delta F_{\mathrm{GR}}\left(\frac{\beta(\Lambda-\epsilon)}{2\Lambda}\right)}}{e^{-\beta\Delta F_{\mathrm{MT}}\left(\frac{\beta(\Lambda-\epsilon)}{2\Lambda}\right)}} \approx \frac{k_{\mathrm{WT}}(\epsilon)}{k_{\mathrm{MT}}(\epsilon)} \approx \frac{k_{\mathrm{GR}}(\epsilon)}{k_{\mathrm{MT}}(\epsilon)}. \tag{3.58}$$

Finally, making the substitution $\lambda = \lambda_{\mathrm{MT}}(\epsilon)$ to convert the integration variable from λ to ϵ in Eq. 3.55, and using the approximation in Eq. 3.58, we can rewrite the quantum enhancement in the rate predicted by iso-RPMD as

$$\frac{k_{\mathrm{iso}}}{k_{\mathrm{MT}}} \approx \frac{1}{2\Lambda}\int_{-\Lambda}^{\Lambda} \mathrm{d}\epsilon \frac{k_{\mathrm{GR}}(\epsilon)}{k_{\mathrm{MT}}(\epsilon)}. \tag{3.59}$$

For both models considered above (model 1 and model 2), this approximation is within 1% of the actual ratio, indicating that the assumptions in Eq. 3.58 are valid and that this does indeed provide a useful way to understand the behaviour of the iso-RP rate.

From Eq. 3.59 we see that the quantum enhancement predicted by iso-RPMD can be interpreted as the average of the true quantum enhancement over the entire Marcus normal regime, $\epsilon \in [-\Lambda, \Lambda]$. This can be used to understand why, for example, iso-RPMD underestimates the rate in the symmetric case and overestimates the rate in the activationless case. Symmetric reactions (with $\epsilon = 0$) have a larger quantum enhancement than other driving forces in the normal regime, due to nuclear tunnelling. The iso-RP rate for a symmetric reaction is therefore contaminated by imaginary-time paths for which the tunnelling is weaker, which leads to an underestimation of the quantum mechanical rate. Conversely in the activationless case, where the exact rate is typically very close to the Marcus theory rate, iso-RPMD considerably overestimates the rate as it is dominated by the large nuclear tunnelling seen around $\epsilon = 0$. In both cases, iso-RPMD is dominated by unphysical imaginary-time paths, which leads to an inaccurate rate. This is in contrast to the situation in the adiabatic limit, where RPMD rate theory accurately captures deep tunnelling due to its connection to the semiclassical instanton approximation.[144] Modifying iso-RPMD so that it is dominated by the correct (non-adiabatic) instanton path in the golden-rule limit may well therefore provide a useful route to improving its accuracy for non-adiabatic reactions.

3.6 Conclusion

In this chapter we have discussed some of the different approaches to generalising Born-Oppenheimer RPMD to calculate non-adiabatic reaction rates. We have seen that at present each of these methods has its limitations. For example KC-RPMD does not reduce to the standard Born-Oppenheimer RPMD in the adiabatic limit and SS-PI fails to recover the exact rate in the high temperature limit. Whilst iso-RPMD is an improvement in both of these regards, our analysis has shown that it is still unable to quantitatively describe reaction rates in the golden-rule limit in systems where nuclear quantum effects are important. We have shown that for the spin-boson model the ansatz leads to a uniform quantum enhancement over the Marcus theory rate, independent of the thermodynamic driving force. Hence it does not capture the quantum asymmetry that is seen in a plot of the logarithm of the rate constant against the thermodynamic driving force. (However, since it correctly describes the high temperature limit, iso-RP will capture the classical asymmetry seen in anharmonic systems.) Furthermore, we have shown that the quantum enhancement predicted by the iso-RP ansatz is approximately the average of the true quantum enhancement over the entire Marcus normal regime. This explains why iso-RP tends to underestimate the rate for symmetric reactions and to overestimate the rate for activationless reactions. Since the average quantum enhancement in the normal regime is typically dominated by reactions near the symmetric limit, iso-RPMD may prove qualitatively useful in describing these reactions. However, it is clear that applying the method to reactions with driving forces nearer the activationless limit, or those in the Marcus inverted regime, would be inadvisable.

By design we have only considered the golden-rule limit of iso-RPMD and it is clear that the failings seen in this regime will not be universal to all coupling strengths. In particular, provided a sensible MQC method is used, iso-RPMD should still accurately describe systems which are close to being electronically adiabatic. Furthermore, even for systems in which there are significant non-adiabatic effects, provided these effects are not rate limiting in the process considered, iso-RPMD may provide accurate results. It does share the single most important feature of standard adiabatic RPMD, in that it

obeys quantum detailed balance by construction (provided a MQC method with this property is used).[33,34] We also expect that iso-RPMD will be accurate for systems in which the non-adiabatic transition is effectively classical and nuclear quantum effects are important for crossing a barrier away from this transition. In fact, the accuracy of iso-RPMD has already been demonstrated in such a situation by Tao *et al.* in their calculation of state-resolved reaction rates for a one-dimensional two-state model of the $F + H_2$ reaction.[33,34] Application of the method to similar but more complex systems will no doubt provide physical insight in the future.

For systems in which nuclear quantum effects are important and the rate limiting step involves passage through the through the diabatic crossing, such as many biological and inorganic electron transfer reactions, more work is clearly needed to make iso-RPMD an accurate method for calculating reaction rates. In order to apply iso-RPMD to such systems one would need to modify the isomorphic Hamiltonian or the dynamics to make it more closely related to an accurate approximation to the exact quantum rate in the golden-rule limit. This might be achieved by making a connection to Wolynes theory,[82] or to one of the newer path-integral based approaches that we will discuss in Chap. 7, which have a very similar functional form to Eq. 3.42. But whether or not such an improvement is possible remains to be seen.

3.A Appendix: Golden-rule limit of $\Delta_n^{\mathrm{iso}}(\mathbf{q})^2$

Here we evaluate the golden-rule limit of the iso-RP coupling, $\Delta_n^{\mathrm{iso}}(\mathbf{q})$. In order to keep the argument as simple as possible, we will consider a position independent $\Delta(\boldsymbol{q}) = \Delta$. It is also simpler to work in path-integral notation, where ring-polymer configurations $\mathbf{q}$ (in the infinite n limit) become cyclic paths $\boldsymbol{q}(\tau)$ parameterised by imaginary time τ. Consequently functions of a single ring-polymer configuration, $A(\mathbf{q})$, become functionals of the imaginary-time path, $A[\boldsymbol{q}(\tau)]$. Making this notational change we can recast Eq. 3.40 in the infinite n limit as

$$k_{\mathrm{iso}} = \left\langle \frac{2\pi}{\hbar} (\Delta^{\mathrm{iso}}[\boldsymbol{q}(\tau)])^2 \delta(V_-^{\mathrm{iso}}[\boldsymbol{q}(\tau)] + \epsilon) \right\rangle_0^{\mathrm{iso}}, \tag{3.60}$$

where

$$V_{-}^{\mathrm{iso}}[\boldsymbol{q}(\tau)] = V_{0}^{\mathrm{iso}}[\boldsymbol{q}(\tau)] - V_{1}^{\mathrm{iso}}[\boldsymbol{q}(\tau)] \tag{3.61}$$

$$V_{i}^{\mathrm{iso}}[\boldsymbol{q}(\tau)] = \frac{1}{\beta\hbar}\int_{0}^{\beta\hbar} V_{i}(\boldsymbol{q}(\tau))\,\mathrm{d}\tau, \tag{3.62}$$

and the expectation value is given by

$$\langle A[\boldsymbol{q}(\tau)]\rangle_{0}^{\mathrm{iso}} = \frac{\oint \mathcal{D}\boldsymbol{q}(\tau)\, e^{-S_{0}^{\mathrm{iso}}[\boldsymbol{q}(\tau)]/\hbar} A[\boldsymbol{q}(\tau)]}{\oint \mathcal{D}\boldsymbol{q}(\tau)\, e^{-S_{0}^{\mathrm{iso}}[\boldsymbol{q}(\tau)]/\hbar}}, \tag{3.63}$$

with

$$S_{0}^{\mathrm{iso}}[\boldsymbol{q}(\tau)] = \int_{0}^{\beta\hbar} \sum_{\nu=1}^{f} \frac{1}{2} m_{\nu}\dot{q}_{\nu}^{2}(\tau) + V_{0}(\boldsymbol{q}(\tau))\,\mathrm{d}\tau. \tag{3.64}$$

Note that the integrals over the positions of the ring-polymer beads have become a "path integral" over all possible paths $\boldsymbol{q}(\tau)$. The circle indicates that the paths are cyclic, $\boldsymbol{q}(\tau + \beta\hbar) = \boldsymbol{q}(\tau)$, and the measure $\mathcal{D}\boldsymbol{q}(\tau)$ contains the integrals over the ring-polymer momenta (which can be done analytically).

In this notation, the isomorphic coupling in Eq. 3.36 becomes

$$\Delta^{\mathrm{iso}}\left[\boldsymbol{q}(\tau)\right]^{2} = \frac{1}{\beta^{2}}\,\mathrm{acosh}^{2}\left[\frac{\mu[\boldsymbol{q}(\tau)]}{2} e^{\beta(V_{+}^{\mathrm{iso}}[\boldsymbol{q}(\tau)]-\epsilon)/2}\right] - \frac{\left(V_{-}^{\mathrm{iso}}[\boldsymbol{q}(\tau)] + \epsilon\right)^{2}}{4}, \tag{3.65}$$

where

$$V_{+}^{\mathrm{iso}}[\boldsymbol{q}(\tau)] = V_{0}^{\mathrm{iso}}[\boldsymbol{q}(\tau)] + V_{1}^{\mathrm{iso}}[\boldsymbol{q}(\tau)] \tag{3.66}$$

and

$$\mu[\boldsymbol{q}(\tau)] = \mathrm{tr_{e}}\left[\mathcal{T}\exp\left(-\frac{1}{\hbar}\int_{0}^{\beta\hbar} \boldsymbol{V}(\boldsymbol{q}(\tau))\,\mathrm{d}\tau\right)\right], \tag{3.67}$$

in which the $\mathcal{T}$ is now an imaginary-time ordering operator and $\boldsymbol{V}(\boldsymbol{q}(\tau))$ is just the diabatic potential matrix evaluated at $\boldsymbol{q}(\tau)$.

To find the golden-rule limit of $\Delta^{\mathrm{iso}}[\boldsymbol{q}(\tau)]^{2}$, we first note that the only term in Eq. 3.65 which depends on the physical coupling, Δ, is $\mu[\boldsymbol{q}(\tau)]$. Hence we begin by expanding $\mu[\boldsymbol{q}(\tau)]$ to second order in Δ as

$$\mu[\boldsymbol{q}(\tau)] = \mu_{0}[\boldsymbol{q}(\tau)] + \Delta^{2}\mu_{2}[\boldsymbol{q}(\tau)] + O(\Delta^{4}). \tag{3.68}$$

In order to evaluate each term in this expansion one can expand the trace as

$$\mu[\boldsymbol{q}(\tau)] = \lim_{n\to\infty} \prod_{j=1}^{n} \Big(\sum_{\sigma_j=0}^{1} \left\langle \sigma_j \right| e^{-\beta_n \boldsymbol{V}(\boldsymbol{q}(\tau_j))} \left| \sigma_{j+1} \right\rangle \Big), \tag{3.69}$$

where $\tau_j = j\beta_n\hbar$ and $\sigma_{n+1} = \sigma_1$. Then noting that

$$\langle 0| e^{-\beta_n \boldsymbol{V}(\boldsymbol{q})} |0\rangle = e^{-\beta_n V_0(\boldsymbol{q})} + O(\beta_n^2) \tag{3.70}$$

$$\langle 1| e^{-\beta_n \boldsymbol{V}(\boldsymbol{q})} |1\rangle = e^{-\beta_n (V_1(\boldsymbol{q})-\epsilon)} + O(\beta_n^2) \tag{3.71}$$

and

$$\langle 0| e^{-\beta_n \boldsymbol{V}(\boldsymbol{q})} |1\rangle = -\beta_n \Delta e^{-\beta_n [V_0(\boldsymbol{q})+V_1(\boldsymbol{q})-\epsilon]/2} + O(\beta_n^2), \tag{3.72}$$

we see that each off-diagonal matrix element in the product in Eq. 3.69 contributes one power of Δ. Equivalently, noting that the set $\{\sigma_j\}$ in the infinite n limit corresponds to a stochastic path $\sigma(\tau)$, we see that every time $\sigma(\tau)$ changes from 0 to 1 (known as a kink) we pick up one power of Δ. Since the path $\sigma(\tau)$ has cyclic symmetry it must have an even number of kinks and hence $\mu[\boldsymbol{q}(\tau)]$ is an even function of Δ.

It is immediately obvious that the only paths which contribute to the zeroth order term are those which do not contain any kinks

$$\mu_0[\boldsymbol{q}(\tau)] = e^{-\beta V_0^{\mathrm{iso}}[\boldsymbol{q}(\tau)]} + e^{-\beta (V_1^{\mathrm{iso}}[\boldsymbol{q}(\tau)]-\epsilon)}, \tag{3.73}$$

corresponding to $\sigma(\tau) = 0$ and $\sigma(\tau) = 1$ for all τ in the trace over diabatic states in Eq. 3.67. Similarly the only paths which contribute to $\mu_2[\boldsymbol{q}(\tau)]$ are those which contain two kinks. Each of these paths can be characterised by two parameters, the total time which the path spends on diabat 1, which we denote $\lambda\hbar$

$$\lambda\hbar = \int_0^{\beta\hbar} \sigma(\tau)\, \mathrm{d}\tau, \tag{3.74}$$

and the time at which $\sigma(\tau)$ changes from 0 to 1, which we label τ'. We can thus write the second order term as

$$\mu_2[\boldsymbol{q}(\tau)] = \frac{1}{\hbar} \int_0^{\beta} \mathrm{d}\lambda \int_0^{\beta\hbar} \mathrm{d}\tau' e^{-(\beta-\lambda)V_0^{\lambda}[\boldsymbol{q}(\tau+\tau')]-\lambda(V_1^{\lambda}[\boldsymbol{q}(\tau+\tau')]-\epsilon)}, \tag{3.75}$$

where

$$V_0^\lambda[\boldsymbol{q}(\tau)] = \frac{1}{(\beta-\lambda)\hbar}\int_{\lambda\hbar}^{\beta\hbar} V_0(\boldsymbol{q}(\tau))\,\mathrm{d}\tau \tag{3.76}$$

$$V_1^\lambda[\boldsymbol{q}(\tau)] = \frac{1}{\lambda\hbar}\int_{0}^{\lambda\hbar} V_1(\boldsymbol{q}(\tau))\,\mathrm{d}\tau. \tag{3.77}$$

Now by first recognising that

$$\frac{\mu_0[\boldsymbol{q}(\tau)]}{2} e^{\beta(V_+^{\mathrm{iso}}[\boldsymbol{q}(\tau)]-\epsilon)/2} = \cosh(\beta(V_-^{\mathrm{iso}}[\boldsymbol{q}(\tau)]+\epsilon)/2), \tag{3.78}$$

and then making use of

$$\mathrm{acosh}^2[\cosh(a)+b\Delta^2]-a^2 = \frac{2b\Delta^2 a}{\sinh(a)} + O(\Delta^4), \tag{3.79}$$

it is straightforward to show that we can write the coupling as

$$\Delta^{\mathrm{iso}}[\boldsymbol{q}(\tau)]^2 = \Delta^2\frac{\mu_2[\boldsymbol{q}(\tau)]}{\mu_2^{\mathrm{iso}}[\boldsymbol{q}(\tau)]} + O(\Delta^4), \tag{3.80}$$

where

$$\mu_2^{\mathrm{iso}}[\boldsymbol{q}(\tau)] = \frac{2\beta\sinh\left(\beta(V_-^{\mathrm{iso}}[\boldsymbol{q}(\tau)]+\epsilon)/2\right)}{e^{\beta(V_+^{\mathrm{iso}}[\boldsymbol{q}(\tau)]-\epsilon)/2}\,(V_-^{\mathrm{iso}}[\boldsymbol{q}(\tau)]+\epsilon)}, \tag{3.81}$$

or equivalently

$$\mu_2^{\mathrm{iso}}[\boldsymbol{q}(\tau)] = \frac{1}{\hbar}\int_0^\beta \mathrm{d}\lambda\int_0^{\beta\hbar}\mathrm{d}\tau' e^{-(\beta-\lambda)V_0^{\mathrm{iso}}[\boldsymbol{q}(\tau)]-\lambda(V_1^{\mathrm{iso}}[\boldsymbol{q}(\tau)]-\epsilon)}. \tag{3.82}$$

Next recognising that

$$\frac{\delta(V_-^{\mathrm{iso}}[\boldsymbol{q}(\tau)]+\epsilon)}{\mu_2^{\mathrm{iso}}[\boldsymbol{q}(\tau)]} = \frac{\delta(V_-^{\mathrm{iso}}[\boldsymbol{q}(\tau)]+\epsilon)}{e^{-\beta V_0^{\mathrm{iso}}[\boldsymbol{q}(\tau)]}\beta^2}, \tag{3.83}$$

and also that

$$\frac{e^{-S_0^{\mathrm{iso}}[\boldsymbol{q}(\tau)]/\hbar}\mu_2[\boldsymbol{q}(\tau)]}{e^{-\beta V_0^{\mathrm{iso}}[\boldsymbol{q}(\tau)]}} = \frac{1}{\hbar}\int_0^\beta \mathrm{d}\lambda\int_0^{\beta\hbar}\mathrm{d}\tau' e^{-S^{(\lambda)}[\boldsymbol{q}(\tau+\tau')]/\hbar+\lambda\epsilon}, \tag{3.84}$$

where

$$S^{(\lambda)}[\boldsymbol{q}(\tau)] = S_0^{(\lambda)}[\boldsymbol{q}(\tau)] + S_1^{(\lambda)}[\boldsymbol{q}(\tau)] \tag{3.85}$$

$$S_0^{(\lambda)}[\boldsymbol{q}(\tau)] = \int_{\lambda\hbar}^{\beta\hbar}\sum_{\nu=1}^{f}\frac{1}{2}m_\nu\dot{q}_\nu^2(\tau) + V_0(\boldsymbol{q}(\tau))\mathrm{d}\tau \tag{3.86}$$

$$S_1^{(\lambda)}[\boldsymbol{q}(\tau)] = \int_{0}^{\lambda\hbar}\sum_{\nu=1}^{f}\frac{1}{2}m_\nu\dot{q}_\nu^2(\tau) + V_1(\boldsymbol{q}(\tau))\mathrm{d}\tau, \tag{3.87}$$

we see that we can rewrite Eq. 3.60 in the golden-rule limit as in Eq. 3.42,

$$k_{\mathrm{iso}} = \frac{2\pi}{\beta\hbar Q_r}\int_0^\beta d\lambda \left\langle \Delta^2\delta(V_-^{\mathrm{iso}}[\boldsymbol{q}(\tau)])\right\rangle_\lambda e^{-\beta F_{\mathrm{GR}}(\lambda)+\lambda\epsilon}, \tag{3.88}$$

with

$$\langle A[\boldsymbol{q}(\tau)]\rangle_\lambda = \frac{\oint \mathcal{D}\boldsymbol{q}(\tau) e^{-S^{(\lambda)}[\boldsymbol{q}(\tau)]/\hbar} A[\boldsymbol{q}(\tau)]}{\oint \mathcal{D}\boldsymbol{q}(\tau) e^{-S^{(\lambda)}[\boldsymbol{q}(\tau)]/\hbar}} \tag{3.89}$$

and

$$\begin{aligned} e^{-\beta F_{\mathrm{GR}}(\lambda)} &= \mathrm{tr_n}[e^{-(\beta-\lambda)\hat{H}_0} e^{-\lambda\hat{H}_1}] \\ &= \oint \mathcal{D}\boldsymbol{q}(\tau)\, e^{-S^{(\lambda)}[\boldsymbol{q}(\tau)]/\hbar} \end{aligned} \tag{3.90}$$

and

$$\begin{aligned} Q_r = e^{-\beta F_{\mathrm{GR}}(0)} &= \mathrm{tr_n}\left[e^{-\beta\hat{H}_0}\right] \\ &= \oint \mathcal{D}\boldsymbol{q}(\tau)\, e^{-S^{(0)}[\boldsymbol{q}(\tau)]/\hbar}. \end{aligned} \tag{3.91}$$

4

A general non-adiabatic quantum instanton

Contents

Summary

In this chapter we present a general quantum instanton approach to calculating reaction rates for systems with two electronic states and arbitrary values of the electronic coupling. This new approach, which we call the non-adiabatic quantum instanton (NAQI) approximation, reduces to Wolynes theory in the golden-rule limit and to a recently proposed projected quantum instanton (PQI) method in the adiabatic limit. As in both of these earlier theories, the NAQI approach is based on making a saddle point approximation to the time integral of a modified reactive flux autocorrelation function, although with a generalised definition of the projection operator onto the product states. We illustrate the accuracy of the approach by comparison with exact rates for one dimensional scattering problems and discuss its applicability to more complex reactions.

4.1 Introduction

When developing new path-integral methods for studying non-adiabatic systems a common approach has been to generalise a pre-existing adiabatic method. One of the most successful path-integral techniques for electronically adiabatic reactions is ring-polymer molecular dynamics (RPMD) reaction rate theory,[18,19] and because of this, as we saw in the previous chapter, much of the work in this area has focussed on trying to extend it to treat non-adiabatic systems.[25–34] The success of RPMD in the deep tunnelling regime has been explained by showing it is connected to the semiclassical instanton approximation,[144] which uses a periodic imaginary-time trajectory through the reaction barrier to describe the tunnelling process.[143] While it is not as generally applicable as RPMD, the semiclassical instanton formula is known to provide a highly accurate description of tunnelling in situations where there is a single dominant tunnelling path. Early work extending the semiclassical instanton approach to treat non-adiabatic reactions was based on assuming that the "Im-F" premise[197–201] could be applied to non-adiabatic systems, and succeeded in providing a theory which bridged between the golden-rule and Born-Oppenheimer limits.[202–204] More recently, Richardson and coworkers[170,195,196] have provided a rigorous derivation of the semiclassical instanton rate in the golden-rule limit,

and found some important differences between the resulting expression and that given by the Im-F formulation. However, their derivation has yet to be extended beyond the golden-rule limit so that it can be applied to reactions with arbitrary electronic coupling strengths.

In this chapter we shall focus on another well known method, the quantum instanton approximation. Unlike the other methods discussed above, this approximation was in fact first suggested in the golden-rule context by Wolynes[82] in 1987 (resulting in the Wolynes theory approximation discussed in Chap. 2), before the adiabatic counterpart was suggested by Miller *et al.*[15] in 2003 (who gave it the name quantum instanton). Wolynes theory and the quantum instanton are both closely related to the semiclassical instanton, and all three can be interpreted as steepest descent approximations to the flux-flux correlation function expression for the reaction rate. However, whereas the semiclassical instanton simultaneously approximates integrals over both position and time, Wolynes theory and the quantum instanton involve just a single steepest descent approximation to the time integral. The resulting expressions only involve time-independent quantities, which can be evaluated by sampling imaginary-time paths.

Recently Vaillant *et al.*[86] have suggested a slight modification of the original adiabatic quantum instanton which they have called the projected quantum instanton (PQI). This enforces sampling of paths close to the semiclassical instanton and results in an expression that is even more closely related to Wolynes theory. In the following we shall present a generalised approach to electronically non-adiabatic reactions that is applicable to arbitrary electronic coupling strengths between the golden-rule and adiabatic limits and which reduces to Wolynes theory and the PQI approximation in these two limits, respectively.

We begin in Sec. 4.2 by discussing how the choice of the projection operators that are used to define the reactants and products affects the functional form of the reactive flux-flux correlation function of an electronically non-adiabatic reaction. Motivated by this discussion, we introduce a simple projection operator onto the product states which can be tuned so as to minimise the recrossing of the transition state dividing surface for any electronic coupling strength. In Sec. 4.3, we summarise the Wolynes theory and quantum instanton approaches to the golden-rule and Born-Oppenheimer limits, before introducing a more general approach for the calculation of reaction rates for arbitrary

electronic coupling strengths, which we shall call the non-adiabatic quantum instanton (NAQI) approximation. In Sec. 4.4 we investigate the accuracy of the NAQI formula for a series of simple one-dimensional scattering problems for which the exact quantum mechanical reaction rates can be computed for comparison. Sec. 4.5 concludes the chapter, discussing several possible applications of the NAQI approach and the scope for further theoretical developments.

4.2 Exact reaction rate theory

Since it suffices for our present purposes, we shall restrict our attention to simple one-dimensional scattering problems, such that the Hamiltonian can be written as

$$\hat{H} = \hat{H}_0|0\rangle\langle 0| + (\hat{H}_1 - \epsilon)|1\rangle\langle 1| + \Delta(|0\rangle\langle 1| + |1\rangle\langle 0|), \tag{4.1}$$

with

$$\hat{H}_i = \frac{\hat{p}^2}{2m} + V_i(\hat{q}), \tag{4.2}$$

in which $V_i(q)$ is the diabatic potential on electronic state $|i\rangle$. We shall also assume that the electronic coupling Δ is a constant, independent of the nuclear configuration q. Within this simple framework, the adiabatic potentials, $U_j(q)$, are

$$U_j(q) = \frac{V_0(q) + V_1(q) - \epsilon}{2} - \frac{(-1)^j}{2}\sqrt{(V_0(q) - V_1(q) + \epsilon)^2 + 4\Delta^2}. \tag{4.3}$$

Everything we shall have to say can readily be generalised to treat more complex multi-dimensional reactions, and to include non-Condon effects. However, Eqs. 4.2 and 4.3 are all we shall need to make the points we would like to make here.

Following from Sec. 2.2.2, we will work with the flux-flux correlation form of the exact quantum mechanical rate[134,136,137]

$$kQ_r = \frac{1}{2}\int_{-\infty}^{\infty} \bar{c}_{\mathrm{ff}}(t)\,\mathrm{d}t, \tag{4.4}$$

where $Q_r = \sqrt{m/2\pi\beta\hbar^2}$ is the reactant partition function per unit length and

$$\bar{c}_{\mathrm{ff}}(t) = \mathrm{Tr}\left[e^{-\beta\hat{H}/2}\hat{F}_p e^{-\beta\hat{H}/2} e^{+i\hat{H}t/\hbar}\hat{F}_p e^{-i\hat{H}t/\hbar}\right] \tag{4.5}$$

is the thermally symmetrised reactive flux autocorrelation function. As discussed in Chap. 2 this formulation applies equally well in both the adiabatic and non-adiabatic limits with appropriate definitions of the projection operator $\hat{P}_p$.

In the adiabatic limit where the Born-Oppenheimer approximation is valid, it is usual to define $\hat{P}_p$ as

$$\hat{P}_p = \theta(s(\hat{q})), \tag{4.6}$$

where $\theta(x)$ is a Heaviside step function and $s(q) = 0$ is a position space dividing surface between the reactants [$s(q) < 0$] and products [$s(q) > 0$]. The flux operator then becomes

$$\hat{F}_p = \frac{\hat{p}}{2m}\frac{\partial s}{\partial q}\delta(s(\hat{q})) + \frac{\partial s}{\partial q}\delta(s(\hat{q}))\frac{\hat{p}}{2m}. \tag{4.7}$$

In the golden-rule limit where $\Delta \to 0$, it is more usual to define the rate in terms of a transition between the diabatic states $|0\rangle$ and $|1\rangle$, which gives

$$\hat{P}_p = |1\rangle\langle 1|, \tag{4.8}$$

and

$$\hat{F}_p = \frac{i}{\hbar}\Delta(|0\rangle\langle 1| - |1\rangle\langle 0|). \tag{4.9}$$

In situations where the reactants and products can equally well be distinguished using either definition of $\hat{P}_p$, the rate constant is independent of the definition used. However, while the choice of projection operator does not change the rate, it does change the functional form of the flux-flux correlation function. To illustrate this we shall consider a simple symmetric curve crossing problem

$$V_0(q) = Ae^{+q/L}, \tag{4.10a}$$

$$V_1(q) = Ae^{-q/L}, \tag{4.10b}$$

with $\beta A = 48$, $mL^2/\beta\hbar^2 = 1/4$, $\epsilon = 0$, and three different values of the electronic coupling strength ($\beta\Delta$).

Figure 4.1 shows the flux-flux correlation functions for this model problem with $\log_{10}(\beta\Delta) = 1.5$ (approximately in the adiabatic limit), as calculated using both the adiabatic and non-adiabatic projection operators. The position space projection operator

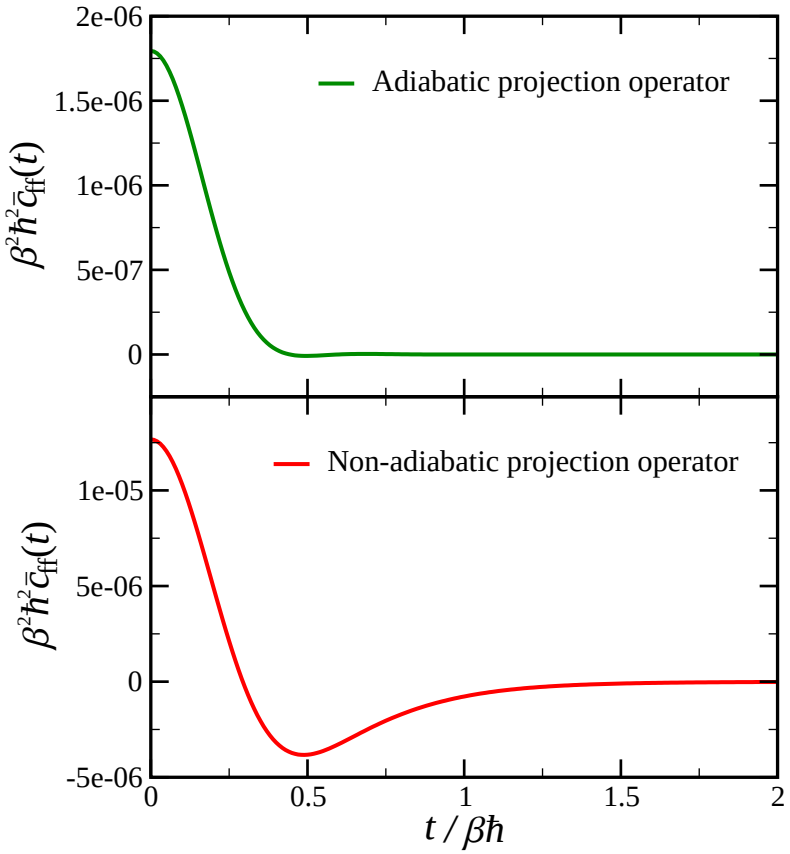

Figure 4.1: Flux-flux correlation functions for an exponential crossing model in the adiabatic regime (with $\beta A = 48$, $mL^2/\beta\hbar^2 = 1/4$ and $\log_{10}(\beta\Delta) = 1.5$). Note the different scales on the y-axes in the two panels. The areas under both curves are the same. However the non-adiabatic projection operator clearly leads to a much longer-lived correlation function with a negative tail, which indicates recrossing of the dividing surface between reactants and products.[205]

leads to a correlation function which decays quickly with almost no negative correlation, whereas the diabatic projection operator gives a correlation function that is much larger at $t = 0$ and has a slowly decaying negative tail. The position space projection operator is thus seen to lead to far less recrossing than the diabatic projection operator in this regime.

Figure 4.2 shows the flux-flux correlation function for $\log_{10}(\beta\Delta) = -2$, which is in the opposite (non-adiabatic) limit. In this case the amount of recrossing is reversed, with the diabatic projection operator leading to an approximately Gaussian flux-flux correlation function with minimal recrossing, whereas the position space projection operator gives rise to significant recrossing. Here the recrossing arises from the high probability that when the system passes through the dividing surface it will remain on

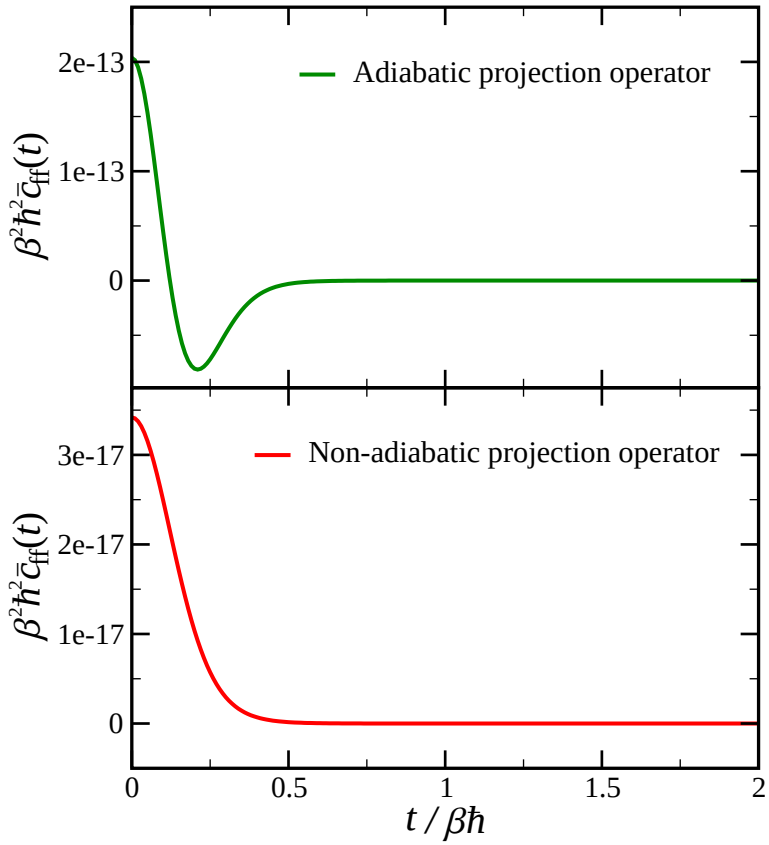

Figure 4.2: Flux-flux correlation functions for an exponential crossing model in the golden-rule regime (with $\beta A = 48$, $mL^2/\beta\hbar^2 = 1/4$ and $\log_{10}(\beta\Delta) = -2$). Note the different scales on the y-axes in the two panels. The areas under both curves are the same. However the adiabatic projection operator clearly leads to a correlation function with a negative tail, which indicates recrossing of the dividing surface between reactants and products.[205]

the same diabatic surface, and hence will a short time later be reflected by the potential wall and return through the dividing surface.

The projection operators in Eqs. 4.6 and 4.8 are clearly quite different. However we note that it is possible to recast the projection operator on to the products in the golden-rule limit in a form that more closely resembles Eq. 4.6,

$$\hat{P}_p = \theta(-\hat{\sigma}_z), \tag{4.11}$$

where $\hat{\sigma}_z$ is the Pauli spin operator $\hat{\sigma}_z = |0\rangle\langle 0| - |1\rangle\langle 1|$. This suggests an obvious generalisation in which the argument of the Heaviside step function is taken to be a linear combination of $s(\hat{q})$ and $\hat{\sigma}_z$,

$$\hat{P}_p(\alpha) = \theta(\cos(\alpha)s(\hat{q}) - \sin(\alpha)\hat{\sigma}_z), \tag{4.12}$$

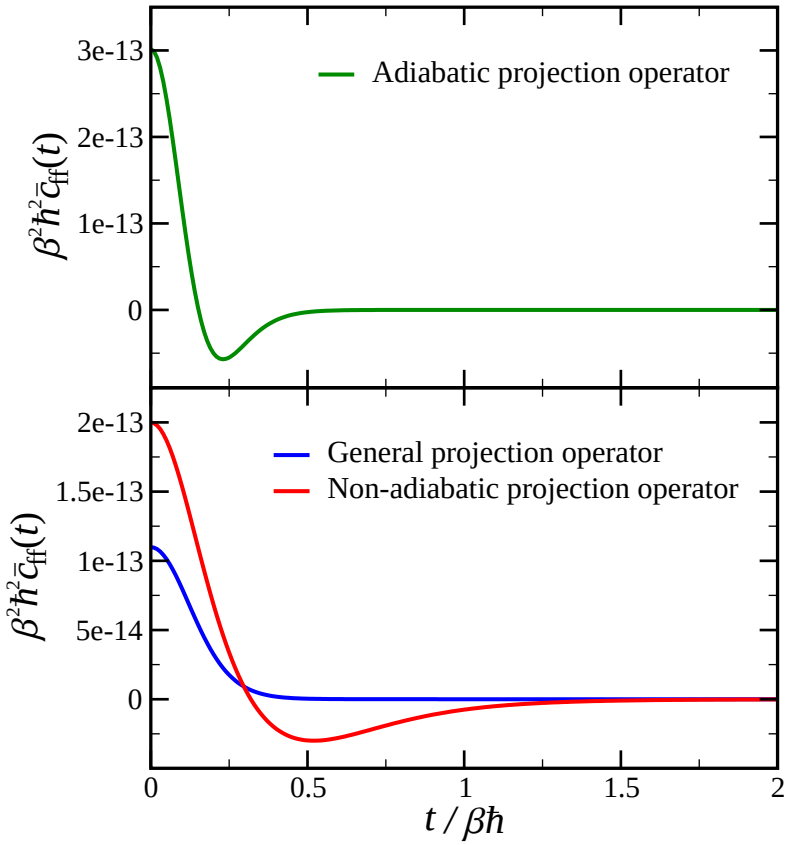

Figure 4.3: Flux-flux correlation functions for an exponential crossing model with parameters intermediate between the golden-rule and the adiabatic limits ($\beta A = 48$, $mL^2/\beta\hbar^2 = 1/4$ and $\log_{10}(\beta\Delta) = -0.25$). Note the different scales on the y-axes in the two panels. The plot clearly illustrates that in this regime the adiabatic projection operator leads to a correlation function with significant recrossing of the dividing surface and the non-adiabatic projection operator leads to a much longer lived correlation function with a negative tail. The generalised projection operator is seen to give a correlation function with almost no recrossing.

or equivalently, provided $0 \leq \alpha < \pi/2$, using the properties of the step function,

$$\hat{P}_p(\alpha) = \theta(s(\hat{q}) - \tan(\alpha)\hat{\sigma}_z). \tag{4.13}$$

This $\hat{P}_p(\alpha)$ is diagonal in the electronic basis with diagonal matrix elements

$$\langle 0| \hat{P}_p(\alpha) |0\rangle = \theta(s(\hat{q}) - \tan(\alpha)), \tag{4.14a}$$

$$\langle 1| \hat{P}_p(\alpha) |1\rangle = \theta(s(\hat{q}) + \tan(\alpha)), \tag{4.14b}$$

and so we see that we can also think of the generalised projection operator as effectively giving rise to two separate position space dividing surfaces, one for each diabatic state.

In the Born-Oppenheimer limit it is clear that $\alpha \to 0$, and in the non-adiabatic limit that $\alpha \to \pi/2$. In Figure 4.3 we show the flux-flux correlation functions for the system with $\log_{10}(\beta\Delta) = -0.25$, which is intermediate between the adiabatic and non-adiabatic limits. The results for all three projection operators are shown, with $s(q) = q/L$ and $\tan(\alpha) = 12/5$ in the case of the generalised projection operator in Eq. 4.12. We see that with this choice of α the correlation function is approximately Gaussian with minimal recrossing. In contrast both the purely position space and purely diabatic state projection operators have significantly higher initial values, along with regions of negative correlation corresponding to recrossing.

4.3 Flux-flux based quantum transition state theories

The advantage of writing the rate in terms of the integral of a flux-flux correlation function with minimal recrossing is that one can then use this to develop a kind of quantum transition state theory, i.e. an approximate expression for the rate which depends only on time independent quantities. The approach we take here follows the Wolynes theory approximation, introduced in Chap. 2, and the closely related quantum instanton approximation to the Born-Oppenheimer rate. We begin this section by recapping the derivation of Wolynes theory[82] and giving a summary of the quantum instanton approximation,[15] before showing how they can be generalised to give a method that is applicable to electronically non-adiabatic reactions with arbitrary coupling strength.

4.3.1 Wolynes theory

As discussed in Chap. 2, in order to derive the Wolynes theory expression for the rate one begins by taking the golden-rule limit of the flux-flux correlation function, with the flux operator defined as in Eq. 4.9, to give

$$\bar{c}_{\mathrm{ff}}(t) = \frac{2\Delta^2}{\hbar^2}\,\mathrm{Re}\left(c_{\mathrm{GR}}(t + i\beta\hbar/2)\right), \tag{4.15}$$

where

$$c_{\mathrm{GR}}(t + i\beta\hbar/2) = \mathrm{tr_n}\left[e^{-\beta\hat{H}_0/2 - i\hat{H}_0 t/\hbar} e^{-\beta(\hat{H}_1 - \epsilon)/2 + i(\hat{H}_1 - \epsilon)t/\hbar}\right]. \tag{4.16}$$

Hence, a non-zero bias to products, ϵ, introduces an oscillatory component into the correlation function, $e^{+\beta\epsilon/2-i\epsilon t/\hbar}$. In order to remove this oscillation and restore the approximately Gaussian behaviour seen for the symmetric problem in the lower panel of Fig. 4.2, one makes use of the relation, $c_{\mathrm{GR}}(-t+i\beta\hbar/2) = c^{*}_{\mathrm{GR}}(t+i\beta\hbar/2)$ to rewrite the rate as

$$kQ_r = \frac{\Delta^2}{\hbar^2}\int_{-\infty}^{\infty} c_{\mathrm{GR}}(t+i\beta\hbar/2)\,\mathrm{d}t, \tag{4.17}$$

and then performs the integration over time by shifting the contour of integration to pass through a saddle point of $c_{\mathrm{GR}}(t)$ on the imaginary-time axis. This leads to the Wolynes theory approximation to the rate[82]

$$k_{\mathrm{WT}}Q_r = \frac{\Delta^2}{\hbar}\sqrt{\frac{2\pi}{-\beta F''_{\mathrm{WT}}(\lambda_{\mathrm{sp}})}}e^{-\beta F_{\mathrm{WT}}(\lambda_{\mathrm{sp}})}, \tag{4.18}$$

where

$$\begin{aligned} e^{-\beta F_{\mathrm{WT}}(\lambda)} &= \mathrm{tr}_{\mathrm{n}}\left[e^{-(\beta-\lambda)\hat{H}_0}e^{-\lambda(\hat{H}_1-\epsilon)}\right] \\ &= c_{\mathrm{GR}}(i\lambda\hbar) \end{aligned} \tag{4.19}$$

and the saddle point condition is $\beta F'_{\mathrm{WT}}(\lambda_{\mathrm{sp}}) = 0$.*

4.3.2 Adiabatic quantum instanton

In the adiabatic limit, for reactions which can be considered to proceed on the lower adiabatic surface, the flux-flux correlation function becomes

$$\bar{c}_{\mathrm{ff}}(t) = \mathrm{tr}_{\mathrm{n}}\left[e^{-\beta\hat{H}_{\mathrm{BO}}/2}\hat{F}_p e^{-\beta\hat{H}_{\mathrm{BO}}/2}e^{+i\hat{H}_{\mathrm{BO}}t/\hbar}\hat{F}_p e^{-i\hat{H}_{\mathrm{BO}}t/\hbar}\right], \tag{4.20}$$

where

$$\hat{H}_{\mathrm{BO}} = \frac{\hat{p}^2}{2m} + \hat{U}_0(q) \tag{4.21}$$

and the flux operator is defined by Eq. 4.7. The original paper by Miller *et al.*[15] proposed two closely related "quantum instanton" methods. The conceptually simpler of the two makes a second order cumulant approximation to the flux-flux correlation function,

$$\bar{c}_{\mathrm{ff}}(t) \simeq \bar{c}_{\mathrm{ff}}(0)\exp\left(\frac{\ddot{\bar{c}}_{\mathrm{ff}}(0)}{2\bar{c}_{\mathrm{ff}}(0)}t^2\right), \tag{4.22}$$

*Note that for consistency of notation with the PQI and NAQI approaches introduced later we have here defined the free energy to include the external bias $F_{\mathrm{WT}}(\lambda) = F_{\mathrm{GR}}(\lambda) - \epsilon\lambda/\beta$.

and then integrates over time to give

$$k_{\mathrm{QI}}Q_r = \sqrt{\frac{\pi\bar{c}_{\mathrm{ff}}(0)}{-2\ddot{\bar{c}}_{\mathrm{ff}}(0)}}\bar{c}_{\mathrm{ff}}(0). \tag{4.23}$$

The problem with this approach is that the second order cumulant expansion of the flux-flux correlation function can be a poor approximation for asymmetric reactions. This can be understood as arising for essentially the same reason as we have discussed above for Wolynes theory. Vaillant *et al.*[86] have recently examined the problem in detail with a semiclassical analysis in which they showed that neither Eq. 4.23 nor the alternative formulation of the quantum instanton method in the original paper by Miller *et al.*[15] reduces to the semiclassical instanton approximation in the limit as $\hbar \to 0$.

In order to fix this problem, Vaillant *et al.* have suggested a modified method, the projected quantum instanton (PQI), in which the flux-flux correlation function is approximated as[86]

$$\bar{c}_{\mathrm{ff}}(t) \simeq 2\mathrm{Re}\left[c_{\mathrm{PQI}}(t + i\beta\hbar/2)\right], \tag{4.24}$$

where

$$c_{\mathrm{PQI}}(t + i\beta\hbar/2) = \mathrm{tr_n}\left[\hat{W}_r(i\beta\hbar/2 - t)\,\hat{F}_p\hat{W}_p(i\beta\hbar/2 + t)\,\hat{F}_p\right], \tag{4.25}$$

with

$$\hat{W}_s(t) = e^{+i\hat{H}_{\mathrm{BO}}t/2\hbar}\hat{P}_s e^{+i\hat{H}_{\mathrm{BO}}t/2\hbar} \tag{4.26}$$

for $s = r$ and p, with $\hat{P}_r = \hat{1} - \hat{P}_p$. The difference between Eqs. 4.20 and 4.24 is that the exact $\bar{c}_{\mathrm{ff}}(t)$ contains two additional terms of the form

$$\mathrm{tr_n}\left[\hat{W}_s(i\beta\hbar/2 - t)\,\hat{F}_p\hat{W}_s(i\beta\hbar/2 + t)\,\hat{F}_p\right]$$

with $s = r$ and p. However, Vaillant *et al.* argue that since the time integrals of these terms vanish in the semiclassical ($\hbar \to 0$) limit, they can safely be neglected when calculating the reaction rate.[86]

Substituting Eq. 4.24 into Eq. 4.4 and noting that $c_{\mathrm{PQI}}(-t + i\beta\hbar/2) = c^*_{\mathrm{PQI}}(t + i\beta\hbar/2)$ gives

$$kQ_r \simeq \int_{-\infty}^{\infty} c_{\mathrm{PQI}}(t + i\beta\hbar/2)\,\mathrm{d}t. \tag{4.27}$$

This time integral can be evaluated by steepest descent as in Wolynes theory to give

$$k_{\mathrm{PQI}}Q_r = \frac{1}{\beta^2\hbar}\sqrt{\frac{2\pi}{-\beta F''_{\mathrm{PQI}}(\lambda_{\mathrm{sp}})}}e^{-\beta F_{\mathrm{PQI}}(\lambda_{\mathrm{sp}})}, \tag{4.28}$$

where

$$\begin{aligned} e^{-\beta F_{\mathrm{PQI}}(\lambda)} &= (\beta\hbar)^2 \mathrm{tr}_{\mathrm{n}}\left[\hat{W}_r(i(\beta-\lambda)\hbar)\,\hat{F}_p\hat{W}_p(i\lambda\hbar)\,\hat{F}_p\right] \\ &= (\beta\hbar)^2 c_{\mathrm{PQI}}(i\lambda\hbar), \end{aligned} \tag{4.29}$$

in which the factor of $(\beta\hbar)^2$ has been introduced to ensure dimensional consistency in Eq. 4.29 and then compensated for in Eq. 4.28. The saddle point condition is now $F'_{\mathrm{PQI}}(\lambda_{\mathrm{sp}}) = 0$, which is satisfied by the value of λ that maximises $F_{\mathrm{PQI}}(\lambda)$ and minimises $c_{\mathrm{PQI}}(i\lambda\hbar)$.

4.3.3 Non-adiabatic quantum instanton

It is clear from the above discussion that the PQI method is very closely related to Wolynes theory.[82] This connection can be made more explicit by noting that Wolynes theory and the PQI method can be regarded as the golden-rule limit and adiabatic limit, respectively, of a more general non-adiabatic QI method.

In order to derive this NAQI method one simply proceeds as in Eqs. 4.24 to 4.29, but using the flux operator corresponding to the generalised projection operator, $\hat{P}_p(\alpha)$, in Eq. 4.12. The final result has the same form as Eq. 4.28,

$$k_{\mathrm{NAQI}}Q_r = \frac{1}{\beta^2\hbar}\sqrt{\frac{2\pi}{-\beta F''_{\alpha^\star}(\lambda_{\mathrm{sp}})}}e^{-\beta F_{\alpha^\star}(\lambda_{\mathrm{sp}})}, \tag{4.30}$$

where

$$\begin{aligned} e^{-\beta F_\alpha(\lambda)} &= (\beta\hbar)^2\,\mathrm{Tr}\left[\hat{W}_r(i(\beta-\lambda)\hbar)\,\hat{F}\hat{W}_p(i\lambda\hbar)\,\hat{F}\right] \\ &= (\beta\hbar)^2 c_\alpha(i\lambda\hbar) \end{aligned} \tag{4.31}$$

and we have defined $\alpha^\star$ and λ_{sp} as the values of α and λ that maximise $F_\alpha(\lambda)$ and minimise $c_\alpha(i\lambda\hbar)$. Note that now the projected propagators are

$$\hat{W}_s(t) = e^{+i\hat{H}t/2\hbar}\hat{P}_s e^{+i\hat{H}t/2\hbar}. \tag{4.32}$$

When $\Delta \to 0$ and $\alpha^\star \to \pi/2$, as is the case in the golden-rule limit, Eq. 4.30 reduces to Wolynes theory,[82] and when the upper adiabatic electronic state becomes thermally inaccessible and $\alpha^\star \to 0$, it reduces to the adiabatic PQI of Vaillant *et al.*[86] The NAQI method is thus a generalisation of these pre-existing methods which can be applied to reactions that are intermediate between the two limiting regimes.

4.4 Results and discussion

To illustrate the accuracy of the NAQI approach we shall again consider the exponential curve crossing model from Sec. 4.2, now with a series of different values for the bias, ϵ. Defining the transition state, $q^\ddagger$, as the solution to the equation $V_0(q^\ddagger) = V_1(q^\ddagger) - \epsilon$, and the value of the potential at the crossing point as $V^\ddagger = V_0(q^\ddagger)$, the behaviour of this model can be fully characterised by the four dimensionless parameters, $\beta\Delta$, $\beta V^\ddagger$, $\beta\epsilon$ and $mL^2/\beta\hbar^2$. Note that $A = \sqrt{(V^\ddagger + \epsilon/2)^2 - \epsilon^2/4}$.

To demonstrate the behaviour of the NAQI method in different regimes we shall consider three systems in which the values of $\beta V^\ddagger$, $\beta\epsilon$ and $mL^2/\beta\hbar^2$ are fixed while $\beta\Delta$ is varied so as to span the range from golden-rule to Born-Oppenheimer like behaviour. For each value of $\beta\Delta$, the NAQI rate was evaluated using a sine finite basis representation (FBR) in the barrier region, with α and λ optimised along with the location of the position space dividing surface, $s(q) = (q - q_0)/L$, so as to minimise $c_\alpha(i\lambda\hbar)$. The exact rate was computed for comparison by integrating the cumulative reaction probability

$$kQ_r\beta\hbar = \frac{1}{2\pi}\int_0^\infty e^{-\beta E}N(E)\beta \mathrm{d}E, \tag{4.33}$$

with $N(E)$ calculated using the coupled channel log derivative method (code written by Prof. David E. Manolopoulos).[206]

In order to illustrate the importance of nuclear quantum effects, we shall compare the exact and NAQI results with the classical Born-Oppenheimer rate

$$k_{\text{cl-BO}}Q_r\beta\hbar = \frac{1}{2\pi}e^{-\beta U_0^\ddagger}, \tag{4.34}$$

where $U_0^{\ddagger} = \frac{1}{2}\Big(\sqrt{4(A-\Delta)^2+\epsilon^2} - \epsilon\Big)$ is the maximum on the lower adiabatic potential, and with the classical golden-rule rate

$$k_{\text{cl-GR}} Q_r \beta\hbar = \frac{\Delta^2\sqrt{2\pi m\beta}}{\hbar|V_0'(q^{\ddagger}) - V_1'(q^{\ddagger})|} e^{-\beta V^{\ddagger}}, \tag{4.35}$$

where $|V_0'(q^{\ddagger}) - V_1'(q^{\ddagger})| = (2V^{\ddagger} + \epsilon)/L$. In terms of the four dimensionless parameters this is simply

$$k_{\text{cl-GR}} Q_r \beta\hbar = \frac{\beta^2\Delta^2}{(2\beta V^{\ddagger} + \beta\epsilon)} \sqrt{\frac{2\pi m L^2}{\beta\hbar^2}} e^{-\beta V^{\ddagger}}. \tag{4.36}$$

The first system we shall consider is the symmetric problem from Sec. 4.2, with $\beta\epsilon = 0$, $\beta V^{\ddagger} = 48$ and $mL^2/\beta\hbar^2 = 1/4$. These parameters were chosen so that when $\log_{10}(\beta\Delta) = 1.5$ the Born-Oppenheimer problem on the lower adiabatic potential is similar to the 300 K symmetric Eckart barrier problem considered by Vaillant *et al.* in Ref. 86. Figure 4.4 compares the NAQI rate with the exact rate for this system. Excellent agreement is obtained for the full range of $\beta\Delta$ considered. The error in the NAQI rate is approximately independent of $\beta\Delta$, and is slightly less than 5%. Comparison with the classical golden-rule and Born-Oppenheimer rates highlights the importance of nuclear quantum effects, showing in particular that the effect of tunnelling on the rate is strongly dependent on the electronic coupling strength. The tunnelling enhancement of the rate ranges from a factor of 30 at the largest value of electronic coupling, $\log_{10}(\beta\Delta) = 1.5$, to 12 orders of magnitude in the golden-rule limit. Clearly there is very efficient tunnelling through the narrow, nearly cusped potential energy barrier at small values of the coupling.

It is interesting to note that the rate constant for the intermediate value of coupling considered in Fig. 4.3, $\log_{10}(\beta\Delta) = -0.25$, is actually very well described by the golden-rule limit in this system. Hence we see that the electronic coupling at which the transition from Born-Oppenheimer to golden-rule behaviour occurs is larger for the rate than the flux-flux correlation function. This results in the optimum value of α remaining close to the adiabatic value while the rate exhibits an approximately quadratic dependence on the electronic coupling characteristic of the golden-rule limit. We do not expect this to be a general feature – it occurs here because this is a symmetric problem in the deep tunnelling regime. In fact, we believe this helps to explain the success of "mean field" methods

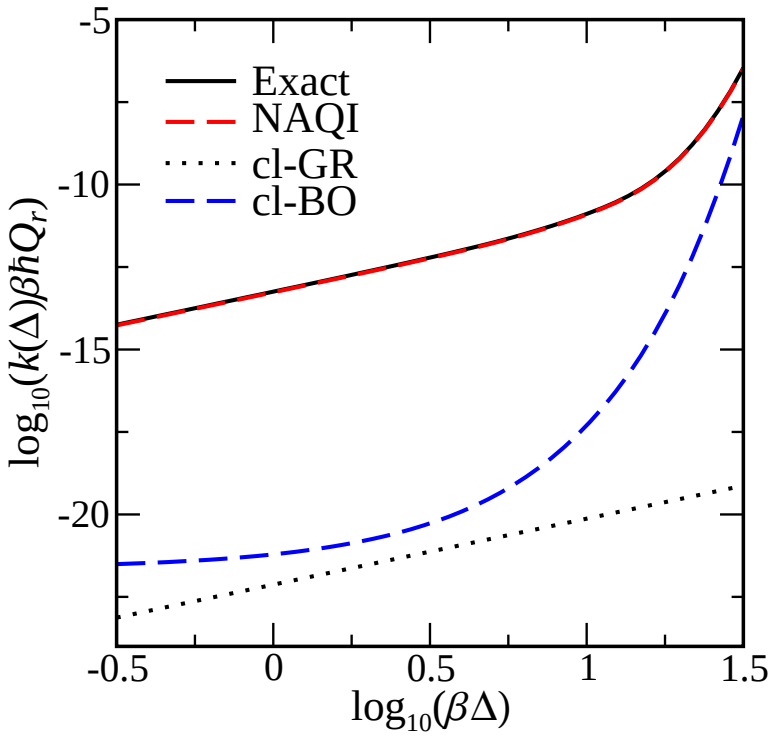

Figure 4.4: Comparison of the exact and NAQI rates as a function of the diabatic coupling $\log(\beta\Delta)$ for a symmetric exponential crossing model with $\beta\epsilon = 0$, $\beta V^{\ddagger} = 48$ and $mL^2/\beta\hbar^2 = 1/4$. The classical Born-Oppenheimer and golden-rule rates are included to illustrate the importance of nuclear quantum effects.

for such problems.[28,178] These methods exploit the fact that at intermediate values of the electronic coupling the dominant contribution to the partition function in the barrier region is the Δ^2 term. The Δ^0 terms have a larger action due to lack of tunnelling whereas the Δ^2 term is dominated by paths near the golden-rule instanton which only spend a brief amount of time near the crossing point and have a smaller action. Note that the mean field instanton based methods all involve some kind of *ad hoc* approximation in which the Δ^0 term is thrown away, whereas this is unnecessary in the present NAQI approach.

Figure 4.5 shows the various rates as a function of the electronic coupling for the second system we shall consider, a strongly asymmetric system with $\beta\epsilon = 50$, $\beta V^{\ddagger} = 44.5$ and $mL^2/\beta\hbar^2 = 16/49$. Again the parameters were chosen such that when $\log(\beta\Delta) = 1.5$ the lower adiabatic potential is similar to that in one of the systems studied by Vaillant *et al.*, in this case the most asymmetric system with $\alpha = 4$ at 300 K in Fig. 5 of Ref. 86. As with the first system we see large nuclear quantum effects at all values of electronic

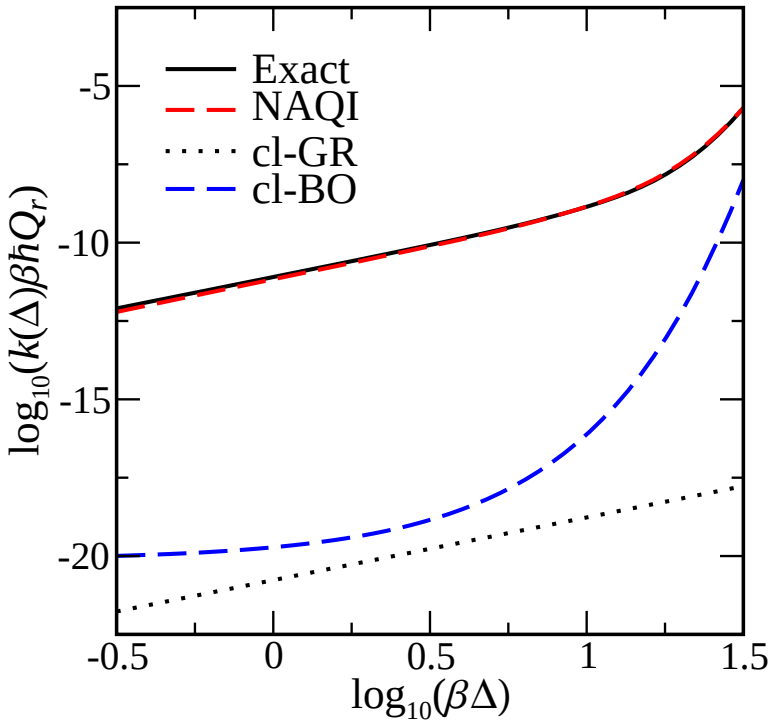

Figure 4.5: Comparison of the exact and NAQI rates as a function of the diabatic coupling $\log(\beta\Delta)$ for an asymmetric exponential crossing model with $\beta\epsilon = 50$, $\beta V^{\ddagger} = 44.5$ and $mL^2/\beta\hbar^2 = 16/49$. The classical Born-Oppenheimer and golden-rule rates are included to illustrate the importance of nuclear quantum effects.

coupling, with the largest quantum enhancement in the golden-rule limit. We find excellent agreement between the exact rate and the NAQI rate, with the largest error near $\log(\beta\Delta) = -0.5$ where the NAQI rate underestimates the exact rate by around 20%. Interestingly the rate is again well described by Fermi's golden rule at this value of $\beta\Delta$ despite the correlation function and the optimum value of α being intermediate between the Born-Oppenheimer and golden-rule regimes. However, in contrast to the symmetric system considered above, the optimum value of α moves significantly away from zero before the rate has begun to exhibit a quadratic dependence on the electronic coupling.

The high accuracy of the method for such an asymmetric system at all values of the electronic coupling is particularly encouraging as it indicates that we are correctly capturing the instanton in this system. In particular, it shows that the introduction of the projection operators into the flux-flux correlation function works not only in the golden-rule and adiabatic limits but also at intermediate values of the electronic

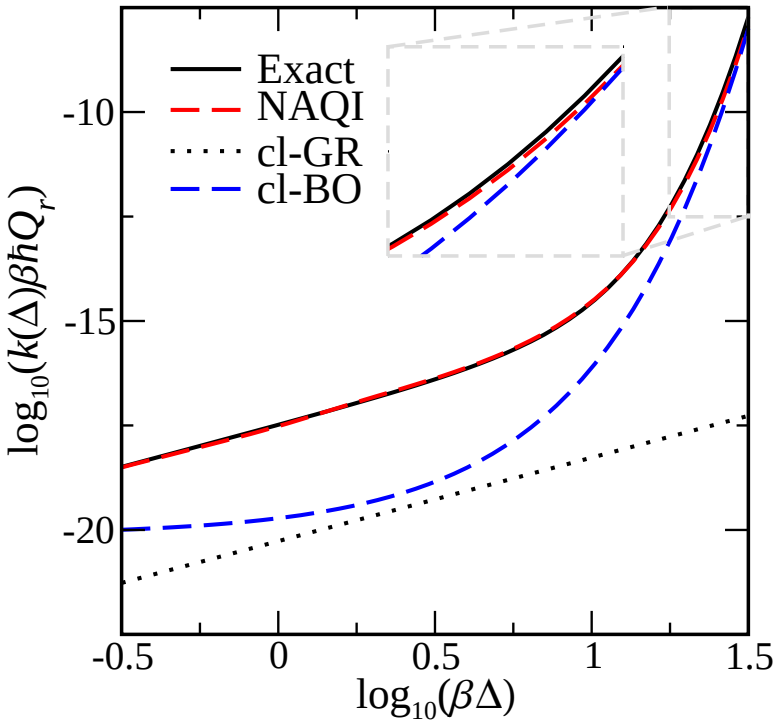

Figure 4.6: Comparison of the exact and NAQI rates as a function of the diabatic coupling $\log(\beta\Delta)$ for an asymmetric exponential crossing model with $\beta\epsilon = 50$, $\beta V^{\ddagger} = 44.5$ and $mL^2/\beta\hbar^2 = 160/49$. The classical Born-Oppenheimer and golden-rule rates are included to illustrate the importance of nuclear quantum effects.

coupling. In this regard the present method provides a significant improvement over previous theories, such as the QTST of Schwieters and Voth,[178,204] which break down for strongly asymmetric systems.

The final system we shall consider is significantly less quantum mechanical while still being strongly asymmetric. This is achieved by increasing the dimensionless mass parameter by a factor of 10 relative to the previous model, so that $\beta\epsilon = 50$, $\beta V^{\ddagger} = 44.5$ and $mL^2/\beta\hbar^2 = 160/49$. Figure 4.6 compares the exact rate with the NAQI rate as well as the classical golden-rule and Born-Oppenheimer rates for this system. We see that for the largest values of electronic coupling the classical adiabatic rate becomes a very good approximation to the exact rate, indicating that nuclear quantum effects are minimal in this regime. The NAQI rate again agrees very closely with exact rate for all values of the electronic coupling, with errors less than 5% for $\log_{10}(\beta\Delta) < 1$. The largest errors are observed at the largest coupling strengths, in the range $1.25 \leq \log_{10}(\beta\Delta) \leq 1.5$. We find

that the NAQI approximation underestimates the exact rate by about 40% at the upper end of this range, where the reaction is approximately classical and adiabatic. This is a well known deficiency of the adiabatic quantum instanton,[15,16,86] and arises because in the classical limit the correlation function (Eq. 2.166) is not well approximated by a Gaussian due to the presence of a long time polynomially decaying tail. Analysis of the free particle correlation function predicts that the adiabatic PQI underestimates the exact rate by 37%,[86] which is entirely consistent with the error seen here in the NAQI rate. Simple fixes have been suggested in the past to correct the adiabatic quantum instanton for this error,[15,16] and it may be possible to apply similar fixes to the NAQI.

4.5 Conclusion

We have demonstrated that it is straightforward to generalise the PQI approximation and Wolynes theory, which are applicable in the Born-Oppenheimer and golden-rule limits respectively, to treat non-adiabatic reactions with arbitrary electronic coupling strengths. The resulting NAQI approximation has been shown to be highly accurate for both symmetric and strongly asymmetric systems at low temperatures where nuclear quantum effects are important. However, as is expected from its connection with the adiabatic quantum instanton, we find that it underestimates the exact rate by approximately 40% in the adiabatic limit at high temperature, where the flux-flux correlation function is not well approximated by a Gaussian but instead exhibits a polynomially decaying tail. This problem has previously been overcome by assuming a different functional form for the correlation function or by going to a higher order asymptotic approximation, and these are both interesting avenues to explore to improve the present method.[15,207–209]

Here we have only applied the NAQI approach to simple one dimensional systems in order to demonstrate the basic features of the method. In order to apply the method to multidimensional systems it will be necessary to develop a path-integral implementation, which we expect to be straightforward to do starting from the standard path-integral implementation of Wolynes theory discussed in Sec. 2.3.3. The path-integral implementation may then be able provide direct information about the imaginary-time trajectories that are important in the reaction, and how these trajectories change as a function of

the electronic coupling. One of the main difficulties associated with the calculation of multidimensional quantum instanton rates in the adiabtatic limit is locating the optimum position space dividing surface. Although the natural reaction coordinate in a two level system is expected to be the diabatic energy gap, this may not always provide a good reaction coordinate, in particular as it is well-known that solvent friction can often drive electron transfer away from the non-adiabatic limit.[63–67] In the next chapter we will suggest an alternative approach to calculating non-adiabatic reaction rates which avoids the need to find an optimum dividing surface altogether.

Finally, we note that by making steepest descent approximations to the integrals over position in PQI and Wolynes theory one can obtain the semiclassical instanton in the Born-Oppenheimer and golden-rule limits respectively.[86,195] Hence, we expect that a steepest descent approximation to the NAQI should lead to an accurate semiclassical instanton which is valid for arbitrary electronic coupling strengths. More speculatively, because the semiclassical instanton in the adiabatic limit has a close connection to (and has been shown to provide a justification for) RPMD rate theory,[144] one might hope that the resulting non-adiabatic semiclassical instanton may help in the development of an accurate generalisation of RPMD for calculating non-adiabatic rates.

4.A Appendix: Diabatic projection operator

The alternative expression for the diabatic projection operator in Eq. 4.11 can be derived by noting that

$$\theta(-\hat{\sigma}_z) = \lim_{\epsilon \to 0_+} \frac{1}{2\pi i} \int_{-\infty}^{\infty} \frac{e^{-ix\hat{\sigma}_z}}{x - i\epsilon} \mathrm{d}x \tag{4.37}$$

and

$$e^{-ix\hat{\sigma}_z} = e^{-ix}|0\rangle\langle 0| + e^{+ix}|1\rangle\langle 1| \tag{4.38}$$

immediately give

$$\theta(-\hat{\sigma}_z) = |1\rangle\langle 1|. \tag{4.39}$$

5
A simple interpolation formula

Contents

Summary

In this chapter we present a simple interpolation formula for calculating non-adiabatic reaction rates as a function of the electronic coupling strength. The formula only requires the calculation of golden-rule and Born-Oppenheimer rates and so can be combined with any methods that are able to calculate these rates. We first demonstrate the accuracy of the formula by applying it to a one dimensional scattering problem for which the exact quantum mechanical, golden-rule, and Born-Oppenheimer rates are readily calculated. We then describe how the formula can be combined with the Wolynes theory approximation to the golden-rule rate, and the ring-polymer molecular dynamics (RPMD) approximation to the Born-Oppenheimer rate, and used to capture the effects of nuclear tunnelling, zero-point energy, and solvent friction on condensed phase electron transfer reactions, provided the Born-Oppenheimer rate is well-defined. Comparison with exact hierarchical equations of motion (HEOM) results for a demanding set of spin-boson models shows that the interpolation formula has an error comparable to that of RPMD rate theory in the adiabatic limit, and that of Wolynes theory in non-adiabatic limit, and is therefore as accurate as any method could possibly be that attempts to generalise RPMD to arbitrary electronic coupling strengths.

5.1 Introduction

We saw in Chap. 2 how RPMD can be used to calculate reaction rates in the adiabatic limit and Wolynes theory can be used to calculate reaction rates in the golden-rule limit. The previous two chapters have explored extensions of each of these methods and found challenges with both. In the case of non-adiabatic generalisations of RPMD we saw that the predicted reaction rates in the golden-rule limit are often not very reliable, as they do not correctly sample the imaginary-time paths involved in non-adiabatic tunnelling. With the non-adiabatic quantum instanton developed in the previous chapter this difficulty is avoided, and the theory was found to be very accurate for arbitrary values of coupling. Unfortunately, unlike RPMD, the resulting theory is dependent on a good choice of dividing surface when one moves away from the non-adiabatic limit. This is expected

to be particularly important for electron transfer in solution, where it is well known that solvent friction can drive a reaction away from the non-adiabatic limit even when the electronic coupling is very small.[63–67]

Here we suggest a simple method for including nuclear quantum effects in the calculation of reaction rates between the adiabatic and non-adiabatic limits, that avoids the need to find a non-adiabatic generalisation of RPMD, and hence also all the difficulties with doing so. In particular, we show how one can perform separate golden-rule and Born-Oppenheimer simulations and then interpolate between their results to calculate the electron transfer rate for an arbitrary electronic coupling strength. Since there already exist well established methods for calculating the Born-Oppenheimer and golden-rule rates, the method we are suggesting is immediately applicable to realistic simulations of condensed phase electron transfer reactions. Importantly, when used with RPMD to calculate the Born-Oppenheimer rate, it is therefore independent of the choice of dividing surface. Furthermore, we shall show that using the interpolation formula gives an error comparable to that of RPMD rate theory in the adiabatic limit, and Wolynes theory in the non-adiabatic limit, and is therefore as good as one could possibly hope to do by generalising RPMD to treat non-adiabatic reactions. The interpolation formula we use here is also closely related to pre-existing theories for the high-temperature limit of the spin-boson model,[63–72] in particular to approaches based on Padé resummations of the perturbative series in Δ, and as we show in Sec. 5.2 our formula reduces to a known analytical result, namely Zusman theory,[63] in the appropriate limit.

Sec. 5.2 introduces our new formula for interpolating between the results of golden-rule and Born-Oppenheimer rate calculations to obtain an expression for the rate at intermediate electronic coupling strengths, and highlights some of its properties. Sec. 5.3 investigates the accuracy of the interpolation formula for a simple one-dimensional scattering problem for which the exact quantum mechanical, golden-rule, and Born-Oppenheimer rates are straightforward to calculate. Sec. 5.4 combines the formula with the RPMD approximation to the Born-Oppenheimer rate and the Wolynes theory approximation to the golden-rule rate and applies it to the spin-boson model in a demanding set of regimes – with small and large nuclear quantum effects, low and

high electronic coupling strengths, weak and strong solvent frictions, and two very different thermodynamic driving forces. The results are shown to agree well with exact quantum mechanical rate constants obtained using the hierarchical equations of motion (HEOM) method[210–216] in all of these regimes. Sec. 5.5 concludes the chapter, leaving Appendix 5.B to describe an efficient implementation of RPMD for system-bath problems such as the spin-boson model considered in Sec. 5.4.

5.2 Interpolation formula

In Chap. 2, we have given expressions for the exact electron transfer rate constant $k(\Delta)$, the golden-rule rate constant $k_{\mathrm{GR}}(\Delta)$, and the Born-Oppenheimer rate constant $k_{\mathrm{BO}}(\Delta)$, all of which can clearly be calculated as a function of the electronic coupling strength Δ. For an electron transfer reaction in solution, Wolynes theory can be used to provide an estimate of $k_{\mathrm{GR}}(\Delta)$, and RPMD rate theory an estimate of $k_{\mathrm{BO}}(\Delta)$, for any value of Δ. However, there is as yet no equally simple and reliable way to estimate the exact electron transfer rate constant $k(\Delta)$ for values of Δ away from the non-adiabatic (golden-rule, $\beta\Delta \ll 1$) and adiabatic (Born-Oppenheimer, $\beta\Delta \gg 1$) limits.

To solve this problem, let us now consider combining the results of the golden-rule and Born-Oppenheimer calculations with the simple interpolation formula

$$k(\Delta) \simeq k_{\mathrm{IF}}(\Delta) = \frac{k_{\mathrm{GR}}(\Delta)k_{\mathrm{BO}}(\Delta)}{k_{\mathrm{GR}}(\Delta) + k_{\mathrm{BO}}(\Delta = 0)}. \tag{5.1}$$

This has the correct limiting behaviour for both small and large Δ, as illustrated in Fig. 5.1. As $\beta\Delta \to 0$, $k_{\mathrm{BO}}(\Delta)$ and $k_{\mathrm{GR}}(\Delta) + k_{\mathrm{BO}}(\Delta = 0)$ both tend to $k_{\mathrm{BO}}(\Delta = 0)$, which then cancels top and bottom in Eq. 5.1 to leave $k_{\mathrm{IF}}(\Delta) \simeq k_{\mathrm{GR}}(\Delta)$, the correct non-adiabatic rate constant. And when $\beta\Delta \gg 1$, $k_{\mathrm{GR}}(\Delta) + k_{\mathrm{BO}}(\Delta = 0)$ tends to $k_{\mathrm{GR}}(\Delta)$, which then cancels with the $k_{\mathrm{GR}}(\Delta)$ in the numerator to leave $k_{\mathrm{IF}}(\Delta) \simeq k_{\mathrm{BO}}(\Delta)$, the correct adiabatic rate constant. In effect, the right-hand side of Eq. 5.1 is a Padé-like approximant to $k(\Delta)$ which is straightforward to compute even for a liquid phase electron transfer reaction, and which interpolates correctly between the non-adiabatic and adiabatic limits.

It is clear that the interpolation formula in Eq. 5.1 can only be used when the Born-Oppenheimer rate constant is well defined for all relevant values of Δ. So the formula

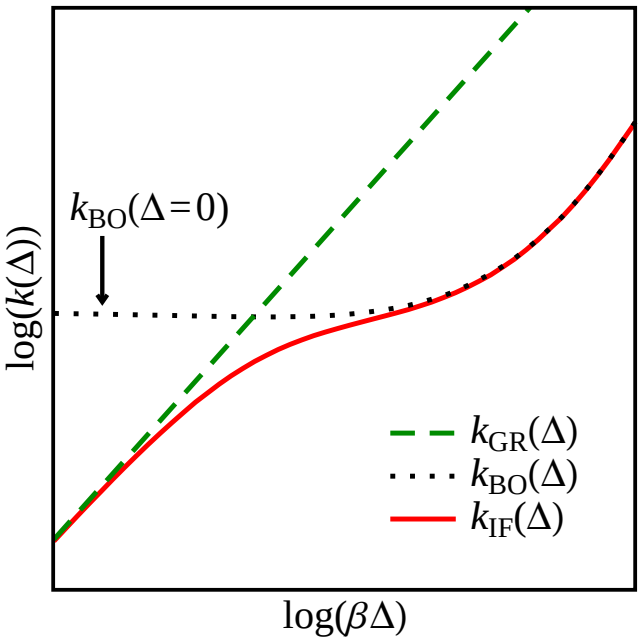

Figure 5.1: Illustration of the behaviour of the interpolation formula in Eq. 5.1. For small $\beta\Delta$, $k_{IF}(\Delta)$ approaches the golden-rule rate constant $k_{GR}(\Delta)$, and for large $\beta\Delta$ it approaches the Born-Oppenheimer rate constant $k_{BO}(\Delta)$, as discussed in more detail the text.

cannot be used in the Marcus inverted regime. In the normal regime, we require that the reaction barrier is large compared to $k_B T$, at least in the non-adiabatic limit. More formally, we require that defining the reactants and products using a position space dividing surface on the lower adiabatic surface is not significantly different to using the diabatic projection operators in the non-adiabatic limit, so that to a good approximation

$$Q_r(\Delta = 0) = \mathrm{tr}_n\left[e^{-\beta\hat{H}_0}\right] \simeq \mathrm{tr}_n\left[e^{-\beta\hat{H}_{BO}(\Delta=0)}\theta(-s(\hat{\boldsymbol{q}}))\right], \tag{5.2}$$

$$Q_p(\Delta = 0) = \mathrm{tr}_n\left[e^{-\beta\hat{H}_1}\right] \simeq \mathrm{tr}_n\left[e^{-\beta\hat{H}_{BO}(\Delta=0)}\theta(s(\hat{\boldsymbol{q}}))\right], \tag{5.3}$$

where $\hat{H}_{BO}(\Delta = 0)$ is the Born-Oppenheimer Hamiltonian on the (cusped) lower adiabatic surface with zero electronic coupling. With this expected range of validity in mind we can now consider two important properties of the interpolation formula.

The first of these properties is that the formula satisfies detailed balance. That is

$$\frac{k_{IF}(\Delta)}{k'_{IF}(\Delta)} = \frac{Q_p(\Delta)}{Q_r(\Delta)}, \tag{5.4}$$

where $k_{\mathrm{IF}}(\Delta)$ and $k'_{\mathrm{IF}}(\Delta)$ are the forward and backward rate constants and $Q_r(\Delta)$ and $Q_p(\Delta)$ are the reactant and product partition functions. This can be seen by first noting that Eq. 5.1 gives

$$\frac{k_{\mathrm{IF}}(\Delta)}{k'_{\mathrm{IF}}(\Delta)} = \frac{k_{\mathrm{BO}}(\Delta)}{k'_{\mathrm{BO}}(\Delta)} \cdot \frac{1 + k'_{\mathrm{BO}}(\Delta = 0)/k'_{\mathrm{GR}}(\Delta)}{1 + k_{\mathrm{BO}}(\Delta = 0)/k_{\mathrm{GR}}(\Delta)}. \tag{5.5}$$

Provided Eqs. 5.2 and 5.3 are satisfied, we also have

$$\frac{Q_p(\Delta = 0)}{Q_r(\Delta = 0)} = \frac{k_{\mathrm{BO}}(\Delta = 0)}{k'_{\mathrm{BO}}(\Delta = 0)} = \frac{k_{\mathrm{GR}}(\Delta)}{k'_{\mathrm{GR}}(\Delta)}, \tag{5.6}$$

because the Born-Oppenheimer and golden-rule rates each satisfy detailed balance. Hence

$$\frac{k_{\mathrm{BO}}(\Delta = 0)}{k_{\mathrm{GR}}(\Delta)} = \frac{k'_{\mathrm{BO}}(\Delta = 0)}{k'_{\mathrm{GR}}(\Delta)}, \tag{5.7}$$

and combining this with Eq. 5.5 gives

$$\frac{k_{\mathrm{IF}}(\Delta)}{k'_{\mathrm{IF}}(\Delta)} = \frac{k_{\mathrm{BO}}(\Delta)}{k'_{\mathrm{BO}}(\Delta)} = \frac{Q_p(\Delta)}{Q_r(\Delta)}. \tag{5.8}$$

The second important property of Eq. 5.1 is that it reduces to a known analytical result, the Zusman equation,[63] under the appropriate conditions. The Zusman equation gives an analytical expression for the rate constant in the classical limit for the spin-boson model, extending Marcus theory to include the effect of friction along the reaction coordinate. The Zusman equation is given explicitly in Section 5.4 but for now we simply note that it can be written in a form reminiscent of Eq. 5.1 as

$$k_{\mathrm{ZUS}}(\Delta) = \frac{k_{\mathrm{MT}}(\Delta)k_{\mathrm{A}}(\Delta = 0)}{k_{\mathrm{MT}}(\Delta) + k_{\mathrm{A}}(\Delta = 0)}, \tag{5.9}$$

where $k_{\mathrm{MT}}(\Delta)$ is the Marcus theory rate and $k_{\mathrm{A}}(\Delta = 0)$ is the classical rate on the cusped ground adiabatic potential in the limit of high friction. The obvious difference between this and Eq. 5.1, which for the classical spin-boson model becomes

$$k_{\mathrm{IF}}(\Delta) = \frac{k_{\mathrm{MT}}(\Delta)k_{\mathrm{A}}(\Delta)}{k_{\mathrm{MT}}(\Delta) + k_{\mathrm{A}}(\Delta = 0)}, \tag{5.10}$$

is that it predicts $k_{\mathrm{ZUS}}(\Delta) \to k_A(\Delta = 0)$ rather than $k_A(\Delta)$ for large Δ. Hence the Zusman equation misses the fact that increasing Δ lowers the adiabatic reaction barrier. This is because the derivation of the Zusman equation assumes that $\beta\Delta \ll 1$. Under these

circumstances $k_A(\Delta) \simeq k_A(\Delta = 0)$, and the classical limit of our interpolation formula reduces to the Zusman equation.

The breakdown of the Zusman equation for large electronic coupling is well known, and there already exist classical theories which can be used to calculate rates in this regime.[68–72] Our approach is naturally closely related to several these methods, when applied to the high temperature limit of the spin-boson model. In particular we note that our interpolation formula is very similar to an interpolation formula proposed by Gladkikh *et al.*,[72] which corrects the Zusman equation by interpolating between the rates for the cusped and parabolic barriers in the adiabatic limit. The present approach can thus also be viewed as a generalisation of these previous interpolation formulas, which is capable of treating general anharmonic condensed phase problems and including the effects of tunnelling and zero-point energy. A simple qualitative perspective on the physical picture which underlies Zusman theory as well as our interpolation formula is given in Appendix 5.A.

5.3 Scattering model

As a first test of the accuracy of the interpolation formula in Eq. 5.1, we shall again consider the simple one-dimensional exponential curve crossing model from Chap. 4 with the following diabatic potential energy curves:

$$V_0(q) = Ae^{+q/L}, \tag{5.11}$$

$$V_1(q) = Ae^{-q/L}. \tag{5.12}$$

This provides a useful test problem because not only can we calculate the exact rate to go from state $|0\rangle$ to $|1\rangle$, but we can also calculate each of the components of the interpolation formula exactly. The exact rate $k(\Delta)$ and the ground adiabatic Born-Oppenheimer rate $k_{\mathrm{BO}}(\Delta)$ can each be calculated as Boltzmann averages of appropriate cumulative reaction probabilities,

$$k(\Delta)\beta\hbar Q_r = \frac{1}{2\pi}\int_0^\infty e^{-\beta E} N(E)\,\beta \mathrm{d}E, \tag{5.13}$$

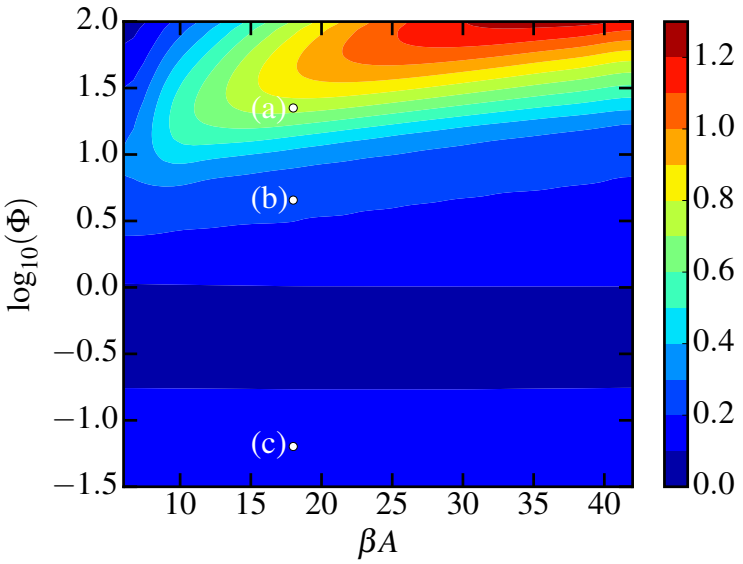

Figure 5.2: Contour plot of the maximum error as defined in Eq. 5.15 for the scattering model. The exact rate $k(\Delta)$ was calculated using the log derivative method, as were $k_{\mathrm{GR}}(\Delta)$ and $k_{\mathrm{BO}}(\Delta)$. The log derivative code was written by Prof. David E. Manolopoulos.

where $Q_r = \sqrt{m/2\pi\beta\hbar^2}$ is the reactant partition function per unit length. The cumulative reaction probability $N(E)$ that determines the exact non-adiabatic rate $k(\Delta)$ can be calculated using the coupled channel log derivative method,[206] and the golden-rule rate $k_{\mathrm{GR}}(\Delta)$ can be extracted from the Δ^2 dependence of $k(\Delta)$ in the limit as $\Delta \to 0$ (the log derivative code was written by Prof. David E. Manolopoulos). For the Born-Oppenheimer rate $k_{\mathrm{BO}}(\Delta)$, $N(E)$ can be calculated using a single channel log derivative method on the ground adiabatic potential energy surface. The fact that all three rates $k(\Delta)$, $k_{\mathrm{GR}}(\Delta)$ and $k_{\mathrm{BO}}(\Delta)$ can be calculated exactly allows us to test the accuracy of the interpolation formula in Eq. 5.1 separately from that of the approximate path-integral techniques (Wolynes theory and RPMD rate theory) which are required for condensed phase problems.

The behaviour of this model system (at $\epsilon = 0$) is completely determined by three dimensionless parameters: $\beta\Delta$, βA, and $mL^2/\beta\hbar^2$. Keeping the last two of these parameters fixed we define the error in the interpolation formula as a function of $\beta\Delta$ using the equation

$$E(\beta\Delta) = \left| \log_2 \left(\frac{k_{\mathrm{IF}}(\beta\Delta)}{k(\beta\Delta)} \right) \right|. \tag{5.14}$$

This allows us to define the maximum error for a particular βA and $mL^2/\beta\hbar^2$ as

$$E_{\max} = \max_{\beta\Delta < 0.8\beta A} E(\beta\Delta), \tag{5.15}$$

where the range of $\beta\Delta$ is limited to ensure that the reaction is always activated. This is a more useful measure of the error than the percentage error as it treats underestimation and over estimation on an equal footing, and is in keeping with the usual way that errors are discussed for RPMD, which is expected to be within a factor of 2 of the exact rate in the deep tunnelling regime. Note that $E_{\max} = 1$ corresponds to the interpolation formula being out by at most a factor of 2 and $E_{\max} = 0$ corresponds to it being exact for all values of $\beta\Delta$.

Figure 5.2 shows $E_{\max}$ as a function of the two remaining free parameters, which we take to be βA and the dimensionless parameter Φ defined as

$$\Phi = \beta A \sqrt{\frac{2\beta\hbar^2}{\pi^3 m L^2}}. \tag{5.16}$$

This parameter can be related to the instanton action for a linear approximation to the diabatic potentials in the non-adiabatic limit and it quantifies how "quantum mechanical" the reaction is. We see that in the classical regime, $\log_{10}(\Phi) < 0$, the error is essentially solely a function of Φ and approaches a plateau with $E_{\max}$ just above 0.1, corresponding to the interpolation formula being within a factor of 1.1 of the exact rate for the full range of $\beta\Delta$. For $\log_{10}(\Phi) > 0$, the error grows as the problem becomes more quantum mechanical. However $E_{\max}$ remains below 1 for $\log_{10}(\Phi) < 1.5$, corresponding to the interpolation formula being within a factor of 2 of the exact rate throughout this regime. As an illustration of the physical regimes that the plot spans, note that the point labelled (a) corresponds to a strongly quantum mechanical system with $\beta A = 18$, $T = 50\,\mathrm{K}$, $L = 0.5\,a_0$, and $m \simeq 1000\,m_\mathrm{e}$, point (b) corresponds to a system where the mass associated with the nuclear motion has been increased to $m \simeq 25000\,m_\mathrm{e}$ and point (c) to $m \simeq 1.3 \times 10^8\,m_\mathrm{e}$.

Figure 5.3 shows the rate as a function of $\beta\Delta$ for the three labelled points in Fig. 5.2. The plot shows the exact rate as well as the result of the interpolation formula evaluated using the exact Born-Oppenheimer and golden-rule rates. To illustrate the importance of nuclear quantum effects we also include the classical limit of the golden-rule rate which is given by

$$k_{\text{cl-GR}}(\Delta) = \frac{\Delta^2}{\hbar^2 Q_r} \sqrt{\frac{\pi m}{2\beta}} \frac{L}{A} e^{-\beta A}. \tag{5.17}$$

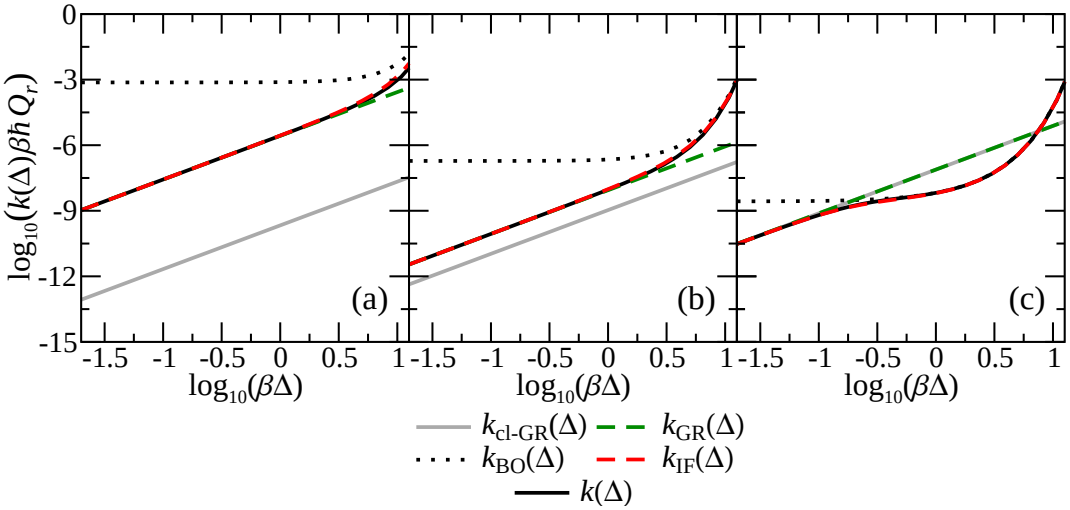

Figure 5.3: Plots demonstrating the accuracy of the interpolation formula for the three points labeled in Fig. 5.2. All three systems have $\beta A = 18$, with (a) $\Phi = 22.4$, (b) $\Phi = 4.54$, and (c) $\Phi = 0.0635$. The exact rate $k(\Delta)$ was calculated using the log derivative method, as were $k_{\text{GR}}(\Delta)$ and $k_{\text{BO}}(\Delta)$. The classical golden-rule rate was calculated using Eq. 5.17. The log derivative code was written by Prof. David E. Manolopoulos.

We see that the interpolation formula is capable of capturing the full range of behaviour, from the highly quantum mechanical in system (a) to the essentially classical in system (c). It is also of note that as Φ decreases the value of $\beta\Delta$ at which the reaction begins to behave adiabatically also decreases. This can be understood by noting that Φ is related to the Landau-Zener adiabaticity parameter[173]

$$P(\Delta) = \frac{2\pi\Delta^2}{\hbar\langle|v|\rangle_{\text{cl}}|\delta F|} \tag{5.18}$$

where $\langle|v|\rangle_{\text{cl}}$ is the classical average thermal velocity,

$$\frac{1}{2}\langle|v|\rangle_{\text{cl}} = \frac{1}{\sqrt{2\pi m\beta}}, \tag{5.19}$$

and $\delta F = 2A/L$. We see that $\Phi = 1/P(k_{\text{B}}T)$ and so gives a measure of how non-adiabatic the reaction is expected to be at $\beta\Delta = 1$. In system (a), $\Phi \gg 1$, and the rate is firmly non-adiabatic at $\beta\Delta = 1$, whereas in system (c), $\Phi \ll 1$, and the rate is firmly adiabatic at $\beta\Delta = 1$. This connection between Φ (or equivalently the instanton action) and the Landau-Zener adiabaticity parameter can be thus be used to account for the fact that increased nuclear tunnelling tends to make a reaction more non-adiabatic.[217,218]

5.4 Spin-boson model

The spin-boson model is the prototypical non-adiabatic system that is used to model electron transfer reactions in condensed phase environments. Written in the "reaction coordinate" form, the diabatic potentials of this model are given by[64]

$$V_0(Q, \boldsymbol{q}) = \frac{1}{2}\Omega^2\left(Q + \sqrt{\frac{\Lambda}{2\Omega^2}}\right)^2 + V_{sb}(Q, \boldsymbol{q}), \tag{5.20}$$

$$V_1(Q, \boldsymbol{q}) = \frac{1}{2}\Omega^2\left(Q - \sqrt{\frac{\Lambda}{2\Omega^2}}\right)^2 + V_{sb}(Q, \boldsymbol{q}), \tag{5.21}$$

where

$$V_{sb}(Q, \boldsymbol{q}) = \sum_{\nu=1}^{N_b} \frac{1}{2}\omega_\nu^2\left(q_\nu - \frac{c_\nu Q}{\omega_\nu^2}\right)^2, \tag{5.22}$$

and Λ is the Marcus theory reorganisation energy (note that we shall work throughout this section with mass-weighted coordinates). The influence of the bath on the reaction coordinate, Q, is fully described by the associated spectral density, which is formally defined as

$$J(\omega) = \frac{\pi}{2}\sum_{\nu=1}^{N_b} \frac{c_\nu^2}{\omega_\nu}\delta(\omega - \omega_\nu). \tag{5.23}$$

The bath is then taken to be infinite, corresponding to a continuous spectral density. Here we choose to consider a purely Ohmic spectral density,

$$J(\omega) = \gamma\omega, \tag{5.24}$$

which gives rise to Langevin dynamics along the reaction coordinate in the classical adiabatic limit. This model problem allows us to investigate the accuracy of our newly proposed method in a variety of different regimes, from underdamped ($\gamma < 2\Omega$) to overdamped ($\gamma > 2\Omega$) motion along the reaction coordinate, from high frequencies (large Ω) to low frequencies (small Ω), and for the full range of non-adiabatic (small Δ) to adiabatic (large Δ) behaviour.

The reaction coordinate form can be related to the conventional spin-boson model by a normal mode transformation.[64,192,193] In the conventional form, the diabatic potentials are just sums of uncoupled displaced harmonic oscillators,

$$V_0(\boldsymbol{x}) = \sum_{\nu=0}^{N_b} \frac{1}{2}\bar{\omega}_\nu^2\left(x_\nu + \frac{\bar{c}_\nu}{\bar{\omega}_\nu^2}\right)^2, \tag{5.25}$$

$$V_1(\boldsymbol{x}) = \sum_{\nu=0}^{N_b} \frac{1}{2}\bar{\omega}_\nu^2\Big(x_\nu - \frac{\bar{c}_\nu}{\bar{\omega}_\nu^2}\Big)^2, \tag{5.26}$$

where x_ν, $\bar{\omega}_\nu$ and $\bar{c}_\nu$ are the transformed (mass weighted) coordinates, frequencies and couplings respectively. In order to map between the two forms one simply needs to know the relation between the spectral density for the coupling of nuclear coordinates to the electronic state

$$J_\sigma(\omega) = \frac{\pi}{2}\sum_{\nu=0}^{N_b} \frac{\bar{c}_\nu^2}{\bar{\omega}_\nu}\delta(\omega - \bar{\omega}_\nu), \tag{5.27}$$

and the spectral density $J(\omega)$ for the coupling of the bath to the reaction coordinate.* This mapping is given by[64,192,193]

$$J_\sigma(\omega) = \frac{\Lambda}{2}\frac{\Omega^2 J(\omega)}{(\omega^2 - \Omega^2 + R(\omega))^2 + J^2(\omega)}, \tag{5.28}$$

where

$$R(\omega) = \frac{2\omega^2}{\pi}P\int_0^\infty \frac{J(u)}{u(u^2-\omega^2)}du, \tag{5.29}$$

and P denotes the Cauchy principal value. For the Ohmic spectral density considered here, $R(\omega) = 0$, and the electronic spectral density becomes

$$J_\sigma(\omega) = \frac{\Lambda}{2}\frac{\gamma\,\Omega^2\omega}{(\omega^2 - \Omega^2)^2 + \gamma^2\omega^2}, \tag{5.30}$$

which is typically referred to as the Brownian oscillator spectral density.

The spin-boson model provides a useful system for testing new methods because it is possible to obtain exact numerical results for this model for comparison. Despite this, previous attempts to extend RPMD to treat non-adiabatic rates have only been tested in certain limiting regimes, for example by comparison with Zusman theory or the quantum golden-rule rate. Here we test the validity of Eq. 5.1 by comparison with numerically exact results generated using the hierarchical equations of motion (HEOM) method,[210–216] which allows us to examine a wider range of physically relevant regimes. The HEOM calculations used in this chapter were performed by Dr. Lachlan P. Lindoy.

In order to calculate the rate using HEOM we again make use of Eq. 2.44 with $\hat{P}_r = |0\rangle\langle 0|$ and $\hat{P}_p = |1\rangle\langle 1|$. Since it is computationally impractical to prepare the initial

*Note that we have changed notation here relative to the previous chapters, and $J_\sigma(\omega)$ is now the spectral density that was introduced in Chap. 2.

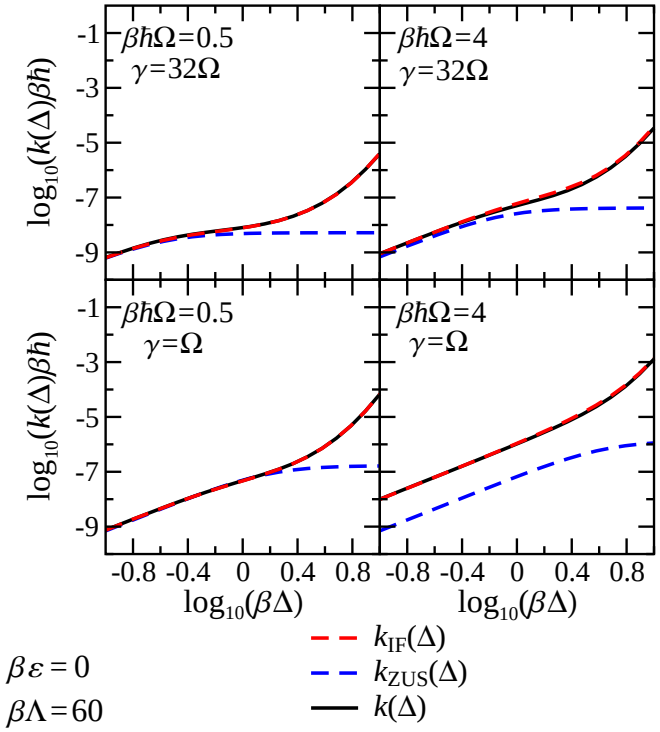

Figure 5.4: Plot comparing the rates predicted by the interpolation formula [Eq. 5.1], Zusman theory [Eq. 5.1], and the numerically exact HEOM method, for the symmetric spin-boson model with Brownian oscillator spectral density [Eq. 5.30]. The Born-Oppenheimer and golden-rule rates used in the interpolation formula were calculated using RPMD rate theory and Wolynes theory, respectively. All HEOM calculations were performed by Dr. Lachlan P. Lindoy.

density matrix in the form of Eq. 2.60, we instead follow the procedure of Shi *et al.*,[219] in which the system is initially prepared on the reactant diabat with the bath in thermal equilibrium on the average diabatic potential, and is then equilibrated in the absence of coupling ($\Delta = 0$). The resulting initial condition can be expressed as

$$\hat{\rho}(0) = \lim_{t\to\infty} \frac{e^{-i\hat{H}_0 t/\hbar} e^{-\beta \hat{H}_+} |0\rangle\langle 0| e^{+i\hat{H}_0 t/\hbar}}{\mathrm{Tr}[e^{-\beta \hat{H}_+}|0\rangle\langle 0|]}. \tag{5.31}$$

where

$$\hat{H}_+ = \frac{\hat{H}_0 + \hat{H}_1}{2}. \tag{5.32}$$

With this modified initial condition the time-dependent populations of the two electronic states again eventually settle down to conform to Eqs. 2.42, allowing the exact HEOM forward electron transfer rate to be calculated from Eq. 2.44.

To highlight the importance of nuclear quantum effects, and the effect of the changes in shape and height of the adiabatic barrier with Δ, we also compare the results of

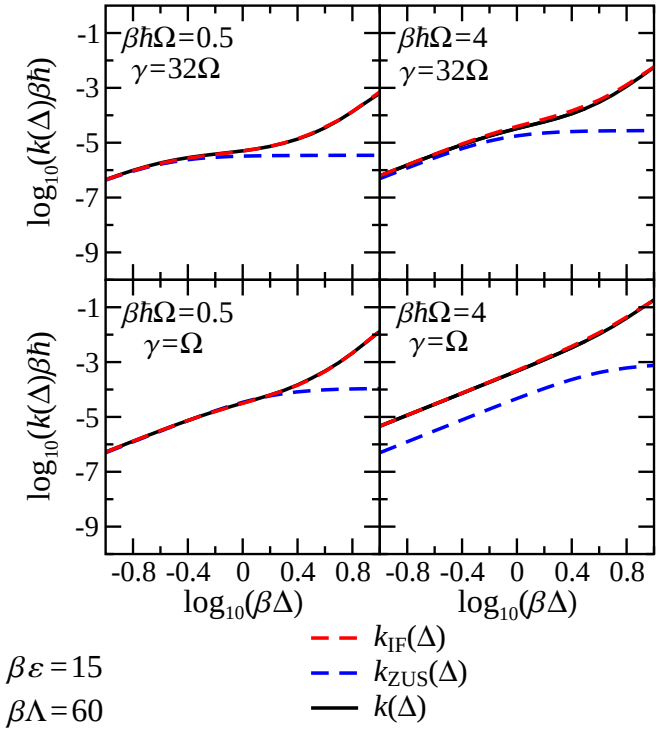

Figure 5.5: Plot comparing the rates predicted by the interpolation formula [Eq. 5.1], Zusman theory [Eq. 5.1], and the numerically exact HEOM method, for the asymmetric spin-boson model with Brownian oscillator spectral density [Eq. 5.30]. The Born-Oppenheimer and golden-rule rates used in the interpolation formula were calculated using RPMD rate theory and Wolynes theory, respectively. All HEOM calculations were performed by Dr. Lachlan P. Lindoy.

the interpolation formula to the Zusman equation, which for the spin-boson model as described here is[63,220]

$$k_{\mathrm{ZUS}}(\Delta) = \frac{\beta\frac{\Delta^2}{\hbar}\frac{\Omega^2}{4\gamma}\left(1-\frac{\epsilon^2}{\Lambda^2}\right)\exp\left(-\beta\frac{(\Lambda-\epsilon)^2}{4\Lambda}\right)}{\frac{\Delta^2}{\hbar}\sqrt{\frac{\pi\beta}{\Lambda}}+\frac{\Omega^2}{4\gamma}\sqrt{\frac{\beta\Lambda}{\pi}}\left(1-\frac{\epsilon^2}{\Lambda^2}\right)}. \tag{5.33}$$

This can be seen to be identical to Eq. 5.9 with the identifications

$$k_{\mathrm{MT}}(\Delta) = \frac{\Delta^2}{\hbar}\sqrt{\frac{\pi\beta}{\Lambda}}\exp\left(-\beta\frac{(\Lambda-\epsilon)^2}{4\Lambda}\right), \tag{5.34}$$

and

$$k_{\mathrm{A}}(\Delta=0) = \frac{\Omega^2}{4\gamma}\sqrt{\frac{\beta\Lambda}{\pi}}\left(1-\frac{\epsilon^2}{\Lambda^2}\right)\exp\left(-\beta\frac{(\Lambda-\epsilon)^2}{4\Lambda}\right). \tag{5.35}$$

In the following we use RPMD to calculate the Born-Oppenheimer rate constant, $k_{\mathrm{BO}}(\Delta)$, and Wolynes theory to calculate the golden-rule rate constant, $k_{\mathrm{GR}}(\Delta)$, although we reiterate that the interpolation formula can be used with any methods which are applicable

to these two limits. Previous path-integral studies of system-bath models have opted to discretise the spectral density using a procedure such as that described in the original RPMD rate theory paper,[18] increasing the number of modes in the discretisation until the results were converged to the infinite bath limit. Here instead we note that, working in the reaction coordinate form, we can analytically integrate out all but one nuclear degree of freedom.[221] This results in an effective renormalised ring-polymer Hamiltonian for the single remaining nuclear coordinate (the reaction coordinate, Q), which makes the calculations trivial. In the case of RPMD the dynamics of the full system plus bath are then recovered using a generalised Langevin equation (GLE). Full details of the derivation of this GLE and the renormalised Hamiltonian, along with how they are implemented numerically, are given in Appendix 5.B.

Figures 5.4 and 5.5 compare the rates obtained using the interpolation formula with the exact HEOM results for the spin-boson model described above. In these calculations we used a typical Marcus reorganisation energy of $\Lambda = 60\,k_{\mathrm{B}}T$, with a series of different driving forces (ϵ), solvent frictions (γ), and reaction coordinate frequencies (Ω). The interpolation formula is seen to give excellent agreement with the exact results in all of the regimes considered, with the largest error, of just under 30%, observed in the overdamped high frequency systems at intermediate values of $\beta\Delta$ ($\beta\hbar\Omega = 4$, $\gamma = 32\Omega$, $\beta\epsilon = 0$ and 15). The interpolation formula is also seen to be most accurate for the overdamped low frequency systems. This is to be expected from its connection with the Zusman equation (see Section 5.2), which is derived in the limit of low frequency and high friction. It is of note, however, that the interpolation formula is much more accurate than the Zusman equation at even moderate values of $\beta\Delta$, due to the failure of Zusman theory to capture the effect of Δ on the adiabatic reaction barrier. As we have already discussed, more accurate classical theories for the spin-boson model exist,[70,72] but this breakdown illustrates the advantage of testing new methods against numerically exact results, as we do here, rather than relying on comparison to simple analytical formulas which can turn out to have rather limited accuracy.

The Zusman equation also fails to capture the effects of nuclear tunnelling and zero-point energy, which for the underdamped high frequency systems lead to over an order of

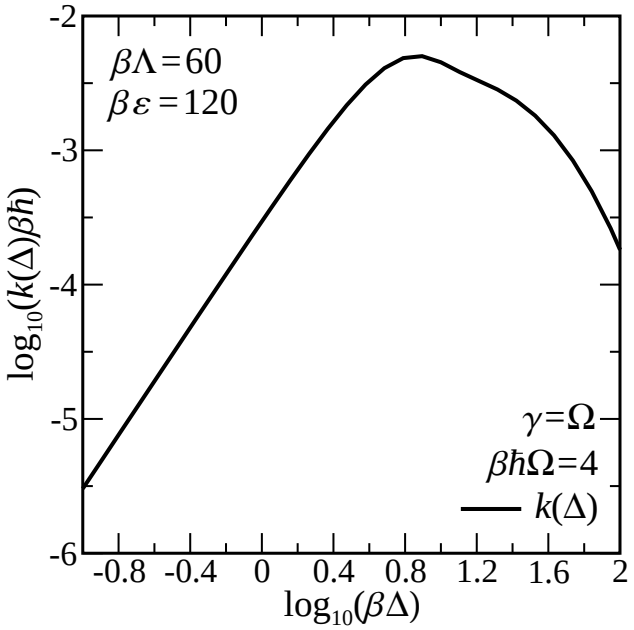

Figure 5.6: Plot of the exact HEOM rate versus $\beta\Delta$ for a spin-boson model with a Brownian oscillator spectral density, deep in the Marcus inverted regime ($\epsilon = 2\Lambda$). The interpolation formula in Eq. (38) cannot be used for this problem because the Born-Oppenheimer rate is not well-defined. Calculations performed by Dr. Lachlan P. Lindoy.

magnitude increase in the rate constant in the non-adiabatic limit. Since both Wolynes theory and RPMD are able to accurately capture the effect of tunnelling and zero-point energy, so too is the interpolation formula when these two theories are used as input. The success of the interpolation formula in this regime (large Ω and underdamped) is particularly encouraging as it is the opposite of the regime where the Zusman equation is valid. We note that, as was seen in Section 5.3, the greater nuclear tunnelling in this regime means that the golden-rule expression for the rate continues to be accurate even for $\beta\Delta > 1$. The much smaller increase in the rate observed for the overdamped high frequency systems illustrates the reduction of nuclear tunnelling due to friction.[192] This can be understood in the ring-polymer perspective by considering the renormalisation of the normal mode frequencies of the ring-polymer due to friction, $\omega_k \rightarrow \sqrt{\omega_k^2 + \gamma\omega_k}$ (see Appendix 5.B). It follows from this renormalisation that a larger value of γ leads to a smaller radius of gyration of the ring-polymer and a more classical-like dynamics.

The success of the interpolation formula in such a wide range of parameter regimes is clearly encouraging. However, it is important to remember its limitations. The formula is

only expected to be accurate when the reactants and products can equally well be defined using either a position space dividing surface or diabatic state projection operators in the non-adiabatic limit. In the most extreme case of the Marcus inverted regime there is no position space description of the reaction and a Born-Oppenheimer rate cannot be defined. Figure 5.6 illustrates the behaviour of the exact HEOM rate as a function of $\beta\Delta$ for an underdamped high frequency system with a driving force of $\epsilon = 2\Lambda$, deep inside the inverted regime. At small $\beta\Delta$ the rate is well described by the golden-rule, but at large $\beta\Delta$ the rate begins to decrease as it approaches an adiabatic limit in which there is no transfer of population between the upper and lower adiabats. This kind of system clearly cannot be studied with the interpolation formula in Eq. 5.1. We have included it here to provide both an honest illustration of one of the limitations of the current approach and a challenge for future work.

Despite this limitation we would like to stress that the interpolation formula can still be very accurate even when the barrier to reaction is low. For example, in Fig. 5.5 the barrier on the lower adiabatic surface becomes very small as $\beta\Delta$ becomes large, dropping all the way to $1.2\,k_{\mathrm{B}}T$ when $\beta\Delta = 10$. But the rate predicted using the interpolation formula still agrees very well with the exact rate calculated using HEOM with diabatic state projection operators.

5.5 Conclusion

In this chapter, we have shown how the RPMD rate theory and Wolynes theory approximations to Born-Oppenheimer and golden-rule rates can be combined in a simple interpolation formula that accurately predicts the rates of non-adiabatic reactions with arbitrary electronic coupling strengths. The accuracy of the interpolation formula has been demonstrated by comparison with exact results for both a simple one-dimensional scattering problem and a demanding series of spin-boson models. In particular, the use of the exact HEOM method to provide benchmark results for these spin-boson models has allowed us to explore a wide range of chemically relevant regimes, from underdamped to overdamped dynamics, small to large nuclear quantum effects, and the full range

of electronic coupling strengths, from the non-adiabatic to adiabatic limits. Previous methods have not been tested in such wide ranging and challenging regimes.

Since RPMD rate theory and Wolynes theory are both readily applicable to truly complex (anharmonic and multidimensional) problems, it will be interesting in future work to apply the interpolation formula to more realistic models of electronically non-adiabatic reactions and use it to answer some chemically interesting questions. We note in particular that the formula is well suited to quantifying the degree of electronic non-adiabaticity in a reaction, as well as assessing the relative importance of electronic coupling and solvent friction in driving a reaction away from the non-adiabatic limit, as we have shown in some of our examples. Further qualitative insights into the reaction mechanism can also clearly be gained from the Born-Oppenheimer and golden-rule calculations that the interpolation formula combines.

Having said this, there are clearly still some open issues which warrant further theoretical work. In addition to the inability of the interpolation formula to treat systems in the Marcus inverted regime, we still need to investigate its accuracy for systems which can have multiple competing reaction pathways such as proton-coupled electron transfer reactions. Further work is also needed in order to treat systems in which multiple electronic states are involved, such as in superexchange mediated electron transfer, and to develop approaches that can treat both the incoherent rate processes considered in this thesis and also the coherent dynamics relevant to condensed phase electronic spectra, which current non-adiabatic methods such as Wolynes theory cannot describe.

5.A Appendix: A qualitative perspective of the interpolation formula

A qualitative perspective of the Zusman rate equation and the interpolation formula can be gained by noting that the functional form of both corresponds to a consecutive reaction scheme of the form,

$$r \underset{k_0^-}{\overset{k_0^+}{\rightleftharpoons}} \mathrm{TS}_r \underset{k_\mathrm{e}}{\overset{k_\mathrm{e}}{\rightleftharpoons}} \mathrm{TS}_p \underset{k_1^-}{\overset{k_1^+}{\rightleftharpoons}} p, \tag{5.36}$$

where r corresponds to reactants, TS_r and TS_p correspond to two reactive intermediates and p corresponds to the products. Physically this is tantamount to assuming that the reaction can be described as consisting of a series of steps consistent with the qualitative description of a non-adiabatic reaction given in Chap. 1, along with the assumption that each of these steps can be treated via an incoherent rate constant. Following this perspective k_0^+ and k_0^- correspond to the rates for thermal fluctuations to take the system to and from the transition state region on the reactant surface, k_e corresponds to the rate for transfer between the reactant and product electronic states in the transition state region, and k_1^+ and k_1^- correspond to the rates for thermal fluctuations to take the system to and from the transition state region on the product surface.

Solving the rate equations, under the assumption of steady state for the populations of TS_r and TS_p, gives the rate constant for transfer from r to p as

$$k = \frac{k_0^+ k_\mathrm{e} k_1^+}{k_0^- k_\mathrm{e} + k_0^- k_1^+ + k_\mathrm{e} k_1^+}. \tag{5.37}$$

With the identification of k_e as corresponding to the electronic transition, it follows that in the adiabatic limit $k_\mathrm{e} \gg k_1^+$ and $k_\mathrm{e} \gg k_0^-$ such that the Born-Oppenheimer rate is given by

$$k_\mathrm{BO}(\Delta) = \frac{k_0^+(\Delta) k_1^+(\Delta)}{k_0^-(\Delta) + k_1^+(\Delta)}. \tag{5.38}$$

In the opposite non-adiabatic limit, it follows that $k_\mathrm{e} \ll k_1^+$ and $k_\mathrm{e} \ll k_0^-$, such that the golden-rule rate obeys the relation

$$k_\mathrm{GR}(\Delta) = \Delta^2 \lim_{\Delta \to 0} \left[\frac{k_\mathrm{e}(\Delta) k_0^+(\Delta = 0)}{\Delta^2 k_0^-(\Delta = 0)} \right]. \tag{5.39}$$

Making use of the first of these two identities it is simple to show that Eq. 5.37 is equivalent to

$$k(\Delta) = \frac{k_\mathrm{e}(\Delta) k_\mathrm{BO}(\Delta)}{k_\mathrm{e}(\Delta) + k_0^-(\Delta) k_\mathrm{BO}(\Delta)/k_0^+(\Delta)}. \tag{5.40}$$

This now has a form more reminiscent of the interpolation formula. To simplify further we write the Born-Oppenheimer rate in the Arrhenius form as,

$$k_\mathrm{BO}(\Delta) = A_\mathrm{BO}(\Delta) e^{-\Delta F^\ddagger(\Delta)}, \tag{5.41}$$

and define the exponential term to be equivalent to the ratio of forwards and reverse rate constants between the reactants and transition state

$$e^{-\Delta F^{\ddagger}(\Delta)} = \frac{k_0^+(\Delta)}{k_0^-(\Delta)}. \tag{5.42}$$

Using this in Eq. 5.40 and multiplying the numerator and denominator by $e^{-\beta\Delta F^{\ddagger}(\Delta=0)}$ then gives

$$k(\Delta) = \frac{k_{\mathrm{e}}(\Delta)e^{-\beta\Delta F^{\ddagger}(\Delta=0)}A_{\mathrm{BO}}(\Delta)e^{-\beta\Delta F^{\ddagger}(\Delta)}}{k_{\mathrm{e}}(\Delta)e^{-\beta\Delta F^{\ddagger}(\Delta=0)} + A_{\mathrm{BO}}(\Delta)e^{-\beta\Delta F^{\ddagger}(\Delta=0)}}. \tag{5.43}$$

To arrive at the final result we now make two simplifying approximations, the first of which is to assume that the transition between TS_r and TS_p can always be treated using Fermi's golden rule, such that $k_{\mathrm{e}}(\Delta) \propto \Delta^2$ and

$$k_{\mathrm{GR}}(\Delta) \simeq \frac{k_{\mathrm{e}}(\Delta)k_0^+(\Delta=0)}{k_0^-(\Delta=0)} = k_{\mathrm{e}}(\Delta)e^{-\beta\Delta F^{\ddagger}(\Delta=0)}. \tag{5.44}$$

The second approximation is that the pre-exponential factor $A_{\mathrm{BO}}(\Delta) \simeq A_{\mathrm{BO}}(\Delta=0)$, such that

$$k_{\mathrm{BO}}(\Delta=0) = A_{\mathrm{BO}}(\Delta=0)e^{-\beta\Delta F^{\ddagger}(\Delta=0)} \simeq A_{\mathrm{BO}}(\Delta)e^{-\beta\Delta F^{\ddagger}(\Delta=0)}, \tag{5.45}$$

which corresponds classically to assuming that changes to the curvature of the potential surface do not change the rate of passage through the transition state region. Inserting these two approximations into Eq. 5.43 we then arrive at the interpolation formula given in Eq. 5.1,

$$k(\Delta) \simeq \frac{k_{\mathrm{GR}}(\Delta)k_{\mathrm{BO}}(\Delta)}{k_{\mathrm{GR}}(\Delta) + k_{\mathrm{BO}}(\Delta=0)}. \tag{5.46}$$

The interpolation formula can thus be thought to rest on four basic assumptions. Firstly that the reaction can be considered as a stepwise process, involving motion to and from a high energy transition state region where the electronic transition takes place. Secondly that each of these steps can be treated as an incoherent rate like process. Thirdly that the electronic transition in the transition state region can be treated using Fermi's golden rule, and finally that the prefactor of the Born-Oppenheimer rate is approximately independent of the electronic coupling, Δ. Hence the interpolation formula is most likely to be accurate if these approximations can be justified. However, the interpolation formula is guaranteed

to reduce to the golden-rule and Born-Oppenheimer rates in the appropriate limit even when these approximations are not well justified, and so the formula may still give rate predictions which are practically accurate in a much wider regime.

To arrive at the Zusman equation one makes the approximation,

$$A_{\mathrm{BO}}(\Delta)e^{-\beta\Delta F^{\ddagger}(\Delta)} \simeq A_{\mathrm{BO}}(\Delta=0)e^{-\beta\Delta F^{\ddagger}(\Delta=0)} \text{ or equivalently } k_{\mathrm{BO}}(\Delta) \simeq k_{\mathrm{BO}}(\Delta=0), \quad (5.47)$$

in place of Eq. 5.45, and then replaces each of the rate constants by the classical rates for the spin-boson model in the limit of high friction along the diabatic energy gap coordinate. The assumption of a consecutive reaction mechanism is of course valid classically in this high friction limit, just as assuming k_{e} is given by the golden-rule is consistent with the assumption that $k_{\mathrm{BO}}(\Delta) \simeq k_{\mathrm{BO}}(\Delta=0)$. However, due to the exponential sensitivity of the barrier height on Δ, assuming that the entire Born-Oppenheimer rate is independent of Δ rather than just the pre-exponential factor is of course a much more drastic approximation.

In fact, in situations where one can analytically separate the rate expression into exponential and pre-exponential components one need not make the second of the two approximations at all, and instead one can simply approximate the rate as[72]

$$k(\Delta) \simeq \frac{A_{\mathrm{GR}}(\Delta)A_{\mathrm{BO}}(\Delta)}{A_{\mathrm{GR}}(\Delta)+A_{\mathrm{BO}}(\Delta)}e^{-\beta\Delta F^{\ddagger}(\Delta)}, \quad (5.48)$$

where

$$k_{\mathrm{GR}}(\Delta) = A_{\mathrm{GR}}(\Delta)e^{-\beta\Delta F^{\ddagger}(\Delta=0)}. \quad (5.49)$$

This could, for example, be used as a simple way to combine the semiclassical instanton approximations in the golden-rule and Born-Oppenheimer limits.[143,146,170,195]

5.B Appendix: Efficient implementation of RPMD for system-bath problems

In this appendix we describe an efficient implementation of RPMD and other path-integral based methods for system-bath problems with a harmonic bath, which is based on analytically integrating out the effect of the bath in the ring-polymer picture. In Sec. 5.B.1 we give an overview of the approach, detailing the key equations that were implemented. In Sec. 5.B.2 we show how one can integrate out the effect of the bath in RPMD/Wolynes

theory for the general case of an arbitrary number of system coordinates coupled to a harmonic bath. In Sec. 5.B.3 we specialise the general result for the model problem considered in Sec. 5.4. Finally, in Sec. 5.B.4, we describe how we numerically integrated the GLE satisfied by the system variables in RPMD.

5.B.1 Overview

Both RPMD and Wolynes theory calculations for system-bath models such as the spin-boson model can be transformed into trivial problems, which only explicitly include one nuclear degree of freedom, the reaction coordinate.* Starting from the diabatic potentials [Eqs. 5.20-5.22], we can write both the RPMD and Wolynes theory Hamiltonians in the form

$$H^{(n)}(\mathbf{P},\mathbf{Q},\mathbf{p},\mathbf{q}) = H_s^{(n)}(\mathbf{P},\mathbf{Q}) + H_{sb}^{(n)}(\mathbf{Q},\mathbf{p},\mathbf{q}) \tag{5.50}$$

where

$$\begin{aligned} H_{sb}^{(n)}(\mathbf{Q},\mathbf{p},\mathbf{q}) = \sum_{j=1}^{n}\sum_{\nu=1}^{N_b}\Bigg[&\frac{p_{j,\nu}^2}{2m_\nu} + \frac{1}{2}m_\nu\omega_n^2(q_{j+1,\nu}-q_{j,\nu})^2 \\ &+ \frac{1}{2}m_\nu\omega_\nu^2\left(q_{j,\nu} - \frac{c_\nu Q_j}{m_\nu\omega_\nu^2}\right)^2\Bigg]. \end{aligned} \tag{5.51}$$

Integrating out the effect of the bath on the system allows us to write an effective Hamiltonian which only contains the reaction coordinate. For the Ohmic spectral density this renormalised ring-polymer Hamiltonian is simply

$$\tilde{H}_s^{(n)}(\mathbf{P},\mathbf{Q}) = H_s^{(n)}(\mathbf{P},\mathbf{Q}) + \sum_{k=0}^{n-1}\frac{1}{2}\gamma\omega_k\tilde{Q}_k^2 \tag{5.52}$$

where $\tilde{Q}_k$ and $\omega_k = 2\omega_n \sin(k\pi/n)$ are the position and frequency of the k^{th} normal mode of the free ring-polymer along the reaction coordinate. We see that friction has the effect of increasing the stiffness of the ring-polymer springs. As discussed in the main part of this chapter, this is consistent with the well known effect of friction in reducing tunnelling and making the system behave more classically.[192]

*Note that in the case of the spin-boson model itself the exact expression for $F_{\text{GR}}(\lambda)$ can be used to evaluate Wolynes theory without the use of path integrals, however the approach described here can be used to calculate the Wolynes rate for anharmonic system coordinates.

For static quantities such as the Wolynes rate and the quantum transition state theory (QTST) part of the RPMD rate, one can simply do path-integral molecular dynamics (PIMD) with the renormalised system Hamiltonian in Eq. 5.52. However, when evaluating dynamical quantities such as the RPMD transmission coefficient, the dynamical effect of the bath must also be included. This results in a generalised Langevin equation (GLE) for the motion along the reaction coordinate, which for the problem considered in Sec. 5.4 takes the form

$$\dot{\tilde{Q}}_k = \tilde{P}_k \tag{5.53a}$$

$$\dot{\tilde{P}}_k = -\frac{\partial \tilde{H}_s^{(n)}}{\partial \tilde{Q}_k} - \int_0^t K_k(t-\tau)\tilde{P}_k(\tau)\mathrm{d}\tau + F_k(t) \tag{5.53b}$$

where

$$\begin{aligned} K_k(t) = {} & 2\gamma\delta(t) - \gamma\omega_k \\ & + \gamma\omega_k^2 t \mathrm{J}_0(\omega_k t)\left(1 - \frac{\pi}{2}\mathrm{H}_1(\omega_k t)\right) \\ & - \gamma\omega_k \mathrm{J}_1(\omega_k t)\left(1 - \frac{\pi}{2}\omega_k t \mathrm{H}_0(\omega_k t)\right) \end{aligned} \tag{5.54}$$

is the friction kernel, $\mathrm{J}_n(x)$ is the n^{th} Bessel function of the first kind, and $\mathrm{H}_n(x)$ is the n^{th} Struve H function. To integrate these equations of motion we use a modified form of the algorithm suggested by Berkowitz, Morgan and McCammon[222] which makes use of the exact evolution of the free ring-polymer (as detailed in Sec. 5.B.4). Note that, since $\omega_0 = 0$, the centroid friction kernel is proportional to a delta function, and so the non-Markovian behaviour originates in the internal ring-polymer modes. This reflects the fact that whilst the Ohmic spectral density in the classical limit corresponds to Markovian dynamics of the reaction coordinate, this is not true quantum mechanically.

5.B.2 Derivation

Here we derive the generalised Langevin equation (GLE) for a ring-polymer Hamiltonian with N_s physical system coordinates which are linearly coupled to N_b harmonic oscillators, applying the approach of Cortés *et al.*[221] to the ring-polymer system bath model. We begin by writing the total ring-polymer Hamiltonian as

$$H^{(n)}(\mathbf{P},\mathbf{Q},\mathbf{p},\mathbf{q}) = H_s^{(n)}(\mathbf{P},\mathbf{Q}) + H_{sb}^{(n)}(\mathbf{Q},\mathbf{p},\mathbf{q}) \tag{5.55}$$

where $(\mathbf{Q}, \mathbf{P})$ and $(\mathbf{q}, \mathbf{p})$ denote coordinates and momenta of the system and bath respectively, and

$$H_{sb}^{(n)}(\mathbf{Q}, \mathbf{p}, \mathbf{q}) = \sum_{j=1}^{n} \sum_{\nu=1}^{N_b} \left[\frac{p_{j,\nu}^2}{2m_\nu} + \frac{1}{2} m_\nu \omega_n^2 (q_{j+1,\nu} - q_{j,\nu})^2 + \frac{1}{2} m_\nu \omega_\nu^2 \left(q_{j,\nu} - \sum_{\mu=1}^{N_s} \frac{c_{\mu\nu} Q_{j,\mu}}{m_\nu \omega_\nu^2} \right)^2 \right]. \tag{5.56}$$

Throughout we use Latin subscripts to denote ring-polymer coordinates and Greek subscripts for physical degrees of freedom. Transforming from the bead representation to the normal mode representation of the free ring-polymer gives

$$H_{sb}^{(n)}(\tilde{\mathbf{Q}}, \tilde{\mathbf{q}}, \tilde{\mathbf{p}}) = \sum_{k=0}^{n-1} \sum_{\nu=1}^{N_b} \left[\frac{\tilde{p}_{k,\nu}^2}{2m_\nu} + \frac{1}{2} m_\nu \omega_k^2 \tilde{q}_{k,\nu}^2 + \frac{1}{2} m_\nu \omega_\nu^2 \left(\tilde{q}_{k,\nu} - \sum_{\mu=1}^{N_s} \frac{c_{\mu\nu} \tilde{Q}_{k,\mu}}{m_\nu \omega_\nu^2} \right)^2 \right], \tag{5.57}$$

where again $\omega_k = 2\omega_n \sin(k\pi/n)$ are the normal mode frequencies of the free ring-polymer. From this it is clear that the bath does not couple the normal modes of the system ring-polymer and hence it is straightforward to integrate out the effect of the bath on the system in this representation. The equations of motion are

$$\dot{\tilde{Q}}_{k,\lambda} = \frac{\tilde{P}_{k,\lambda}}{m_\lambda}, \tag{5.58a}$$

$$\dot{\tilde{P}}_{k,\lambda} = -\frac{\partial H_s^{(n)}}{\partial \tilde{Q}_{k,\lambda}} + \sum_{\nu=1}^{N_b} c_{\lambda\nu} \left(\tilde{q}_{k,\nu} - \frac{\boldsymbol{c}_\nu \cdot \tilde{\boldsymbol{Q}}_k}{m_\nu \omega_\nu^2} \right), \tag{5.58b}$$

$$\dot{\tilde{q}}_{k,\nu} = \frac{\tilde{p}_{k,\nu}}{m_\nu}, \tag{5.58c}$$

$$\dot{\tilde{p}}_{k,\nu} = -m_\nu \tilde{\omega}_{k,\nu}^2 \tilde{q}_{k,\nu} + \boldsymbol{c}_\nu \cdot \tilde{\boldsymbol{Q}}_k, \tag{5.58d}$$

where $\tilde{\omega}_{k,\nu} = \sqrt{\omega_\nu^2 + \omega_k^2}$ and we have rewritten $\sum_{\mu=1}^{N_s} c_{\mu\nu} \tilde{Q}_{k,\mu} = \boldsymbol{c}_\nu \cdot \tilde{\boldsymbol{Q}}_k$.

The equations of motion for the bath degrees of freedom

$$\ddot{\tilde{q}}_{k,\nu} + \tilde{\omega}_{k,\nu}^2 \tilde{q}_{k,\nu} = \frac{\boldsymbol{c}_\nu \cdot \tilde{\boldsymbol{Q}}_k}{m_\nu}, \tag{5.59}$$

can be solved using the standard method of undetermined coefficients. The corresponding homogeneous differential equation is

$$\ddot{\tilde{q}}_{k,\nu} + \tilde{\omega}_{k,\nu}^2 \tilde{q}_{k,\nu} = 0, \tag{5.60}$$

giving the complementary function

$$\tilde{q}_{k,\nu}(t) = a_{k,\nu}\cos(\tilde{\omega}_{k,\nu}t) + b_{k,\nu}\sin(\tilde{\omega}_{k,\nu}t). \tag{5.61}$$

Hence we consider the particular solution

$$\tilde{q}_{k,\nu}(t) = a_{k,\nu}(t)\cos(\tilde{\omega}_{k,\nu}t) + b_{k,\nu}(t)\sin(\tilde{\omega}_{k,\nu}t), \tag{5.62}$$

and require that

$$\dot{a}_{k,\nu}(t)\cos(\tilde{\omega}_{k,\nu}t) + \dot{b}_{k,\nu}(t)\sin(\tilde{\omega}_{k,\nu}t) = 0. \tag{5.63}$$

Differentiating Eq. 5.62 twice and using Eq. 5.63 gives

$$\begin{aligned}\dot{\tilde{q}}_{k,\nu}(t) = &-\tilde{\omega}_{k,\nu}a_{k,\nu}(t)\sin(\tilde{\omega}_{k,\nu}t)\\ &+\tilde{\omega}_{k,\nu}b_{k,\nu}(t)\cos(\tilde{\omega}_{k,\nu}t)\end{aligned} \tag{5.64}$$

and then

$$\begin{aligned}\ddot{\tilde{q}}_{k,\nu}(t) = &-\tilde{\omega}_{k,\nu}^2 a_{k,\nu}(t)\cos(\tilde{\omega}_{k,\nu}t)\\ &-\tilde{\omega}_{k,\nu}^2 b_{k,\nu}(t)\sin(\tilde{\omega}_{k,\nu}t)\\ &-\tilde{\omega}_{k,\nu}\dot{a}_{k,\nu}(t)\sin(\tilde{\omega}_{k,\nu}t)\\ &+\tilde{\omega}_{k,\nu}\dot{b}_{k,\nu}(t)\cos(\tilde{\omega}_{k,\nu}t).\end{aligned} \tag{5.65}$$

Hence using Eq. 5.59 it follows that

$$\begin{aligned}\frac{\boldsymbol{c}_\nu \cdot \tilde{\boldsymbol{Q}}_k(t)}{m_\nu} = &-\tilde{\omega}_{k,\nu}\dot{a}_{k,\nu}(t)\sin(\tilde{\omega}_{k,\nu}t)\\ &+\tilde{\omega}_{k,\nu}\dot{b}_{k,\nu}(t)\cos(\tilde{\omega}_{k,\nu}t),\end{aligned} \tag{5.66}$$

which can be rearranged using Eq. 5.63 to give

$$\frac{\boldsymbol{c}_\nu \cdot \tilde{\boldsymbol{Q}}_k(t)}{m_\nu\tilde{\omega}_{k,\nu}}\sin(\tilde{\omega}_{k,\nu}t) = -\dot{a}_{k,\nu}(t) \tag{5.67a}$$

$$\frac{\boldsymbol{c}_\nu \cdot \tilde{\boldsymbol{Q}}_k(t)}{m_\nu\tilde{\omega}_{k,\nu}}\cos(\tilde{\omega}_{k,\nu}t) = \dot{b}_{k,\nu}(t). \tag{5.67b}$$

Integrating gives

$$a_{k,\nu}(t) = a_{k,\nu}(0) - \int_0^t \frac{\boldsymbol{c}_\nu \cdot \tilde{\boldsymbol{Q}}_k(\tau)}{m_\nu\tilde{\omega}_{k,\nu}}\sin(\tilde{\omega}_{k,\nu}\tau)\mathrm{d}\tau \tag{5.68a}$$

$$b_{k,\nu}(t) = b_{k,\nu}(0) + \int_0^t \frac{\boldsymbol{c}_\nu \cdot \tilde{\boldsymbol{Q}}_k(\tau)}{m_\nu\tilde{\omega}_{k,\nu}}\cos(\tilde{\omega}_{k,\nu}\tau)\mathrm{d}\tau, \tag{5.68b}$$

which when substituted into Eq. 5.62 gives

$$\begin{aligned}\tilde{q}_{k,\nu}(t) = &\int_0^t \frac{\boldsymbol{c}_\nu \cdot \tilde{\boldsymbol{Q}}_k(\tau)}{m_\nu \tilde{\omega}_{k,\nu}} \sin(\tilde{\omega}_{k,\nu}(t-\tau))\mathrm{d}\tau \\ &+ a_{k,\nu}(0)\cos(\tilde{\omega}_{k,\nu}t) + b_{k,\nu}(0)\sin(\tilde{\omega}_{k,\nu}t).\end{aligned} \tag{5.69}$$

Finally, integrating by parts and inserting the appropriate boundary conditions gives

$$\begin{aligned}\tilde{q}_{k,\nu}(t) = &\frac{\boldsymbol{c}_\nu \cdot \tilde{\boldsymbol{Q}}_k(t)}{m_\nu \tilde{\omega}_{k,\nu}^2} - \frac{\boldsymbol{c}_\nu \cdot \tilde{\boldsymbol{Q}}_k(0)}{m_\nu \tilde{\omega}_{k,\nu}^2}\cos(\tilde{\omega}_{k,\nu}t) \\ &- \int_0^t \frac{\boldsymbol{c}_\nu \cdot \dot{\tilde{\boldsymbol{Q}}}_k(\tau)}{m_\nu \tilde{\omega}_{k,\nu}^2}\cos(\tilde{\omega}_{k,\nu}(t-\tau))\mathrm{d}\tau \\ &+ \tilde{q}_{k,\nu}(0)\cos(\tilde{\omega}_{k,\nu}t) + \frac{\tilde{p}_{k,\nu}(0)}{m_\nu \tilde{\omega}_{k,\nu}}\sin(\tilde{\omega}_{k,\nu}t).\end{aligned} \tag{5.70}$$

Having solved for $\tilde{q}_{k,\nu}(t)$, we can now substitute this back into Eq. 5.58b to obtain the GLE for an arbitrary system bath model,

$$\dot{\tilde{\boldsymbol{P}}}_k(t) = -\frac{\partial \tilde{H}_s^{(n)}}{\partial \tilde{\boldsymbol{Q}}_k} - \int_0^t \mathbf{K}^{(k)}(t-\tau)\cdot\dot{\tilde{\boldsymbol{Q}}}_k(\tau)\mathrm{d}\tau + \mathbf{F}^{(k)}(t). \tag{5.71}$$

Here we have defined

$$\frac{\partial \tilde{H}_s^{(n)}}{\partial \tilde{\boldsymbol{Q}}_k} = \frac{\partial H_s^{(n)}}{\partial \tilde{\boldsymbol{Q}}_k} + \boldsymbol{\alpha}^{(k)}\cdot\tilde{\boldsymbol{Q}}_k \tag{5.72}$$

with

$$\alpha_{\lambda\mu}^{(k)} = \sum_{\nu=1}^{N_b}\left(\frac{c_{\lambda\nu}c_{\mu\nu}}{m_\nu\omega_\nu^2} - \frac{c_{\lambda\nu}c_{\mu\nu}}{m_\nu\tilde{\omega}_{k,\nu}^2}\right), \tag{5.73}$$

which accounts for the renormalisation of the system Hamiltonian due to the presence of the bath, and we have collected together the remaining effects of the bath into a friction kernel

$$K_{\lambda\mu}^{(k)}(t-\tau) = \sum_{\nu=1}^{N_b}\frac{c_{\lambda\nu}c_{\mu\nu}}{m_\nu\tilde{\omega}_{k,\nu}^2}\cos(\tilde{\omega}_{k,\nu}(t-\tau)) \tag{5.74}$$

and a fluctuating force

$$F_\lambda^{(k)}(t) = \sum_{\nu=1}^{N_b} c_{\lambda\nu}\left(\left(\tilde{q}_{k,\nu}(0) - \frac{\boldsymbol{c}_\nu\cdot\tilde{\boldsymbol{Q}}_k(0)}{m_\nu\tilde{\omega}_{k,\nu}^2}\right)\cos(\tilde{\omega}_{k,\nu}t) + \frac{\tilde{p}_{k,\nu}(0)}{m_\nu\tilde{\omega}_{k,\nu}}\sin(\tilde{\omega}_{k,\nu}t)\right). \tag{5.75}$$

It is straightforward to show that, for a system at thermal equilibrium, the fluctuating force and the friction kernel are related by the fluctuation-dissipation theorem

$$\langle F_\lambda^{(k)}(0)F_\mu^{(k)}(t)\rangle = \frac{1}{\beta_n}K_{\lambda\mu}^{(k)}(t). \tag{5.76}$$

The easiest way to see this is to note that the ring-polymer Hamiltonian in Eq. 5.55 can be rewritten as

$$H^{(n)} = \tilde{H}_s^{(n)} + \tilde{H}_{sb}^{(n)} \tag{5.77}$$

where each term is written in renormalised form as

$$\tilde{H}_s^{(n)} = H_s^{(n)} + \sum_{k=0}^{n-1} \frac{1}{2} \tilde{\boldsymbol{Q}}_k^T \boldsymbol{\alpha}^{(k)} \tilde{\boldsymbol{Q}}_k \tag{5.78a}$$

$$\tilde{H}_{sb}^{(n)} = \sum_{k=0}^{n-1} \sum_{\nu=1}^{N_b} \left[\frac{\tilde{p}_{k,\nu}^2}{2m_\nu} + \frac{1}{2} m_\nu \tilde{\omega}_{k,\nu}^2 \left(\tilde{q}_{k,\nu} - \frac{\boldsymbol{c}_\nu \cdot \tilde{\boldsymbol{Q}}_k}{m_\nu \tilde{\omega}_{k,\nu}^2} \right)^2 \right]. \tag{5.78b}$$

Hence integrating first over the $\tilde{q}_{k,\nu}$ it is straightforward to see that the correlation function of the fluctuating force in Eq. 5.75 leads directly to Eq. 5.76. Note also that, in the infinite bath limit, the fluctuating force is Gaussian (by the Central Limit Theorem), and since $\langle F_\lambda^{(k)}(0) \rangle = 0$, a knowledge of the friction kernel completely specifies the form of the fluctuating force.

Finally, we note that the expressions for $\alpha_{\lambda\mu}^{(k)}$ and $K_{\lambda\mu}^{(k)}(t)$ in Eqs. 5.73 and 5.74 can be recast in terms of the spectral density

$$J_{\lambda\mu}(\omega) = \frac{\pi}{2} \sum_{\nu=1}^{N_b} \frac{c_{\lambda\nu} c_{\mu\nu}}{m_\nu \omega_\nu} \delta(\omega - \omega_\nu), \tag{5.79}$$

either as

$$\alpha_{\lambda\mu}^{(k)} = \frac{2}{\pi} \int_0^\infty \frac{J_{\lambda\mu}(\omega)}{\omega} - \frac{J_{\lambda\mu}(\omega)\omega}{\omega^2 + \omega_k^2} \mathrm{d}\omega \tag{5.80}$$

and

$$K_{\lambda\mu}^{(k)}(t) = \frac{2}{\pi} \int_0^\infty \frac{J_{\lambda\mu}(\omega)\omega}{\omega^2 + \omega_k^2} \cos\left(\sqrt{\omega^2 + \omega_k^2}\, t \right) \mathrm{d}\omega, \tag{5.81}$$

or equivalently as

$$\alpha_{\lambda\mu}^{(k)} = \frac{2}{\pi} \int_0^\infty \frac{J_{\lambda\mu}(\omega)}{\omega} - \frac{J_{\lambda\mu}^{(k)}(\omega)}{\omega} \mathrm{d}\omega \tag{5.82}$$

and

$$K_{\lambda\mu}^{(k)}(t) = \frac{2}{\pi} \int_0^\infty \frac{J_{\lambda\mu}^{(k)}(\omega)}{\omega} \cos(\omega t) \mathrm{d}\omega, \tag{5.83}$$

where we have defined

$$J_{\lambda\mu}^{(k)}(\omega) = \theta(\omega - \omega_k) J_{\lambda\mu}\left(\sqrt{\omega^2 - \omega_k^2} \right) \tag{5.84}$$

with $\theta(x)$ being the Heaviside step function.

5.B.3 One dimensional system with Ohmic spectral density

The problem considered in Sec. 5.4 consists of a single system coordinate (the reaction coordinate) coupled to a bath with an Ohmic spectral density $J(\omega) = \gamma\omega$. The frequencies which enter the renormalisation of the system Hamiltonian are therefore simply

$$\alpha_k = \frac{2}{\pi}\int_0^\infty \frac{\gamma\omega_k^2}{\omega^2+\omega_k^2}\mathrm{d}\omega, \tag{5.85}$$

where, since there is only one physical system coordinate, we have changed notation slightly so that the subscript refers to the normal mode. This integral is easily evaluated to give

$$\alpha_k = \gamma\omega_k. \tag{5.86}$$

The friction kernel can also be evaluated analytically for this problem by considering

$$K_k(t) = \frac{2}{\pi}\int_0^\infty \frac{J_k(\omega)}{\omega}\cos(\omega t)\,\mathrm{d}\omega \tag{5.87}$$

with

$$J_k(\omega) = \theta(\omega-\omega_k)\gamma\sqrt{\omega^2-\omega_k^2}. \tag{5.88}$$

This can be rearranged into the form

$$K_k(t) = \frac{2}{\pi}\int_{\omega_k}^\infty \frac{\gamma\sqrt{\omega^2-\omega_k^2}-\gamma\omega}{\omega}\cos(\omega t)\mathrm{d}\omega + 2\gamma\delta(t) - \frac{2}{\pi}\int_0^{\omega_k}\gamma\cos(\omega t)\mathrm{d}\omega, \tag{5.89}$$

and then straightforwardly evaluated to give

$$\begin{aligned} K_k(t) =& 2\gamma\delta(t) - \gamma\omega_k \\ &+ \gamma\omega_k^2 t\mathrm{J}_0(\omega_k t)\left(1-\frac{\pi}{2}\mathrm{H}_1(\omega_k t)\right) \\ &- \gamma\omega_k\mathrm{J}_1(\omega_k t)\left(1-\frac{\pi}{2}\omega_k t\mathrm{H}_0(\omega_k t)\right), \end{aligned} \tag{5.90}$$

where $\mathrm{J}_n(x)$ is the n^{th} Bessel function of the first kind and $\mathrm{H}_n(x)$ is the n^{th} Struve H function.

The GLE for each internal mode of the ring polymer in a one-dimensional system coupled to a bath with Ohmic spectral density can thus be written as

$$\dot{\tilde{Q}}_k = \frac{\tilde{P}_k}{m} \tag{5.91a}$$

$$\dot{\tilde{P}}_k = -\frac{\partial\tilde{H}_s^{(n)}}{\partial\tilde{Q}_k} - \frac{1}{m}\int_0^t K_k(t-\tau)\tilde{P}_k(\tau)\mathrm{d}\tau + F_k(t), \tag{5.91b}$$

where

$$\frac{\partial\tilde{H}_s^{(n)}}{\partial\tilde{Q}_k} = \frac{\partial V_s^{(n)}}{\partial\tilde{Q}_k} + \omega_k^2\tilde{Q}_k + \gamma\omega_k\tilde{Q}_k. \tag{5.92}$$

5.B.4 Generalised Langevin equation: Numerical integration

The standard integration scheme used to evolve RPMD can be written in the form

$$\tilde{P}'_k \leftarrow \tilde{P}^{(i)}_k + \frac{\Delta t}{2} f^{(i)}_k \tag{5.93a}$$

$$\tilde{Q}^{(i+1)}_k \leftarrow \cos(\omega_k \Delta t)\tilde{Q}^{(i)}_k + \frac{1}{m\omega_k}\sin(\omega_k \Delta t)\tilde{P}'_k \tag{5.93b}$$

$$\tilde{P}'_k \leftarrow \cos(\omega_k \Delta t)\tilde{P}'_k - m\omega_k \sin(\omega_k \Delta t)\tilde{Q}^{(i)}_k \tag{5.93c}$$

$$\tilde{P}^{(i+1)}_k \leftarrow \tilde{P}'_k + \frac{\Delta t}{2} f^{(i+1)}_k \tag{5.93d}$$

where $f^{(i)}_k$ is the external force on the the k^{th} normal mode (excluding the ring-polymer spring force) at time step i, and $\tilde{P}'_k$ is a temporary value of the momentum (between the two time steps). For simplicity we shall consider just a single system coordinate; the extension to more degrees of freedom is straightforward but notationally cumbersome. Following Berkowitz *et al.*,[222] we start by considering the standard ring-polymer integration scheme in its position only form (analogous to the difference between the Verlet and velocity Verlet algorithms)

$$\tilde{Q}^{(i+1)}_k \leftarrow 2C_k \tilde{Q}^{(i)}_k - \tilde{Q}^{(i-1)}_k + f^{(i)}_k \frac{\Delta t^2}{m} S_k \tag{5.94a}$$

$$\tilde{P}^{(i)}_k \leftarrow \frac{m}{S_k}\frac{\tilde{Q}^{(i+1)}_k - \tilde{Q}^{(i-1)}_k}{2\Delta t}, \tag{5.94b}$$

where $C_k = \cos(\omega_k \Delta t)$ and $S_k = \frac{1}{\omega_k \Delta t}\sin(\omega_k \Delta t)$.

Firstly we incorporate the renormalisation of the Hamiltonian in the exact ring-polymer evolution by replacing $C_k \to \tilde{C}_k = \cos(\tilde{\omega}_k \Delta t)$ and $S_k \to \tilde{S}_k = \frac{1}{\tilde{\omega}_k \Delta t}\sin(\tilde{\omega}_k \Delta t)$, with $\tilde{\omega}_k = \sqrt{\omega_k^2 + \gamma\omega_k}$. Then we use the fact that the external force

$$f_k(t) = -\frac{\partial V^{(n)}_s}{\partial \tilde{Q}_k} - \frac{1}{m}\int_0^t K_k(t-\tau)\tilde{P}_k(\tau)\mathrm{d}\tau + F_k(t) \tag{5.95}$$

can be discretised using the trapezium rule to give

$$f^{(i)}_k \simeq -\frac{\partial V^{(n)}_s}{\partial \tilde{Q}^{(i)}_k} - \frac{1}{m}\sum_{j=0}^{i} w_j K^{(j)}_k \tilde{P}^{(i-j)}_k \Delta t + F^{(i)}_k, \tag{5.96}$$

where w_j are the integration weights and $F^{(i)}_k$ is a particular realisation of the fluctuating force, the generation of which is discussed later. Using this with Eq. 5.94b for

the momenta gives

$$\begin{aligned}\tilde{Q}_k^{(i+1)}\left(1+\frac{\Delta t^2}{4m}K_k^{(0)}\right) =& 2\tilde{C}_k\tilde{Q}_k^{(i)} - \tilde{Q}_k^{(i-1)}\left(1-\frac{\Delta t^2}{4m}K_k^{(0)}\right) \\ &- \frac{1}{m}\sum_{j=1}^{i} w_j K_k^{(j)}\tilde{P}_k^{(i-j)}\Delta t\frac{\Delta t^2}{m}\tilde{S}_k \\ &- \frac{\partial V_s^{(n)}}{\partial \tilde{Q}_k^{(i)}}\frac{\Delta t^2}{m}\tilde{S}_k + F_k^{(i)}\frac{\Delta t^2}{m}\tilde{S}_k.\end{aligned} \tag{5.97}$$

Finally, we rearrange this into a form analogous to the usual ring-polymer integration scheme to obtain

$$\tilde{P}'_k \leftarrow \tilde{P}_k^{(i)}\left(1-\frac{\Delta t^2}{4m}K_k^{(0)}\right) \tag{5.98a}$$

$$\tilde{P}'_k \leftarrow \tilde{P}'_k - \frac{\Delta t^2}{2m}\sum_{j=1}^{i} w_j K_k^{(j)}\tilde{P}_k^{(i-j)} + \frac{\Delta t}{2}F_k^{(i)} \tag{5.98b}$$

$$\tilde{P}'_k \leftarrow \tilde{P}'_k - \frac{\Delta t}{2}\frac{\partial V_s^{(n)}}{\partial \tilde{Q}_k^{(i)}} \tag{5.98c}$$

$$\tilde{Q}_k^{(i+1)} \leftarrow \cos(\tilde{\omega}_k\Delta t)\tilde{Q}_k^{(i)} + \frac{1}{m\tilde{\omega}_k}\sin(\tilde{\omega}_k\Delta t)\tilde{P}'_k \tag{5.98d}$$

$$\tilde{P}'_k \leftarrow \cos(\tilde{\omega}_k\Delta t)\tilde{P}'_k - m\tilde{\omega}_k\sin(\tilde{\omega}_k\Delta t)\tilde{Q}_k^{(i)} \tag{5.98e}$$

$$\tilde{P}'_k \leftarrow \tilde{P}'_k - \frac{\Delta t}{2}\frac{\partial V_s^{(n)}}{\partial \tilde{Q}_k^{(i+1)}} \tag{5.98f}$$

$$\tilde{P}'_k \leftarrow \tilde{P}'_k - \frac{\Delta t^2}{2m}\sum_{j=1}^{i+1} w_j K_k^{(j)}\tilde{P}_k^{(i+1-j)} + \frac{\Delta t}{2}F_k^{(i+1)} \tag{5.98g}$$

$$\tilde{P}_k^{(i+1)} \leftarrow \tilde{P}'_k\left(1+\frac{\Delta t^2}{4m}K_k^{(0)}\right)^{-1}. \tag{5.98h}$$

This can be implemented by noting that Eqs. 5.98c-5.98f are just the usual integration scheme with modified spring constants, to which one simply needs to add the thermostatting steps in Eqs. 5.98a, 5.98b, 5.98g and 5.98h. We also note that, since the dynamics of the centroid ($k = 0$) mode is Markovian, we can simply use the usual path-integral Langevin equation (PILE)[223] integration scheme for this mode with the appropriate friction constant.

As described by Berkowitz *et al.*,[222] the fluctuating force $F_k(t)$ can be obtained on the necessary time grid using a discrete Fourier transform. This can be achieved by

first writing the fluctuating force as

$$F_k(t) = \int_0^\infty G_k(\omega)\Big(\xi_a(\omega)\cos(\omega t) + \xi_b(\omega)\sin(\omega t)\Big)\mathrm{d}\omega, \tag{5.99}$$

where $\xi_a(\omega)$ and $\xi_b(\omega)$ are Gaussian random noise terms satisfying

$$\langle \xi_a(\omega)\rangle = \langle \xi_b(\omega)\rangle = 0 \tag{5.100a}$$

$$\langle \xi_a(\omega)\xi_a(\omega')\rangle = \delta(\omega - \omega') \tag{5.100b}$$

$$\langle \xi_b(\omega)\xi_b(\omega')\rangle = \delta(\omega - \omega') \tag{5.100c}$$

$$\langle \xi_a(\omega)\xi_b(\omega')\rangle = 0, \tag{5.100d}$$

and

$$G_k(\omega) = \sqrt{\frac{2}{\pi\beta_n}\frac{J_k(\omega)}{\omega}}. \tag{5.101}$$

More formally $\xi_a(\omega)$ and $\xi_b(\omega)$ are derivatives of Wiener processes, $w_a(\omega)$ and $w_b(\omega)$ respectively, and as such we can write

$$F_k(t) = \int_0^\infty G_k(\omega)\cos(\omega t)\mathrm{d}w_a(\omega) + \int_0^\infty G_k(\omega)\sin(\omega t)\mathrm{d}w_b(\omega). \tag{5.102}$$

Here the integrals are Stratanovich stochastic integrals defined as

$$\int_0^{\omega_{\max}} g(\omega)\mathrm{d}w(\omega) = \underset{N\to\infty}{\text{ms-lim}}\left[\sum_{j=0}^{N-1}\frac{g(\omega_j) + g(\omega_{j+1})}{2}\big(w(\omega_{j+1}) - w(\omega_j)\big)\right], \tag{5.103}$$

in which the nodes ω_j form an ordered subdivision $0 = \omega_0 < \omega_1 < \cdots \omega_N = \omega_{\max}$ of the interval $[0, \omega_{\max}]$ and 'ms-lim' denotes a limit in mean square. Note that from the definition of a Wiener process

$$w(\omega_{j+1}) - w(\omega_j) = \sqrt{(\omega_{j+1} - \omega_j)}\xi^{(j)} \tag{5.104}$$

where $\{\xi^{(j)};\ j = 0, \ldots, N\}$ is a Gaussian stochastic process with zero mean and unit variance.

Since we wish to obtain $F_k(t)$ on a discrete time grid, with spacing Δt, we truncate the integrals in Eq. 5.102 at the Nyquist critical frequency

$$F_k(i\Delta t) \simeq \int_0^{\frac{\pi}{\Delta t}} G_k(\omega)\cos(\omega i\Delta t)\mathrm{d}w_a(\omega) + \int_0^{\frac{\pi}{\Delta t}} G_k(\omega)\sin(\omega i\Delta t)\mathrm{d}w_b(\omega) \tag{5.105}$$

and then take a finite N approximation to each integral, using a evenly spaced grid in frequency space with $\omega_j = j\Delta\omega$ and $\Delta\omega = \frac{\pi}{N\Delta t}$. This gives

$$F_k(i\Delta t) \simeq F_k^{(i)} = \sum_{j=0}^{N} a_k^{(j)} \cos(ij\pi/N) + b_k^{(j)} \sin(ij\pi/N), \tag{5.106}$$

where we have defined

$$a_k^{(j)} = \begin{cases} G_k(\omega_j)\xi_a^{(j)}\sqrt{\Delta\omega} & \text{if } 0 < j < N \\ G_k(\omega_j)\xi_a^{(j)}\frac{\sqrt{\Delta\omega}}{2} & \text{if } j = 0 \text{ or } N \end{cases} \tag{5.107a}$$

$$b_k^{(j)} = \begin{cases} G_k(\omega_j)\xi_b^{(j)}\sqrt{\Delta\omega} & \text{if } 0 < j < N \\ G_k(\omega_j)\xi_b^{(j)}\frac{\sqrt{\Delta\omega}}{2} & \text{if } j = 0 \text{ or } N, \end{cases} \tag{5.107b}$$

in which $\{\xi_a^{(j)}\}$ and $\{\xi_b^{(j)}\}$ are independent sets of uncorrelated normal deviates with zero mean and unit variance. Since this has the form of a discrete half-complex-to-real Fourier transform it is straightforward to implement numerically. This will return a series of $2N$ time points, of which only the first N should be used since the average of the force-force correlation function will recur. Hence N must be at least as large as the number of time-steps. Note that one must also ensure that N is sufficiently large to avoid aliasing.

This scheme is very simple to implement and proved efficient enough for the present calculations. However, we note that if one were to consider a problem with a larger system dimension it might become advantageous to use a multivariate Ornstein-Uhlenbeck process, in a manner analogous to that adopted by Ceriotti *et al.*[224] in their construction of methods for solving GLEs.

6

Analytic continuation of Wolynes theory into the Marcus inverted regime

Contents

Summary

In this chapter we discuss the difficulty associated with applying Wolynes theory to the Marcus inverted regime. Wolynes theory is based on a saddle point approximation to the time integral of a reactive flux autocorrelation function in the non-adiabatic (golden-rule) limit. The dominant saddle point is on the imaginary-time axis at $t_{\mathrm{sp}} = i\lambda_{\mathrm{sp}}\hbar$, and provided λ_{sp} lies in the range $0 \leq \lambda_{\mathrm{sp}} \leq \beta$, it is straightforward to evaluate the rate constant using information obtained from an imaginary-time path-integral calculation. However, if λ_{sp} lies outside this range, as it does in the Marcus inverted regime, the path integral diverges. This has led to claims in the literature that Wolynes theory cannot describe the correct behaviour in the inverted regime. Here we show how the imaginary-time correlation function obtained from a path-integral calculation can be numerically analytically continued to $\lambda_{\mathrm{sp}} < 0$, and the continuation used to evaluate the rate in the inverted regime. Comparisons with exact golden-rule results for a spin-boson model and a more demanding (asymmetric and anharmonic) model of electronic pre-dissociation show that the theory it is just as accurate in the inverted regime as it is in the normal regime.

6.1 Introduction

Up to this point in the thesis we have focussed on the difficulty associated with calculating reaction rates between the golden-rule and adiabatic limits, however we now turn our attention to the non-adiabatic limit. We have seen that Wolynes theory[82] is very accurate in a wide range of physical regimes, and that it compares favourably to non-adiabatic generalisations of RPMD[23–34] in the calculation of golden-rule rates. Unfortunately, the path-integral implementation of Wolynes theory cannot be directly applied to the Marcus inverted regime.

The difficulty in applying Wolynes theory to the Marcus inverted regime stems from the fact that $\langle \boldsymbol{q}| \, e^{+\alpha \hat{H}_i} \, |\boldsymbol{q}'\rangle$ diverges for Hamiltonians $\hat{H}_i$ that are not bounded from above when $\mathrm{Re}\,\alpha > 0$. This means that for λ outside the range $[0,\beta]$ the path-integral representation of the correlation function,

$$c_{\mathrm{GR}}(t + i\lambda\hbar) = \int \mathrm{d}^f \boldsymbol{q} \int \mathrm{d}^f \boldsymbol{q}' \, \langle \boldsymbol{q}| \, e^{-(\beta-\lambda+it/\hbar)\hat{H}_0} \, |\boldsymbol{q}'\rangle \, \langle \boldsymbol{q}'| \, e^{-(\lambda-it/\hbar)(\hat{H}_1-\epsilon)} \, |\boldsymbol{q}\rangle \,, \tag{6.1}$$

does not converge. To see why this presents a problem in the Marcus inverted regime, note that the saddle point condition requires that $\beta F'_{\mathrm{GR}}(\lambda_{\mathrm{sp}}) = \epsilon$, and that for the spin-boson model the reorganisation energy Λ is defined as

$$\Lambda = \left\langle (V_1(\boldsymbol{q}_0) - V_0(\boldsymbol{q}_0)) \right\rangle_0 = \beta F'_{\mathrm{GR}}(0). \tag{6.2}$$

Hence, when $\epsilon > \Lambda$, corresponding to the Marcus inverted regime, it follows that $\lambda_{\mathrm{sp}} < 0$ and the quantities needed to evaluate the Wolynes rate cannot be directly calculated using the path-integral expressions given in Sec. 2.3.3. However, as the path-integral expression for $c_{\mathrm{GR}}(t + i\lambda\hbar)$ is a convergent representation of an analytic function for $0 \leq \lambda \leq \beta$, it follows that in principle it can be analytically continued from this line to any nonsingular point in the complex t plane. In the following we describe a simple numerical procedure by which the Wolynes theory rate can be calculated for λ_{sp} in the range $[0, \beta]$, and then discuss how this can be used to perform a simple numerical analytic continuation to calculate the Wolynes rate for λ_{sp} outside this strip.*

6.2 Numerical evaluation of Wolynes theory

We begin by writing the Wolynes rate in the form

$$k_{\mathrm{WT}} = \frac{\Delta^2}{\hbar} \sqrt{\frac{2\pi}{-\beta F''_{\mathrm{GR}}(\lambda_{\mathrm{sp}})}} e^{-\beta \Delta F_{\mathrm{GR}}(\lambda_{\mathrm{sp}}) + \lambda_{\mathrm{sp}} \epsilon}. \tag{6.3}$$

where we have eliminated the reactant partition function by defining $\Delta F_{\mathrm{GR}}(\lambda)$ to be the free energy at λ minus the free energy of the reactants

$$\Delta F_{\mathrm{GR}}(\lambda) = F_{\mathrm{GR}}(\lambda) - F_{\mathrm{GR}}(0). \tag{6.4}$$

It is clear from this that the required quantities are λ_{sp}, $\Delta F_{\mathrm{GR}}(\lambda_{\mathrm{sp}})$, and $F''_{\mathrm{GR}}(\lambda_{\mathrm{sp}})$. The method we propose begins by assuming a suitable (physically motivated) functional form $\Delta \tilde{F}_{\mathrm{GR}}(\lambda)$ for $\Delta F_{\mathrm{GR}}(\lambda)$, and least-squares fitting the parameters in this functional form to the path-integral data $\left\{F'_{\mathrm{GR}}(\lambda_l)\right\}$ and $\left\{F''_{\mathrm{GR}}(\lambda_l)\right\}$. The choice of a suitable functional

*Note that an alternative to this approach is to use the well-known maximum entropy analytic continuation method, this has been suggested before and used to directly calculate reaction rates in the normal regime (i.e. without making the Wolynes theory approximation) where it was found to suffer from quite large statistical errors.[225]

form will be discussed in detail for each of the model problems we shall consider below. For each required ϵ, we then solve $\beta\tilde{F}'_{\mathrm{GR}}(\lambda_{\mathrm{sp}}) = \epsilon$ for λ_{sp}, and use $\Delta\tilde{F}_{\mathrm{GR}}(\lambda_{\mathrm{sp}})$ and $\tilde{F}''_{\mathrm{GR}}(\lambda_{\mathrm{sp}})$ in Eq. 6.3 to calculate k_{WT}.

It is clear that this procedure will work when λ_{sp} lies in the range $0 \leq \lambda_{\mathrm{sp}} \leq \beta$, for two reasons. First, one can show, by expanding Eq. 2.104 in terms of the eigenvalues and eigenstates of $\hat{H}_0$ and $\hat{H}_1$, that $F''_{\mathrm{GR}}(\lambda) \leq 0$ for all $0 \leq \lambda \leq \beta$. This implies that $F'(\lambda)$ is a monotonically decreasing function of λ in this range and that the equation $\beta F'_{\mathrm{GR}}(\lambda_{\mathrm{sp}}) = \epsilon$ has a unique solution for λ_{sp}. Secondly, the use of $\Delta\tilde{F}_{\mathrm{GR}}(\lambda_{\mathrm{sp}})$ and $\tilde{F}''_{\mathrm{GR}}(\lambda_{\mathrm{sp}})$ in Eq. 6.3 is tantamount to interpolating the path-integral data to the saddle point when $0 \leq \lambda_{\mathrm{sp}} \leq \beta$, and interpolation is generally quite reliable.

It is less clear that the same procedure will work when $\lambda_{\mathrm{sp}} < 0$, as occurs in the Marcus inverted regime. One reason to suspect that it might work is that the exact $F_{\mathrm{GR}}(\lambda)$ for the spin-boson model [see Eq. 6.9 below] satisfies $F''_{\mathrm{GR}}(\lambda) < 0$ for all λ, and not just in the strip $0 \leq \lambda \leq \beta$. The solution of $\beta F'(\lambda_{\mathrm{sp}}) = \epsilon$ is therefore unique for this model in both the normal and inverted regimes. Another reason is that the physically-motivated functional form for $\Delta\tilde{F}_{\mathrm{GR}}(\lambda)$ for the second (asymmetric and anharmonic) model problem we shall consider below also satisfies $\tilde{F}''_{\mathrm{GR}}(\lambda) < 0$ for all $\lambda < \beta$, and so again gives a unique saddle point in both the normal and inverted regimes. But one cause for concern is that the use of $\Delta\tilde{F}_{\mathrm{GR}}(\lambda_{\mathrm{sp}})$ and $\tilde{F}''_{\mathrm{GR}}(\lambda_{\mathrm{sp}})$ in Eq. 6.3 is tantamount to *extrapolating* the path-integral data when $\lambda_{\mathrm{sp}} < 0$, and extrapolation is typically less reliable than interpolation.

This difference between the normal and inverted regimes is illustrated in Fig. 6.1, with data from the spin-boson model we shall consider in Sec. 6.3.1. Again the reorganisation energy Λ is defined as

$$\Lambda = \left\langle (V_1(\boldsymbol{q}_0) - V_0(\boldsymbol{q}_0)) \right\rangle_0 = \beta F'_{\mathrm{GR}}(0), \tag{6.5}$$

from which it is clear that the transition to the inverted regime at $\epsilon = \Lambda$ occurs when $\lambda_{\mathrm{sp}} = 0$. Defining the reorganisation energy of a general system in terms of the average energy gap, it is clear that this result carries over more generally to systems other than the spin-boson model. In the normal regime where $\epsilon < \Lambda$, the solution of $\beta F'_{\mathrm{GR}}(\lambda_{\mathrm{sp}}) = \epsilon$ is in the range between the dotted vertical lines in Fig. 6.1, where the path-integral data $\{F'_{\mathrm{GR}}(\lambda_l)\}$

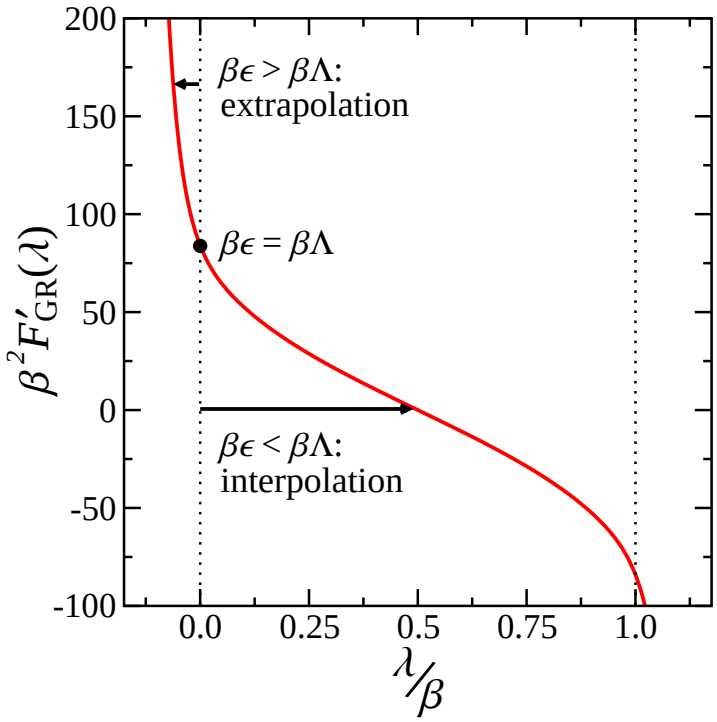

Figure 6.1: Solutions of $\beta F'_{GR}(\lambda_{sp}) = \epsilon$, for a spin-boson model. Systems in the normal regime, $\epsilon < \Lambda$, are solved by interpolation, while systems in the Marcus inverted regime $\epsilon > \Lambda$ require the fitted curve to be extrapolated. But it does not have to be extrapolated very far beyond the dotted lines within which the path-integral data is available, even when $\epsilon = 2\Lambda$.

and $\{F''_{GR}(\lambda_l)\}$ has been calculated and fitted to obtain the red curve. In the inverted regime where $\epsilon > \Lambda$, the curve has to be extrapolated to find the solution of $\beta F'(\lambda_{sp}) = \epsilon$. But fortunately, for this problem, which has physically reasonable parameters as a model for condensed phase electron transfer, the extrapolation does not extend very far beyond the region where the path-integral data is available, even deep in the inverted regime at $\epsilon = 2\Lambda$. This suggests that, while extrapolation can in general be problematic, it is on relatively safe ground in this case and can indeed be used in conjunction with Eq. 6.3 to calculate Wolynes rate constants in the Marcus inverted regime.

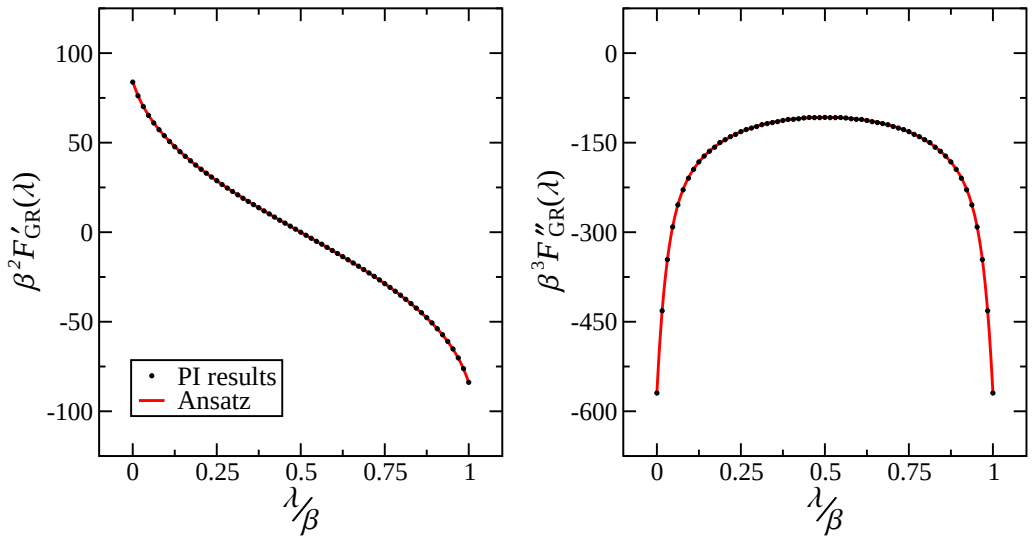

Figure 6.2: Comparison of the path-integral data for the spin-boson model with $\epsilon = 0$ and the fit obtained to it using Eq. 6.10 with $N = 3$. The standard errors in the path-integral results are smaller than the size of the dots.

6.3 Results and discussion

6.3.1 The spin-boson model

The first system we shall consider is the spin-boson model. Although very simple, consisting of two sets of displaced harmonic oscillators with a constant coupling (Δ), this model contains much of the important physics of condensed phase electron transfer and is commonly used in the study of real physical problems.[109–111] For clarity we give the diabatic potentials again here

$$V_0(\boldsymbol{q}) = \sum_{\nu=1}^{f} \frac{1}{2} m\omega_\nu^2 (q_\nu + \xi_\nu)^2, \tag{6.6}$$

and

$$V_1(\boldsymbol{q}) = \sum_{\nu=1}^{f} \frac{1}{2} m\omega_\nu^2 (q_\nu - \xi_\nu)^2, \tag{6.7}$$

with the spectral density defined as

$$J(\omega) = \frac{\pi}{2} \sum_{\nu=1}^{f} \frac{c_\nu^2}{m\omega_\nu} \delta(\omega - \omega_\nu) \tag{6.8}$$

where $c_\nu = m\omega_\nu^2 \xi_\nu$.

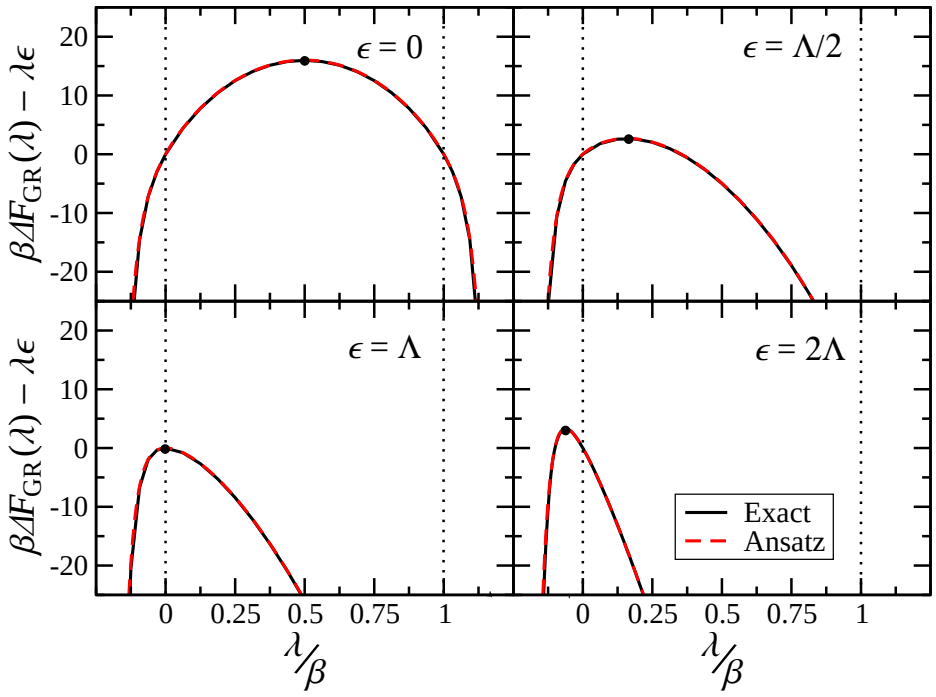

Figure 6.3: A comparison of the exact $\Delta F_{GR}(\lambda)$ [calculated using Eq. 6.9] and the result of fitting the ansatz in Eq. 6.10 to path-integral data, for the spin-boson model. The solid black circle in each panel shows the saddle point, which moves from $\lambda_{sp} = 0$ for symmetric electron transfer ($\epsilon = 0$) to $\lambda_{sp} = -\beta/2$ for activationless electron transfer ($\epsilon = \Lambda$) to $\lambda_{sp} < -\beta/2$ in the Marcus inverted regime ($\epsilon > \Lambda$).

Using the exact expression for $\Delta F_{GR}(\lambda)$ given in Eq. 3.49 it follows that in its discretised form, $\Delta F_{GR}(\lambda)$ is given exactly by

$$\Delta F_{GR}(\lambda) = \sum_{\nu=1}^{f} \frac{2c_\nu\xi_\nu}{\beta\hbar\omega_\nu}\left(\frac{\cosh\left(\frac{1}{2}\beta\hbar\omega_\nu\right) - \cosh\left((\lambda-\beta/2)\hbar\omega_\nu\right)}{\sinh\left(\frac{1}{2}\beta\hbar\omega_\nu\right)}\right). \tag{6.9}$$

This suggests an obvious ansatz for $\Delta\tilde{F}_{GR}(\lambda)$ of the form

$$\Delta\tilde{F}_{GR}(\lambda) = -\frac{\lambda}{\beta}\Delta F + \sum_{i=1}^{N}\frac{a_i}{b_i^2}\left(\cosh\left(\tfrac{1}{2}b_i\beta\right) - \cosh\left(b_i(\lambda-\beta/2)\right)\right), \tag{6.10}$$

in which $\{a_i\}$ and $\{b_i\}$ are real fitting parameters with $a_i > 0$, and we include the possibility of an intrinsic free energy difference between reactants and products $\Delta F = -\Delta F_{GR}(\beta)$. Eq. 6.10 is clearly capable of giving an accurate fit to the path-integral data when $N = f$. However, we expect that it will also give a good fit that can be extrapolated some way

outside $0 \leq \lambda \leq \beta$ for $N \ll f$. This is because the exact function contains information about the behaviour of $c_{\mathrm{GR}}(t)$ well away from the imaginary-time axis, which is not important for the evaluation of Eq. 6.3.

Given the success of the spin-boson model in describing real physical systems,[226] we expect that this ansatz will also work well for other "symmetric" problems, i.e. those for which $-\beta \Delta F_{\mathrm{GR}}(\lambda) + \lambda\epsilon$ is symmetric about $\lambda = \beta/2$ when $\epsilon = -\Delta F$. Systems which do not have this property will require an extension of the ansatz, and this is discussed in Sec. 6.3.2.

To test the method described in Sec. 6.2, we consider a spin-boson model with Debye spectral density

$$J(\omega) = \frac{\Lambda}{2} \frac{\omega\omega_c}{\omega^2 + \omega_c^2}, \tag{6.11}$$

with reorganisation energy $\Lambda = 50\,\mathrm{kcal/mol}$ and characteristic frequency $\omega_c = 500\,\mathrm{cm}^{-1}$, at 300 K. These parameters are similar to those used in several earlier studies and they were chosen here because they give a significant quantum mechanical effect on the rate constant: they lead to a rate constant for symmetric electron transfer ($\epsilon = 0$) around two orders of magnitude larger than the Marcus theory prediction, which is at the upper limit of earlier estimates of the quantum enhancement for the ferrous-ferric system in aqueous solution.[84,111]

The spectral density was discretised in the standard way, with[227]

$$\omega_\nu = \omega_c \tan \frac{(\nu - \frac{1}{2})\pi}{2f}, \tag{6.12}$$

and

$$c_\nu = \sqrt{\frac{m\Lambda}{2f}}\omega_\nu, \tag{6.13}$$

and

$$\xi_\nu = \sqrt{\frac{\Lambda}{2mf}}\frac{1}{\omega_\nu}, \tag{6.14}$$

for $\nu = 1, \ldots, f$. (Note that since neither ω_ν nor $c_\nu\xi_\nu$ in Eq. 6.9 depends on m this is a redundant parameter that does not need to be specified to define the problem.) It was found that $f = 12$ degrees of freedom were sufficient to converge the exact rate to graphical accuracy for all ϵ considered.

The parameters a_i and b_i were determined by simultaneously fitting $\{F'_{\mathrm{GR}}(\lambda_l)\}$ and $\{F''_{\mathrm{GR}}(\lambda_l)\}$ to the ansatz in Eq. 6.10. This was done by minimising the objective function

$$L(\mathbf{a},\mathbf{b}) = \frac{\sum_l \left[\tilde{F}'_{\mathrm{GR}}(\lambda_l) - F'_{\mathrm{GR}}(\lambda_l)\right]^2}{2\sum_l \left[\bar{F}'_{\mathrm{GR}} - F'_{\mathrm{GR}}(\lambda_l)\right]^2} + \frac{\sum_l \left[\tilde{F}''_{\mathrm{GR}}(\lambda_l) - F''_{\mathrm{GR}}(\lambda_l)\right]^2}{2\sum_l \left[\bar{F}''_{\mathrm{GR}} - F''_{\mathrm{GR}}(\lambda_l)\right]^2}, \tag{6.15}$$

where $\bar{F}'_{\mathrm{GR}} = \frac{1}{N_l}\sum_l F'_{\mathrm{GR}}(\lambda_l)$ and $\bar{F}''_{\mathrm{GR}} = \frac{1}{N_l}\sum_l F''_{\mathrm{GR}}(\lambda_l)$ with N_l being the number of l values at which the derivatives were calculated.

As this is a non-linear optimisation problem there may be many local minima. We therefore used a global optimisation algorithm[228,229] on the domain defined by $0 \leq a_i \leq |F''_{\mathrm{GR}}(\beta/2)|$ and $0 < b_i \leq \hbar\omega_{\max}$, with $\omega_{\max} = 22000\,\mathrm{cm}^{-1}$. The path-integral results were calculated using path-integral molecular dynamics with the PILE thermostat[223] at 65 equally spaced points in the interval $0 \leq \lambda_l \leq \beta$, with $n = 256$ path-integral beads. We found that $N = 3$, corresponding to 6 free parameters, was sufficient to fit the results to within their statistical error bars. Fig. 6.2 shows the first and second derivatives of $\Delta F_{\mathrm{GR}}(\lambda)$ along with the corresponding fit obtained for $N = 3$, for which $\beta^3\mathbf{a} = (1.4205\times10^{-5}, 1.0787\times10^{1}, 9.6756\times10^{1})$ and $\beta\mathbf{b} = (3.4972\times10^{1}, 7.0368, 9.5562\times10^{-1})$.

As $\Delta F_{\mathrm{GR}}(\lambda)$ is known analytically for this problem we can compare the exact curve to the result of fitting to the path-integral data. Fig. 6.3 shows $\Delta\tilde{F}_{\mathrm{GR}}(\lambda) - \epsilon\lambda/\beta$ (with the parameters given above) and the exact $\Delta F_{\mathrm{GR}}(\lambda) - \epsilon\lambda/\beta$ for a variety of driving forces, ranging from the normal regime to activationless electron transfer and on into the Marcus inverted regime. The agreement is clearly excellent even for $\epsilon = 2\Lambda$, deep inside the inverted regime. This justifies the assertion that the behaviour on the imaginary axis can be captured by including only a small number of terms $N \ll f$ in Eq. 6.10.

Having found the parameters in $\Delta\tilde{F}_{\mathrm{GR}}(\lambda)$, we are now in a position to evaluate Eq. 6.3 for arbitrary ϵ, as described in Sec. 6.2. Fig. 6.4 compares the exact rate constants to those calculated using Eq. 6.3 with $\Delta F_{\mathrm{GR}}(\lambda)$ replaced by $\Delta\tilde{F}_{\mathrm{GR}}(\lambda)$. The exact rate constants were obtained by numerically integrating the exact spin-boson rate in given in Eq. 2.217. For comparison the rate constants predicted by Marcus theory (Eq. 2.114), which is exact in the classical ($\beta \to 0$) limit for this problem, are also included. Since all the rate constants in Fig. 6.4 are given relative to the classical rate at $\epsilon = 0$ we do not need to specify the value of Δ. However, for the results to be accurate Δ must be small enough for

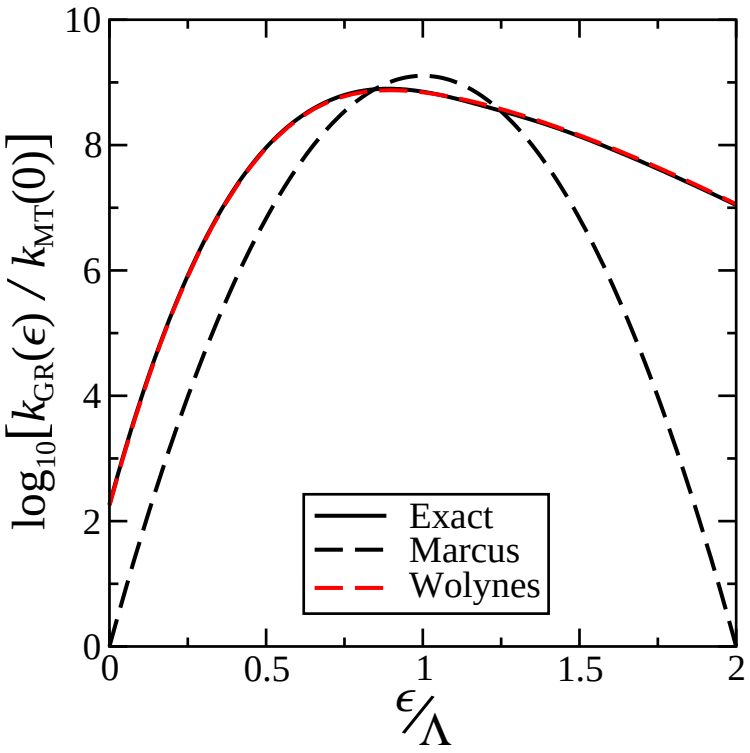

Figure 6.4: Rate constants for the spin-boson model, relative to the Marcus theory result for $\epsilon = 0$. The exact results were calculated using Eq. 2.217 and the Wolynes results were calculated using Eq. 6.3 with the fitted $\Delta\tilde{F}_{GR}(\lambda)$.

the golden rule to apply. It is apparent that Wolynes theory gives excellent agreement with the exact rate for all physically relevant values of ϵ. Note that this is a situation in which nuclear quantum effects are vitally important: the quantum mechanical rate is 7 orders of magnitude larger than the classical rate at $\epsilon = 2\Lambda$. The success of the ansatz in Eq. 6.10 for this problem is striking and suggests that the same approach is likely to work for a wide variety of "symmetric" condensed phase electron transfer reactions. The extension of the approach to more general (asymmetric and anharmonic) problems is discussed next.

6.3.2 An electronic pre-dissociation model

The second system we shall consider is a one-dimensional model of electronic pre-dissociation that was introduced by Richardson and Thoss to illustrate the oscillatory nature of non-adiabatic reactive flux correlation functions.[230] Analogous to a condensed

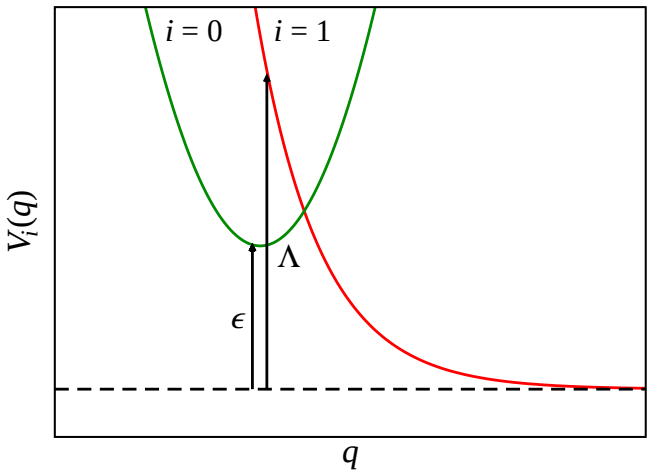

Figure 6.5: The diabatic potential energy curves for the one-dimensional electronic predissociation model, along with the driving force ϵ and reorganisation energy Λ.

phase problem, this system has a continuum of product states, and it provides a useful test case because the exact non-adiabatic rate constant can again be calculated for comparison (in this case using quantum scattering theory).

The diabatic potential energy curves of the model are

$$V_0(q) = \frac{1}{2}m\omega^2 q^2, \tag{6.16}$$

and

$$V_1(q) = De^{-2\alpha(q-\xi)}, \tag{6.17}$$

in which we shall use the same parameters as Richardson and Thoss:[230] $m = 1, \omega = 1, D = 2, \alpha = 0.2, \xi = 5, \beta = 3$, and $\hbar = 1$. Note that for this problem the reorganisation energy as defined (at $\epsilon = 0$) in Eq. 6.5 is temperature-dependent, because although $V_0(q)$ is still harmonic $V_1(q) - V_0(q)$ is no longer a linear function of q. When presenting our results as a function of ϵ/Λ we shall therefore simply define Λ as $\Lambda = De^{2\alpha\xi}$, as illustrated in Fig. 6.5.

This model presents two obvious challenges which will require modifications of the ansatz for $\Delta\tilde{F}_{\mathrm{GR}}(\lambda)$ in Eq. 6.10. Firstly the system is not symmetric and secondly, since $V_1(q)$ is unbounded, the product partition function is infinite and the imaginary-time correlation function $c_{\mathrm{GR}}(i\lambda\hbar)$ diverges at $\lambda = \beta$. Assuming a power law divergence,

$$c_{\mathrm{GR}}(i\lambda\hbar) \sim A(\beta - \lambda)^{-\gamma} \text{ as } \lambda \to \beta \tag{6.18}$$

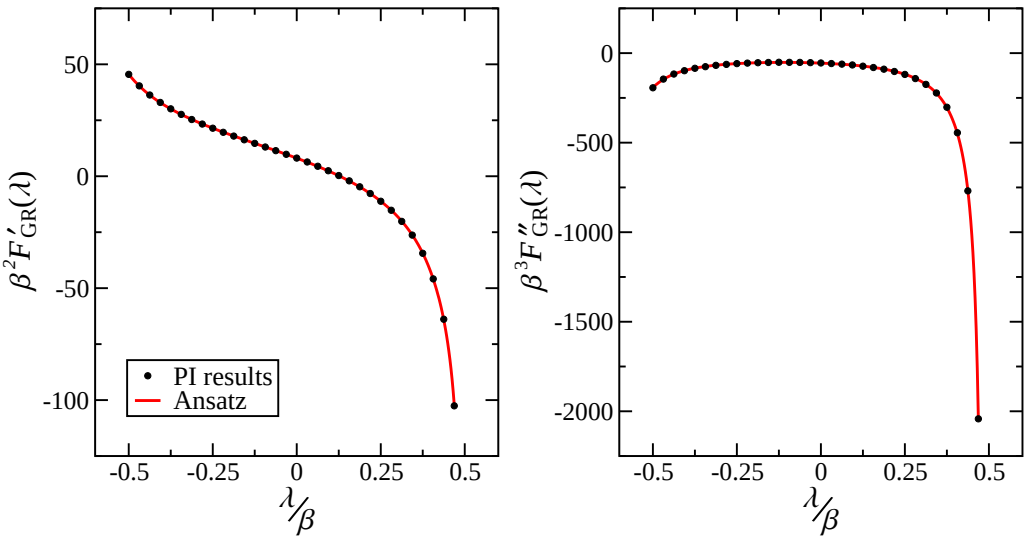

Figure 6.6: Comparison of the path-integral data for the electronic pre-dissociation model with $\epsilon = 0$ and the fit obtained to it using Eq. 6.20 with $N = 3$. The standard errors in the path-integral results are smaller than the size of the dots.

for some positive constant γ, it follows from the definition of $F_{GR}(\lambda)$ that

$$F_{GR}(\lambda) \sim \frac{\gamma}{\beta} \ln(\beta - \lambda) \text{ as } \lambda \to \beta. \tag{6.19}$$

On the basis of these observations, we arrive at the following generalisation of Eq. 6.10:

$$\Delta\tilde{F}_{GR}(\lambda) = d \ln\left(1 - \frac{\lambda}{\beta}\right) - \frac{\lambda}{\beta}\Delta F + \sum_{i=1}^{N} \frac{a_i}{b_i^2}\left(\cosh\left(b_i\left[\tfrac{1}{2}\beta + c_i\right]\right) - \cosh\left(b_i[\lambda - \tfrac{1}{2}\beta - c_i]\right)\right). \tag{6.20}$$

Here again $a_i > 0$, and in addition to the logarithmic term we have accounted for asymmetry in $\Delta F_{GR}(\lambda)$ by adding the additional parameters c_i which shift the origins of the hyperbolic cosines.

The parameters were again determined by minimising the objective function

$$L(\mathbf{a}, \mathbf{b}, \mathbf{c}, d) = \frac{\sum_j \left[\tilde{F}'_{GR}(\lambda_j) - F'_{GR}(\lambda_j)\right]^2}{2\sum_j \left[\bar{F}'_{GR} - F'_{GR}(\lambda_j)\right]^2} + \frac{\sum_j \left[\tilde{F}''_{GR}(\lambda_j) - F''_{GR}(\lambda_j)\right]^2}{2\sum_j \left[\bar{F}''_{GR} - F''_{GR}(\lambda_j)\right]^2}, \tag{6.21}$$

with the same non-linear optimisation algorithm.[228,229] The search was performed on the domain defined by $0 \le a_i \le |F''_{GR}(\beta/2)|$, $0 < b_i \le \hbar\omega_{max}$ (with $\omega_{max} = 10$), $-\beta < c_i < \beta$,

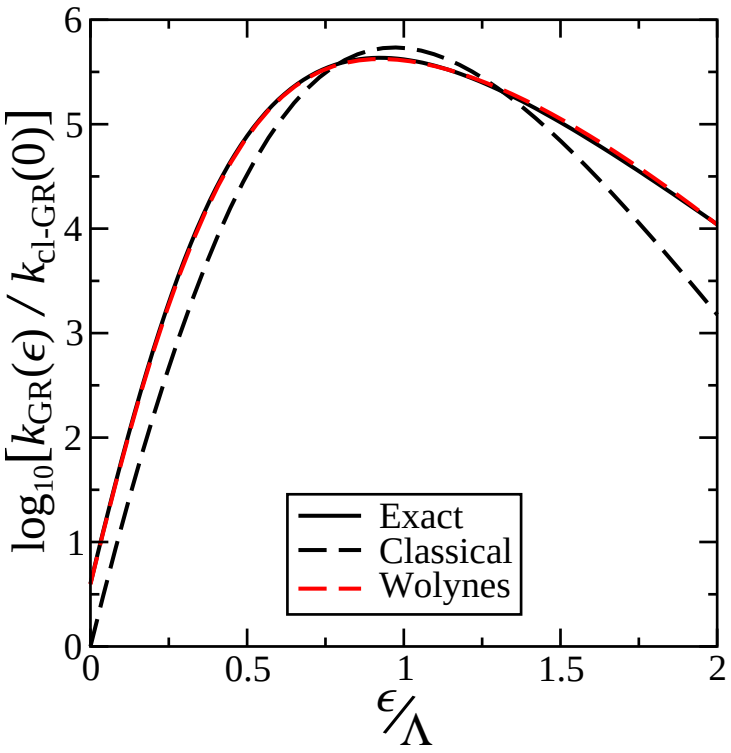

Figure 6.7: Rate constants for the electronic pre-dissociation model, relative to the classical golden-rule rate at $\epsilon = 0$. The exact results were calculated using Eq. 6.22 and the Wolynes results were calculated using Eq. 6.20. The code used for the exact rate calculations was written by Prof. David E. Manolopoulos.

and $0 \leq d \leq 15/\beta$. The path-integral results were calculated in the same way as for the spin-boson model at 32 equally spaced points in the interval $0 \leq \lambda_l \leq 31\beta/32$, with $n = 256$ path-integral beads. $\lambda_n = \beta$ was not included because $\Delta F_{GR}(\beta)$ is undefined.

We found that $N = 3$ in Eq. 6.20 was again sufficient to fit the path-integral results to within their statistical error bars. Fig. 6.6 shows the first and second derivatives of $\Delta F_{GR}(\lambda)$ along with the corresponding fit, for which $\beta^3\mathbf{a} = (1.8281 \times 10^1, 3.4729 \times 10^{-2}, 2.8976 \times 10^1)$, $\beta\mathbf{b} = (8.4376 \times 10^{-3}, 1.9063 \times 10^1, 4.6062)$, $\mathbf{c}/\beta = (7.4223 \times 10^{-1}, -6.1285 \times 10^{-2}, -8.9571 \times 10^{-2})$ and $\beta d = 1.3762$.

The exact golden-rule rate for this problem was also calculated for comparison. This was done by using a Lobatto shape function discrete variable representation[231] (code

written by Prof. David E. Manolopoulos) to calculate

$$kQ_r = -\frac{2\Delta^2}{\hbar} \sum_\nu e^{-\beta E_\nu} \operatorname{Im} \langle \nu | \hat{G}_1^+(E_\nu) | \nu \rangle \,, \tag{6.22}$$

and

$$Q_r = \sum_\nu e^{-\beta E_\nu}, \tag{6.23}$$

where

$$\hat{H}_0 | \nu \rangle = E_\nu | \nu \rangle \,, \tag{6.24}$$

and

$$\hat{G}_1^+(E_\nu) = \lim_{\eta \to 0_+} (E_\nu + i\eta - \hat{H}_1 + \epsilon)^{-1}. \tag{6.25}$$

For this problem the appropriate classical limit of the rate constant is given by the classical golden rule, which here reduces to

$$k_{\text{cl-GR}} = \frac{\Delta^2}{\hbar} \sqrt{2\pi\beta m\omega^2} \frac{e^{-\beta V_0(q^\ddagger)}}{|V_0'(q^\ddagger) - V_1'(q^\ddagger)|}, \tag{6.26}$$

in which $q^\ddagger$ is defined by the equation $V_0(q^\ddagger) = V_1(q^\ddagger) - \epsilon$.

Fig. 6.7 compares the exact, Wolynes and classical golden-rule rate constants for this problem relative to $k_{\text{cl-GR}}(\epsilon = 0)$. Once again Wolynes theory gives excellent agreement with the exact rate well into the Marcus inverted regime. The quantum mechanical enhancement of the rate is not as pronounced as it was for the spin-boson model considered in Sec. 6.3.1, but it is still almost an order of magnitude at $\epsilon = 2\Lambda$. And this problem is more challenging in many other respects, including its asymmetry, its anharmonicity, and the divergent behaviour of its free energy as $\lambda \to \beta$. We therefore regard the results in Fig. 6.7 to be just as encouraging for future applications of the theory as those in Fig. 6.4.

6.4 Conclusions

In this chapter, we have established that an appropriate implementation of Wolynes theory[82] works equally well in both the normal and inverted electron transfer regimes. The only difference between the two regimes is that, whereas the treatment of the normal

regime involves the interpolation of imaginary-time path-integral data, the treatment of the inverted regime involves its extrapolation. While extrapolation can often be problematic, this is not the case in the present context, because one does not have to extrapolate very far along the imaginary-time axis to reach the saddle point that determines the Wolynes rate. This is certainly true for both of the model problems we have considered – a typical spin-boson problem and a one-dimensional model of electronic pre-dissociation – and we would expect it to be true more generally.

7

Breakdown of Wolynes theory - Alternative path-integral methods

Contents

Summary

In this chapter we present a simple method for the calculation of reaction rates in the golden-rule limit, which accurately captures the effects of tunnelling and zero-point energy. The method is based on a modification of the recently proposed golden-rule quantum transition state theory (GR-QTST) of Thapa, Fang and Richardson. We show that whilst GR-QTST is not size consistent, leading to the possibility of unbounded errors in the rate, our modified method has no such issue and so can be reliably applied to condensed phase systems. Both methods involve path-integral sampling in a constrained ensemble; the two methods differ, however, in the choice of constraint functional. We demonstrate numerically that our modified method is as accurate as GR-QTST for the one-dimensional model considered by Thapa and coworkers. We then study a multi-dimensional spin-boson model, for which our method accurately predicts the true quantum rate, while GR-QTST breaks down with an increasing number of boson modes in the discretisation of the spectral density. Our method is able to accurately predict reaction rates in the Marcus inverted regime, without the need for the analytic continuation required by Wolynes theory.

7.1 Introduction

Despite its success there are several remaining issues with Wolynes theory. The first is that, although it recovers Marcus theory in the high temperature limit for the spin-boson model, it does not recover the correct (classical golden rule) expression for the high-temperature rate of an anharmonic reaction.[170] The second issue, which we met in the previous chapter, is that the path-integral representation of the Wolynes rate is only valid when λ_{sp} lies in the interval $[0,\beta]$. In the Marcus inverted regime, where the driving force is larger than the reorganisation energy, it turns out that $\lambda_{\mathrm{sp}} < 0$, and hence Wolynes theory cannot be directly applied to reactions in this regime. We have shown, in the previous chapter, that it is possible to evaluate the Wolynes rate even when $\lambda_{\mathrm{sp}} < 0$, by analytically continuing along the imaginary-time axis. However, it would clearly be desirable to have a method which avoided the need for this kind of numerical analytic continuation. The third issue, which has recently been pointed out by Richardson

and coworkers, is that for systems with multiple transition states, Wolynes theory can significantly overestimate the rate.[232,233] This is again because the Wolynes rate must be evaluated at $i\lambda_{sp}\hbar$. For systems with only one transition state, evaluating the Wolynes expression away from the correct value of λ_{sp} leads to a significant overestimation of the rate. Hence when applied to systems with two or more transition states, which when treated separately would have different values of λ_{sp}, Wolynes theory is forced to take an intermediate value which overestimates the rate via both channels.[233]

In the high temperature limit, one can simply use the classical golden-rule expression for the rate.[141,142] This is independent of the imaginary time $i\lambda\hbar$ at which it is evaluated, and can therefore be used both in the inverted regime and for systems with multiple transition states. One might hope that it would be possible to find a quantum generalisation of the classical golden-rule expression that is applicable to lower temperatures and remains independent of the imaginary time at which it is evaluated. Recently Thapa, Fang and Richardson have suggested such a generalisation, which they call golden-rule quantum transition state theory (GR-QTST).[232,233] This is based on introducing an energy matching constraint which is satisfied by the semiclassical instanton. Unlike Wolynes theory, GR-QTST correctly captures the classical golden-rule rate in the high temperature limit for all systems (with harmonic or anharmonic potentials). For a one dimensional system of linear crossing potentials, it is also exact at all temperatures and is independent of the imaginary time $i\lambda\hbar$ at which it is evaluated. Thapa *et al.*[232] demonstrated that for other one dimensional problems the GR-QTST rate remains approximately independent of λ, which enables the calculation of rates in the Marcus inverted regime without the need for analytic continuation (when $\lambda_{sp} < 0$ the GR-QTST rate can be calculated using $\lambda = 0$.)

Despite these attractive features, GR-QTST has a major drawback which limits its applicability to multidimensional problems: it is not size consistent. The multidimensional generalisation of GR-QTST is affected by adding additional degrees of freedom, even when they are not coupled to the degrees of freedom that participate in the reaction. For a small but finite number of uncoupled degrees of freedom this makes the method more sensitive to the value of λ at which the rate is evaluated, which poses problems when $\lambda = 0$ is used to calculate rates in the Marcus inverted regime. However, for

a realistic condensed phase system, the problem is more severe: the calculation can become dominated by the physically unimportant degrees of freedom, leading to an unbounded error in the rate. This means for example that the results do not converge for a spin-boson model as one increases the number of bath modes in the discretisation of the spectral density, as we shall show below.

In this chapter we suggest a modified method which fixes the size consistency problem. Unlike GR-QTST our expression for the rate only involves the diabatic energy gap and projections onto its gradient. This means that adding uncoupled modes does not affect our approximation to the rate. The modified method retains the desirable features of GR-QTST, being exact in the high temperature limit and in one dimension for two linear crossing potentials. For want of a better name we will therefore refer to the method as the "Linear Golden-Rule" (LGR) approximation. We shall show that this method gives rates that are approximately independent of λ, and hence that it is able to calculate rates deep in the inverted regime (without any analytic continuation). Although LGR is very similar to GR-QTST, we do not base our constraint on an energy matching condition. As such the two methods are not equivalent even in one dimension, except in the high temperature and linear crossing cases. This means that the LGR approximation does not have the same connection to the semiclassical instanton[170,195,196] as GR-QTST, and so it may become less accurate at very low temperatures. This does not however appear to be the case for the problems studied here, which we believe to be representative of typical chemically relevant regimes.

Sec. 7.2 summarises existing theory. Sec. 7.3 introduces the GR-QTST approximation, and elaborates on its size inconsistency. Sec. 7.4 introduces the LGR approximation, and explains how it solves the size consistency problem. Sec. 7.5 discusses the numerical implementation of the LGR. Sec. 7.6 presents example applications to two model problems for which exact results are available for comparison: a one dimensional model of electronic pre-dissociation and a multidimensional spin-boson model. Sec. 7.7 concludes the chapter.

7.2 Background theory

7.2.1 Exact theory

In order to understand the approximate theories we shall discuss below it is helpful to consider the exact golden-rule rate in terms of the distribution $\rho_\lambda(E)$. As such we recap this form of the exact golden-rule rate, and for simplicity we continue to focus on systems for which $\Delta(\boldsymbol{q}) = \Delta$ is a constant, briefly discussing the generalisation beyond this in Appendix 7.A. As was shown in Sec. 2.2.3 the exact golden-rule rate can be written in the form,

$$k_{\mathrm{GR}}(\epsilon) = \frac{2\pi\Delta^2}{Q_r\hbar}\rho_\lambda(\epsilon)e^{-\beta F_{\mathrm{GR}}(\lambda)+\lambda\epsilon}, \tag{7.1}$$

where $\rho_\lambda(E)$ is a probability distribution given by the Fourier transform

$$\rho_\lambda(E) = \frac{1}{2\pi\hbar}\int_{-\infty}^{\infty}\left\langle e^{-i\hat{H}_0 t/\hbar}e^{+i\hat{H}_1 t/\hbar}\right\rangle_\lambda e^{-iEt/\hbar}\mathrm{d}t, \tag{7.2}$$

with

$$\left\langle e^{-i\hat{H}_0 t/\hbar}e^{+i\hat{H}_1 t/\hbar}\right\rangle_\lambda = \frac{c_\lambda(t)}{c_\lambda(0)}, \tag{7.3}$$

and the Boltzmann factor can be written in terms of a path-integral as

$$e^{-\beta F_{\mathrm{GR}}(\lambda)} = \oint \mathcal{D}\boldsymbol{q}(\tau)e^{-S^{(\lambda)}[\boldsymbol{q}(\tau)]/\hbar}. \tag{7.4}$$

Importantly we stress that the exact rate is independent of the shift in imaginary time $i\lambda\hbar$. This is an important property of the exact rate and as we shall see later it is a desirable property for any approximate theory. Note also that knowledge of the distribution, $\rho_\lambda(E)$ in Eq. 7.1, calculated with $\epsilon = 0$, allows one to calculate the rate at any other driving force.

7.2.2 Wolynes theory

The Wolynes theory approximation to the non-adiabatic rate constant is normally thought of as a steepest descent approximation to the integral of $c_{\mathrm{GR}}(t + i\lambda\hbar)$ in Eq. 2.89. This gives[82]

$$k_{\mathrm{WT}} = \frac{\Delta^2}{Q_r\hbar}\sqrt{\frac{2\pi}{-\beta F''(\lambda_{\mathrm{sp}})}}e^{-\beta F(\lambda_{\mathrm{sp}})+\lambda_{\mathrm{sp}}\epsilon}, \tag{7.5}$$

in which λ_{sp} is given by the saddle point condition

$$\beta F'(\lambda_{\mathrm{sp}}) = \epsilon. \tag{7.6}$$

We note here that Wolynes theory can equivalently be thought of as a Gaussian approximation to the distribution $\rho_\lambda(E)$ in Eq. 7.2 that is constructed so as to reproduce the 0th, 1st and 2nd moments of the exact distribution:

$$\rho_{\mathrm{WT},\lambda}(E) = \sqrt{\frac{1}{2\pi\mu_{2,\lambda}}}\exp\left(-\frac{(E-\mu_{1,\lambda})^2}{2\mu_{2,\lambda}}\right), \tag{7.7}$$

where

$$\mu_{1,\lambda} = \int_{-\infty}^{\infty} E\rho_\lambda(E)\,\mathrm{d}E = \beta F'_{\mathrm{GR}}(\lambda) \tag{7.8}$$

and

$$\mu_{2,\lambda} = \int_{-\infty}^{\infty} (E^2-\mu_{1,\lambda}^2)\rho_\lambda(E)\,\mathrm{d}E = -\beta F''(\lambda). \tag{7.9}$$

Viewed from this perspective we see that the saddle point condition is equivalent to choosing the distribution which is peaked at the driving force, ϵ, which (provided that the exact distribution is also singly peaked) is likely to be where the approximation is most accurate.

Although Wolynes theory is very accurate for many systems, including the spin-boson model, recent work by Richardson and co-workers has demonstrated that it can breakdown for systems with multiple transition states.[233] This can be understood by considering a reaction which can be separated into two distinct reaction pathways a and b, such that the rate can be written in terms of a contribution from each as,

$$k_{\mathrm{GR}}(\epsilon) = k_{a,\mathrm{GR}}(\epsilon) + k_{b,\mathrm{GR}}(\epsilon). \tag{7.10}$$

For such a system it follows that the distribution can be written as,

$$\rho_\lambda(E) = \rho_{a,\lambda}(E) + \rho_{b,\lambda}(E), \tag{7.11}$$

and hence approximating $\rho_\lambda(E)$ as a single Gaussian may become very inaccurate, leading to significant overestimation of the rate. An important corollary of this is that the correlation function at λ_{sp} is also poorly approximated by a Gaussian. Since Wolynes theory is exact at short time, this means that the exact correlation function, $c_{\mathrm{GR}}(t + i\lambda_{\mathrm{sp}}\hbar)$, typically exhibits significant oscillatory behaviour leading to a large reduction in the rate compared to using the short time approximation.

7.2.3 High temperature limit

As discussed in Sec. 2.2.3, in the high-temperature limit the exact rate tends to the well-known classical golden-rule rate[141,142]

$$k_{\text{cl-GR}}(\epsilon) = \frac{2\pi\Delta^2}{Q_r\hbar}\left\langle\delta(V_-(\boldsymbol{q})+\epsilon)\right\rangle_{\text{cl},\lambda} e^{-\beta F_{\text{cl-GR}}(\lambda)+\lambda\epsilon}, \tag{7.12}$$

with

$$e^{-\beta F_{\text{cl-GR}}(\lambda)} = \frac{1}{(2\pi\hbar)^f}\int \mathrm{d}^f\boldsymbol{p}\int \mathrm{d}^f\boldsymbol{q}\, e^{-(\beta-\lambda)H_0(\boldsymbol{p},\boldsymbol{q})-\lambda H_1(\boldsymbol{p},\boldsymbol{q})}, \tag{7.13}$$

and where $\rho_{\text{cl},\lambda}(E) = \left\langle\delta(V_-(\boldsymbol{q})+E)\right\rangle_{\text{cl},\lambda}$ is the classical limit of the distribution, $\rho_\lambda(E)$, which is the probability density for the system to be found with $V_-(\boldsymbol{q})+\epsilon = 0$. As it is just the high temperature limit of the exact rate, it is clear that the classical golden-rule rate is also entirely *independent* of the λ at which it is evaluated, (although Eq. 7.13 may not be convergent for λ outside the interval $[0,\beta]$). This is in stark contrast to the Wolynes rate, which not only fails to give the correct result in the high-temperature limit but must still be evaluated at λ_{sp} in this limit. This also means that classically there is no issue with the evaluation of rates in the inverted regime, where one can simply set $\lambda = 0$ in Eq. 7.12. It would clearly be desirable to find a path-integral generalisation of this equation that was capable of accurately capturing the effects of tunnelling and zero-point energy on the rate.

7.3 GR-QTST

7.3.1 Formulation

Recently Thapa, Fang and Richardson have attempted to do precisely this. They have proposed a new method (GR-QTST) for calculating golden-rule rates, which like Wolynes theory involves path-integral sampling.[232,233] They argued that the rate could be approximated by introducing an energy constraint into Eq. 7.4, which would be exactly satisfied by the semiclassical instanton.[170,195,196] Following this logic, for a system with no external bias $\epsilon = 0$, they suggested the following approximation to the rate[232]

$$k_{\text{GR-QTST}}(\lambda) = \frac{2\pi\Delta^2}{Q_r\hbar}\left\langle\delta\left(\frac{2}{3}\mathcal{E}_-^{(\lambda)}[\boldsymbol{q}(\tau)]\right)\right\rangle_\lambda e^{-\beta F_{\text{GR}}(\lambda)}, \tag{7.14}$$

where the constraint functional is given by

$$\mathcal{E}_{-}^{(\lambda)}[\boldsymbol{q}(\tau)] = \mathcal{T}_{-}^{(\lambda)}[\boldsymbol{q}(\tau)] + \mathcal{V}_{-}^{(\lambda)}[\boldsymbol{q}(\tau)]. \tag{7.15}$$

Here the first term corresponds to the difference of the virial estimator for the kinetic energy,[12,234] averaged around each segment of the ring-polymer

$$\mathcal{T}_{-}^{(\lambda)}[\boldsymbol{q}(\tau)] = \mathcal{T}_{0}^{(\lambda)}[\boldsymbol{q}(\tau)] - \mathcal{T}_{1}^{(\lambda)}[\boldsymbol{q}(\tau)] \tag{7.16}$$

with

$$\mathcal{T}_{0}^{(\lambda)}[\boldsymbol{q}(\tau)] = \int_{\lambda\hbar}^{\beta\hbar} \frac{\nabla V_0(\boldsymbol{q}(\tau)) \cdot (\boldsymbol{q}(\tau) - \boldsymbol{s}(\boldsymbol{q}^+))}{2(\beta-\lambda)\hbar} \mathrm{d}\tau \tag{7.17a}$$

$$\mathcal{T}_{1}^{(\lambda)}[\boldsymbol{q}(\tau)] = \int_{0}^{\lambda\hbar} \frac{\nabla V_1(\boldsymbol{q}(\tau)) \cdot (\boldsymbol{q}(\tau) - \boldsymbol{s}(\boldsymbol{q}^+))}{2\lambda\hbar} \mathrm{d}\tau \tag{7.17b}$$

and

$$\boldsymbol{s}(\boldsymbol{q}^+) = \boldsymbol{q}^+ - \frac{V_-(\boldsymbol{q}^+)\nabla V_-(\boldsymbol{q}^+)}{|\nabla V_-(\boldsymbol{q}^+)|^2} \tag{7.18}$$

with $\boldsymbol{q}^+ = \frac{1}{2}(\boldsymbol{q}(0) + \boldsymbol{q}(\lambda\hbar))$. The second term in Eq. 7.15 corresponds to the difference between the potential energies averaged around the two segments

$$\mathcal{V}_{-}^{(\lambda)}[\boldsymbol{q}(\tau)] = \mathcal{V}_{0}^{(\lambda)}[\boldsymbol{q}(\tau)] - \mathcal{V}_{1}^{(\lambda)}[\boldsymbol{q}(\tau)] \tag{7.19}$$

where

$$\mathcal{V}_{0}^{(\lambda)}[\boldsymbol{q}(\tau)] = \int_{\lambda\hbar}^{\beta\hbar} \frac{V_0(\boldsymbol{q}(\tau))}{(\beta-\lambda)\hbar} \mathrm{d}\tau \tag{7.20a}$$

$$\mathcal{V}_{1}^{(\lambda)}[\boldsymbol{q}(\tau)] = \int_{0}^{\lambda\hbar} \frac{V_1(\boldsymbol{q}(\tau))}{\lambda\hbar} \mathrm{d}\tau. \tag{7.20b}$$

Comparison with Eq. 7.1 allows us to identify the approximation that GR-QTST is making to $\rho_\lambda(E)$ as

$$\rho_{\text{GR-QTST},\lambda}(E) = \left\langle \delta\left(\frac{2}{3}\mathcal{E}_{-}^{(\lambda)}[\boldsymbol{q}(\tau)] + E\mathcal{G}^{(\lambda)}[\boldsymbol{q}(\tau)]\right)\right\rangle_{\lambda} \tag{7.21}$$

where

$$\mathcal{G}^{(\lambda)}[\boldsymbol{q}(\tau)] = \frac{2}{3} + \frac{\mathcal{G}_{0}^{(\lambda)}[\boldsymbol{q}(\tau)] - \mathcal{G}_{1}^{(\lambda)}[\boldsymbol{q}(\tau)]}{3} \tag{7.22}$$

with

$$\mathcal{G}_0^{(\lambda)}[\boldsymbol{q}(\tau)] = \int_{\lambda\hbar}^{\beta\hbar} \frac{\nabla V_0(\boldsymbol{q}(\tau)) \cdot \nabla V_-(\boldsymbol{q}^+)}{(\beta-\lambda)\hbar|\nabla V_-(\boldsymbol{q}^+)|^2} \mathrm{d}\tau \tag{7.23a}$$

$$\mathcal{G}_1^{(\lambda)}[\boldsymbol{q}(\tau)] = \int_{0}^{\lambda\hbar} \frac{\nabla V_1(\boldsymbol{q}(\tau)) \cdot \nabla V_-(\boldsymbol{q}^+)}{\lambda\hbar|\nabla V_-(\boldsymbol{q}^+)|^2} \mathrm{d}\tau. \tag{7.23b}$$

One can show from these expressions that, unlike Wolynes theory, GR-QTST does not in general give the exact 1st, 2nd or even 0th moments of $\rho_\lambda(E)$.

As with Wolynes theory, GR-QTST is expected to be most accurate when $\rho_\lambda(0)$ is near the peak of the distribution and so ideally $k_{\text{GR-QTST}}(\lambda)$ should be evaluated at $\lambda = \lambda_{\text{sp}}$. However, when λ_{sp} is outside the interval $[0,\beta]$, such that evaluation at λ_{sp} is not possible, Thapa *et al.* suggest evaluating the rate at the end point closest to λ_{sp}.[232]

In low dimensions Thapa *et al.* found their method gave very good agreement with exact quantum mechanical golden-rule rates, and that since $k_{\text{GR-QTST}}(\lambda)$ is approximately independent of λ it gives accurate predictions of rates in the Marcus inverted regime and for systems with multiple transition states.[232,233] Unfortunately, however, their method is not size consistent. Although this size inconsistency has been discussed previously by Fang *et al.*,[232,233] its origins and implications have not yet been fully explored.

7.3.2 Size inconsistency

To explain the lack of size consistency in GR-QTST, we shall consider a system for which the coordinates can be separated into two uncoupled sets $\boldsymbol{q}_a$ and $\boldsymbol{q}_b$, and for which only $\boldsymbol{q}_a$ are coupled to the diabatic states. We note that this is not a physically unreasonable model as in a real atomistic simulation there may be many degrees of freedom which are essentially uncoupled from the non-adiabatic reaction of interest. The diabatic potentials for such a system can be written as

$$V_0(\boldsymbol{q}) = U_{0,a}(\boldsymbol{q}_a) + U_b(\boldsymbol{q}_b) \tag{7.24a}$$

$$V_1(\boldsymbol{q}) = U_{1,a}(\boldsymbol{q}_a) + U_b(\boldsymbol{q}_b), \tag{7.24b}$$

with corresponding diabatic Hamiltonians

$$\hat{H}_0 = \hat{H}_{0,a} + \hat{H}_b \tag{7.25a}$$

$$\hat{H}_1 = \hat{H}_{1,a} + \hat{H}_b. \tag{7.25b}$$

It is clear physically that the rate of transfer from state $|0\rangle$ to state $|1\rangle$ is completely independent of the "b" degrees of freedom. This can be confirmed by considering Eq. 2.89 and noting that since $[\hat{H}_{i,a}, \hat{H}_b] = 0$

$$\begin{aligned} c_{\lambda=0}(t) &= \mathrm{tr_n}\left[e^{-\beta\hat{H}_0} e^{-i\hat{H}_0 t/\hbar} e^{+i\hat{H}_1 t/\hbar}\right] \\ &= \mathrm{tr}_{a,\mathrm{n}}\left[e^{-\beta\hat{H}_{0,a}} e^{-i\hat{H}_{0,a} t/\hbar} e^{+i\hat{H}_{1,a} t/\hbar}\right] \mathrm{tr}_{b,\mathrm{n}}\left[e^{-\beta\hat{H}_b}\right] \end{aligned} \tag{7.26}$$

such that the "b" dependent terms cancel exactly with those in the reactant partition function

$$Q_r = \mathrm{tr}_{a,\mathrm{n}}\left[e^{-\beta\hat{H}_{0,a}}\right] \mathrm{tr}_{b,\mathrm{n}}\left[e^{-\beta\hat{H}_b}\right], \tag{7.27}$$

where $\mathrm{tr}_{a,\mathrm{n}}[\dots]$ denotes a trace just over the a degrees of freedom and $\mathrm{tr}_{b,\mathrm{n}}[\dots]$ just the b degrees of freedom.

The GR-QTST expression for the rate, however, does not have this property. To see this we first define the probability distribution

$$p_\lambda(E) = \left\langle \delta\left(\frac{2}{3}\mathcal{E}_-^{(\lambda)}[\boldsymbol{q}(\tau)] - E\right)\right\rangle_\lambda \tag{7.28}$$

which is equivalent to the pre-exponential term in $k_{\text{GR-QTST}}(\lambda)$, for $\epsilon = 0$, when evaluated at $E = 0$. (Note that, this is not quite the same as $\rho_{\text{GR-QTST},\lambda}(-E)$ in Eq. 7.21). Noting that the constraint functional can be separated into two parts, each of which only depends on one of the two uncoupled sets of degrees of freedom, we can write

$$\mathcal{E}_-^{(\lambda)}[\boldsymbol{q}(\tau)] = \mathcal{E}_{-,a}^{(\lambda)}[\boldsymbol{q}_a(\tau)] + \mathcal{E}_{-,b}^{(\lambda)}[\boldsymbol{q}_b(\tau)]. \tag{7.29}$$

It then follows straightforwardly that

$$p_\lambda(E) = \int_{-\infty}^{\infty} p_{a,\lambda}(E - E') p_{b,\lambda}(E')\,\mathrm{d}E', \tag{7.30}$$

where

$$p_{\alpha,\lambda}(E) = \left\langle \delta\left(\frac{2}{3}\mathcal{E}_{-,\alpha}^{(\lambda)}[\boldsymbol{q}_\alpha(\tau)] - E\right)\right\rangle_\lambda \tag{7.31}$$

with $\alpha = a$ or b.

If it were true that $\mathcal{E}_{-,b}^{(\lambda)}[\boldsymbol{q}_b(\tau)] = 0$, then $p_{b,\lambda}(E)$ would simply be $\delta(E)$, and GR-QTST would correctly predict that the spectator degrees of freedom did not affect the rate. However, this is not in general the case as the instantaneous quantum fluctuations in the

virial energy estimators for these degrees of freedom averaged around the two segments of the ring polymer do not perfectly cancel. It follows that $p_{b,\lambda}(E)$ is a distribution with non-zero standard deviation. Hence, when it is convoluted with $p_{a,\lambda}(E)$, the resulting distribution will not in general satisfy $p_\lambda(0) = p_{a,\lambda}(0)$. This problem becomes worse with increasing system size, as the variance of the distribution $p_{b,\lambda}(E)$ grows linearly with the number of uncoupled degrees of freedom. While the fluctuations may be small when there are only a few uncoupled degrees of freedom, they will clearly eventually come to dominate the rate. Although Richardson and coworkers have discussed the size inconsistency of GR-QTST previously,[232,233] the analysis presented here clarifies under what circumstances the GR-QTST rate will break down. In particular we can see that the rate will be significantly affected when the variance due to fluctuations in degrees of freedom uncoupled to the reaction becomes comparable to the variance of the exact distribution. As the variance of the exact distribution is on the order of Λ/β, where Λ is the Marcus reorganisation energy, it is simple to assess whether uncoupled degrees of freedom are likely to dominate the rate. The size inconsistency will be most pronounced in the tails of the distribution, and for singly peaked $\rho_\lambda(E)$ the error is thus expected to be smallest when the GR-QTST rate is evaluated at λ_{sp}.*

We shall show in the following chapter that, for a realistic atomistic simulation of aqueous ferrous-ferric electron transfer, the solvent degrees of freedom that are uncoupled from the reaction do indeed dominate the GR-QTST approximation to $\rho_\lambda(E)$, leading to a spurious prediction of the rate. Unfortunately, even in relatively small systems, where all degrees of freedom are significantly coupled to the diabatic electronic states, the lack of size consistency in GR-QTST can lead to large errors in the predicted rates, as we shall illustrate for a spin-boson model in Sec. 7.6.

*Whilst we have only here considered the case of $\epsilon = 0$, the same argument can of course be made for any other value of the driving force.

7.4 An improved method

7.4.1 Linear crossing potentials

GR-QTST does have some desirable features which would make it quite attractive if it were not for its size inconsistency. We believe the most important of these is that, for a one-dimensional system of linear crossing potentials,

$$V_0(q) = \kappa_0(q - q^\ddagger) + V^\ddagger \tag{7.32a}$$

$$V_1(q) = \kappa_1(q - q^\ddagger) + V^\ddagger, \tag{7.32b}$$

the method gives the exact quantum mechanical rate constant[195]

$$k_{\mathrm{GR}} Q_r = \sqrt{\frac{2\pi m}{\beta\hbar^2}} \frac{\Delta^2}{\hbar|\kappa_0 - \kappa_1|} e^{-\beta V^\ddagger} \exp\left(\frac{\beta^3\hbar^2\kappa_0^2\kappa_1^2}{24m(\kappa_0 - \kappa_1)^2}\right), \tag{7.33}$$

independent of the choice of λ. In order to show this, Thapa *et al.*[232] demonstrated that for this system the exact rate can be written in terms of an imaginary-time path integral as

$$k = \frac{2\pi\Delta^2}{\hbar Q_r} \oint \mathcal{D}q(\tau)\, e^{-S^{(\lambda)}[q(\tau)]/\hbar} \delta(\mathcal{V}_-^{(\lambda)}[q(\tau)]) \tag{7.34}$$

where

$$\mathcal{V}_-^{(\lambda)}[q(\tau)] = \mathcal{V}_0^{(\lambda)}[q(\tau)] - \mathcal{V}_1^{(\lambda)}[q(\tau)] \tag{7.35}$$

with

$$\mathcal{V}_0^{(\lambda)}[q(\tau)] = V_0(\tilde{q}) + \int_{\lambda\hbar}^{\beta\hbar} \frac{\kappa_0(q(\tau) - \tilde{q})}{(\beta - \lambda)\hbar} \mathrm{d}\tau \tag{7.36a}$$

$$\mathcal{V}_1^{(\lambda)}[q(\tau)] = V_1(\tilde{q}) + \int_0^{\lambda\hbar} \frac{\kappa_1(q(\tau) - \tilde{q})}{\lambda\hbar} \mathrm{d}\tau, \tag{7.36b}$$

for any choice of $\tilde{q}$. Instead of merely being a step on the way to showing that GR-QTST is exact in the linear case, we believe that this result is instead fundamental to the success of the method for more general one-dimensional problems.

7.4.2 Linear golden-rule approximation

Following this perspective, let us now suggest a modified method which directly generalises Eqs. 7.34 to 7.36 for multidimensional and non-linear potentials. The most obvious generalisation of Eqs. 7.35 and 7.36 would be to simply use the difference between diabatic potential energies averaged around each segment of the imaginary-time path,

$$\mathcal{V}_{-}^{(\lambda)}[\boldsymbol{q}(\tau)] = \int_{\lambda\hbar}^{\beta\hbar} \frac{V_0(\boldsymbol{q}(\tau))}{(\beta-\lambda)\hbar}\mathrm{d}\tau - \int_{0}^{\lambda\hbar} \frac{V_1(\boldsymbol{q}(\tau))}{\lambda\hbar}\mathrm{d}\tau. \tag{7.37}$$

However, for the reasons we have already discussed, this is not size consistent. For a two dimensional system described by the diabats

$$V_i(\boldsymbol{q}) = U_{i,a}(q_a) + U_b(q_b) \tag{7.38a}$$

$$U_{i,a}(q_a) = \kappa_i(q - q^{\ddagger}) + V^{\ddagger}, \tag{7.38b}$$

it is clear that the multidimensional generalisation of Eqs. 7.35 and 7.36 that avoids the size consistency problem would need to be equivalent to

$$\mathcal{U}_{-}^{(\lambda)}[q_a(\tau)] = \int_{\lambda\hbar}^{\beta\hbar} \frac{U_{0,a}(q_a(\tau))}{(\beta-\lambda)\hbar}\mathrm{d}\tau - \int_{0}^{\lambda\hbar} \frac{U_{1,a}(q_a(\tau))}{\lambda\hbar}\mathrm{d}\tau, \tag{7.39}$$

rather than Eq. 7.37. This suggests that we would ideally like to "project out" degrees of freedom uncoupled to $V_{-}(\boldsymbol{q})$. In this simple example this can clearly be achieved by letting

$$\mathcal{U}_{-}^{(\lambda)}[\boldsymbol{q}(\tau)] = \int_{\lambda\hbar}^{\beta\hbar} \frac{V_0(\tau,\tau')}{(\beta-\lambda)\hbar}\mathrm{d}\tau - \int_{0}^{\lambda\hbar} \frac{V_1(\tau,\tau')}{\lambda\hbar}\mathrm{d}\tau \tag{7.40}$$

where

$$V_i(\tau,\tau') = V_i(q_a(\tau), q_b(\tau')), \tag{7.41}$$

i.e. by fixing degrees of freedom orthogonal to the diabatic energy gap coordinate at some specified imaginary time $i\tau'$.

In order to generalise this to more complex multidimensional systems we first define the local diabatic energy gap coordinate as

$$x_{\tau'}(\tau) = V_{-}(\boldsymbol{q}(\tau')) + \nabla V_{-}(\boldsymbol{q}(\tau')) \cdot (\boldsymbol{q}(\tau) - \boldsymbol{q}(\tau')), \tag{7.42}$$

and then consider changes in the diabatic potentials as a function of $x_{\tau'}(\tau)$ whilst keeping orthogonal degrees of freedom fixed at τ',

$$V_i(\tau,\tau') = V_i(\boldsymbol{q}(\tau')) + \left.\frac{\partial V_i}{\partial x_{\tau'}}\right|_{\tau'} (x_{\tau'}(\tau) - x_{\tau'}(\tau')) + \dots . \tag{7.43}$$

In order to obtain a practical expression for the constraint functional we assume that along the imaginary-time path the diabatic potential can be treated as a harmonic function of $x_{\tau'}$, such that

$$\left.\frac{\partial^2 V_i}{\partial x_{\tau'}^2}\right|_{\tau'} \simeq \frac{\left.\frac{\partial V_i}{\partial x_{\tau'}}\right|_{\tau} - \left.\frac{\partial V_i}{\partial x_{\tau'}}\right|_{\tau'}}{x_{\tau'}(\tau) - x_{\tau'}(\tau')}, \tag{7.44}$$

and

$$V_i(\tau,\tau') \simeq V_i(\boldsymbol{q}(\tau')) + \frac{\left.\frac{\partial V_i}{\partial x_{\tau'}}\right|_{\tau} + \left.\frac{\partial V_i}{\partial x_{\tau'}}\right|_{\tau'}}{2}(x_{\tau'}(\tau) - x_{\tau'}(\tau')). \tag{7.45}$$

This can then be rewritten explicitly in terms of the original coordinates by noting that

$$x_{\tau'}(\tau) - x_{\tau'}(\tau') = \nabla V_-(\boldsymbol{q}(\tau')) \cdot (\boldsymbol{q}(\tau) - \boldsymbol{q}(\tau')) \tag{7.46}$$

and

$$\left.\frac{\partial V_i}{\partial x_{\tau'}}\right|_{\tau} = \frac{\nabla V_i(\boldsymbol{q}(\tau)) \cdot \nabla V_-(\boldsymbol{q}(\tau'))}{|\nabla V_-(\boldsymbol{q}(\tau'))|^2}, \tag{7.47}$$

which having defined the projected diabatic gradients

$$\boldsymbol{\kappa}_{i,\tau'}(\tau) = \frac{\nabla V_i(\boldsymbol{q}(\tau)) \cdot \nabla V_-(\boldsymbol{q}(\tau'))}{|\nabla V_-(\boldsymbol{q}(\tau'))|^2} \nabla V_-(\boldsymbol{q}(\tau')) \tag{7.48}$$

allows us to rewrite Eq. 7.45 in the form

$$V_i(\tau,\tau') \simeq V_i(\boldsymbol{q}(\tau')) + \frac{\boldsymbol{\kappa}_{i,\tau'}(\tau) + \boldsymbol{\kappa}_{i,\tau'}(\tau')}{2} \cdot (\boldsymbol{q}(\tau) - \boldsymbol{q}(\tau')). \tag{7.49}$$

It is clear that in general this approach depends on the value of τ' about which the expansion is taken. We suggest averaging τ' over the two hopping times, $\lambda\hbar$ and $\beta\hbar$, which we have found generally gives the most accurate results. Our approximation to the rate, in the case of $\epsilon = 0$, can then be written as

$$k_{\mathrm{LGR}}(\lambda) = \frac{2\pi\Delta^2}{\hbar Q_r} \langle \delta(\bar{V}_-^{(\lambda)}[\boldsymbol{q}(\tau)] + \bar{\mathcal{K}}_-^{(\lambda)}[\boldsymbol{q}(\tau)]) \rangle_\lambda e^{-\beta F_{\mathrm{GR}}(\lambda)}, \tag{7.50}$$

in which the argument of the delta function consists of two terms. The first of these is simply the diabatic energy gap averaged over the two bridging beads,

$$\bar{V}_{-}^{(\lambda)}[\boldsymbol{q}(\tau)] = \frac{V_{-}(\boldsymbol{q}(\lambda\hbar)) + V_{-}(\boldsymbol{q}(\beta\hbar))}{2}, \tag{7.51}$$

and the second is a gradient-based correction of the form

$$\bar{\mathcal{K}}_{-}^{(\lambda)}[\boldsymbol{q}(\tau)] = \bar{\mathcal{K}}_{0}^{(\lambda)}[\boldsymbol{q}(\tau)] - \bar{\mathcal{K}}_{1}^{(\lambda)}[\boldsymbol{q}(\tau)] \tag{7.52}$$

where

$$\bar{\mathcal{K}}_{i}^{(\lambda)}[\boldsymbol{q}(\tau)] = \frac{\mathcal{K}_{i,\lambda\hbar}^{(\lambda)}[\boldsymbol{q}(\tau)] + \mathcal{K}_{i,\beta\hbar}^{(\lambda)}[\boldsymbol{q}(\tau)]}{2} \tag{7.53}$$

with

$$\mathcal{K}_{0,\tau'}^{(\lambda)}[\boldsymbol{q}(\tau)] = \int_{\lambda\hbar}^{\beta\hbar} \frac{\bar{\boldsymbol{\kappa}}_{0}(\tau,\tau')\cdot(\boldsymbol{q}(\tau)-\boldsymbol{q}(\tau'))}{(\beta-\lambda)\hbar}\mathrm{d}\tau \tag{7.54a}$$

$$\mathcal{K}_{1,\tau'}^{(\lambda)}[\boldsymbol{q}(\tau)] = \int_{0}^{\lambda\hbar} \frac{\bar{\boldsymbol{\kappa}}_{1}(\tau,\tau')\cdot(\boldsymbol{q}(\tau)-\boldsymbol{q}(\tau'))}{\lambda\hbar}\mathrm{d}\tau \tag{7.54b}$$

and

$$\bar{\boldsymbol{\kappa}}_{i}(\tau,\tau') = \frac{\boldsymbol{\kappa}_{i,\tau'}(\tau) + \boldsymbol{\kappa}_{i,\tau'}(\tau')}{2}. \tag{7.55}$$

Since this method is based directly on the exact result in the linear case and only involves the gradients of the diabatic potentials we call it the linear golden-rule (LGR) approximation. In view of the assumption we have made we expect it will be most accurate when the gradients of the diabatic potentials do not change dramatically around the imaginary-time path. The LGR approximation does not have the same connection to the semiclassical instanton that Thapa *et al.*[232] chose to prioritise in their definition of GR-QTST, and hence is likely to be less accurate for low dimensional systems at low temperatures. It is however clear by construction that it retains the property of being exact for a one dimensional system of two linear crossing potentials, as well as reducing to Eq. 7.12 in the high temperature limit (where $|\boldsymbol{q}(\tau) - \boldsymbol{q}(\tau')| \to 0$ and $\bar{\mathcal{K}}_{-}^{(\lambda)}[\boldsymbol{q}(\tau)] \to 0$). In addition to this we note that, unlike GR-QTST, the LGR approximation to the distribution $\rho_{\lambda}(E)$,

$$\rho_{\mathrm{LGR},\lambda}(E) = \left\langle \delta(\bar{V}_{-}^{(\lambda)}[\boldsymbol{q}(\tau)] + \bar{\mathcal{K}}_{-}^{(\lambda)}[\boldsymbol{q}(\tau)] + E)\right\rangle_{\lambda}, \tag{7.56}$$

correctly integrates to one, and hence is a true distribution.

Except in the linear case and the high temperature limit, $k_{\mathrm{LGR}}(\lambda)$ will not be completely independent of λ. Hence, just as with Wolynes theory and GR-QTST, we expect that $k_{\mathrm{LGR}}(\lambda)$ will be most accurate when evaluated at the saddle point λ_{sp}. As with GR-QTST, we thus suggest that the LGR rate is evaluated at λ_{sp} or at the closest end point when λ_{sp} falls outside the range $[0,\beta]$.

We note that the first of the two terms appearing in the delta function in Eq. 7.56 is precisely the same as arrises from making the static approximation,[67]

$$e^{-i\hat{H}_0 t/2\hbar} e^{+i\hat{H}_1 t/2\hbar} \simeq e^{-i\hat{V}_- t/2\hbar} \tag{7.57}$$

symmetrically in Eq. 2.90 to give

$$c_{\mathrm{GR}}(t + i\lambda\hbar) \simeq \mathrm{tr_n}[e^{-(\beta-\lambda)\hat{H}_0} e^{-i\hat{V}_- t/2\hbar} e^{-\lambda\hat{H}_1} e^{-i\hat{V}_- t/2\hbar}] e^{\epsilon(\lambda - it/\hbar)}. \tag{7.58}$$

Although it is exact at high temperature, the static approximation is generally only valid at short time. Hence at low temperatures the static approximation to the distribution,

$$\rho_{\mathrm{st},\lambda}(E) = \left\langle \delta(\bar{V}_-^{(\lambda)}[\boldsymbol{q}(\tau)] + E) \right\rangle_\lambda, \tag{7.59}$$

is typically not accurate in the tails of the distribution. The second term in the argument of the delta function in Eq. 7.56, $\bar{\mathcal{K}}_-^{(\lambda)}[\boldsymbol{q}(\tau)]$, acts to correct the static approximation to the tails of the distribution, and makes the rate approximately independent of λ. The LGR approximation therefore combines the exact quantum statistics of the system with a local linear approximation to predict how tunnelling and zero-point energy will affect the rate.

7.4.3 Size consistency

The main theoretical improvement of the LGR approximation over GR-QTST is that it is not affected by adding uncoupled modes to the system. To highlight this we shall again consider a system with diabatic potentials

$$V_0(\boldsymbol{q}) = U_{0,a}(\boldsymbol{q}_a) + U_b(\boldsymbol{q}_b) \tag{7.60a}$$

$$V_1(\boldsymbol{q}) = U_{1,a}(\boldsymbol{q}_a) + U_b(\boldsymbol{q}_b), \tag{7.60b}$$

in which the "b" degrees of freedom are not coupled (directly or indirectly) to the diabatic state and hence should have no effect on the rate. Since the diabatic energy gap is then (by definition) independent of $\boldsymbol{q}_b$,

$$V_-(\boldsymbol{q}) = U_{0,a}(\boldsymbol{q}_a) - U_{1,a}(\boldsymbol{q}_a), \tag{7.61}$$

it follows straightforwardly that so too is its average around the imaginary-time path, $\bar{V}_-[\boldsymbol{q}(\tau)] = \bar{V}_-[\boldsymbol{q}_a(\tau)]$. For the correction term we note that since the derivative of the energy gap is independent of $\boldsymbol{q}_b$ it follows simply that both

$$\nabla V_i(\boldsymbol{q}(\tau)) \cdot \nabla V_-(\boldsymbol{q}(\tau')) = \nabla U_{i,a}(\boldsymbol{q}_a(\tau)) \cdot \nabla V_-(\boldsymbol{q}_a(\tau')), \tag{7.62}$$

and

$$\nabla V_-(\boldsymbol{q}(\tau')) \cdot (\boldsymbol{q}(\tau) - \boldsymbol{q}(\tau')) = \nabla V_-(\boldsymbol{q}_a(\tau')) \cdot (\boldsymbol{q}_a(\tau) - \boldsymbol{q}_a(\tau')), \tag{7.63}$$

and hence that the correction term, $\mathcal{K}_-^{(\lambda)}[\boldsymbol{q}(\tau)] = \mathcal{K}_-^{(\lambda)}[\boldsymbol{q}_a(\tau)]$, is also independent of the uncoupled modes. (Note that the gradient operator in Eqs. 7.62 and 7.63 is $\nabla = (\partial/\partial\boldsymbol{q}_a, \partial/\partial\boldsymbol{q}_b)$, and that cross terms between the "a" and "b" coordinates do not contribute to the dot products.) Hence, our method does not suffer the same size consistency issue as GR-QTST. This key difference arrises because of the projection of ∇V_i onto ∇V_-, which ensures that degrees of freedom which are not coupled to $V_-(\boldsymbol{q})$ do not enter the constraint functional.

7.5 Numerical implementation

There are clearly two components to evaluating $k_{\mathrm{LGR}}(\lambda)$, the first of which is the evaluation of the Boltzmann factor, $e^{-\beta F_{\mathrm{GR}}(\lambda)}/Q_r$. This is common to all of the methods we have discussed: Wolynes Theory, GR-QTST and LGR. Since

$$\frac{e^{-\beta F_{\mathrm{GR}}(\lambda)}}{Q_r} = e^{-\beta[F_{\mathrm{GR}}(\lambda) - F_{\mathrm{GR}}(0)]} = e^{-\beta \int_0^\lambda F'_{\mathrm{GR}}(\lambda')\,\mathrm{d}\lambda'}, \tag{7.64}$$

and since $-\beta F'_{\mathrm{GR}}(\lambda_l)$ is given by the simple path-integral expectation value in Eq. 2.188, this factor is straightforward to calculate by evaluating $-\beta F'(\lambda_l)$ on a grid of points and doing a numerical integration.

The second component in $k_{\mathrm{LGR}}(\lambda)$ is the probability density, $\rho_{\mathrm{LGR},\lambda}(\epsilon)$. Since $\rho_{\lambda_{\mathrm{sp}}}(E)$ tends to be peaked around $E = \epsilon$, this can be evaluated at the same time as $-\beta F'(\lambda_l)$ by histogramming the the n bead discretisation of $\bar{V}_-[\boldsymbol{q}(\tau)] + \mathcal{K}_-^{(\lambda)}[\boldsymbol{q}(\tau)]$ to give $\rho_{\mathrm{LGR},\lambda_l}(E)$. Hence in the normal regime one needs to do no additional calculations beyond those required by Wolynes theory.[82] However, in the inverted regime, for reactions which are sufficiently activated, direct evaluation of $\rho_{\mathrm{LGR},\lambda_l=0}(\epsilon)$ in this way will be insufficient. Instead one will need to use an enhanced sampling technique to sample configurations around the crossing seam $V_0(\boldsymbol{q}) = V_1(\boldsymbol{q}) - \epsilon$. This added complexity is mitigated by the fact that there is no need in this case to do any simulations for values of $\lambda_l > 0$, and the fact that one immediately knows the Boltzmann factor $e^{-\beta F_{\mathrm{GR}}(0)}/Q_r = 1$. Hence, for a similar activation energy, the inverted regime does not introduce any greater simulation effort than that required in the normal regime.

7.6 Results and discussion

In order to test the LGR approximation we have considered two different model problems for which exact results are available for comparison. The first of these is the one dimensional electronic pre-dissociation model considered by Thapa *et al.* in their first paper introducing GR-QTST,[232] and which we also considered in the previous chapter. The second is a multidimensional discretisation of a spin-boson model with an exponentially damped Ohmic spectral density, with parameters chosen to provide a demanding test case exhibiting significant nuclear quantum effects.

7.6.1 One-dimensional pre-dissociation model

The first model we consider is the pre-dissociation model originally introduced by Richardson and Thoss to demonstrate the oscillatory nature of flux-flux correlation functions.[230] This model was also considered by Thapa *et al.*[232] in their paper introducing GR-QTST, and for ease of comparison with their results we consider the same parameter regimes as they did in their paper.

For this system the diabatic potentials take the form

$$V_0(q) = \frac{1}{2}\omega^2 q^2 \tag{7.65}$$

and

$$V_1(q) = De^{-2\alpha(q-\xi)}. \tag{7.66}$$

The model parameters are $m = 1$, $\omega = 1$, $D = 2$, $\alpha = 0.2$, and $\xi = 5$, in units where $\hbar = 1$, and the calculations are performed over a range of values of β and ϵ. We again define the reorganisation energy for this problem as $\Lambda = De^{2\alpha\xi}$.

In order to highlight the relative importance of nuclear quantum effects in different regimes, we shall compare our results with the classical rate in Eq. 7.12. For this simple one dimensional model this can be expressed as[173]

$$k_{\text{cl-GR}} = \frac{\Delta^2}{\hbar}\sqrt{2\pi\beta m\omega^2}\frac{e^{-\beta V_0(q^\ddagger)}}{|V'_-(q^\ddagger)|}, \tag{7.67}$$

where $q^\ddagger$ satisfies the equation $V_0(q^\ddagger) = V_1(q^\ddagger) - \epsilon$. The exact quantum mechanical rate

$$k_{\text{GR}} = -\frac{2\Delta^2}{\hbar Q_r}\sum_j e^{-\beta E_j}\,\text{Im}\,\langle j|\,\hat{G}_1^+(E_j)\,|j\rangle\,, \tag{7.68}$$

with

$$Q_r = \sum_j e^{-\beta E_j} \tag{7.69}$$

where

$$\hat{H}_0\,|j\rangle = E_j\,|j\rangle \tag{7.70}$$

and

$$\hat{G}_1^+(E_j) = \lim_{\eta\to 0^+}\left(E_j + i\eta - \hat{H}_1 + \epsilon\right)^{-1}, \tag{7.71}$$

was calculated using a Lobatto shape function discrete variable representation, using code written by Prof. David E. Manolopoulos.[231]

Figure 7.1 compares the rate as a function of the driving force for this model at a fixed temperature, with all rates plotted relative to the classical rate at zero driving force. We do not include the GR-QTST results in Fig. 7.1 as they are the same as the LGR rates to graphical accuracy. The LGR rates are also almost graphically indistinguishable from the exact rates for this problem, both in the normal regime and all the way out to

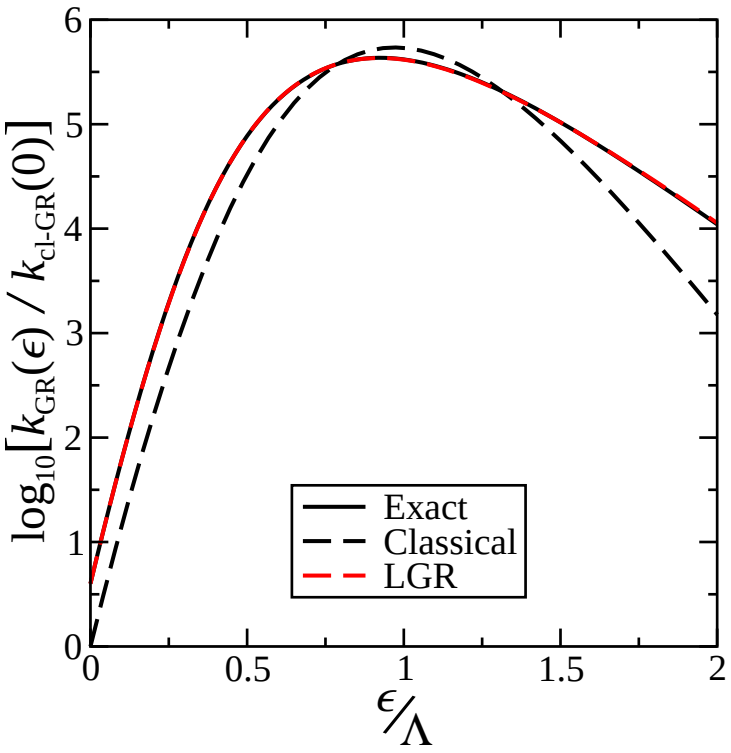

Figure 7.1: Rate constants for the electronic pre-dissociation model at $\beta = 3$, relative to the classical result at $\epsilon = 0$. The exact results were calculated using Eq. 7.68 and the LGR results as described in Sec. 7.5, using 256 ring-polymer beads. Exact results were calculated using code written by Prof. David E. Manolopoulos.

$\epsilon = 2\Lambda$ in the inverted regime. The accuracy of the method in the inverted regime is particularly pleasing given the simplicity with which the LGR calculation is performed, in particular when compared with the approach of the previous chapter, which requires numerical analytic continuation to obtain the Wolynes theory rate in the inverted regime. Comparison with the classical rate shows that at this temperature nuclear quantum effects only have a moderate effect on the rate, with the largest difference, occurring at $\epsilon = 2\Lambda$, corresponding to less than an order of magnitude speed up relative to the classical rate.

Figure 7.2 shows how the rate constants vary as a function of temperature at zero driving force, $\epsilon = 0$. We see clearly the break down of Wolynes theory at high temperature, as is highlighted in the inset of the figure. GR-QTST and LGR do not suffer from this problem, and instead correctly recover the exact rate in the high temperature

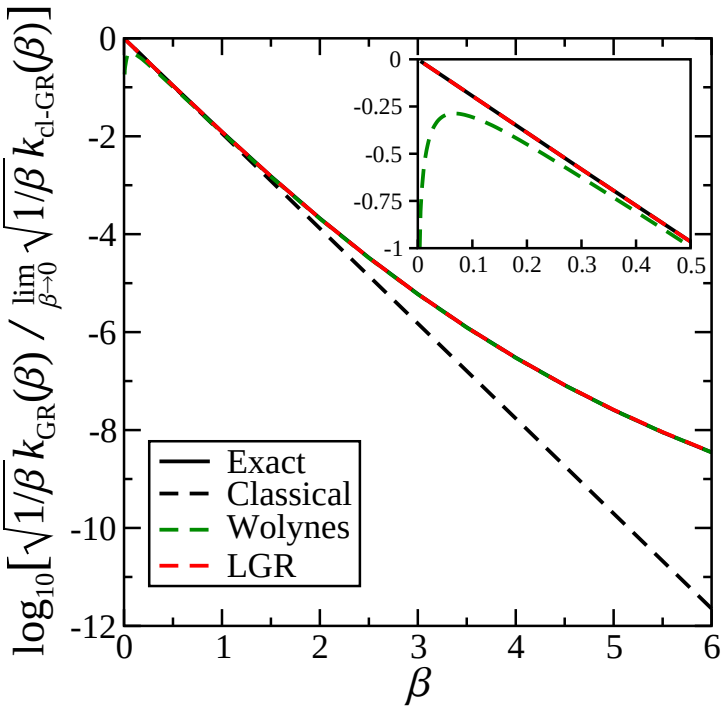

Figure 7.2: Rate constants as a function of inverse temperature for the pre-dissociation model, with $\epsilon = 0$. The exact results were calculated using Eq. 7.68. The results for Wolynes Theory and LGR were calculated using 512 beads at the lowest temperature. The inset shows the break down of Wolynes theory at high temperature. The GR-QTST results are not included as they are essentially indistinguishable from the LGR rates on this plot. They can be found in Ref. 232. Exact rates were calculated using code written by Prof. David E. Manolopoulos

limit. At lower temperatures we see that both LGR and Wolynes theory are graphically indistinguishable from the exact rate (which is hidden under the LGR and Wolynes curves in the figure). We find that the LGR rates are very accurate for this problem, with an error of less than 5% for all values of β considered. This is particularly impressive considering that at the lowest temperature there are 3 orders of magnitude difference between the classical and quantum rates. The LGR rate is in fact slightly more accurate at this temperature than the GR-QTST rate, which has an error of about 8% at $\beta = 6$.[232]

7.6.2 Multi-dimensional spin-boson model

The second system we shall consider is a multi-dimensional spin-boson model,

$$V_0(\boldsymbol{q}) = \sum_{\nu=1}^{f} \frac{1}{2} m\omega_\nu^2 q_\nu^2 + c_\nu q_\nu \tag{7.72a}$$

$$V_1(\boldsymbol{q}) = \sum_{\nu=1}^{f} \frac{1}{2} m\omega_\nu^2 q_\nu^2 - c_\nu q_\nu, \tag{7.72b}$$

in which the bosonic bath modes are described by an exponentially damped Ohmic spectral density

$$J(\omega) = \Lambda \frac{\pi\omega}{4\omega_c} e^{-\omega/\omega_c}, \tag{7.73}$$

with a reorganisation energy of $\Lambda = 50\,\mathrm{kcal\,mol^{-1}}$ and a cutoff frequency of $\beta\hbar\omega_c = 8$ at 300 K.

This model was chosen to be strongly quantum mechanical, so as to provide a stringent test of the accuracy of GR-QTST and LGR. The exact quantum mechanical golden-rule rate can be calculated for comparison by numerical integration of the exact expression for $c_{\mathrm{GR}}(t)$ given by Eq. 2.217, and the classical limit of the rate is given by Marcus theory (Eq. 2.224).[46–49]

In order to calculate the exact, GR-QTST, and LGR rates for this problem we use a discretised form of the spectral density with f modes, which in the limit as $f \to \infty$ becomes equivalent to the continuous form:

$$J(\omega) = \frac{\pi}{2} \sum_{\nu=1}^{f} \frac{c_\nu^2}{m\omega_\nu} \delta(\omega - \omega_\nu). \tag{7.74}$$

The discretisation we employ is defined by

$$\omega_\nu = -\omega_c \ln(x_\nu), \tag{7.75}$$

and

$$c_\nu = \omega_\nu \sqrt{\frac{m\Lambda w_\nu}{2}}, \tag{7.76}$$

where w_ν and x_ν are the weights and nodes of an f-point Gauss-Legendre quadrature on the interval $[0, 1]$. Discretising using Gauss-Legendre quadrature rather than the

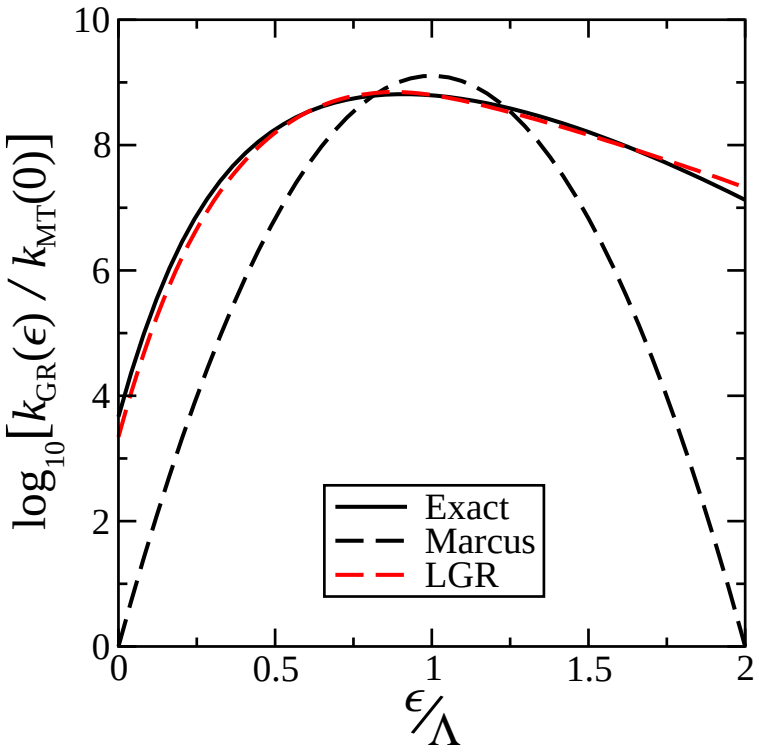

Figure 7.3: Exact, LGR and Marcus theory reaction rate constants as a function of the driving force for a multi-dimensional spin-boson model. All three rate constants are plotted relative to the classical (Marcus theory) rate at zero driving force ($\epsilon = 0$). The LGR rates were computed using 256 path-integral beads and the exact rate was calculated by numerical integration of Eq. 2.217. Both the exact and LGR rates are converged to graphical accuracy with $f = 16$ bath modes.

more commonly used midpoint rule[227] leads to more rapid convergence of the exact golden-rule rate with respect to the number of bath modes. Since GR-QTST is not size consistent the GR-QTST rates do not converge with increasing f, and by using a rapidly convergent discretisation we will be able to more clearly illustrate the breakdown of GR-QTST with increasing system size.

Figure 7.3 shows the exact, LGR and classical (Marcus theory) rates as a function of driving force for this model, relative to the classical rate at zero driving force. We find that both the exact rates and the LGR rates are essentially converged to graphical accuracy using $f = 8$ bath modes, and that they are very well converged with the $f = 16$ modes that we use in this figure. Comparison of the classical rate and the exact quantum

mechanical rate highlights the importance of nuclear quantum effects. We see that the exact rate is well over 3 orders of magnitude larger than the classical rate at $\epsilon = 0$, and 7 orders of magnitude larger at $\epsilon = 2\Lambda$. While the logarithm of the classical rate exhibits the famous parabolic dependence on the driving force, the exact rate is not symmetric about $\epsilon = \Lambda$. This asymmetry of the quantum rate as a function of driving force is well known, and occurs due to the increased efficiency of tunnelling in the Marcus inverted regime. We also note that the large decrease in the quantum compared to the classical rate near the activationless reaction, $\epsilon = \Lambda$, is an indication of the importance of high frequency modes in this system. It can be attributed to zero-point energy broadening the quantum distribution relative to the classical distribution at the same temperature, resulting in a reduced probability of the system being found at the diabatic crossing point.

We see that LGR reproduces the main qualitative features of the exact rate as a function of driving force. The largest errors exhibited by LGR are at $\epsilon = 0$, where it is just over a factor of 2 smaller than the exact rate, and at $\epsilon = 2\Lambda$ where it is just under a factor of 2 larger than the exact rate. Considering the large difference between the classical and quantum rates for these systems, we feel that these are not unreasonable errors. Encouragingly LGR is also most accurate for values of ϵ where the difference between the quantum and classical rates is smallest, showing an error of less than 10% at $\epsilon = \Lambda$. The accuracy of LGR for this system even in the inverted regime, where $\lambda_{\mathrm{sp}} < 0$ and the rate must be evaluated at $\lambda = 0$, is perhaps the most encouraging feature of Fig. 7.3. Especially since this calculation avoids the numerical analytic continuation needed to apply Wolynes theory to the inverted regime. We would conclude from Fig. 7.3 that the LGR provides an accurate approximation to quantum mechanical golden-rule rates for condensed phase systems in both the normal and inverted regimes.

Figure 7.4 shows the GR-QTST results for discretisations with $f = 8, 16$ and 32 bath modes, illustrating the failure of this method to converge with increasing system size. While GR-QTST provides reasonably accurate results for the 8 mode discretisation, as we move to 16 and 32 mode discretisations the error in the GR-QTST rate grows significantly. This is in stark contrast to both the exact and LGR rates which show no significant change with increasing system size. We see that the size consistency error is most pronounced

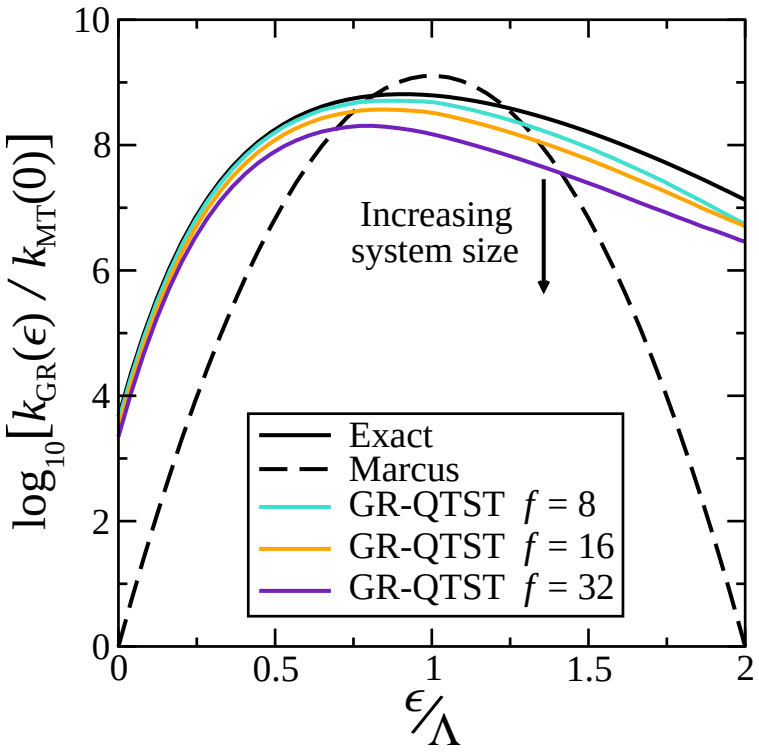

Figure 7.4: Comparison of GR-QTST reaction rate constants as a function of the driving force for the spin-boson model with an increasing number of bath modes, relative to the classical (Marcus theory) rate at zero driving force ($\epsilon = 0$). The GR-QTST rates were computed using 256 path-integral beads and the exact rate was calculated by numerical integration of Eq. 2.217. This plot illustrates that GR-QTST does not converge as the size of the system increases, due to the lack of size consistency discussed in Sec. 7.3.2

in the inverted regime, where the GR-QTST rate is out by as much as a factor of 3 for $f = 16$ and by almost an order of magnitude for $f = 32$. Although the error in the normal regime is not as pronounced, it is important to stress that since the GR-QTST rates do not converge as $f \to \infty$ it is possible to obtain an arbitrarily large error by going to sufficiently large f. We shall demonstrate in the following chapter that, for more realistic atomistic models of condensed phase electron transfer with thousands of degrees of freedom rather than only 32, the error even in the normal regime can become very significant indeed.

7.7 Conclusion and future work

In this chapter, we have proposed an alternative to Wolynes theory for calculating non-adiabatic reaction rates in the golden-rule limit. This alternative, which we have called the "Linear Golden-Rule" approximation, improves on the recent "Golden-Rule Quantum Transition State Theory" approximation of Richardson and coworkers by eliminating its size consistency issues. Like GR-QTST, but unlike Wolynes theory, the method we have proposed recovers the correct classical golden-rule result in the high-temperature limit, and it is exact at all temperatures for the special case of two linearly crossing potentials in one dimension. Its advantage over GR-QTST is that it is size consistent, and can therefore be used without issue in large-scale simulations of condensed phase reactions: the uncoupled "spectator" modes that are not involved in the reaction do not contribute to the calculated reaction rate. Its advantages over Wolynes theory are threefold: it is exact in the high-temperature limit, it can be applied to reactions with more than one transition state, and it can be used to calculate electron transfer rates in the Marcus inverted regime without the need for any numerical analytic continuation.

In the previous section we have demonstrated the accuracy of LGR for both a one dimensional anharmonic pre-dissociation model and a multidimensional spin-boson model. The approximate independence of the LGR approximation to the rate on λ allows for direct evaluation of reaction rates in the Marcus inverted regime. It also means that LGR can be applied to systems with multiple transition states, which when treated separately would have different values of λ_{sp}. Application of LGR to System I from Ref. 233 at $\beta = 3$ reduced units, which was designed to exhibit two transition states, confirms the accuracy of LGR for such systems, with $k_{\mathrm{LGR}}/\Delta^2 = 2.2 \pm 0.2 \times 10^{-28}$ reduced units compared to $k_{\mathrm{GR}}/\Delta^2 = 1.98 \times 10^{-28}$ for the exact golden-rule rate, $k_{\text{cl-GR}}/\Delta^2 = 1.1 \pm 0.2 \times 10^{-29}$ for the classical golden-rule rate and $k_{\text{GR-QTST}}/\Delta^2 = 2.3 \pm 0.2 \times 10^{-28}$ for the GR-QTST rate.[233] In contrast, Wolynes theory overestimates the rate by more than a factor of 300 for this system.[233] Although LGR eliminates the size inconsistency seen in GR-QTST, it also loses the connection to the semiclassical instanton.[170,195,196,232] As such, in low dimensional models, LGR is expected to become less accurate than

GR-QTST at sufficiently low temperatures. However, we feel that for simulations of condensed phase reactions, such as electron transfer in solution, size consistency is more important than a formal connection to the semiclassical instanton. It may of course be possible to develop a method which is both size consistent and has a close connection to the semiclassical instanton, and this is an interesting avenue of future work.

As we showed in Chap. 4, Wolynes theory can be generalised to calculate reaction rates beyond the golden-rule limit, to give a non-adiabatic quantum instanton approximation, which reduces to the projected quantum instanton in the adiabatic limit.[15,16,86] The development of a generalisation of LGR, capable of treating systems with arbitrary couplings, is an important target of future work. In particular, one might speculatively hope that this would provide further insight into the development of an accurate non-adiabatic generalisation of RPMD, which is an area of active research in the field.[25–34] However, we note that, LGR can already be used to calculate reaction rates in systems with arbitrary coupling strength, by combining it with Born-Oppenheimer RPMD using the simple interpolation formula introduced in Chap. 5. Future work will look to investigate the accuracy of this approach in systems where Wolynes theory is known to break down in the golden-rule limit.

For now, LGR provides an accurate approach to calculating reaction rates in the golden-rule limit, which is straightforward to apply to condensed phase systems in both the normal and inverted regimes. In the following chapter, we shall apply it to an atomistic model of aqueous ferrous-ferric electron transfer, and compare the results to those of Wolynes theory and GR-QTST. This will allow us to assess the recent suggestion that ferrous-ferric electron transfer exhibits a range of qualitatively different tunnelling pathways, leading to a breakdown of Wolynes theory and also the assumptions of linear response inherent in the Marcus picture of electron transfer.[235] The conclusions of this study will turn out to be entirely consistent with what we have found here.

7.A Non-constant diabatic coupling

A detailed investigation of the effects of non-constant diabatic coupling, $\Delta(\boldsymbol{q})$, is unfortunately beyond the scope of this thesis. However, we note that an obvious general-

isation of Eq. 7.50, which reduces to the correct high temperature limit (Eq. 2.105) is simply given by

$$k_{\mathrm{LGR}}(\lambda) = \frac{2\pi}{\hbar}\Big\langle \Delta(\boldsymbol{q}(0))\Delta(\boldsymbol{q}(\lambda\hbar))\delta(\bar{V}_-^{(\lambda)}[\boldsymbol{q}(\tau)] + \bar{\mathcal{K}}_-^{(\lambda)}[\boldsymbol{q}(\tau)] + \epsilon)\Big\rangle_\lambda e^{-\beta F_{\mathrm{GR}}(\lambda)+\lambda\epsilon}. \tag{7.77}$$

7.B Ring-polymer discretisation

For completeness we give here the n bead discretisation of Eqs. 7.51-7.54. The diabatic energy gap averaged over the two bridging beads is simply

$$\bar{V}_{-,n}^{(l)}(\mathbf{q}) = \frac{V_-(\boldsymbol{q}_0) + V_-(\boldsymbol{q}_l)}{2}, \tag{7.78}$$

and the correction term is given by

$$\bar{\mathcal{K}}_{-,n}^{(l)}(\mathbf{q}) = \bar{\mathcal{K}}_{0,n}^{(l)}(\mathbf{q}) - \bar{\mathcal{K}}_{1,n}^{(l)}(\mathbf{q}) \tag{7.79}$$

in which

$$\bar{\mathcal{K}}_{i,n}^{(l)}(\mathbf{q}) = \frac{\mathcal{K}_{i,n}^{(l)}(\mathbf{q}, \boldsymbol{q}_0) + \mathcal{K}_{i,n}^{(l)}(\mathbf{q}, \boldsymbol{q}_l)}{2} \tag{7.80}$$

where, for $l = 1, \ldots, n-1$,

$$\mathcal{K}_{0,n}^{(l)}(\mathbf{q}, \boldsymbol{q}_j) = \sum_{k=l}^{n} w_{kl} \frac{\bar{\boldsymbol{\kappa}}_0(\boldsymbol{q}_k, \boldsymbol{q}_j)\cdot(\boldsymbol{q}_k - \boldsymbol{q}_j)}{(n-l)} \tag{7.81a}$$

$$\mathcal{K}_{1,n}^{(l)}(\mathbf{q}, \boldsymbol{q}_j) = \sum_{k=0}^{l} w_{kl} \frac{\bar{\boldsymbol{\kappa}}_1(\boldsymbol{q}_k, \boldsymbol{q}_j)\cdot(\boldsymbol{q}_k - \boldsymbol{q}_j)}{l}, \tag{7.81b}$$

and w_{kl} are the weights in Eq. 2.187. Here the effective diabatic gradients are

$$\bar{\boldsymbol{\kappa}}_i(\boldsymbol{q}_k, \boldsymbol{q}_j) = \frac{(\nabla V_i(\boldsymbol{q}_k) + \nabla V_i(\boldsymbol{q}_j))\cdot\nabla V_-(\boldsymbol{q}_j)}{2|\nabla V_-(\boldsymbol{q}_j)|^2}\nabla V_-(\boldsymbol{q}_j). \tag{7.82}$$

The end points $l = 0$ ($\lambda_0 = 0$) and $l = n$ ($\lambda_n = \beta$) are special cases, for which

$$\bar{\mathcal{K}}_{0,n}^{(l)}(\mathbf{q}) = \sum_{k=0}^{n-1} \frac{\bar{\boldsymbol{\kappa}}_0(\boldsymbol{q}_k, \boldsymbol{q}_0)\cdot(\boldsymbol{q}_k - \boldsymbol{q}_0)}{n} \tag{7.83a}$$

$$\bar{\mathcal{K}}_{1,n}^{(l)}(\mathbf{q}) = 0, \tag{7.83b}$$

and

$$\bar{\mathcal{K}}_{0,n}^{(l)}(\mathbf{q}) = 0 \tag{7.84a}$$

$$\mathcal{K}_{1,n}^{(l)}(\mathbf{q}) = \sum_{k=0}^{n-1} \frac{\bar{\boldsymbol{\kappa}}_1(\boldsymbol{q}_k, \boldsymbol{q}_0)\cdot(\boldsymbol{q}_k - \boldsymbol{q}_0)}{n}, \tag{7.84b}$$

respectively.

8

Application to aqueous ferrous-ferric electron transfer

Contents

Summary

In this chapter we revisit the well-known aqueous ferrous-ferric electron transfer reaction in order to address recent suggestions that nuclear tunnelling can lead to significant deviation from the linear response assumption inherent in the Marcus picture of electron transfer. A recent study of this reaction by Richardson and coworkers has found a large difference between their new path-integral method, GR-QTST, and the saddle point approximation of Wolynes (Wolynes theory). They suggested that this difference could be attributed to the existence of multiple tunnelling pathways, leading Wolynes theory to significantly overestimate the rate. This was used to argue that the linear response assumptions of Marcus theory may break down for liquid systems when tunnelling is important. If true, this would imply that the commonly used method for studying such systems, where the problem is mapped onto a spin-boson model, is invalid. However, as we showed in the previous chapter, a size inconsistency in GR-QTST can lead to poor predictions of the rate in systems with many degrees of freedom. Here we demonstrate that the GR-QTST results for ferrous-ferric electron transfer are indeed dominated by its size consistency error. Furthermore, by comparing the results of LGR and Wolynes theory, we confirm the established picture of nuclear tunnelling in this system. We then go on to compare our path-integral results to those obtained by mapping onto the spin-boson model, in order to reassess the importance of anharmonic effects and the accuracy of this commonly used mapping approach. Finally we consider the effect of introducing an artificial bias towards the products, and use this to test the applicability of both the LGR approach and analytic continuation of Wolynes theory for calculating reaction rates in the inverted regime in a fully atomistic simulation.

8.1 Introduction

The most commonly used approach to understand electron electron transfer, in biological, inorganic and materials chemistry, is Marcus theory.[1–9] In its basic form, the Marcus picture of electron transfer consists of two steps: spontaneous thermal fluctuations of the solvent polarisation (assumed to be harmonic) first bringing the reactant and product

charge transfer states to the same energy, followed by a golden-rule transition from one charge transfer state to the other.[46–49] While there are many analytical theories which go beyond the simplest form of Marcus theory, for example by including nuclear quantum effects,[53–62] the majority still assume that the relaxation of the solvent polarisation (or diabatic energy gap) can be treated within linear response theory, which is equivalent to assuming a harmonic (spin-boson) model for the diabatic potentials.[236]

Perhaps the prototypical example of electron transfer, commonly used to introduce Marcus theory in undergraduate text books,[237,238] is the aqueous ferrous-ferric electron transfer reaction,*

$$\mathrm{Fe}^{2+}(\mathrm{aq}) + \mathrm{Fe}^{3+}(\mathrm{aq}) \rightarrow \mathrm{Fe}^{3+}(\mathrm{aq}) + \mathrm{Fe}^{2+}(\mathrm{aq}), \tag{8.1}$$

which, along with other similar self-exchange reactions, has been the subject of numerous theoretical studies.[84,107,109–111,239–245] In the classical limit the pioneering atomistic studies of ferrous-ferric electron transfer by Chandler and coworkers demonstrated that the assumptions of Marcus theory are well founded.[107,241] By calculating the free-energy as a function of solvent polarisation they showed that the resulting surfaces were essentially parabolic in line with the Marcus assumption,[107] and by studying the solvent relaxation immediately after electron transfer they were able to illustrate the close agreement between the exact and linear response results.[241]

In addition to investigating the ferrous-ferric system in the classical limit, Chandler and coworkers also carried out one of the first atomistic studies of the influence nuclear tunnelling on electron transfer.[84] In this work, they used imaginary-time path-integral simulations to directly calculate the Wolynes theory[82] approximation to the electron transfer rate, as well as performing classical equilibrium simulations to map the problem onto the spin-boson model. Mapping the problem onto the spin-boson model provides an alternative approach to calculating the influence of nuclear tunnelling on the electron transfer rate, as once the problem has been mapped the exact quantum mechanical golden-rule rate can simply be evaluated using Eq. 2.217. Mapping to the spin-boson Hamiltonian is equivalent to assuming the relaxation of the solvent polarisation can be described via

*Note that consistent with previous studies we will take ferrous-ferric electron transfer to be well described by the golden-rule limit throughout this chapter.

linear response. It provides a simple way to estimate nuclear quantum effects from classical atomistic simulations, by calculating the spectral density from the classical energy gap autocorrelation function in the reactant ensemble.[246,247] This approach has since become a popular way to use atomistic simulation to study electron transfer, finding application in a diverse range of problems from electron transfer in enzymes to device physics.[3,109,248–251] Using both methods Chandler and coworkers found surprisingly large tunnelling enhancements of the ferrous-ferric electron transfer rate, with Wolynes theory predicting a quantum enhancement factor of ~60 and the spin-boson mapping a factor of ~40 at room temperature.[84] These large quantum enhancements proved quite controversial and have since been the focus of several papers.[111,242,243] The general consensus that has emerged from these papers is that the large enhancement is due to a lack of polarisability in the SPC water model that Chandler and coworkers used in their calculations.[84] Unfortunately, unlike in the classical limit where the approximations of Marcus theory can be validated using the exact classical golden-rule rate, in the quantum regime it is not possible to calculate the exact quantum rate for anything beyond simple model systems and hence the accuracy of Wolynes theory and mapping onto the spin-boson model can only be inferred indirectly.

As we discussed in the previous chapter, Richardson and coworkers have reassessed the accuracy of Wolynes theory, and have pointed out that its Gaussian (saddle point) approximation can breakdown severely for systems with multiple transition states.[233] As an alternative to Wolynes theory, they have suggested a new path-integral based approach, GR-QTST.[232,233] They have shown that, for low-dimensional model systems designed to exhibit multiple transition states as well as significant nuclear quantum effects, GR-QTST gives accurate rate predictions, while Wolynes theory can overestimate the rate by more than two orders of magnitude.[233] On applying GR-QTST to a fully atomistic model of ferrous-ferric electron transfer, they found a tunnelling enhancement around 7 times smaller than that of Wolynes theory, and used this to argue that Wolynes theory may be overestimating the rate due to the presence of multiple tunnelling pathways.[235] This is a significant claim, because if true it would imply that the picture offered by the spin-boson model was not only quantitatively inaccurate, but also qualitatively incorrect.[235]

In the previous chapter, however, we have demonstrated that GR-QTST can suffer from a serious size inconsistency issue for large systems. Here we argue that it is this size inconsistency that is responsible for the large difference between the Wolynes and GR-QTST predictions of the rate in ferrous-ferric electron transfer, rather than a breakdown of Wolynes theory. To support this argument, and help assess both the accuracy of Wolynes theory and the spin-boson mapping for this system, we also apply an alternative path-integral method, the linear golden-rule (LGR) approximation. Since it is both size consistent and does not assume the correlation function is Gaussian, LGR provides an independent way to assess whether the assumptions of Wolynes theory break down in ferrous-ferric electron transfer and to assess the accuracy of the spin-boson mapping method for including nuclear quantum effects in condensed phase electron transfer reactions.

Sec. 8.2 gives an overview of the mapping approach. Sec. 8.3 provides some details of our simulations of the ferrous-ferric system. Sec. 8.4 analyses how a lack of size consistency in GR-QTST affects its prediction of the ferrous-ferric rate, and investigates the recent suggestion that Wolynes theory is breaking down for this reaction.[235] Sec. 8.5 reassesses the validity of the spin-boson mapping in the light of the preceding sections. In Sec. 8.6 we consider the effect of an external bias on the reaction rates and investigate the applicability of these methods to calculate reaction rates in the inverted regime. Sec. 8.7 concludes the chapter.

8.2 Mapping to the spin-boson model

The spin-boson model assumes that from the perspective of the electron transfer the nuclear potentials in both charge transfer states can be modelled as being purely harmonic with the same frequencies in both states,

$$V_0(\boldsymbol{q}) = \sum_{\nu=1}^{f} \frac{1}{2} m\omega_\nu^2 q_\nu^2 + c_\nu q_\nu \tag{8.2a}$$

$$V_1(\boldsymbol{q}) = \sum_{\nu=1}^{f} \frac{1}{2} m\omega_\nu^2 q_\nu^2 - c_\nu q_\nu - \Delta F, \tag{8.2b}$$

where we have introduced the intrinsic bias $\Delta F = F_{\mathrm{GR}}(0) - F_{\mathrm{GR}}(\beta)$; note that for the ferrous-ferric electron transfer considered here $\Delta F = 0$. The effect of the nuclear dynamics on the electronic coordinate is then completely described by the spectral density, which is formally defined as

$$J(\omega) = \frac{\pi}{2} \sum_{\nu=1}^{f} \frac{c_\nu^2}{m\omega_\nu} \delta(\omega - \omega_\nu), \tag{8.3}$$

and the exact rate can be calculated using[53,54,59–61]

$$\frac{c_{\mathrm{GR}}(t)}{Q_r} = \exp(-i(\epsilon + \Delta F)t/\hbar - \phi(t)/\hbar), \tag{8.4}$$

where

$$\phi(t) = \frac{4}{\pi} \int_{-\infty}^{\infty} \frac{J(\omega)}{\omega^2} \left[\frac{1 - \cos(\omega t)}{\tanh(\beta\hbar\omega/2)} - i \sin(\omega t) \right] \mathrm{d}\omega. \tag{8.5}$$

To map a real system onto the spin-boson model one must therefore choose a method for defining the spectral density of the system. There are many ways that this can be achieved, using either simulation or experimental data.[59,243,252] The approach we will focus on here is the use of classical molecular dynamics to define the spectral density according to the relation[3,84,246]

$$\frac{J(\omega)}{\omega} = \frac{\Lambda}{2} \int_0^{\infty} \frac{\langle \delta V_-(0)\, \delta V_-(t) \rangle_{\mathrm{cl},0}}{\langle \delta V_-^2(0) \rangle_{\mathrm{cl},0}} \cos(\omega t) \mathrm{d}t. \tag{8.6}$$

Here the averages are taken in the classical canonical ensemble of the reactants, $V_-(t) = V_0(t) - V_1(t)$ is the energy gap between the reactant and product diabats at time t along a microcanonical trajectory sampled from this ensemble, and the energy gap fluctuation is defined as

$$\delta V_-(t) = V_-(t) - \langle V_- \rangle_{\mathrm{cl},0}. \tag{8.7}$$

The Marcus theory reorganisation energy Λ in Eq. 8.6 is taken to be

$$\Lambda = \Delta F - \langle V_- \rangle_{\mathrm{cl},0}, \tag{8.8}$$

with the driving force given by

$$\Delta F = \frac{1}{\beta} \ln \left(\frac{\mathrm{tr}_{\mathrm{cl}} \left[e^{-\beta H_1} \right]}{\mathrm{tr}_{\mathrm{cl}} \left[e^{-\beta H_0} \right]} \right), \tag{8.9}$$

which is clearly zero for the symmetric ferrous-ferric system we shall consider here.

(We note in passing that an alternative choice of mapping gives the Marcus theory reorganisation energy as

$$\Lambda_2 = \frac{\beta}{2}\langle \delta V_-(0)\, \delta V_-(0)\rangle_{\mathrm{cl},0}. \tag{8.10}$$

While this is equivalent to Eq. 8.8 for the spin-boson model, the two expressions differ for more realistic (atomistic and anharmonic) models of electron transfer. For completeness Appendix 8.A gives a detailed discussion of the origin of this choice of mapping, including a discussion of why Eq. 8.8 is to be preferred over Eq. 8.10).

There are a number of obvious difficulties with trying to map a complex anharmonic system onto a model as simple as the spin-boson model. While it may be reasonable for a symmetric reaction such as ferrous-ferric electron transfer to treat the reactants and product states as having the same frequencies, it is not clear that this should be valid for asymmetric reactions. Furthermore it is not clear how well in general, even for a symmetric reaction such as ferrous-ferric electron transfer, the motion to the transition state can be described by a collection of small fluctuations from equilibrium, given that the underlying potential is anharmonic.

8.3 Computational details

The model of ferrous-ferric electron transfer we consider here is chosen to be the same as that considered in the study of Richardson and coworkers in which they found a large difference between the GR-QTST and Wolynes theory rates.[235] The system consists of 265 water molecules in a periodic cubic box of length 20 Å at 300 K. The Fe^{2+} and Fe^{3+} ions are fixed at a distance of 5.5 Å in the centre of the box, with the internuclear axis parallel to the edge of the box. The water model is the flexible q-TIP4P/F model (designed for use with path-integral simulations),[253] and the interatomic potential for the water-Fe interaction is the same as in the original study by Chandler and coworkers.[84,107,241] Consistent with these previous studies we assume that the diabatic coupling can be taken as a constant and that the reaction can be treated as being in the golden-rule limit. As was discussed by Richardson and coworkers, this model is not designed to give a quantitatively

accurate description of the real system. In addition to artificially fixing the positions of the Fe ions, the lack of polarisability and the relatively small size of the system are expected to lead to significant errors in the predicted reorganisation energy.[111,242,243] Despite this, the model provides a useful test of methods for calculating reaction rates in complex systems, and a qualitative representation of the physical system that will be sufficient to address the key questions of this chapter (whether the assumptions of Wolynes theory are valid, and whether ferrous-ferric electron transfer can be mapped onto the spin-boson model).

The system was first equilibrated for 1 ns in the classical canonical ensemble, from which we took 10 configurations equally spaced in time from the final 0.5 ns to initialise the path-integral simulations. Following Ref. 235 all path-integral simulations were found to be converged using $n = 24$ beads and a time step of 0.5 fs was used throughout. Each of the 10 initial configurations was equilibrated in the path-integral ensemble for a further 7 ps before the production runs were performed. Calculations of $F'(\lambda)$ were performed for 13 equally spaced points with $\lambda \in [0, \beta/2]$. At each value of λ an additional 7 ps of equilibration was performed starting from the final configuration from the previous value of λ. All the necessary ensemble averages were then accumulated in a final production run at each value of λ amounting to 700 ps of simulation time. All path-integral simulations were performed using the Cayley integrator with a Langevin thermostat.[254,255]

We find the Marcus reorganisation energy calculated using Eq. 8.8 to be $\Lambda = 110.3 \pm 0.3$ mHartree, and that calculated using Eq. 8.10 to be $\Lambda_2 = 113.7 \pm 0.3$ mHartree. Both are the same to within the error bars as those found by Richardson and coworkers.[235] The close agreement between the two definitions of the reorganisation energy indicates that in the classical limit ferrous-ferric electron transfer is well described by the spin-boson model, in agreement with previous studies.[107,241] As discussed above the large value of the reorganisation energy for the present model, 3.0 eV, compared to the experimental estimate of 2.1 eV, can be attributed in large part as being due to the lack of polarisability of the q-TIP4P/F water model.[111,242,243]

8.4 In defence of Wolynes theory

In this section we shall address the recent finding, in the study by Richardson and coworkers,[235] of a large discrepancy between the rates predicted by Wolynes theory and GR-QTST for ferrous-ferric electron transfer. This was used to argue that the assumptions of Wolynes theory may be breaking down for this system, leading to an overestimate of the exact rate. Here we will demonstrate that the opposite is true. In fact it is GR-QTST which is breaking down and the assumptions of Wolynes theory are well justified. We begin by demonstrating that the lack of size consistency in GR-QTST dominates its estimate of the rate, before using a comparison of the results of Wolynes theory and LGR to demonstrate that the Wolynes theory result is highly accurate for this system.

8.4.1 Size consistency error in GR-QTST

As we have shown in the previous chapter, GR-QTST is not size consistent: its prediction of the rate can be affected by degrees of freedom which are entirely uncoupled from the reaction. We found that this issue has only a relatively small effect on the GR-QTST rate for low dimensional models, however we expect it to become much more pronounced for realistic simulations which contain thousands of degrees of freedom. We thus believe that this size consistency issue is leading GR-QTST to underestimate the exact rate for the model of ferrous-ferric electron transfer described above.

To understand this issue we need to consider the pre-factor in the GR-QTST rate. To this end let us define the probability distribution

$$p_{\text{GR-QTST},\lambda}(E) = \left\langle \delta\left(\frac{2}{3}\left(\mathcal{E}_0^{(\lambda)} - \mathcal{E}_1^{(\lambda)}\right) + E\right)\right\rangle_\lambda , \tag{8.11}$$

for which $p_{\text{GR-QTST},\lambda}(0) = \rho_{\text{GR-QTST},\lambda}(0)$. In order to evaluate the probability distribution $p_{\text{GR-QTST},\lambda}(E)$, one simply histograms the constraint functional $\frac{2}{3}(\mathcal{E}_0^{(\lambda)} - \mathcal{E}_1^{(\lambda)})$ in the appropriate ensemble. The lack of size consistency of GR-QTST arises because the value of $p_{\text{GR-QTST},\lambda}(0)$ – the probability density for the virial energy on one half of the ring polymer to be the same as that on the other – is in general dependent on all of the degrees of freedom in the simulation, and not just those which are involved in the reaction. To see why this leads to a lack of size consistency note that, even for an electronically adiabatic

reaction with only one electronic state, the two halves of the ring polymer do not have the same instantaneous virial energies. Because the spontaneous energy fluctuations are size extensive, for a large enough system, the difference in virial energy between the two halves of the ring polymer will be dominated by these fluctuations rather than the difference between the diabatic potentials. Therefore, instead of constraining the system to the transition state, the GR-QTST constraint becomes dominated by quantum energy fluctuations in degrees of freedom entirely uncoupled from the reaction.

To show that this lack of size consistency is dominating the GR-QTST calculation for ferrous-ferric electron transfer, we need to demonstrate that the spontaneous fluctuations are indeed dominating $p_{\text{GR-QTST},\lambda}(E)$. To do this we consider a modified system in which the reactant and product electronic states are the same, and hence the nuclear dynamics are uncoupled from any electron transfer reaction. We define the nuclear potentials for this uncoupled system as the average of the two diabatic potentials in the real system,

$$V_{\text{u},0}(\boldsymbol{q}) = V_{\text{u},1}(\boldsymbol{q}) = \frac{V_0(\boldsymbol{q}) + V_1(\boldsymbol{q})}{2}, \tag{8.12}$$

which of course just corresponds to both iron ions being $Fe^{2.5+}$. Since both electronic states are the same, $\hat{H}_{\text{u},0} = \hat{H}_{\text{u},1}$, and the exact distribution for the uncoupled model is simply $\rho_\lambda(E) = \delta(E)$. It is clear that GR-QTST cannot satisfy this exactly, but in order for it to be accurate when applied to the real ferrous-ferric electron transfer, it must hold approximately. This means that we must have $p_{\text{GR-QTST},\lambda}(E) \simeq \delta(E)$ for the uncoupled model, i.e. the variance must be much smaller than the variance of the exact distribution (which is on the order of Λ/β).

Figure 8.1 compares the distribution $p_{\text{GR-QTST},\lambda}(E)$ for both the real ferrous-ferric system and for the uncoupled system, in which the two diabatic electronic states are the same. We see that, not only is the variance of $p_{\text{GR-QTST},\lambda}(E)$ in the uncoupled system not significantly smaller than in the real system, but it is actually essentially the same, indicating that spontaneous quantum fluctuations in the energy are dominating the GR-QTST constraint functional and hence the GR-QTST approximation of $\rho_\lambda(0)$. This demonstrates clearly that the GR-QTST rate is not a reliable approximation to the exact rate for this system, and hence cannot be used to assess the accuracy of Wolynes theory or mapping to the spin-boson model.

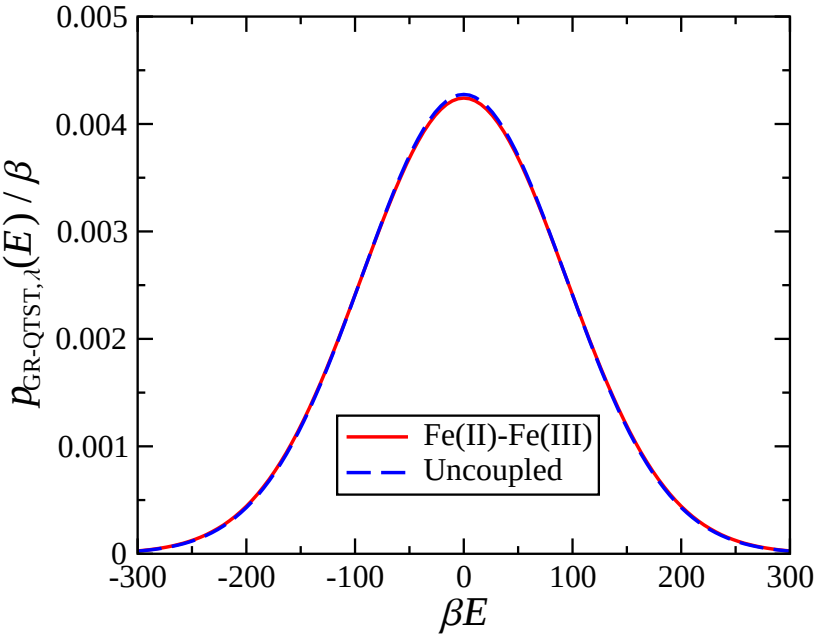

Figure 8.1: Comparison of the GR-QTST distribution (Eq. 8.11) for both the real Fe(II)-Fe(III) system and for an uncoupled system in which the nuclear potentials are the same in both diabatic states (corresponding to both iron ions having a charge of 2.5). The close agreement between the two curves illustrates that the size consistency error of GR-QTST is dominating the calculation of the rate in ferrous-ferric electron transfer. Note for reference that $\beta\Lambda \simeq 116$.

8.4.2 Accuracy of Wolynes theory

Although we have demonstrated that the GR-QTST rate is not reliable for ferrous-ferric electron transfer this does not, by itself, disprove the suggestion that Wolynes theory is overestimating the exact rate. One way to address this possibility is to apply a method which does not assume that the correlation function is Gaussian and compare the results with Wolynes theory. Whilst GR-QTST cannot be used for this purpose, we can apply the LGR approximation, which although closely related to GR-QTST is size consistent. In addition to providing a useful way to independently assess the assumptions of Wolynes theory, this will also serve as the first demonstration of the applicability of LGR to a fully atomistic simulation.

Table 8.1 compares the rate constants for ferrous-ferric electron transfer calculated using each of the methods under consideration. Just as in the study by Richardson and

Table 8.1: Comparison of the rate constants for each of the methods considered, given in atomic units. Note that errors are given as two standard errors in the mean.

	k_{GR}/Δ^2
Classical	$5.4 \pm 0.6 \times 10^{-11}$
Marcus	$4.3 \pm 0.4 \times 10^{-11}$
Wolynes	$3.9 \pm 0.6 \times 10^{-9}$
LGR	$3.7 \pm 0.6 \times 10^{-9}$
SB Mapping	$2.8 \pm 0.3 \times 10^{-9}$
GR-QTST	$5.3 \pm 0.8 \times 10^{-10}$

coworkers,[235] we find that Wolynes theory predicts a rate which is around 7 times larger than that predicted by GR-QTST. In contrast, the Wolynes rate is only about 5% larger than the LGR rate. The close agreement of Wolynes theory and LGR, which are based on very different approximations, is a strong indication that the assumptions of Wolynes theory are likely to be valid for ferrous-ferric electron transfer. We would also note that the errors given in Table 8.1 are dominated by the thermodynamic integration of $F'_{\mathrm{GR}}(\lambda)$ to give $e^{-\beta F_{\mathrm{GR}}(\lambda_{\mathrm{sp}})}$, and hence we can give a much more detailed comparison of the methods by separately considering their approximations to $\rho_{\lambda_{\mathrm{sp}}}(E)$.

The upper panel of Fig. 8.2 compares the LGR and Wolynes theory approximations to $\rho_\lambda(E)$ with $\lambda = \lambda_{\mathrm{sp}} = \beta/2$. It is clear that both agree very closely, with LGR having an approximately Gaussian functional form. Using the fact that the distribution is just the Fourier transform of the correlation function we can also compare the Wolynes and LGR approximations to the normalised correlation function, by taking the inverse Fourier transform to give

$$\frac{c_\lambda(t)}{c_\lambda(0)} = \int_{-\infty}^{\infty} \rho_\lambda(E) e^{+iEt/\hbar} \mathrm{d}E. \tag{8.13}$$

The LGR and Wolynes correlation functions are shown in the lower panel of Fig. 8.2 and unsurprisingly we find that the LGR correlation function looks essentially like a Gaussian in the time domain as well, again indicating that the assumptions of Wolynes theory are valid. The small 5% difference in the rates of the two methods is visible in

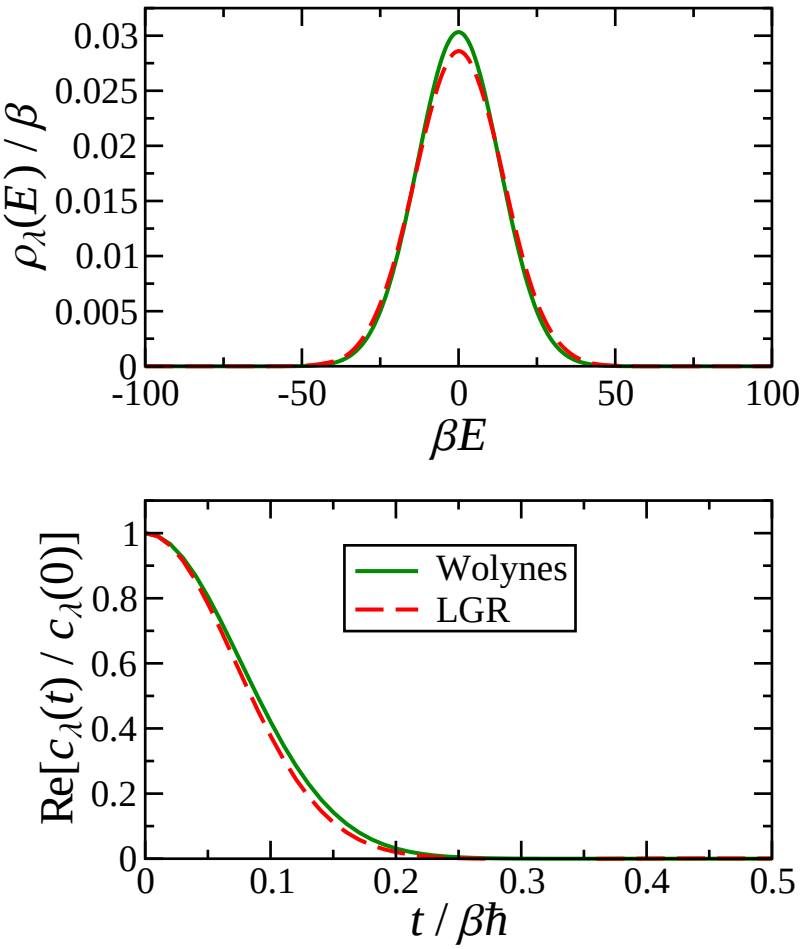

Figure 8.2: LGR and Wolynes theory approximations to $\rho_\lambda(E)$ (upper panel) and Re$[c_\lambda(t)/c_\lambda(0)]$ (lower panel) for the present atomistic model of ferrous-ferric electron transfer. In both panels calculations are done with $\lambda = \lambda_{\rm sp} = \beta/2$, using 24 path-integral beads.

both panels, from the relative heights of the distributions and areas under the correlation functions. What is difficult to see by eye is whether this difference is due to the LGR correlation function not being perfectly Gaussian, or if it is due to a small error in the LGR approximation to the second moment of the exact distribution, $\rho_\lambda(E)$.

Since LGR does not in general give the exact first and second moments of the distribution $\rho_\lambda(E)$,* one test of its accuracy is to compare the rates obtained using the original LGR distribution with those obtained using a corrected LGR distribution in which

*For ferrous-ferric electron transfer, the LGR approximation to the first moment of the distribution $\rho_\lambda(E)$ is correct at $\lambda = \lambda_{\rm sp} = \beta/2$ by symmetry, but the LGR approximation to the second moment is slightly off.

the first and second moments are adjusted to the exact results. This can be achieved by defining the "moment corrected LGR" distribution according to

$$\rho_{\text{mc-LGR},\lambda}(E) = \sqrt{\frac{\tilde{\mu}_{2,\lambda}}{\mu_{2,\lambda}}}\rho_{\text{LGR},\lambda}\left(\sqrt{\frac{\tilde{\mu}_{2,\lambda}}{\mu_{2,\lambda}}}(E-\mu_{1,\lambda})+\tilde{\mu}_{1,\lambda}\right) \tag{8.14}$$

where

$$\tilde{\mu}_{1,\lambda} = \int_{-\infty}^{\infty} E\rho_{\text{LGR},\lambda}(E)\mathrm{d}E \tag{8.15}$$

and

$$\tilde{\mu}_{2,\lambda} = \int_{-\infty}^{\infty} (E^2-\tilde{\mu}_{1,\lambda}^2)\rho_{\text{LGR},\lambda}(E)\mathrm{d}E. \tag{8.16}$$

We find that the moment corrected LGR rate agrees with the Wolynes theory rate to within 1%, indicating that the small difference between the LGR and Wolynes theory rates is almost entirely due to the small error in the LGR approximation to $\mu_{2,\lambda}$. This therefore strongly supports the assertion that the Wolynes theory approximation is valid for ferrous-ferric electron transfer.

It is now clear that the difference between the GR-QTST rate and the Wolynes rate for ferrous-ferric electron transfer is due to GR-QTST underestimating the exact rate rather than Wolynes theory overestimating it. The error in GR-QTST originates from the fluctuations in the virial energies of modes uncoupled to the reaction, which dominate the GR-QTST constraint functional. Given this perspective it seems natural to ask whether these background fluctuations can be subtracted from the GR-QTST calculation to yield an accurate rate. In particular, the above discussion would seem to suggest that the small difference between the GR-QTST distribution for the real system and the uncoupled system in Fig. 8.1 should be related to the "correct" GR-QTST result. That is, the result that would be obtained if the contribution from the uncoupled modes could be removed. A detailed discussion of how this can be done is left to Appendix 8.B, but the result is that one can indeed approximately remove the spurious background signal from the GR-QTST distribution. In doing so, we find that the resulting corrected GR-QTST rate is about 10% larger than the Wolynes rate, rather than 7 times smaller. This further confirms our assertion that it is GR-QTST and not Wolynes theory that is breaking down for this problem.

8.5 Validity of mapping to the spin-boson model

The study by Richardson and coworkers also concluded that the common practice of mapping to the spin-boson model is invalid for ferrous-ferric electron transfer.[235] In this section we give an overview of their arguments, and discuss how their results can be reinterpreted in the light of our present findings. We then go on to reassess the validity of mapping to the spin-boson model for ferrous-ferric electron transfer and discuss what conclusions can be drawn for more general systems. When it comes to assessing the validity of the mapping there are two main questions one might ask: is the spin-boson perspective qualitatively accurate, and can it give quantitatively accurate predictions of the rate?

Richardson and coworkers used the difference between the Wolynes theory results and GR-QTST results to argue that mapping to the spin-boson model was invalid.[235] Their argument focussed on the close agreement between GR-QTST and Wolynes theory in a previous study, which consisted of a series of different spin-boson models, as evidence that the ferrous-ferric system could not be spin-boson like. However, that previous study only looked at spin-boson models with up to 8 degrees of freedom,[232] compared to the over 2000 degrees of freedom in their atomistic model of ferrous-ferric electron transfer.[235] As we have demonstrated in the previous chapter, the size consistency error of GR-QTST only becomes apparent when there a large number of uncoupled degrees of freedom. Hence the difference between GR-QTST and Wolynes theory for ferrous-ferric electron transfer cannot be used to argue that mapping to a spin-boson model is invalid for this problem.

In order to provide further evidence that Wolynes theory was breaking down in their ferrous-ferric simulation, and to justify the claim that it is not valid to map this problem onto a spin-boson model, Richardson and coworkers also performed an instanton analysis.[235] They took a series of configurations from an equilibrium simulation and fixed all atoms more than 5Å away from the Fe ions, before performing an instanton optimisation on the remaining degrees of freedom. They found that the resulting instantons had a wide range of different saddle point values, λ_{sp}, which they used to argue that the system exhibits a continuum of different transition states with different

Table 8.2: Quantum correction factors for the different methods considered in this chapter. In order to provide a fair comparison, the quantum correction factors for the atomistic methods are defined relative to the atomistic classical golden-rule rate, whereas the spin-boson quantum correction factor is defined relative to the classical golden-rule rate for the same spin-boson model (i.e. Marcus theory).

	Γ
Wolynes	73 ± 14
LGR	69 ± 13
SB Mapping	66 ± 2
GR-QTST	10 ± 2

tunnelling characters.[235] However, we note that if one were to do the same thing to the spin-boson model, for example by fixing the coordinates of some of the bath modes at configurations sampled from an equilibrium simulation, one would also see a range of different saddle points. Fixing some degrees of freedom stops them from relaxing and reduces the reorganisation energy, while also giving a random bias either to products or reactants. The different biases then lead to a range of different saddle points, and the distribution of these saddle points is further broadened by the reduced reorganisation energy. Since the spin-boson model is known to have just a single instanton at any given temperature, this seems to us to refute the claim that the same analysis can be used to show that the ferrous-ferric problem has multiple transition states.

With this established, let us now return to the qualitative Marcus picture of electron transfer, in which collective solvent motion takes the system to the transition state. This picture is strongly supported by the close agreement between the classical golden-rule and Marcus theory rates, and the Wolynes theory and quantum mechanical spin-boson rates, in Table 8.1. However, this close agreement is not perfect in either (classical or quantum) case: we find small but significant quantitative differences between the atomistic and spin-boson-mapped calculations, reflecting the fact that the real potential energy surface is anharmonic.

Anharmonic effects are also apparent in the difference between the two definitions of the Marcus reorganisation energy, Λ and Λ_2 [Eqs. 8.8 and 8.10, respectively]. Although

there is only a 3% difference between the two, the rates predicted by Λ_2 are significantly less accurate – more than a factor of 2 smaller in both the classical and quantum cases – because using Λ_2 overestimates the activation energy of the reaction. This highlights the fact that the quality of the mapping is strongly dependent on how well it captures the activation energy. In fact, if we adjust the reorganisation energy so that Marcus theory agrees with the exact classical golden-rule rate (corresponding to $\Lambda = 109.45$ mHartree), this also brings the quantum rate predicted by the spin-boson model up to agree with the Wolynes and LGR predictions to within their error bars, giving $k_{\mathrm{GR}}/\Delta^2 \simeq 3.5 \times 10^{-9}$ atomic units. Hence, we find that accounting for the small anharmonic effects in an average manner can make mapping to the spin-boson model essentially quantitative for this model of ferrous-ferric electron transfer.

Table 8.2 shows the quantum correction factors, $\Gamma = k_{\mathrm{GR}}/k_{\text{cl-GR}}$, obtained using each of the methods discussed in this chapter. It is worth noting that the quantum correction factors predicted by Wolynes theory, LGR and the spin-boson mapping, are much larger than the experimental estimates. As we have now demonstrated the accuracy of these approaches, it follows that this difference is caused by deficiencies in the atomistic model we have used, and as has been discussed at length before this is likely due in large part to a lack of polarisability in the water model.[111,242,243] The inclusion of polarisability is expected to significantly reduce the reorganisation energy and hence the importance of tunnelling in the system. These changes are likely to make the assumptions behind mapping to a spin-boson model more rather than less reliable, and hence we expect that the results found here are transferable to more realistic models.

Despite the fact that we find mapping to the spin-boson model can be quantitatively accurate for ferrous-ferric electron transfer, our results have highlighted the sensitivity of the mapping to the exact approach used. It is clear that for any system in which there are modes involved in the reaction that are strongly anharmonic the mapping will be less reliable. Furthermore, even for systems in which the reactants and products can be treated as essentially harmonic, there may be situations in which they have different frequencies, which will again make the spin-boson model less reliable. Whilst there exist many asymmetric generalisations of basic Marcus theory,[256–258] the importance of

nuclear quantum effects in electron transfer can be very pronounced, and hence for any theory to be quantitatively accurate it must be able to capture both asymmetry and nuclear tunnelling. Unlike mapping to the spin-boson model, the path-integral methods we have used in this chapter have no difficulty in dealing with more complicated systems, and hence provide a useful tool in the study of complex electron transfer reactions in solution.

8.6 Effect of an external bias to products

Before we conclude the chapter we briefly consider the effect of an external bias to products ϵ on the reaction rate. This will allow us to demonstrate the applicability of the methods discussed for calculating reaction rates in the Marcus inverted regime in the previous two chapters to a fully atomistic simulation. The LGR rates are thus calculated using $\lambda = 0$ for $\lambda_{\text{sp}} < 0$, and the Wolynes theory rates are calculated by fitting the imaginary-time data for $F'_{\text{GR}}(\lambda)$ and $F''_{\text{GR}}(\lambda)$ to Eq. 6.10 using Eq. 6.15 with $N = 3$ terms. As well as the LGR and Wolynes rates we also calculate the Marcus theory rate, with a reorganisation energy of $\Lambda = 110.3$ mHartree, in order to illustrate the relative importance of nuclear quantum effects at different driving forces. Unlike in the previous chapters we are of course unable to calculate the exact rates in order to validate the results of LGR and Wolynes theory. In the absence of exact results, we also calculate the rates predicted by the spin-boson mapping in order to further validate the LGR and Wolynes results. To ensure that they are as accurate as possible, the mapping rates are calculated using the adjusted reorganisation energy, $\Lambda = 109.45$ mHartree, chosen to reproduce the correct classical activation energy at $\epsilon = 0$.

Figure 8.3 compares the LGR, Wolynes theory, spin-boson mapping and Marcus theory rates as a function of the external driving force relative to the Marcus theory reorganisation energy, $\Lambda = 110.3$ mHartree. The LGR and Wolynes theory rates show very close agreement at all values of the driving force considered, with the largest difference occurring at $\epsilon/\Lambda = 2$, where the LGR rate is just over a factor of 2 larger than the Wolynes results. This is not an unreasonable difference, particularly considering that the quantum rates are around 8 orders of magnitude larger than the Marcus theory rate at this driving force. In fact the Wolynes and spin-boson mapping results agree

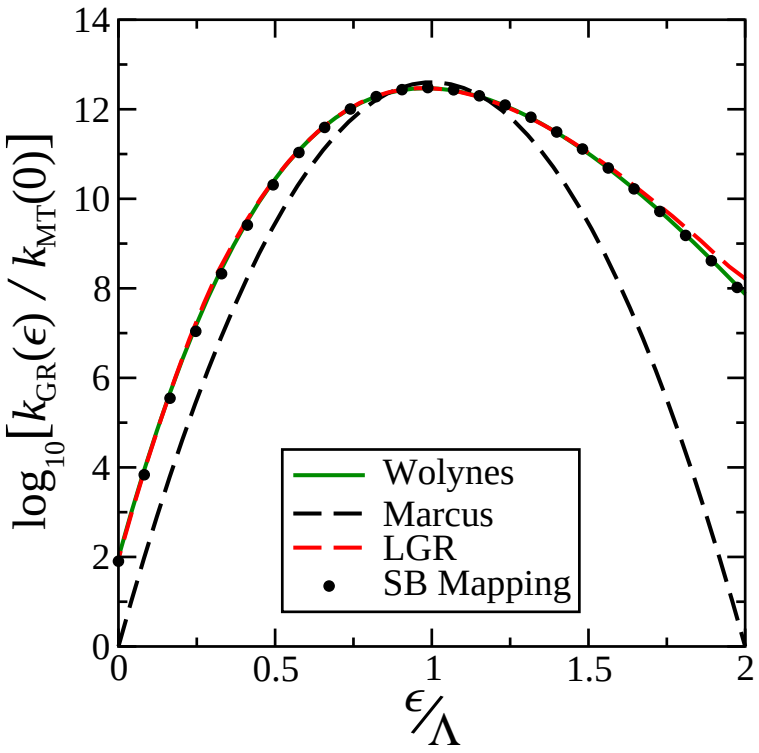

Figure 8.3: Comparison of Wolynes, LGR and Mapping rates as a function of the external driving force, ϵ/Λ, for the ferrous-ferric system, where the Marcus theory reorganisation energy has been defined as $\Lambda = 110.3$ mHartree. Wolynes theory rates are calculated by the fitting procedure described in Chap. 6, using Eq. 6.10 with $N = 3$ terms. Note that the SB mapping results given here are those with the reorganisation energy, $\Lambda = 109.45$ mHartree, adjusted so that the classical and Marcus rates agree at $\epsilon = 0$.

even more closely, and are differ by no more than a factor of 1.5 at all driving forces considered. This close agreement is perhaps unsurprising given that the ansatz used to fit the imaginary-time data is based on the exact result for the spin-boson model, and hence both approaches can be considered as mapping to a spin-boson model. However, the two approaches use different information, and hence the close agreement between the Wolynes and spin-boson mapping results further support the view that the ferrous-ferric system is very well described by a spin-boson model. As such it seems likely that the LGR results are the least accurate of the three approaches deep in the inverted regime, and this would be consistent with the results in the previous chapter where for a similar quantum enhancement the LGR rate was also about a factor of 2 too large.

8.7 Conclusion

For at least 30 years the standard picture of ferrous-ferric electron transfer has been based on linear response theory. Whilst this has been rigorously tested in the high temperature limit where it is possible to calculate all quantities exactly,[84,107,241] it has previously just been assumed that the same approach would carry over to the quantum regime. This assumption has recently been thrown into doubt by the study of Richardson and coworkers,[235] which has suggested that when nuclear tunnelling is important the assumptions of linear response theory may break down due to the existence of a range of tunnelling paths with qualitatively different behaviour. This would imply that, not only was the common practice of mapping electron transfer reactions onto the spin-boson model quantitatively wrong, but also qualitatively so. In this chapter we have addressed these suggestions and confirmed that the linear response assumption in aqueous ferrous-ferric electron transfer is well justified, even in the presence of significant tunnelling.

Richardson and coworkers have previously shown that the saddle point approximation of Wolynes theory can breakdown for systems which exhibit multiple distinct transition states.[233] By showing that GR-QTST and Wolynes theory give very different predictions of the electron transfer rate in ferrous-ferric electron transfer, they argued that this may be due to the existence of multiple transition states, which would be at odds with the assumptions of linear response and hence mapping onto the spin-boson model. Here we have demonstrated that the difference between GR-GTST and Wolynes theory is due to a size consistency error on the part of GR-QTST, and by comparing with an alternative path-integral method, LGR, we have confirmed the accuracy of Wolynes theory. Just as in the original study by Chandler and coworkers,[84] we have found a tunnelling enhancement that is much larger than inferred from experiment. This is most likely due to the lack of polarisability in the water models used in this study and in Ref. 84, and also to the relatively small sizes of the simulations. The model we have investigated is thus not entirely realistic. However, it is clear from the error it has revealed in GR-QTST that it provides a useful test for methods designed to treat non-adiabatic systems, and given that the Wolynes theory results are very accurate for this model it could provide

a useful benchmark for testing other methods in the future. In this spirit, by applying an external bias, we have also tested the LGR and numerical analytic continuation approaches, developed in the preceding chapters, to the calculation of reaction rates in the Marcus inverted regime. The close agreement between both methods, despite quantum enhancements of more than 7 orders of magnitude, indicates that these approaches provide a viable approach to calculating reaction rates in the inverted regime in complex systems.

Comparison of our path-integral results with those from mapping to the spin-boson model show small deviations from the harmonic assumption. We find that these deviations are sufficiently small that they can be essentially accounted for, in an average sense, by choosing the Marcus reorganisation energy so as to give the correct classical activation energy. However our results highlight that even small anharmonic effects can lead to significant changes in the rate, and we note that these effects are likely to be much more pronounced in systems which are more complex than aqueous ferrous-ferric electron transfer. In particular if the reactants and products have different frequencies or if there are modes important in the electron transfer which show more pronounced anharmonicity, such as conformational changes which couple to the electron transfer, then mapping onto the spin-boson model is likely to breakdown.[259,260] In contrast path-integral approaches such as Wolynes theory and the LGR approximation provide a simple approach to the calculation of electron transfer rates in complex systems.

8.A Mapping to the spin-boson model

In this appendix we give a discussion of the basis for mapping electron transfer onto a spin-boson model via classical equilibrium simulation. In order to derive the standard mapping we begin by writing the rate in the form

$$k = \frac{\Delta^2}{\hbar^2}\int_{-\infty}^{\infty}\left\langle e^{-i\hat{H}_0 t/\hbar}e^{+i\hat{H}_1 t/\hbar}\right\rangle_0 e^{-i\epsilon t/\hbar}\mathrm{d}t, \tag{8.17}$$

where $\langle\hat{A}\rangle_0 = \mathrm{tr}[e^{-\beta\hat{H}_0}\hat{A}]/Q_r$. Noting that

$$e^{-i\hat{H}_0 t/\hbar}e^{+i\hat{H}_1 t/\hbar} = \mathcal{T}\exp\left(-\frac{i}{\hbar}\int_0^t e^{-i\hat{H}_0 t'/\hbar}\hat{V}_- e^{+i\hat{H}_0 t'/\hbar}\mathrm{d}t'\right) \tag{8.18}$$

where $\mathcal{T}\exp$ denotes the time ordered exponential, we can then make use of Kubo's generalised cumulant expansion[261] to write

$$k = \frac{\Delta^2}{\hbar^2}\int_{-\infty}^{\infty} e^{-i\langle\hat{V}_-\rangle_0 t/\hbar - \frac{1}{\hbar^2}\int_0^t (t-t')\langle\delta\hat{V}_-(0)\delta\hat{V}_-(t)\rangle_0 \mathrm{d}t' + \cdots}\mathrm{d}t \tag{8.19}$$

where

$$\delta\hat{V}_-(t) = e^{+i\hat{H}_0/\hbar}(\hat{V}_- - \langle\hat{V}_-\rangle_0)e^{-i\hat{H}_0/\hbar}. \tag{8.20}$$

In general there exist infinitely many non-zero cumulants in the exponential, however for the spin-boson model the series truncates at the second cumulant. Hence in order to map onto the spin-boson model one truncates at second order to give

$$\left\langle e^{-i\hat{H}_0 t/\hbar}e^{+i\hat{H}_1 t/\hbar}\right\rangle_0 \simeq e^{-i\langle\hat{V}_-\rangle_0 t/\hbar - \frac{1}{\hbar^2}\int_0^t (t-t')\langle\delta\hat{V}_-(0)\delta\hat{V}_-(t)\rangle_0 \mathrm{d}t'}. \tag{8.21}$$

To simplify this into a form which can be evaluated using classical molecular dynamics, one begins by introducing the Kubo transformed energy gap fluctuation operator

$$\delta\hat{V}_-^{(K)} = \frac{1}{\beta}\int_0^\beta \mathrm{d}\lambda\, e^{\lambda\hat{H}_0}\delta\hat{V}_- e^{-\lambda\hat{H}_0}, \tag{8.22}$$

from which one can define the spectral density, $J(\omega)$, as

$$\frac{J(\omega)}{\omega} = \frac{\beta}{4}\int_0^\infty \left\langle\delta\hat{V}_-^{(K)}(0)\,\delta\hat{V}_-(t)\right\rangle_0 \cos(\omega t)\,\mathrm{d}t. \tag{8.23}$$

Then making use of the relation between the standard correlation function $C(t) = \left\langle\delta\hat{V}_-(0)\delta\hat{V}_-(t)\right\rangle_0$ and its Kubo transformed variant $C^{(K)}(t) = \left\langle\delta\hat{V}_-^{(K)}(0)\delta\hat{V}_-(t)\right\rangle_0$,

$$C(t) = \frac{1}{2\pi}\int_{-\infty}^{\infty}\int_{-\infty}^{\infty} e^{i\omega(t'-t)}\frac{\beta\hbar\omega}{e^{\beta\hbar\omega}-1}C^{(K)}(t')\,\mathrm{d}t'\mathrm{d}\omega, \tag{8.24}$$

we can write

$$\langle\delta\hat{V}_-(0)\delta\hat{V}_-(t)\rangle_0 = \frac{4}{\pi}\int_{-\infty}^{\infty} e^{-i\omega t}\frac{\hbar}{e^{\beta\hbar\omega}-1}J(\omega)\,\mathrm{d}\omega. \tag{8.25}$$

Finally using the relations

$$\int_0^t (t-t')e^{-i\omega t'}\mathrm{d}t' = -\frac{it}{\omega} + \frac{1-e^{-i\omega t}}{\omega^2} \tag{8.26}$$

and

$$\frac{2}{e^{\beta\hbar\omega}-1} = \coth(\beta\hbar\omega/2) - 1 \tag{8.27}$$

along with the definition of the reorganisation energy

$$\frac{4}{\pi}\int_0^\infty \frac{J(\omega)}{\omega}\,\mathrm{d}\omega = \Lambda, \tag{8.28}$$

we can rewrite Eq. 8.21 in the form

$$\left\langle e^{-i\hat{H}_0 t/\hbar} e^{+i\hat{H}_1 t/\hbar}\right\rangle_0 \simeq \exp(-i\Delta F t/\hbar - \phi(t)/\hbar), \tag{8.29}$$

where

$$\phi(t) = \frac{4}{\pi}\int_{-\infty}^\infty \frac{J(\omega)}{\omega^2}\left[\frac{1-\cos(\omega t)}{\tanh(\beta\hbar\omega/2)} - i\sin(\omega t)\right]\mathrm{d}\omega \tag{8.30}$$

and the thermodynamic driving force is

$$\Delta F = \langle \hat{V}_-\rangle_0 + \Lambda. \tag{8.31}$$

For an accurate mapping it is sensible to require this to be the same as the free energy difference between the reactants and products in the system of interest,

$$\Delta F = \frac{1}{\beta}\ln\left(\frac{\mathrm{tr}[e^{-\beta\hat{H}_1}]}{\mathrm{tr}[e^{-\beta\hat{H}_0}]}\right). \tag{8.32}$$

At this stage the only approximation that has been made is to truncate the cumulant expansion to second order in $\delta\hat{V}_-$, which is exact for the spin-boson model. Typically one makes a further simplification by using classical quantities in place of their quantum counterparts, which again is exact in the case of the spin-boson model. In particular, this means using the classical correlation function in place of the Kubo transformed correlation function in the definition of the spectral density

$$\frac{J(\omega)}{\omega} \simeq \frac{\beta}{4}\int_0^\infty \left\langle \delta V_-(0)\,\delta V_-(t)\right\rangle_{\mathrm{cl},0}\cos(\omega t)\,\mathrm{d}t, \tag{8.33}$$

which is straightforward to compute using standard MD codes.

Now comparing Eq. 8.28 with Eqs. 8.31 and 8.32, we note that there are effectively two different definitions of the Marcus reorganisation energy, which can be computed either as the difference between the driving force and mean diabatic energy gap

$$\Lambda = \epsilon - \langle V_-\rangle_{\mathrm{cl},0},, \tag{8.34}$$

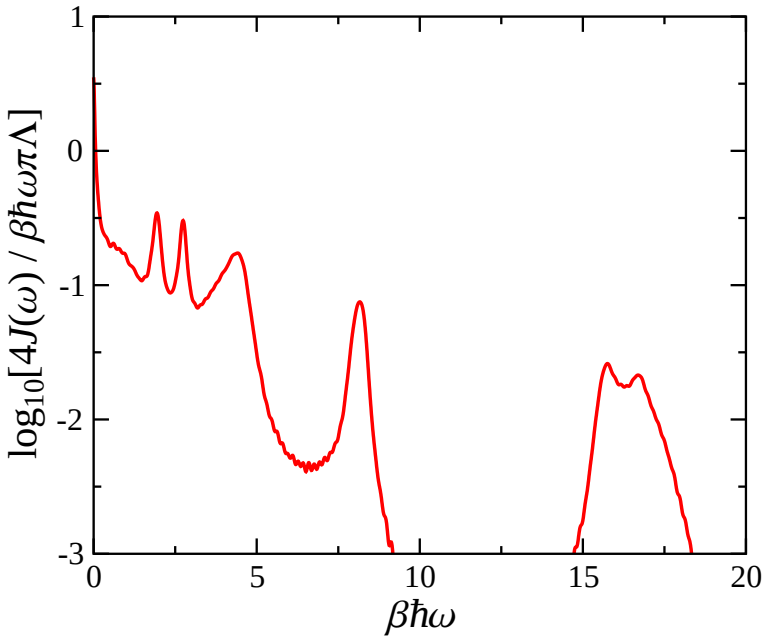

Figure 8.4: Logarithmic plot of the spectral density calculated using Eq. 8.36. This was used to evaluate the spin-boson mapping results in the text.

or from the integral of the spectral density

$$\Lambda_2 = \frac{\beta}{2}\langle \delta V_-(0)\, \delta V_-(0)\rangle_{\mathrm{cl},0}. \tag{8.35}$$

Since the reorganisation energy appears in the exponent in Marcus theory, even small changes in it can result in large changes to the rate. This means that choosing the correct definition is important. Since mapping to the spin-boson model is equivalent to assuming that the free energy $F_{\text{cl-GR}}(\lambda)$ is parabolic, the most consistent way to define Λ for ferrous-ferric electron transfer is such that it passes through the three known points at $\lambda = 0$, $\beta/2$ and β, which corresponds to using Eq. 8.34. Hence for consistency in the main text we define the spectral density such that

$$\frac{J(\omega)}{\omega} = \frac{\Lambda}{2}\int_0^\infty \frac{\langle \delta V_-(0)\, \delta V_-(t)\rangle_{\mathrm{cl},0}}{\langle \delta V_-^2(0)\rangle_{\mathrm{cl},0}} \cos(\omega t)\mathrm{d}t, \tag{8.36}$$

which ensures that the integral of the spectral density now gives the more accurate version of the Marcus reorganisation energy in Eq. 8.34. The calculated spectral density is shown for reference in Fig. 8.4.

We note that alternatively one could use RPMD to approximate the Kubo transformed energy gap correlation function. Whilst this may improve the accuracy of the calculated rates near activationless, $\epsilon \sim \Lambda$, for anharmonic reactions, it still does not allow one to overcome the fundamental limitations of mapping onto a spin-boson model. In particular it is fundamentally limited to sampling equilibrium configurations of the reactants, and hence cannot capture anharmonic features of the potential away from equilibrium that may be important in reaching the transition state. We also note that the above argument can equally be applied to give expressions evaluated in the product rather than the reactant ensemble. Whilst this is the same for the spin-boson model for any realistic asymmetric system there may be significant differences in the reactant and product potential energy surfaces and this can lead to a serious failure of the mapping approach for significantly activated reactions.

8.B Removing the uncoupled modes from GR-QTST

Here we discuss how the spontaneous quantum fluctuations can be approximately removed from the GR-QTST approximation to the ferrous-ferric electron transfer rate. As we discussed in the previous chapter, the GR-QTST approximation to $\rho_\lambda(E)$ is affected by degrees of freedom which are not coupled to the electronic transition. As we have argued in the main text, in a large system such as the atomistic model of ferrous-ferric electron transfer there will be many such degrees of freedom, which will contaminate the GR-QTST distribution leading it to underestimate the true rate.

Let us therefore suppose that we can identify a relatively small subset of degrees of freedom, labelled a, which are involved in the reaction, and a large remainder which are effectively uncoupled from the reaction, labelled b, such that we can write the diabatic potentials in the form

$$V_0(\boldsymbol{q}) = U_{0,a}(\boldsymbol{q}_a) + U_b(\boldsymbol{q}_b) \tag{8.37a}$$

$$V_1(\boldsymbol{q}) = U_{1,a}(\boldsymbol{q}_a) + U_b(\boldsymbol{q}_b). \tag{8.37b}$$

Note that we will not actually need to find the coordinate transformation or identify the coordinates a and b for which this is true, but only assume that it is in principle possible.

Having made this assumption we can simply decompose the contributions to $p_{\text{GR-QTST},\lambda}(E)$ according to

$$\langle \delta(\tfrac{2}{3}\mathcal{E}^{(\lambda)}_{-,a} + \tfrac{2}{3}\mathcal{E}^{(\lambda)}_{-,b} + E)\rangle_\lambda = \int_{-\infty}^{\infty} \langle \delta(\tfrac{2}{3}\mathcal{E}^{(\lambda)}_{-,a} + E' + E)\delta(\tfrac{2}{3}\mathcal{E}^{(\lambda)}_{-,b} - E')\rangle_\lambda \, \mathrm{d}E', \tag{8.38}$$

where $\frac{2}{3}\mathcal{E}^{(\lambda)}_{-,a} + \frac{2}{3}\mathcal{E}^{(\lambda)}_{-,b} = \frac{2}{3}\mathcal{E}^{(\lambda)}_{-}$ is just the GR-QTST constraint functional, separated into contributions from the a and b degrees of freedom. Since the a and b degrees of freedom are uncoupled, it follows that the expectation value in the integrand of Eq. 8.38 can be separated into two terms,

$$\langle \delta(\tfrac{2}{3}\mathcal{E}^{(\lambda)}_{-,a} + E' + E)\delta(\tfrac{2}{3}\mathcal{E}^{(\lambda)}_{-,b} - E')\rangle_\lambda = \langle \delta(\tfrac{2}{3}\mathcal{E}^{(\lambda)}_{-,a} + E' + E)\rangle_\lambda \langle \delta(\tfrac{2}{3}\mathcal{E}^{(\lambda)}_{-,b} - E')\rangle_\lambda.$$

If we now define

$$p_{a\text{-GR-QTST},\lambda}(E) = \langle \delta(\tfrac{2}{3}\mathcal{E}^{(\lambda)}_{-,a} + E)\rangle_\lambda, \tag{8.39}$$

and note that GR-QTST is generally very accurate for systems with a small number of degrees of freedom,[232,233] we are led to speculate that $p_{a\text{-GR-QTST},\lambda}(0)$ will provide a good approximation to the exact $\rho_\lambda(0)$ and hence give a good approximation to the rate.

In order to extract $p_{a\text{-GR-QTST},\lambda}(E)$ from $p_{\text{GR-QTST},\lambda}(E)$, we can consider the uncoupled $Fe^{2.5+}$-$Fe^{2.5+}$ system, for which in the present notation

$$V_0(\boldsymbol{q}) = V_1(\boldsymbol{q}) = \frac{U_{0,a}(\boldsymbol{q}_a) + U_{1,a}(\boldsymbol{q}_a)}{2} + U_b(\boldsymbol{q}_b). \tag{8.40}$$

Since we have assumed that there are only a few a degrees of freedom, it follows that the GR-QTST distribution for this uncoupled system will be

$$p_{\text{un-GR-QTST},\lambda}(E) \simeq \langle \delta(\tfrac{2}{3}\mathcal{E}^{(\lambda)}_{-,b} - E)\rangle_\lambda. \tag{8.41}$$

Hence we could in principle numerically deconvolute Eq. 8.38 to give an approximation to $p_{a\text{-GR-QTST},\lambda}(E)$. However, since we know from the central limit theorem (and from our simulation) that $p_{\text{un-GR-QTST},\lambda}(E)$ will be a Gaussian, and as we have shown that the exact $\rho_\lambda(E)$ is approximately a Gaussian, we can reasonably assume that $p_{a\text{-GR-QTST},\lambda}(E)$ will also be Gaussian. Hence, we can simply use the analytical expression for the convolution of two Gaussians to find that

$$p_{a\text{-GR-QTST},\lambda}(E) \simeq \sqrt{\frac{1}{2\pi\mu^2_{2,a}}} \exp\left(-\frac{E^2}{2\mu^2_{2,a}}\right), \tag{8.42}$$

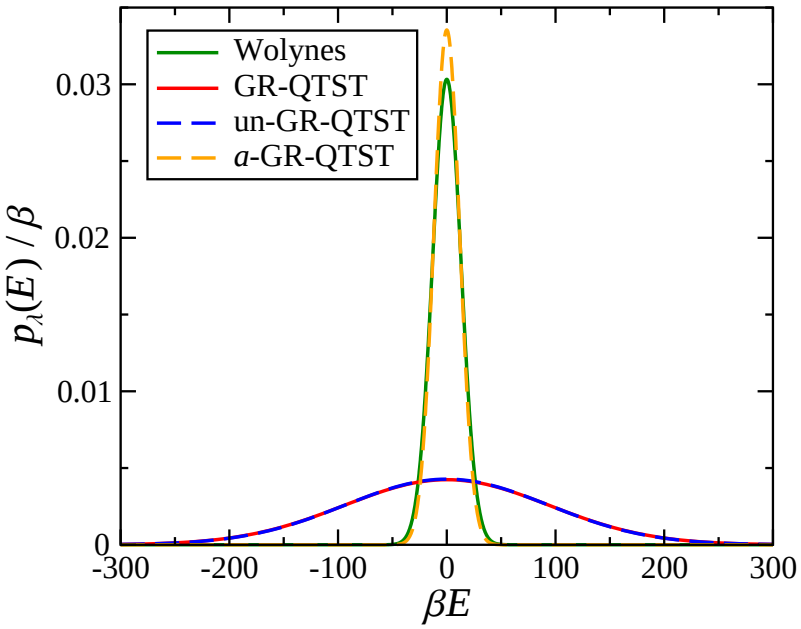

Figure 8.5: Comparison of the corrected GR-QTST distribution obtained via the approximate deconvolution described in Appendix C (a-GR-QTST), with the raw results for the physical (Fe^{2+}-Fe^{3+}; GR-QTST) and uncoupled ($Fe^{2.5+}$-$Fe^{2.5+}$; un-GR-QTST) systems, and with the Wolynes distribution.

where

$$\mu_{2,a}^2 = \int_{-\infty}^{\infty} E^2 [p_{\text{GR-QTST},\lambda}(E) - p_{\text{un-GR-QTST},\lambda}(E)] \, \mathrm{d}E \tag{8.43}$$

and we have made use of the symmetry of the ferrous-ferric system at $\lambda = \lambda_{\text{sp}} = \beta/2$, which implies that the mean of all of the distributions must be zero. Figure 8.5 shows graphically the result of this approximate deconvolution, illustrating the close agreement between the a-GR-QTST results and those of Wolynes theory.

9 Conclusion

In this thesis we have explored some of the challenges associated with the development of accurate path-integral methods for non-adiabatic reaction rates. We have looked to develop simple solutions to these problems which are immediately applicable to realistic condensed phase simulations. This is by no means the first study in this area, and having introduced the established theory in Chap. 2, we continued in Chap. 3 to analyse some of the most recent attempts to solve this problem. We focussed on approaches which aim to generalise RPMD to treat non-adiabatic systems. Standard RPMD rate theory is known to accurately describe the effects of tunnelling and zero-point energy in the adiabatic limit, and one might hope that these non-adiabatic generalisations of RPMD would be able to transfer this accuracy to weaker electronic coupling. Unfortunately, we found that, even the most promising of these approaches, the newly proposed iso-RPMD,[33,34] is not able to accurately describe nuclear quantum effects in the golden-rule limit, highlighting the need for further work in this area.

In Chap. 4 and Chap. 5 we introduced two approaches for calculating non-adiabatic reaction rates, in systems which are intermediate between the golden-rule and Born-Oppenheimer limits. The first of these, the non-adiabatic quantum instanton (NAQI), reduces to Wolynes theory[82] in the golden-rule limit and to the projected quantum instanton[86] in the adiabatic limit. The results for a series of one dimensional scattering models illustrated the accuracy of the method. Having established this, it should be

relatively straightforward to develop a path-integral implementation of NAQI by starting from the existing path-integral versions of Wolynes theory and the adiabatic quantum instanton. Unfortunately, a detailed study of the properties of the path-integral version of the theory was beyond the scope of this thesis. Future work will look to develop the theory further and use it to answer mechanistic questions in condensed phase reactions. An important limitation of the NAQI approach however, is that (like the adiabatic quantum instanton) it requires knowledge of the optimum position space dividing surface. In order to avoid this problem we suggested an alternative approach for calculating reaction rates at arbitrary coupling strength, using a simple interpolation formula. This formula interpolates between the Born-Oppenheimer and golden-rule rates, and can be combined with any method applicable to these two limits, such as Wolynes theory and RPMD. By comparing to exact HEOM results for a series of different spin-boson models,* we demonstrated that the formula gives accurate results in a wide range of physically relevant regimes, and that, in combination with path-integral methods in the adiabatic and non-adiabatic limits, it is immediately applicable to complex multidimensional reactions.

In the second half of this thesis we returned to focus on the golden-rule limit. In Chap. 6 we addressed the difficulty of applying Wolynes theory to the Marcus inverted regime, and showed how this could be overcome using a numerical analytic continuation procedure. Interestingly, since we published this work in 2018, this idea has been carried over by Heller *et al.* to the semiclassical instanton approximation,[170,195] where it was shown[196] that the instanton formula can be directly analytically continued into the inverted regime. In Chap. 7 we addressed the recent work by Richardson and coworkers which showed that Wolynes theory breaks down for systems with multiple transition states.[232,233] We demonstrated that GR-QTST, an alternative to Wolynes theory proposed by Richardson and coworkers to solve this problem,[232,233] itself suffers from a size consistency issue which limits applicability to large scale simulations. We suggested a simple modification to GR-QTST, the linear golden-rule (LGR) approximation, which fixes this size inconsistency, and provides an alternative approach to calculating reaction rates in the inverted regime without the need for analytic continuation. In Chap. 8 we

*HEOM calculations were performed by Dr. Lachlan P. Lindoy.

applied Wolynes theory, LGR and GR-QTST to a fully atomistic model of aqueous ferrous-ferric electron transfer, in order to assess the recent suggestion that Wolynes theory breaks down in this system due to the presence of multiple transition states.[235] We demonstrated that in fact Wolynes theory is very accurate for this system, and that it is actually GR-QTST which breaks down due to its size inconsistency. We also investigated the effect of an artificial bias in the ferrous-ferric system, and used this to illustrate the applicability of both Wolynes theory and LGR to the calculation of reaction rates in the Marcus inverted regime in a realistic condensed phase simulation with anharmonic force fields.

There is still clearly much work to be done in the development of path-integral methods for non-adiabatic reaction rates. In particular, the ultimate goal of the development of an accurate non-adiabatic generalisation of RPMD rate theory is still some way off. However, the methods we have explored in this thesis are capable of tackling many of the questions that one might want to answer with such a method. It will be interesting in the future to apply the methods developed here to study more complex condensed phase reactions, in order to quantify the contribution of nuclear quantum effects, assess the degree of non-adiabaticity, and uncover new reaction mechanisms.

Bibliography

[1] R. H. Holm, P. Kennepohl, and E. I. Solomon, Chem. Rev. **96**, 2239 (1996).

[2] S. Hammes-Schiffer and A. A. Stuchebrukhov, Chem. Rev. **110**, 6939 (2010).

[3] J. Blumberger, Chem. Rev. **115**, 11191 (2015).

[4] D. N. Beratan Annu. Rev. Phys. Chem. **70**, 71 (2019).

[5] V. Balzani, A. Juris, M. Venturi, S. Campagna and S. Serroni, Chem. Rev. **96**, 759 (1996).

[6] J. Brédas, D. Beljonne, V. Coropceanu, and J. Cornil, Chem. Rev. **104**, 4971 (2004).

[7] V. Coropceanu, J. Cornil, D. A. da Silva Filho, Y. Olivier, R. Silbey, and J. Brédas, Chem. Rev. **107**, 926 (2007).

[8] H. Oberhofer, K. Reuter, and J. Blumberger, Chem. Rev. **117**, 10319 (2017).

[9] P. V. Kamat, J. Phys. Chem. C **112**, 18737 (2008).

[10] R. P. Feynman and A. R. Hibbs *Quantum Mechanics and Path Integrals* (McGraw-Hill, New York, 1965).

[11] H. Kleinert *Path Integrals in Quantum Mechanics, Statistics, Polymer Physics and Financial Markets* 5th ed. (World Scientific, Singapore, 2009).

[12] M. E. Tuckerman, *Statistical Mechanics: Theory and Molecular Simulation* (Oxford University Press, New York, 2010).

[13] G. A. Voth, D. Chandler, and W. H. Miller, J. Chem. Phys. **91**, 7749 (1989).

[14] E. Geva, Q. Shi and G. A. Voth, J. Chem. Phys. **115** 9209 (2001).

[15] W. H. Miller, Y. Zhao, M. Ceotto and S. Yang, J. Chem. Phys. **119**, 1329 (2003).

[16] J. Vaníček, W. H. Miller, J. F. Castillo, and F. J. Aoiz, J. Chem. Phys. **123**, 054108 (2005).

[17] I. R. Craig and D. E. Manolopoulos, J. Chem. Phys. **121**, 3368 (2004).

[18] I. R. Craig and D. E. Manolopoulos, J. Chem. Phys. **122**, 084106 (2005).

[19] I. R. Craig and D. E. Manolopoulos, J. Chem. Phys. **123**, 034102 (2005).

[20] R. Collepardo-Guevara, I. R. Craig and D. E. Manolopoulos, J. Chem. Phys. **128**, 144502 (2008).

[21] N. Boekelheide, R. Salomon-Ferrer and T. F. Miller III, Proc. Natl. Acad. Sci. USA **108**, 16159 (2011).

[22] S. Habershon, D. E. Manolopoulos, T. E. Markland and T. F. Miller III, Ann. Rev. Phys. Chem. **64**, 387 (2013).

[23] A. R. Menzeleev, N. Ananth, and T. F. Miller III, J. Chem. Phys. **135**, 074106 (2011).

[24] J. S. Kretchmer and T. F. Miller III, J. Chem. Phys. **138**, 134109 (2013).

[25] P. Shushkov, R. Li and J. C. Tully, J. Chem. Phys. **137**, 22A549 (2012).

[26] J. O. Richardson and M. Thoss, J. Chem. Phys. **139**, 031102 (2013).

[27] N. Ananth, J. Chem. Phys. **139**, 124102 (2013)

[28] J. R. Duke and N. Ananth, Faraday Discuss. **195**, 253 (2016).

[29] A. R. Menzeleev, F. Bell, and T. F. Miller III, J. Chem. Phys. **140**, 064103 (2014).

[30] J. S. Kretchmer and T. F. Miller III, Faraday Discuss. **195**, 191 (2016).

[31] J. S. Kretchmer, N. Boekelheide, J. J. Warren, J. R. Winkler, H. B. Gray, and T. F. Miller III, Proc. Natl. Acad. Sci. USA **115**, 6129 (2018)

[32] S. N. Chowdhury and P. Huo, J. Chem. Phys. **147**, 214109 (2017).

[33] X. Tao, P. Shushkov and T. F. Miller III, J. Chem. Phys. **148**, 102327 (2018).

[34] X. Tao, P. Shushkov and T. F. Miller III, J. Phys. Chem. A **123**, 3013 (2019).

[35] M. Born and R. Oppenheimer, Ann. Phys. **84**, 457 (1927).

[36] D. R. Yarkony, Rev. Mod. Phys. **68**, 985 (1996).

[37] G. A. Worth and L. S. Cederbaum, Annu. Rev. Phys. Chem. **55**, 127 (2004).

[38] J. C. Tully, J. Chem. Phys. **137**, 22A301 (2012).

[39] M. G. Evans and M. Polanyi, Trans. Faraday Soc. **31**, 875 (1935).

[40] M. G. Evans and M. Polanyi, Trans. Faraday Soc. **34**, 11 (1938).

[41] E. Wigner, Trans. Faraday Soc. **34**, 29 (1938).

[42] H. Eyring, Trans. Faraday Soc., **34**, 41 (1938).

[43] L. Landau, Phys. Z. Sowjetunion **2**, 46 (1932).

[44] C. Zener, Proc. R. Soc. London, Ser. A **137**, 696 (1932).

[45] M. Born and V. Fock, Z. Physik **51**, 165 (1928).

[46] R. A. Marcus, J. Chem. Phys. **24**, 966 (1956).

[47] R. A. Marcus and N. Sutin, Biochim. Biophys. Acta **811**, 265 (1985).

[48] N. S. Hush, Trans. Faraday Soc. **57**, 577 (1961).

[49] N. S. Hush, J. Electroanal. Chem. **470**, 170 (1999).

[50] E. Fermi, *Nuclear Physics* (University of Chicago Press, Chicago, 1950).

[51] D. E. Manolopoulos, K. Stark, H. Werner, D. W. Arnold, S. E. Bradforth and D. M. Neumark, Science **262**, 1852 (1993).

[52] E. C. G. Stückelberg, Helv. Phys. Acta **5**, 369 (1932).

[53] V. G. Levich and R. R. Dogonadze, Dokl. Acad. Nauk. SSSR **124**, 123 (1959).

[54] A. A. Ovchinnikov and M. Ya. Ovchinnikova, Sov. Phys. JETP **29**, 688 (1969).

[55] V. G. Levich, R. R. Dogonadze, E. D. German, A. M. Kuznetsov, and Yu. I. Kharkats, Electrochim. Acta **15**, 353 (1970).

[56] N. R. Kestner, J. Logan, and J. Jortner, J. Phys. Chern. **78**, 2148 (1974).

[57] J. Ulstrup and J. Jortner, J. Chem. Phys. **63**, 4358 (1975).

[58] J. Jortner, J. Chem. Phys. **64**, 4860 (1976).

[59] J. Ulstrup, *Charge Transfer in Condensed Media* (Springer, Berlin, 1979).

[60] R. R. Dogonadze, A. M. Kuznetsov, and T. A. M. Marsagishvili, Electrochim. Acta **25**, 1 (1980).

[61] U. Weiss, *Quantum Dissipative Systems*, 3rd ed. (World Scientific, Singapore, 2008).

[62] X. Song and A. A. Stuchebrukhov, J. Chem. Phys. **99**, 969 (1993).

[63] L. D. Zusman, Chem. Phys. **49**, 295 (1980).

[64] A. Garg, J. N. Onuchic and V. J. Ambegaokar, J. Chem. Phys. **83**, 4491 (1985).

[65] J. T. Hynes, J. Phys. Chem. **90**, 3701 (1986).

[66] I. Rips and J. Jortner, J. Chem. Phys. **87**, 2090 (1987).

[67] M. Sparpaglione and S. Mukamel, J. Chem. Phys. **88**, 3263 (1988).

[68] D. F. Calef and P. G. Wolynes, J. Phys. Chem. **87**, 3387 (1983).

[69] E. Pollak, J. Chem. Phys. **93**, 1116 (1990).

[70] I. Rips and E. Pollak, J. Chem. Phys. **103**, 7912 (1995).

[71] A. Starobinets, I. Rips and E. Pollak, J. Chem. Phys. **104**, 6547 (1996).

[72] V. Gladkikh, A. I. Burshtein, and I. Rips, J. Phys. Chem. A **109**, 4983 (2005).

[73] J. C. Tully, J. Chem. Phys. **93**, 1061 (1990).

[74] H-D. Meyer and W. H. Miller, J. Chem. Phys. **70**, 3214 (1979).

[75] G. Stock and M. Thoss, Phys. Rev. Lett. **78**, 578 (1997).

[76] P. Ehrenfest, Z. Physik **45**, 455 (1927).

[77] X. Li and J. C. Tully, J. Chem. Phys. **123**, 084106 (2005).

[78] D. Chandler and P. G. Wolynes, J. Chem. Phys. **74**, 4078 (1981).

[79] M. Parrinello and A. Rahman, J. Chem. Phys. **80**, 860 (1984).

[80] J. S. Cao and G. A. Voth, J. Chem. Phys. **100**, 5106 (1994).

[81] J. S. Cao and G. A. Voth, J. Chem. Phys. **101**, 6168 (1994).

[82] P. G. Wolynes, J. Chem. Phys. **87**, 6559 (1987).

[83] C. Zheng, J. A. McCammon and P. G. Wolynes, Proc. Natl. Acad. Sci. USA **86**, 6441 (1989).

[84] J. S. Bader, R. A. Kuharski, and D. Chandler, J. Chem. Phys. **93**, 230 (1990).

[85] C. Zheng, J. A. McCammon and P. G. Wolynes, Chem. Phys. **158**, 261 (1991).

[86] C. L. Vaillant, M. J. Thapa, J. Vaníček, and J. O. Richardson, J. Chem. Phys. **151**, 144111 (2019).

[87] A. Szabo and N. S. Ostlund. *Modern Quantum Chemistry* (McGraw-Hill Publishing Company, New York, 1989).

[88] M. Born and K. Huang, *Dynamical Theory of Crystal Lattices* (Oxford University Press, Oxford, 1954).

[89] P. Atkins and J. de Paula, *Physical Chemistry* 8th ed. (Oxford University Press, Oxford, 2006).

[90] T. Van Voorhis, T. Kowalczyk, B. Kaduk, L. Wang, C. Cheng and Q. Wu, Annu. Rev. Phys. Chem. **61**, 149 (2010).

[91] C. A. Mead and D. G. Truhlar,. J. Chem. Phys. **77**, 6090 (1982).

[92] M. Baer, Mol. Phys. **40**, 1011 (1980).

[93] T. Pacher, L. S. Cederbaum and H. Köppel, J. Chem. Phys. **89**, 7367 (1988).

[94] T. Pacher, L. S. Cederbaum and H. Köppel, J. Chem. Phys. **95**, 6668 (1991).

[95] G. J. Atchity and K. Ruedenberg, Theor. Chem. Acc. **97**, 47 (1997).

[96] H. Nakamura and D. G. Truhlar, J. Chem. Phys. **117**, 5576 (2002).

[97] R. Muliken, J. Am. Chem. Soc. **78**, 811 (1952).

[98] N. Hush, Prog. Inorg. Chem. **8**, 391 (1967).

[99] S. F. Boys, Rev. Mod. Phys. **32**, 296 (1960).

[100] J. E. Subotnik, S. Yeganeh, R. J. Cave and M. A. Ratner, J. Chem. Phys. **129**, 244101 (2008).

[101] D. G. Truhlar, J. Comp. Chem. **28**, 73 (2007).

[102] T. A. Wesolowski and A. Warshel, J. Phys. Chem. **97**, 8050 (1993).

[103] M. H. M. Olsson, G. Y. Hong and A. Warshel, J. Am. Chem. Soc. **125** 5025 (2003).

[104] Q. Wu and T. Van Voorhis, J. Phys. Chem. A **110**, 9212 (2006).

[105] A. Warshel and R. M. Weiss, J. Am. Chem. Soc. **102**, 6218 (1980).

[106] V. May and O. Kühn, *Charge and Energy Transfer Dynamics in Molecular Systems* (Wiley-VCH, Berlin, 2000).

[107] R. A. Kuharski, J. S. Bader, D. Chandler, M. Sprik, M. L. Klein, and R. W. Impey, J. Chem. Phys. **89**, 3248 (1988).

[108] A. Soudackov and S. Hammes-Schiffer, J. Chem. Phys. **113**, 2385 (2000)

[109] K. Ando, J. Chem. Phys. **114**, 9470 (2001).

[110] J. Blumberger and M. Sprik, Theor. Chem. Acc. **115**, 113 (2006).

[111] J. Blumberger and G. Lamoureux, Mol. Phys. **106**, 1597 (2008).

[112] X. Sun, P. Zhang, Y. Lai, K. L. Williams, M. S. Cheung, B. D. Dunietz, and E. Geva, J. Phys. Chem. C. **122**, 11288 (2018).

[113] M. Head-Gordon and J. C. Tully, J. Chem. Phys. **103**, 10137 (1995).

[114] W. Dou and J. E. Subotnik, J. Chem. Phys. **148**, 230901 (2018).

[115] J. Jortner, M. Bixon, T. Langenbacher, M. E. Michel-Beyerle, Proc. Natl. Acad. Sci. U.S.A. **95**, 12759 (1998).

[116] L. D. Zusman and D. N. Beratan, J. Chem. Phys. **110**, 10468 (1999).

[117] E. G. Petrov, Y. V. Shevchenko, V. I. Teslenko and V. May, J. Chem. Phys. **115**, 7107 (2001).

[118] B. P. Paulson, J. R. Miller, W. Gan, and G. Closs, J. Am. Chem. Soc. **127**, 4860 (2005).

[119] I. R. Craig, M. Thoss and H. Wang, J. Chem. Phys. **127**, 144503 (2007).

[120] D. Chandler, J. Chem. Phys. **68**, 2959 (1978).

[121] D. Chandler, *Introduction to Modern Statistical Mechanics*, (Oxford University Press, New York, 1987).

[122] D. Chandler, J. Stat. Phys. **42**, 49 (1986).

[123] D. Chandler, Discuss. Faraday Soc. **85**, 341 (1988).

[124] P. Hänggi, P. Talkner, and M. Borkovec, Rev. Mod. Phys. **62**, 251 (1990).

[125] R. D. Coalson, D. G. Evans, and A. Nitzan, J. Chem. Phys. **101**, 436 (1994).

[126] M. Cho and R. J. Silbey, J. Chem. Phys. **103**, 595 (1995).

[127] X. Sun and E. Geva, J. Chem. Theory Comput. **12**, 2926 (2016).

[128] X. Sun and E. Geva, J. Chem. Phys. **145**, 064109 (2016).

[129] K. Song and Q. Shi, J. Chem. Phys. **146**, 184108 (2017).

[130] L. Onsager, Phys. Rev. **37**, 405 (1931).

[131] L. Onsager, Phys. Rev. **38**, 2265 (1931).

[132] R. Kubo, J. Phys. Soc. Japan **12**, 570 (1957).

[133] R. Kubo, M. Yokota, and S. Nakajima, J. Phys. Soc. Japan **12**, 1203 (1957).

[134] T. Yamamoto, J. Chem. Phys. **33**, 281 (1960).

[135] R. Zwanzig, *Nonequilibrium Statistical Mechanics*, (Oxford University Press, Oxford, 2001).

[136] W. H. Miller, S. D. Schwartz and J. W. Tromp, J. Chem. Phys. **79**, 4889 (1983).

[137] W. H. Miller, J. Chem. Phys. **61**, 1823 (1974).

[138] M. Lax, J. Chem. Phys. **20**, 1752 (1952).

[139] R. Kubo and Y. Toyozawa, Prog. Theor. Phys. 13, 160 (1955).

[140] S. Habershon, B. J. Braams, and D. E. Manolopoulos, J. Chem. Phys. **127**, 174108 (2007).

[141] D. Chandler, in *Classical and Quantum Dynamics in Condensed Phase Simulations* edited by B. J. Berne, G. Cicootti, and D. F. Coker (World Scientific, Singapore, 1997).

[142] H. Sumi, in *Electron Transfer in Chemistry* (Wiley-VCH Verlag, 2001).

[143] W. H. Miller, J. Chem. Phys. **62**, 1899 (1975).

[144] J. O. Richardson and S. C. Althorpe, J. Chem. Phys. **131**, 214106 (2009).

[145] S. Andersson, G. Nyman, A. Arnaldsson, U. Manthe and H. Jónsson J. Phys. Chem. A **113**, 4468 (2009).

[146] J. O. Richardson, J. Chem. Phys. **148**, 200901 (2018).

[147] T. J. H. Hele and Stuart C. Althorpe, J. Chem. Phys. 138, 084108 (2013).

[148] Stuart C. Althorpe and T. J. H. Hele, J. Chem. Phys. **139**, 084115 (2013).

[149] H. F. Trotter, Proc. Amer. Math. Soc. **10**, 545 (1959).

[150] M. Suzuki, Commun. math. Phys. **51**, 183 (1976).

[151] T. E. Markland and D. E. Manolopoulos, J. Chem. Phys. **129**, 024105 (2008).

[152] T. E. Markland, D. E. Manolopoulos, Chem. Phys. Lett. **464**, 256 (2008).

[153] G. S. Fanourgakis, T. E. Markland, D. E. Manolopoulos, J. Chem. Phys. **131** 094102 (2009).

[154] M. Ceriotti, D. E. Manolopoulos, M. Parrinello, J. Chem. Phys. **134**, 084104 (2011).

[155] V. Kapil, D. M. Wilkins, J. Lan, and M. Ceriotti, J. Chem. Phys. **152**, 124104 (2020).

[156] A. Perez and M. E. Tuckerman, J. Chem. Phys. **135**, 064104 (2011).

[157] V. Kapil, J. Behler, and M. Ceriotti, J. Chem. Phys. **145**, 234103 (2016).

[158] J. S. Kretchmer and T. F. Miller III, Inorg. Chem., **55**, 1022 (2016).

[159] J. R. Cendagorta, A. Powers, T. J. H. Hele, O. Marsalek, Z. Bacic and M. E. Tuckerman, Phys. Chem. Chem. Phys., **18**, 32169 (2016).

[160] W. H. Miller, Faraday Discuss. **110**, 1 (1998).

[161] D. Chandler and D. E. Manolopoulos, Faraday Discuss. **195**, 699 (2016).

[162] B. J. Braams and D. E. Manolopoulos, J. Chem. Phys. **125**, 124105 (2006).

[163] M. Rossi, M. Ceriotti, and D. E. Manolopoulos J. Chem. Phys. **140**, 234116 (2014).

[164] C. H. Bennett, in *Algorithms for Chemical Computations*, ACS Symposium Series No. 46, edited by R. E. Christoffersen (American Chemical Society, Washington, 1977), p. 63.

[165] R. Collepardo-Guevara, Y. V. Suleimanov and D. E. Manolopoulos, J. Chem. Phys. **130**, 174713 (2009); J. Chem. Phys. **133**, 049902 (2010).

[166] Y. V. Suleimanov, R. Collepardo-Guevara and D. E. Manolopoulos, J. Chem. Phys. **134**, 044131 (2011).

[167] R. Perez de Tudela, F. J. Aoiz, Y. V. Suleimanov and D. E. Manolopoulos, J. Phys. Chem. Lett. **3**, 493 (2012).

[168] Y. V. Suleimanov, R. Perez de Tuleda, P. G. Jambrina, J. F. Castillo, V. Saez-Rabanos, D. E. Manolopoulos and F. J. Aoiz, Phys. Chem. Chem. Phys. **15**, 3655 (2013).

[169] C. M. Bender and S. A. Orszag, *Advanced Mathematical Methods for Scientists and Engineers: Asymptotic Methods and Perturbation Theory* (McGraw-Hill, New York, 1978).

[170] J. O. Richardson, R. Bauer, and M. Thoss, J. Chem. Phys. **143**, 134115 (2015).

[171] A. Troisi, A. Nitzan and M. A. Ratner, J. Chem. Phys. **119**, 5783 (2003).

[172] S. S. Skourtis, I. A. Balabin, T. Kawatsu and D. N. Beratan, Proc. Natl. Acad. Sci. USA **102**, 3552 (2005).

[173] A. Nitzan, *Chemical Dynamics in Condensed Phases* (Oxford University Press, Oxford, 2006).

[174] T. J. H. Hele, M. J. Willatt, A. Muolo, and S. C. Althorpe, J. Chem. Phys. **142**, 134103 (2015).

[175] T. J. H. Hele, M. J. Willatt, A. Muolo, and S. C. Althorpe, J. Chem. Phys. **142**, 191101 (2015).

[176] T. J. H. Hele and N. Ananth, Faraday Discuss. **195**, 269 (2016).

[177] T. Hele, *An Electronically Non-Adiabatic Generalisation of Ring Polymer Molecular Dynamics* Part II thesis, Oxford (2011).

[178] C. D. Schwieters and G. A. Voth, J. Chem. Phys. **111**, 2869 (1999).

[179] S. Jang and J. Cao, J. Chem. Phys. **114**, 9959 (2001).

[180] M. H. Alexander, Chem. Phys. Lett. **347**, 436 (2001).

[181] S. Ghosh, S. Giannini, K. Lively and J. Blumberger, Faraday Discuss. **221**, 501 (2020).

[182] J. Lu and Z. Zhou, J. Chem. Phys. **146**, 154110 (2017).

[183] E. R. Bittner and P. J. Rossky, J. Chem. Phys. **103**, 8130 (1995).

[184] B. J. Schwartz, E. R. Bittner, O. V. Prezhdo, and P. J. Rossky, J. Chem. Phys. **104**, 5942 (1996).

[185] O. V. Prezhdo and P. J. Rossky, J. Chem. Phys. **107**, 825 (1997).

[186] J.-Y. Fang and S. Hammes-Schiffer, J. Phys. Chem. A **103**, 9399 (1999).

[187] C. Zhu, S. Nangia, and D. G. Truhlar, J. Chem. Phys. **121**, 7658 (2004).

[188] G. Granucci and M. Persico, J. Chem. Phys. **126**, 134114 (2007).

[189] N. Shenvi, J. E. Subotnik and W. Yang, J. Chem. Phys. **134** 144102 (2011).

[190] B. R. Landry and J. E. Subotnik, J. Chem. Phys. **135**, 191101 (2011).

[191] M. J. Falk, B. R. Landry and J. E. Subotnik, J. Phys. Chem. B **118**, 8108 (2014).

[192] A. J. Leggett, Phys. Rev. B **30**, 1208 (1984).

[193] M. Thoss, H. Wang and W. H. Miller, J. Chem. Phys. **115**, 2991 (2001).

[194] J. R. Miller, L. T. Calcaterra and G. L. Closs, J. Am. Chem. Soc. **106**, 3047 (1984).

[195] J. O. Richardson, J. Chem. Phys. **143**, 134116 (2015).

[196] E. R. Heller and J. O. Richardson, J. Chem. Phys. **152**, 034106 (2020).

[197] S. Chapman, B. C. Garrett and W. H. Miller, J. Chem. Phys. **63**, 2710 (1975).

[198] C. G. Callan and S. Coleman, Phys. Rev. D **16**, 1762 (1977).

[199] I. Affleck, Phys. Rev. Lett. **46**, 388 (1981).

[200] V. A. Benderskii, D. E. Makarov, and C. A. Wight, Adv. Chem. Phys. **88**, 55 (1994).

[201] S. C. Althorpe, J. Chem. Phys. **134**, 114104 (2011).

[202] J. S. Cao, C. Minichino, and G. A. Voth, J. Chem. Phys. **103**, 1391 (1995).

[203] J. S. Cao and G. A. Voth, J. Chem. Phys. **106**, 1769 (1997).

[204] C. D. Schwieters and G. A. Voth, J. Chem. Phys. **108**, 1055 (1998).

[205] J. W. Tromp and W. H. Miller, Faraday Discuss. **84**, 441 (1987).

[206] B. R. Johnson, J. Comp. Phys. **13**, 445 (1973).

[207] J. Cao and B. J. Berne, J. Chem. Phys. **92**, 7531 (1990).

[208] J. Cao and G. A. Voth, J. Chem. Phys. **102**, 3337 (1995).

[209] S. Yang and J. Cao, J. Chem. Phys. **122**, 094108 (2005).

[210] Y. Tanimura and R. Kubo, J. Phys. Soc. Jpn. **58**, 101 (1989).

[211] Y. Tanimura, Phys. Rev. A **41**, 6676 (1990).

[212] Y. Tanimura, J. Phys. Soc. Jpn. **75**, 082001 (2006).

[213] Y. A. Yan, F. Yang, Y. Liu, and J. S. Shao, Chem. Phys. Lett. **395**, 216 (2004).

[214] R. X. Xu, P. Cui, X. Q. Li, Y. Mo, and Y. J. Yan, J. Chem. Phys. **122**, 041103 (2005).

[215] R. X. Xu and Y. J. Yan, Phys. Rev. E **75**, 031107 (2007).

[216] J. S. Jin, X. Zheng, and Y. J. Yan, J. Chem. Phys. **128**, 234703 (2008).

[217] Y. Georgievskii and A. A. Stuchebrukhov, J. Chem. Phys. **113**, 10438 (2000).

[218] A. V. Soudackov and S. Hammes-Schiffer, Faraday Discuss. **195**, 171 (2016).

[219] Q. Shi, L. Chen, G. Nan, R. Xu and Y. Yan, J. Chem. Phys. **130**, 164518 (2009).

[220] L. Hartmann, I. Goychuk and P. Hänggi, J. Chem. Phys. **113**, 11159 (2000).

[221] E. Cortés, B. J. West and K. Lindenberg, J. Chem. Phys. **82**, 2708 (1985).

[222] M. Berkowitz, J. D. Morgan and J. A. McCammon, J. Chem. Phys. **78**, 3256 (1983).

[223] M. Ceriotti, M. Parrinello, T. E. Markland and D. E. Manolopoulos, J. Chem. Phys. **133**, 124104 (2010).

[224] M. Ceriotti, G. Bussi and M. Parrinello, J. Chem. Theor. Comput. **6**, 1170 (2010).

[225] A. A. Golosov, D. R. Reichman and E. Rabani, J. Chem. Phys. 118, **457** (2003).

[226] D. Chandler, Chemica Scripta **29A**, 61 (1989).

[227] H. Wang, M. Thoss, and W. H. Miller, J. Chem. Phys. **115**, 2979 (2001).

[228] S. G. Johnson, *The NLopt nonlinear-optimization package*, http://ab-initio.mit.edu/nlopt.

[229] T. P. Runarsson and X. Yao, IEEE Trans. Syst., Man, Cybern. C **35**, 233 (2005).

[230] J. O. Richardson and M. Thoss, J. Chem. Phys. **141**, 074106 (2014).

[231] D. E. Manolopoulos and R. E. Wyatt, Chem. Phys. Lett. **152**, 23 (1988).

[232] M. J. Thapa, W. Fang and J. O. Richardson, J. Chem. Phys. **150**, 104107 (2019).

[233] W. Fang, M. J. Thapa and J. O. Richardson, J. Chem. Phys. **151**, 214101 (2019).

[234] M. F. Herman, E. J. Bruskin, and B. J. Berne, J. Chem. Phys. **76**, 5150 (1982).

[235] W. Fang, R. A. Zarotiadis and J. O. Richardson, Phys. Chem. Chem. Phys. **22** 10687 (2020).

[236] Y. Georgievskii, C. Hsu, and R. A. Marcus J. Chem. Phys. **110**, 5307 (1999).

[237] R. Henderson, *The Mechanisms of Reactions at Transition Metal Sites (Oxford Chemistry Primers)* (Oxford University Press, Oxford, 1993).

[238] M. Weller, T. Overton, J. Rourke, and F. Armstrong, *Inorganic Chemistry* (Oxford University Press, Oxford, 2018).

[239] B. S. Brunschwig, J. Logan, M. D. Newton, and N. Sutin, J. Am. Chem. Soc. **102**, 5798 (1980).

[240] P. Siders and R. A. Marcus, J. Am. Chem. Soc. **103**, 741 (1981).

[241] J. S. Bader and D. Chandler, Chem. Phys. Lett. **157**, 501 (1989).

[242] M. Marchi, J. N. Gehlen, D. Chandler, and M. Newton, J. Am. Chem. Soc. 115, 4178 (1993).

[243] X. Song and R.A. Marcus, J. Chem. Phys. 99, 7768 (1993).

[244] J. Blumberger and M. Sprik, J. Phys. Chem. B, **109**, 6793 (2005).

[245] C. Drechsel-Graua and M. Sprik, J. Chem. Phys. 136, 034506 (2012).

[246] A. Warshel, J. K. Hwang, J. Chem. Phys. **84**, 4938 (1986).

[247] J. K. Hwang and A. Warshel, Chem. Phys. Lett. **271**, 223 (1997).

[248] K. Ando, J. Chem. Phys. **106**, 116 (1997).

[249] L. W. Ungar, M. D. Newton, and G. A. Voth, J. Phys. Chem. B **103**, 7367 (1999).

[250] V. Tipmanee, H. Oberhofer, M. Park, K. S. Kim, and J. Blumberger, J. Am. Chem. Soc. **132**, 17032 (2010).

[251] T. Firmino, E. Mangaud, F. Cailliez, A. Devolder, D. Mendive-Tapia, F. Gatti, C. Meier, M. Desouter-Lecomte, and A. de la Lande, Phys. Chem. Chem. Phys. 18, 21442 (2016).

[252] J. Gilmore and R. H. McKenzie, J. Phys. Chem. A **112**, 2162 (2008).

[253] S. Habershon, T. E. Markland and D. E. Manolopoulos, J. Chem. Phys. **131**, 024501 (2009).

[254] R. Korol, N. Bou-Rabee, and T. F. Miller III, J. Chem. Phys. **151**, 124103 (2019).

[255] R. Korol, J. L. Rosa-Raíces, N. Bou-Rabee, and T. F. Miller III, J. Chem. Phys. **152**, 104102 (2020).

[256] R. A. Marcus, J. Chem. Phys. **43**, 679 (1965).

[257] E. Laborda, M. C. Henstridge, C. Batchelor-McAuley and R. G. Compton, Chem. Soc. Rev. **42**, 4894 (2013).

[258] J. Mattiat and J. O. Richardson, J. Chem. Phys. **148**, 102311 (2018).

[259] J. Blumberger, I. Tavernelli, M. L. Klein, and M. Sprik, J. Chem. Phys. **124**, 064507 (2006).

[260] S. Krapf, S. Weber, and T. Koslowski, Phys. Chem. Chem. Phys. **14**, 11518 (2012).

[261] R. Kubo, J. Phys. Soc. Jpn. **17**, 1100 (1962).